



Terrin, Anna (2011) *Signalling of cAMP at the centrosome*. PhD thesis.

<http://theses.gla.ac.uk/2767/>

Copyright and moral rights for this thesis are retained by the author

A copy can be downloaded for personal non-commercial research or study, without prior permission or charge

This thesis cannot be reproduced or quoted extensively from without first obtaining permission in writing from the Author

The content must not be changed in any way or sold commercially in any format or medium without the formal permission of the Author

When referring to this work, full bibliographic details including the author, title, awarding institution and date of the thesis must be given



# **SIGNALLING OF cAMP AT THE CENTROSOME**

**Anna Terrin**

Submitted in fulfilment of the requirements for the  
Degree of Doctor of Philosophy

Institute of Neuroscience and Psychology  
Centre for Molecular Pharmacology  
University of Glasgow

© Anna Terrin, 2011

Anna Terrin: Signalling of cAMP at the centrosome,  
Doctor of Philosophy,  
Institute of Neuroscience and Psychology,  
Centre of Molecular Pharmacology, University of Glasgow  
© 2011

EXAMINER:  
Prof Nigel J. Pyne, Strathclyde University  
Dr Martin Cann, Durham University  
Dr George Baillie, University of Glasgow

ADVISOR:  
Prof Manuela Zaccolo

# Abstract

---

The compartmentalisation of cAMP/PKA signalling pathway within specific regions of the cell plays a critical role to achieve the specificity of response. Adenylyl cyclases (AC) are localised at discrete regions of the plasma membrane and phosphodiesterases (PDEs), the only enzymes that degrade cAMP, have been shown to be pivotal in generating spatially restricted pools of cAMP, therefore underpinning spatial control of this second messenger signal. In addition, A-kinase anchoring proteins (AKAPs) are of key importance as they anchor PKA in proximity of its specific targets, thus favouring target selective phosphorylation. Such organisation leads to local activation of PKA subsets through the generation of confined intracellular gradients of cAMP.

Interestingly it has been shown that AKAP450 localises to the centrosome, the major microtubule-organising centre, where it functions as a 'multi-scaffolding' protein by simultaneously associating PKA with PDE4D3 as well as other kinases and phosphatases. Beside this a large body of evidence suggests that the centrosome is essential for the regulation of the cell cycle progression by acting as a scaffold protein for a network of signalling pathways which in turn trigger cellular division.

In the past few years the development of FRET-based sensors has allowed the study of cAMP dynamics with high spatial-temporal resolution. By using this approach it is now possible to monitor real-time fluctuations of cAMP and PKA activity in distinct subcellular compartments and to investigate their physiological role.

The aim of the research presented in this dissertation is to exploit FRET-based sensor to investigate the signalling of cAMP at the centrosome and to define the role of PDE4D3 anchored to AKAP450 in shaping a cAMP pool in such specific compartment. The centrosomal AKAP450/PKA/PDE4D3 macromolecular complex may play a role in the control of cell cycle progression.

To this purpose a CHO clone stably expressing the FRET sensor based on PKA was generated. As expected fluorescence microscopy analysis of this clone indicated that the sensor anchors to endogenous centrosomal AKAPs. Further real-time imaging of basal cAMP provided evidence that the centrosome is a domain with lower cAMP concentration as compared to the bulk cytosol and that PDE4D3 activity is required to maintain a low cAMP level in the centrosomal area.

Interestingly the same cells challenged with the cAMP raising agent forskolin show a larger FRET change at the centrosome as compared to the bulk cytosol.

By using the unimolecular FRET EPAC-based sensor for cAMP, targeted to the centrosome, it was possible to exclude that the level of cAMP generated at the centrosome by forskolin was higher than the level of cAMP generated in the cytosol. Thus, it has been hypothesised that anchoring of PKA to AKAP450 lowers the activation constant of the enzyme leading to a higher FRET change at the centrosome as compare to the bulk cytosol. This hypothesis has been confirmed by expressing in the cytosol the fragment of AKAP450 that anchors PKA and by showing that binding of PKA to the cytosolic fragment also results in increased sensitivity of the enzyme to cAMP. Eventually analysis of PKA activity, by using a FRET-based A-kinase activity reporter (AKAR), indicated that anchoring of PKA to the cytosolic fragment of AKAP450 accounts also for an increased PKA activity.

The molecular mechanism involved in the increased sensitivity of PKA-bound to AKAP450 was also investigated. Interestingly anchoring of PKA to AKAP450 increases the auto-phosphorylation of PKA. Generation of a non-phosphorylatable version of PKA-RII subunit (mutRII) and further generation of a CHO clone stably expressing the mutPKA FRET based sensor strongly indicates that the high sensitivity of PKA bound to AKAP450 is mediated by the auto-phosphorylation site and more specifically the binding of PKA to AKAP450 seems to favour the auto-phosphorylation of PKA.

Finally the role of AKAP450/PKA/PDE4D3 macromolecular complex in the regulation of cell cycle progression was analysed. Displacement of endogenous PDE4D3 from the centrosome by over-expression of a catalytically dead version of PDE4D3 (dnPDE4D3), results not only in the abolishment of difference in cAMP concentration between centrosome and cytosol, but also in an altered cell cycle progression, suggesting that PDE4D3 plays a key role in the regulation of the cell cycle.

In conclusion this study provided evidence for a novel mechanism by which anchoring of PKA to AKAPs modulate the activation constant of the enzyme, thereby providing a mean to regulate enzyme activity locally.

*To my parents  
Who gave me the strength, the tenacity  
And the passion for life*

*...in scientific research  
nor the degree of intelligence  
nor the ability to perform and complete the task at hand  
are essential for success and personal satisfaction.  
In both counts the most total devotion and  
closing our eyes to the difficulties:  
In this way we can address the problems that other, more critical and more  
acute, did not address.*

*[Rita Levi Montalcini]*

*Ai miei genitori  
Che mi hanno trasmesso la forza, la tenacia  
E la passione per la vita*

*...nella ricerca scientifica  
né il grado di intelligenza  
né la capacità di eseguire e portare a termine il compito intrapreso  
sono fattori essenziali per la riuscita e per la soddisfazione personale.  
Nell'uno e nell'altro contano maggiormente la totale dedizione e  
il chiudere gli occhi davanti alle difficoltà:  
in tal modo possiamo affrontare i problemi che altri, più critici e più acuti,  
non affronterebbero.*

*[Rita Levi Montalcini]*

# Acknowledgments

---

I would like to acknowledge my supervisor and mentor Professor Manuela Zaccolo who actively contributed to this research through valuable advices and constructive criticisms as well as for careful review of this dissertation.

Manuela, I wish to thank you because you were the first and have always believed in me as a scientist in this long period of collaboration. You trust in my abilities and encourage me every day, contributing in this way to my development into a stronger and confident person. Your exquisite ability to make everything simple and clear allowed me to be captured by the fascinating aspects of cAMP signalling transduction and let my enthusiasm for this scientific topic to only grow.

I sincerely thank all my colleagues for their help and support in the lab, for the scientific discussions and for putting up with me during these years: thanks to Alessandra, Andreas, Anna, Frank, Laura, Marco, Nicoletta, Stefania and Graham. I also would like to add a special thanks to Alessandra, Frank and Laura for helping me with the proofreading of the thesis and to Anna for some experiments of static FRET.

I wish to acknowledge Ms Niove Jordanides and Dr Joanne Mountford for the fruitful collaboration and the flow cytometry scan analysis experiments.

My warmest thanks to Fiona, Dave, Marie-Ann, Laura and Ian for creating a pleasant atmosphere in the office.

Thanks to all my friends who by being close to me everyday helped me to overcome the difficult moments during the years of my PhD. I am grateful to Camilla, Olga, Agata, Elisa, Federica, Martina, Michele, Morena and Roberto for the affection you show me every day. Wherever the life will take us I know that you will always be with me.

Un grazie speciale a tutta la mia famiglia. Grazie nonna per tutte le preghiere che ogni giorno mi hai dedicato. Grazie a mia mamma e a mio papa' per tutto quello che avete fatto e fate per me. Spero possiate essere orgogliosi di me.

Finally I would like to give my acknowledgements to the examiners: Prof Nigel J. Pyne from Strathclyde University, Dr Martin Cann from Durham University and Dr George Baillie from University of Glasgow for the exciting and challenging discussion; and to Dr Jo Mountford for the organisation of the Viva.

# Table of Contents

---

SIGNALLING OF cAMP AT THE CENTROSOME.....	I
ABSTRACT.....	III
ACKNOWLEDGMENTS.....	VIII
TABLE OF CONTENTS.....	X
LIST OF TABLES.....	XIV
LIST OF FIGURES.....	XV
ABBREVIATIONS.....	XXIII
<b>1 INTRODUCTION.....</b>	<b>1</b>
1.1 THE “SECOND MESSENGER CONCEPT” AND THE “SIGNAL TRANSDUCTION”: A CASCADE OF NOBEL PRIZES.....	1
1.2 CAMP SIGNALLING PATHWAY.....	4
1.3 CAMP PRODUCTION AND DEGRADATION.....	6
1.3.1 <i>Adenylyl cyclase</i> .....	6
1.3.2 <i>Phosphodiesterases</i> .....	9
CATALYTIC DOMAIN.....	11
REGULATORY DOMAIN.....	12
REGULATORY DOMAIN.....	16
TARGETING AND COMPARTMENTALISATION OF PDE4.....	17
1.4 CAMP EFFECTORS.....	18
1.4.1 <i>PKA</i> .....	18
REGULATORY SUBUNIT.....	19
1.4.2 <i>EPAC</i> .....	21
1.4.3 <i>Cyclic nucleotide-Gated Channels (CNG)</i> .....	23
1.5 CAMP COMPARTMENTALISATION.....	25
1.5.1 <i>AKAPs and the physical compartmentalisation of PKA pathway</i> .....	28
PKA BINDING MOTIF.....	29
TARGETING MOTIF.....	30
1.5.2 <i>PDEs and the biochemical compartmentalisation of cAMP</i> .....	37
1.6 OVERVIEW ON CAMP DETECTION MECHANISM.....	42
1.6.1 <i>Classical approach</i> .....	42
1.6.2 <i>CNG-based sensors</i> .....	43
1.6.3 <i>GFP and FRET: seeing is believing</i> .....	44
1.7 A PKA SIGNALLING DOMAIN LOCALISED TO THE CENTROSOME.....	55
1.7.1 <i>Centrosome structure</i> .....	55
1.7.2 <i>Centrosome functions</i> .....	61
1.7.3 <i>The cell cycle and its regulation</i> .....	62
1.7.4 <i>Cell and centrosome coordinating cycles</i> .....	63
1.8 CAMP AND PKA IN CELL CYCLE PROGRESSION.....	68
<b>2 AIM OF THE THESIS.....</b>	<b>74</b>

<b>3</b>	<b>MATERIALS AND METHODS.....</b>	<b>75</b>
3.1	MOLECULAR BIOLOGY.....	75
3.1.1	Generation of competent cells.....	75
3.1.2	Bacterial transformation.....	76
3.1.3	DNA extraction and purification.....	76
3.1.4	mRNA extraction.....	77
3.1.5	Nucleic acid quantification.....	78
3.1.6	cDNA preparation.....	79
3.1.7	PCR and DNA purification.....	79
3.1.8	De-phosphorylation reaction.....	80
3.1.9	Restriction enzymes and Ligation.....	80
3.1.10	Sub-cloning of RII-CFP in pCDNA3.1/Zeo (+).....	80
3.1.11	Sub-cloning of C-YFP in pCDNA3.....	81
3.1.12	Generation of RII_epac.....	81
3.1.13	Generation of RII-RFP.....	81
3.1.14	Generation of SuperAKAP-IS and RIAD.....	81
3.1.15	Generation of AKAP450-2 fragment and mutAKAP450-2 fragment.....	82
3.1.16	Generation of $\Delta$ PKA-GFP.....	82
3.1.17	AKAP79 and AKAP149.....	82
3.1.18	Generation of the Rt31 fragment.....	82
3.1.19	Generation of RII_AKAR3 and GIT1_AKAR3.....	83
3.1.20	Generation of mutRII-CFP.....	83
3.1.21	Generation of dnPDE4D3mRFP.....	83
3.1.22	dnPDE4A4-GFP.....	84
3.2	CELL BIOLOGY.....	84
3.2.1	Cell culture and transfection.....	84
3.2.2	Stable clone selection.....	86
	ZEOCINE™.....	86
	GENETICIN® (G418 SULPHATE, NEOMYCIN).....	86
	HYGROMYCIN B.....	86
3.2.3	PDE4D knock-down.....	88
3.3	FRET BASED ANALYSIS OF CAMP.....	89
3.3.1	Imaging set up.....	90
	MICROSCOPE.....	90
	LIGHT SOURCE:.....	90
	EXCITATION FILTERS:.....	90
	EMISSION FILTERS:.....	91
	OBJECTIVE:.....	92
	CAMERA:.....	92
	IMAGE ACQUISITION AND ANALYSIS:.....	92
3.3.2	FRET experiment.....	92
3.3.3	Stimuli and reagent.....	98
3.4	BIOCHEMISTRY.....	98
3.4.1	Western Blotting.....	98
3.4.2	Immunostaining and Confocal Imaging.....	100

3.5	FLOW CYTOMETRY SCAN ANALYSIS OF CELL CYCLE DISTRIBUTION OF A CELL POPULATION USING PROPIDIUM IODIDE.....	101
<b>4</b>	<b>THE CENTROSOME IS A SUBCELLULAR DOMAIN CHARACTERISED BY LOW BASAL cAMP LEVELS.....</b>	<b>103</b>
	BACKGROUND: .....	103
	HYPOTHESIS:.....	105
	EXPERIMENTAL PROCEDURE: .....	106
4.1	RESULTS.....	106
4.1.1	<i>Generation of a CHO clone stably expressing a FRET sensor based on PKA (PKA-GFP).....</i>	<i>106</i>
4.1.2	<i>The PKA-GFP FRET sensor localises to the centrosome in CHO cells via binding to endogenous AKAPs .....</i>	<i>108</i>
4.1.3	<i>A microdomain with low cAMP concentration at the centrosome.....</i>	<i>111</i>
4.1.4	<i>Generation and characterisation of a stable clone expressing the RII<sub>ε</sub> epac cAMP sensor.....</i>	<i>113</i>
4.1.5	<i>Low cAMP centrosomal microdomain in SH-SY5Y .....</i>	<i>115</i>
4.1.6	<i>Role of PDE4D3 in the regulation of cAMP levels at the centrosome.....</i>	<i>117</i>
4.2	DISCUSSION.....	124
<b>5</b>	<b>ANCHORING OF PKA TO AKAP450 LOWERS PKA ACTIVATION THRESHOLD</b>	<b>126</b>
	BACKGROUND: .....	126
	HYPOTHESIS:.....	126
	EXPERIMENTAL PROCEDURE: .....	127
5.1	RESULTS.....	127
5.1.1	<i>Upon forskolin stimulation the PKA-GFP sensor responds with a larger FRET change at the centrosome than in the cytosol .....</i>	<i>127</i>
5.1.2	<i>PKA anchored to AKAP450 shows increased sensitivity to cAMP.....</i>	<i>129</i>
5.1.3	<i>The increased sensitivity to cAMP of AKAP-anchored PKA is specific for the PKA/AKAP450 interaction .....</i>	<i>137</i>
5.2	DISCUSSION.....	139
<b>6</b>	<b>STUDY OF PKA ACTIVITY AT THE CENTROSOME.....</b>	<b>143</b>
	BACKGROUND: .....	143
	HYPOTHESIS:.....	143
	EXPERIMENTAL PROCEDURE: .....	143
6.1	RESULTS.....	144
6.1.1	<i>AKAR3 as a sensor to measure PKA activity.....</i>	<i>144</i>
6.1.2	<i>Binding of PKA to AKAP450-2 increases PKA activity.....</i>	<i>146</i>
6.1.3	<i>Generation of targeted AKAR3 sensors to monitor centrosomal PKA activity</i>	<i>148</i>
6.2	DISCUSSION.....	154
<b>7</b>	<b>ANCHORING OF PKA TO AKAP450 FAVOURS AUTO-PHOSPHORYLATION OF THE PKA REGULATORY SUBUNIT .....</b>	<b>156</b>

BACKGROUND.....	156
HYPOTHESIS:.....	157
EXPERIMENTAL PROCEDURE: .....	157
7.1 RESULTS.....	157
7.1.1 Anchoring of PKA to AKAP450 enhances auto-phosphorylation of the RII subunit.....	157
7.1.2 Generation of a non-phosphorylatable mutant of the PKA-GFP sensor (mutPKA-GFP) .....	158
7.1.3 mutPKA-GFP anchored to AKAP450-2 does not show increased sensitivity to cAMP 160	
7.1.4 Generation of a stable clone over-expressing mutPKA-GFP.....	161
7.2 DISCUSSION.....	163
<b>8 DISPLACEMENT OF CENTROSOMAL PDE4D3 FROM AKAP450 RESULTS IN ALTERED CELL CYCLE PROGRESSION.....</b>	<b>164</b>
BACKGROUND: .....	164
HYPOTHESIS:.....	166
EXPERIMENTAL PROCEDURE: .....	166
8.1 RESULTS.....	166
8.1.1 Generation of a CHO cell line stably expressing the dominant negative variant of PDE4D3 .....	166
8.1.2 Generation of a CHO cell line stably expressing the dominant negative variant of PDE4A4.....	170
8.1.3 Flow cytometry scan analysis of cell cycle progression .....	170
8.2 DISCUSSION.....	174
<b>9 CONCLUSION AND FUTURE PERSPECTIVES.....</b>	<b>177</b>
<b>10 REFERENCES .....</b>	<b>182</b>

# List of Tables

---

Table 1 Adenylyl cyclase regulation system.....	8
Table 2 Correlation between the AKAPs molecular weight-based nomenclature and the gene-based nomenclature. Adapted from (Pidoux and Tasken).....	33

# List of Figures

---

Figure 1-1 Schematic representation of the “signal transduction” and “second messenger” concept. Adapted from (Sutherland, 1972). .....	2
Figure 1-2 Schematic representation of adenylyl cyclase. TM1 and TM2 are the transmembrane domains; C1 and C2 are the cytosolic loops that form the catalytic core. Adapted from (Willoughby and Cooper, 2007). .....	7
Figure 1-3 Structural formula of cAMP. Arrow points at the bond hydrolysed by PDE. Adapted from (Bender and Beavo, 2006). .....	10
Figure 1-4 Schematic representation of PDEs families. Adapted from (Conti and Beavo, 2007). .....	14
Figure 1-5 Schematic representation of PDE4 subfamily. Adapted from (McCahill et al., 2008) .....	15
Figure 1-6 Schematic representation of A) the regulatory and B) the catalytic subunit of PKA. Star in the regulatory subunit A) indicates the pseudo-phosphorylation or the auto-phosphorylation site of R type I and type II respectively. C) Schematic representation of the quaternary structure of PKA.....	21
Figure 1-7 A) Schematic representation of Epac1 and Epac 2 and B) its activation mechanism.....	23
Figure 1-8 Schematic representation of a CNG channel member. Adapted from (Biel and Michalakis, 2009). .....	25
Figure 1-9 Schematic representation of AKAP-PKA interaction.....	28
Figure 1-10 Schematic representation of a negative feedback loop regulation mechanism involving an AKAP-anchored PDE4. 1) mAKAP anchors PKA and PDE4D3 at the perinuclear region of cardiomyocytes. 2) When cAMP increases, PKA is activated and 3) it phosphorylates the associated PDE4D3 4) which in turn degrades cAMP re-establishing the cAMP level below the threshold of PKA activation.....	36
Figure 1-11 Schematic representation of intracellular cAMP compartmentalisation. cAMP is locally degraded by different compartmentalised subsets of PDEs that can act either as an enzymatic barrier or as a sink to prevent cAMP free diffusion and to generate spatially restricted pools of cAMP. In this way PDEs prevent the inappropriate activation of PKA. Activation of a specific GPCR generates a specific pool of cAMP whereas the activation of a different GPCR leads to the generation of a different pool of cAMP.....	41
Figure 1-12 Schematic representation of the dependence of the energy transfer efficiency (E) on distance. $R_0$ is the Förster distance. ....	47
Figure 1-13 Schematic representation of PKA-GFP FRET based sensor for cAMP and its mechanism of activation.....	49
Figure 1-14 Subcellular localisation of PKA-GFP sensor in neonatal rat ventricular cardiomyocytes. Bar 10 $\mu$ m.....	50
Figure 1-15 Subcellular localisation of mpPKA-GFP sensor in HEK293 cells. Bar 10 $\mu$ m. ....	53

Figure 1-16 Subcellular localisation of RI_epac and RII_epac sensors in neonatal rat ventricular cardiomyocytes. Bars 10µm.....	54
Figure 1-17 Schematic representation of the centrosome and centrosomal proteins distribution according to their proximal-distal polarity. Adapted from (Bornens, 2002).....	56
Figure 3-1 Representation of the slide holder used for live fluorescence imaging experiments.....	93
Figure 3-2 CHO cell stably expressing the PKA-GFP sensors. Black line represents a typical region of interest (ROI) drawn on the cytosol; grey line represents a typical region of interest (ROI) drawn around the centrosome. Bar 10 µm.....	96
Figure 4-1 CHO stably expressing the PKA-GFP sensor. The two panels show the signal generated by the RII-CFP (left panel) and C-YFP (right panel) subunit in interphase cells A) and mitotic cells B). The arrows point to the centrosome A) and centrioles B). The region of the cell in which the fluorescent signal of the probe is excluded is the nucleus in interphase cells A) and the metaphasic plate in mitotic cells B). Bars 10µm.....	108
Figure 4-2 Detail of a CHO cell stably expressing the PKA-GFP sensor (left panel) and imaged at the confocal microscope. The cell shows a clear localisation of the sensor in correspondence of a perinuclear structure in which it is possible to recognise two elements organised orthogonally to each other. Bar 10µm; and schematic representation of a centrosome (right panel).....	109
Figure 4-3 Immunostaining of CHO cells stably expressing the PKA-GFP FRET sensor. Images show co-localisation of RII-CFP with CTR453 (antibody specific for AKAP450), top panel; and with γ-tubulin (specific marker for centrosome) middle panel. Secondary antibody (nc) control in the bottom panel. The signal from the C-YFP component of the sensor is not shown. Bars 10µm.....	110
Figure 4-4 CHO cells over-expressing RII-RFP (upper and lower panel on the left) in combination with SuperAKAP-IS-GFP (right upper panel) or RIAD-GFP (right lower panel). The arrows point to the centrosome. Bars 10µm.....	111
Figure 4-5 RII-CFP signal and pseudo-colour image of a CHO cell stably expressing the PKA-GFP sensor. The signal generated by the C-YFP component of the PKA-GFP sensor is not shown. On the left, a higher magnification of the cell area delimited by the white box is shown. Bar 10µm.....	112
Figure 4-6 Summary of the CFP/YFP ratio values recorder in the bulk cytosol and in the centrosome of cells stably expressing the PKA-GFP sensor. Data are normalised to the ratio value in the cytosol. (Error bar represents SEM. Two tailed; paired t-test, *** p<0.001).....	113
Figure 4-7 Schematic representation of RII_epac sensor. D/D=PKA-RIIβ dimerization docking domain; CFP=cyan variant of the green fluorescent protein (GFP); cAMP BD=cAMP binding domain of Epac1; YFP=yellow variant of the green fluorescent protein.....	114
Figure 4-8 CHO stably expressing the RII_epac sensor. The two panels show the signal generated by the CFP (left panel) and YFP (right panel) emission. The arrows point to the centrosome. Bar 10µm.....	114

- Figure 4-9 Summary of the differences of basal CFP/YFP ratio between the cytosol and the centrosome of CHO cells stably expressing RII\_epac sensor. Data are normalised to the ratio value in the cytosol. (Error bar represents SEM. Two tailed; paired t-test, \*\*\*  $p < 0.001$ ). ..... 115
- Figure 4-10 SH-SY5Y stably expressing the RII\_epac sensor. The two panels show the signal generated by the CFP (left panel) and YFP (right panel) emission. The arrows point to the centrosome. Bar 10 $\mu$ m. .... 116
- Figure 4-11 Top panel: CFP signal and pseudo-colour image of SH-SY5Y cells stably expressing RII\_epac. The box shows the magnification of the centrosome region. Bar 10 $\mu$ m. Bottom panel: summary of the differences of basal CFP/YFP ratio values in the cytosol and in the centrosome of SH-SY5Y cells stably expressing RII\_epac sensor. Data are normalised to the CFP/YFP value in the cytosol. (Error bar represents SEM. Two tailed; paired t-test, \*\*\*  $p < 0.001$ ). ..... 117
- Figure 4-12 Subcellular localisation of PDE4D3 in CHO cells. Images show co-localisation of PDE4D3, top left panel, with  $\gamma$ -tubulin (specific antibody for centrosome) middle panel. Secondary antibody control in the bottom panels. Bars 10 $\mu$ m. .... 118
- Figure 4-13 Top panel: RII-CFP signal and pseudo-colour image of a CHO cell stably expressing PKA-GFP and treated with 10  $\mu$ M rolipram. The box shows the magnification of the centrosome region. Bar 10 $\mu$ m. Bottom panel: summary of the basal CFP/YFP ratio values in the cytosol and in the centrosome of cells stably expressing either PKA-GFP or RII\_epac sensor, as indicated, and treated with rolipram. Data are normalised to the CFP/YFP value in the cytosol (Error bars represent SEM. Two tailed; paired t-test)..... 119
- Figure 4-14 Top panel: RII-CFP signal and pseudo-colour image of a CHO cell stably expressing PKA-GFP and treated with 10  $\mu$ M EHNA. The box shows the magnification of the centrosome region. Bar 10 $\mu$ m. Bottom panel: summary of the differences of basal CFP/YFP ratio value in the cytosol and at the centrosome of cells stably expressing PKA-GFP and treated, as indicated, with EHNA 10  $\mu$ M or cilostamide (cilo) 10  $\mu$ M. Data are normalised to the CFP/YFP value in the cytosol (Error bars represent SEM. Two tailed; paired t-test, \*\*\*  $p < 0.001$ ). ..... 120
- Figure 4-15 Western blot of PDE4D and  $\gamma$ -tubulin obtained from cells treated as follows: untreated CHO (CTRL), CHO over-expressing the control siGLO@ (siGLO) and CHO over-expressing the small RNA interference of PDE4D (siRNAPDE4D). ..... 121
- Figure 4-16 Top panel: RII-CFP signal and pseudo-colour image of a CHO cell co-expressing PKA-GFP and siRNA for PDE4D. The box shows the magnification of the centrosome region. Bar 10 $\mu$ m. Bottom panel: summary of the differences of basal CFP/YFP ratio value in the cytosol and at the centrosome of cells expressing either siRNA for PDE4D or the control siGLO@, as indicated. Data are normalised to the CFP/YFP value in the cytosol. (Error bars represent SEM. Two tailed; paired t-test, \*\*\*  $p < 0.001$  with siGLO@). ..... 122
- Figure 4-17 Top panel: RII-CFP signal and pseudo-colour image of a CHO cell co-expressing PKA-GFP and dnPDE4D3. The box shows the magnification of the centrosome region. Bar 10 $\mu$ m. Bottom panel: summary of the differences of basal

CFP/YFP ratio values in the cytosol and at the centrosome of cells expressing either dnPDE4D3 or the control dnPDE4A4, as indicated. Data are normalised to the CFP/YFP value in the cytosol. (Error bars represent SEM. Two tailed; paired t-test, * p<0.5).....	123
Figure 4-18 Comparison between the effect of rolipram, siRNA for PDE4D and dnPDE4D3 on cytosolic (cyt) and centrosomal (centr) ratio increase compared to untreated control. (Error bars represent SEM. Two tailed; un-paired t-test; *** p<0.001, * p<0.05).....	124
Figure 5-1 Normalised average kinetics of FRET change detected in response to 25 $\mu$ M forskolin (frsk) and recorded in the cytosol (cyt; black circles) and at the centrosome (centr; grey circles) in CHO cells stably expressing PKA-GFP. (Error bar represents SEM. Two tailed; un-paired t-test, *** p<0.001).....	128
Figure 5-2 Normalised average kinetics of FRET change induced by 25 $\mu$ M forskolin (frsk) in CHO cells stably expressing RII_epac and recorded in the cytosol (cyt; black circles) and at the centrosome (centr; grey circles). (Error bar represents SEM. Two tailed; un-paired t-test). ....	129
Figure 5-3 Schematic representation of AKAP450 and AKAP450-2 fragment.....	130
Figure 5-4 Effect of PKA-GFP binding to AKAP450-2 fragment. A) Schematic representation of PKA-GFP and AKAP450-2 fragment interaction; B) Summary of FRET changes induced by 25 $\mu$ M forskolin in the presence or absence of the AKAP450-2 fragment. (Error bar represents SEM. Two tailed; un-paired t-test, * p<0.05).....	131
Figure 5-5 Percentage of cells responding to increasing concentration of forskolin. Open and full bars represent CHO cells expressing PKA-GFP in the presence or absence of the AKAP450-2 fragment, respectively. [n<10].....	132
Figure 5-6 Dose-response curve. FRET change induced by increasing concentration of forskolin in CHO cells expressing PKA-GFP in the presence or absence of AKAP450-2 [n<10]. (Error bars represent SEM. Two tailed; un-paired t-test, * p<0.05, ** 0.01<p<0.001, *** p<0.001). ....	133
Figure 5-7 Effect of disrupting PKA-GFP/AKAP450-2 interaction with SuperAKAP-IS (SuperIS). A) Schematic representation of PKA-GFP, AKAP450-2 and SuperAKAP-IS interaction (SuperIS, red helix); B) Summary of FRET change induced by 25 $\mu$ M forskolin in the presence or absence of AKAP450-2 fragment and SuperAKAP-IS. (Error bars represent SEM. Two tailed; un-paired t-test, * p<0.05, ** 0.01<p<0.001).....	134
Figure 5-8 Effect of AKAP450-2 on $\Delta$ PKA-GFP. A) Schematic representation of AKAP450-2 fragment and $\Delta$ PKA-GFP; B) Summary of FRET change induced by 25 $\mu$ M forskolin in the presence or absence of AKAP450-2 fragment on $\Delta$ PKA-GFP. (Error bar represents SEM. Two tailed un-paired t-test).....	135
Figure 5-9 Effect of PKA-GFP binding to mutAKAP450-2 fragment compared to the binding to the AKAP450-2 (wild type). A) Schematic representation of PKA-GFP and mutAKAP450 2; B) Summary of FRET change induced by 25 $\mu$ M forskolin in the presence or absence of the AKAP450-2 and mutAKAP450-2 fragments. (Error bars represent SEM. Two tailed; un-paired t-test, * p<0.05). ....	136

Figure 5-10 Effect of RII_epac binding to AKAP450-2 fragment. A) Schematic representation of RII_epac/AKAP450-2 fragment interaction; B) Summary of FRET change induced by 25 $\mu$ M forskolin in the presence or absence of the AKAP450-2 fragment. (Error bar represents SEM. Two tailed un-paired t-test). .....	137
Figure 5-11 Effect of PKA-GFP interaction with AKAP79, AKAP149 and Rt31 fragments on the sensitivity of PKA-GFP to cAMP. A) Schematic representation of PKA-GFP anchored to AKAP79 fragment (top) and summary of FRET change induced by 25 $\mu$ M forskolin in the presence or in the absence of the AKAP79 fragment (bottom); B) Schematic representation of PKA-GFP anchored to AKAP149 fragment (top) and summary of FRET change induced by 25 $\mu$ M forskolin in the presence or absence of the AKAP149 fragment (bottom); C) Schematic representation of PKA-GFP anchored to Rt31 fragment (top) and summary of FRET change induced by 25 $\mu$ M forskolin in the presence or absence of the Rt31 fragments (bottom). (Error bars represent SEM. Two tailed; un-paired t-test). .....	138
Figure 6-1 Schematic representation of AKAR3 reporter and its mechanism of function. ....	144
Figure 6-2 Representative kinetics of FRET change induced by 25 $\mu$ M forskolin (frsk) in CHO cells expressing AKAR3 reporter. ....	145
Figure 6-3 Representative kinetics of FRET change induced by 25 $\mu$ M forskolin (frsk) in CHO cells expressing AKAR3 and pre-treated with 10 $\mu$ M H-89. ....	146
Figure 6-4 Effect of over-expression of AKAP450-2 on endogenous PKA activity. Error bar represents SEM. Two tailed; un-paired t-test, ** 0.01<p<0.001). ....	147
Figure 6-5 Effect of over-expression of AKAP79 on endogenous PKA activity. (Error bar represents SEM. Two tailed; un-paired t-test). .....	147
Figure 6-6 Schematic representations of centrosome-targeted AKAR3 reporters: A) RII_AKAR3 and B) GIT1_AKAR3. ....	148
Figure 6-7 Subcellular localisation of RII_AKAR3 and GIT1_AKAR3 in CHO cells. The arrows point to the centrosome. Bars 10 $\mu$ m. ....	149
Figure 6-8 Representative kinetics of FRET change generated by 25 $\mu$ M forskolin (frsk) in CHO cells expressing A) RII_AKAR sensor or B) GIT1_AKAR3 sensor. ....	149
Figure 6-9 Effect of 25 $\mu$ M forskolin on endogenous cytosolic and centrosomal PKA activity. Summary of FRET changes recorded in the cytosol (cyt) and at the centrosome (centr) of CHO cells expressing A) RII_AKAR3 or B) GIT1_AKAR3 sensor. (Error bars represent SEM. Two tailed; paired t-test, *** p<0.001). .....	150
Figure 6-10 Effect of 25 $\mu$ M forskolin on endogenous PKA activity in the presence of the PP1 and PP2A inhibitor calyculin A. Summary of FRET changes induced by 25 $\mu$ M forskolin in CHO cells expressing AKAR3 and in the absence or in the presence of 20 nM calyculin A (CLA). (Error bar represents SEM. Two tailed; un-paired t-test, *** p<0.001). .....	151
Figure 6-11 Effect of 25 $\mu$ M forskolin on endogenous cytosolic and centrosomal PKA activity after inhibition of PP1 and PP2A. Summary of FRET changes recorded in the cytosol (cyt) and at the centrosome (centr) of CHO cells expressing A) RII_AKAR3 or B) GIT1_AKAR3 sensor and pre-treated with 20 nM calyculin A	

(CLA). (Error bars represent SEM. Two tailed; paired t-test, * $p < 0.01$ , ** $0.01 < p < 0.001$ ).....	152
Figure 6-12 Effect of 100 nM forskolin on endogenous cytosolic and centrosomal PKA activity with or without inhibition of PP1 and PP2A. Summary of FRET changes recorded in the cytosol (cyt) and at the centrosome (centr) of CHO cells expressing A) RII_AKAR3 or B) GIT1_AKAR3 sensor and pre-treated with or without 20 nM calyculin A (CLA). (Error bars represent SEM. Two tailed; paired t-test, * $p < 0.05$ ).....	153
Figure 7-1 Effect of over-expression of AKAP450-2 on endogenous PKA RII $\beta$ -subunit auto-phosphorylation. A) Representative western blot of total RII $\beta$ and phospho-RII $\beta$ . B) Western Blot quantification (mean of 5 separate experiments). (Error bar represents SEM. Two tailed; paired t-test, * $p < 0.05$ ).....	158
Figure 7-2 Schematic representation of A) RII-CFP and B) mutRII-CFP subunit with the substitution S114A. D/D=PKA-RII $\beta$ dimerisation docking/domain; IS=inhibitory site (or auto-phosphorylation site); DomainA=cAMP binding domain A; DomainB=cAMP binding domain B; CFP=cyan variant of the green fluorescent protein (GFP). .....	159
Figure 7-3 Western blot showing auto-phosphorylation of PKA-GFP and mutPKA-GFP. The PKA <sub>RII<math>\beta</math></sub> (pS114) antibody recognised only the auto-phosphorylation of the endogenous PKA in lysates from CHO cells over-expressing the mutPKA-CFP. 159	159
Figure 7-4 Comparison between PKA-GFP (wild type) and mutPKA-GFP FRET sensors. Summary of FRET changes induced by 25 $\mu$ M forskolin in CHO cells over-expressing PKA-GFP or mutPKA-GFP. (Error bar represents SEM. Two tailed; unpaired t-test, * $p < 0.05$ ).....	160
Figure 7-5 Effect of AKAP450-2 on the FRET change detected by PKA-GFP and mutPKA-GFP. Summary of FRET changes induced by 25 $\mu$ M forskolin and detected by PKA-GFP (wild type) and mutPKA-GFP in the presence (white columns) or absence (black columns) of the AKAP450-2 fragment. (Error bars represent SEM. Two tailed; un-paired t-test, * $p < 0.05$ ).....	161
Figure 7-6 Subcellular localisation of mutPKA-GFP in CHO cells. The centrosome is indicated by the arrow. Bar 10 $\mu$ m.....	162
Figure 7-7 Effect of 25 $\mu$ M forskolin on the FRET change detected in the cytosol (cyt) and at the centrosome (centr) by mutPKA-GFP and PKA-GFP. (Error bars represent SEM. Two tailed; paired t-test, *** $p < 0.001$ ).....	163
Figure 8-1 Western blot of cell lysates from CHO cells, CHO lines (“Old clone dn4D3” and “New clone dnPDE4D3mRFP”) stably expressing the dnPDE4D3 tagged to mRFP and CHO cells transiently transfected with the dnPDE4D3mRFP (CHO+dn4D3) probed with an antibody directed to PDE4D. “Old clone dn4D3” is the first clone selected, in which it is not possible to detect the dnPDE4D3mRFP; “New clone dnPDE4D3mRFP” is the newly selected clone in which it is possible to detect the PDE4D3, the PDE4D5 and the PDE4D3mRFP as well as these PDEs isoforms appear in lysate from CHO cells transiently transfected with dnPDE4D3mRFP. Lysates from CHO cells and from the “Old clone dn4D3” show only the bands for the endogenous PDE4D3 and PDE4D5.....	167

- Figure 8-2 RT-PCR analysis of PDE4D3 wild type and dominant negative variant in CHO cells, CHO lines stably expressing the dnPDE4D3 tagged to mRFP, “Old clone dn4D3” and “New clone dn4D3” respectively, and CHO cells transiently transfected with the dnPDE4D3mRFP. The 650 bp band expected from the wild type isoform of the PDE4D3 is detectable in the entire set of samples analysed (left panel), whereas only the “New clone dn4D3” and CHO cells transiently expressing the dnPDE4D3mRFP show amplification of the dominant negative variant of PDE4D3. .... 168
- Figure 8-3 Fluorescence microscopy image of a “New clone dn4D3” cell. Image show the subcellular localisation of the recombinant protein. Arrow points to the centrosome. Bar 10µm. .... 169
- Figure 8-4 Subcellular localisation of dnPDE4D3mRFP in CHO cells. Images show co-localisation of dnPDE4D3mRFP (left panel) with RII-CFP (middle panel); arrows point to the centrosome. Bar 10µm. .... 169
- Figure 8-5 CHO stably expressing the dnPDE4A4-GFP. Bar 10µm. .... 170
- Figure 8-6 Quantification of flow cytometry scan analysis (mean of 6 independent experiments) for CHO, CHO-dnPDE4D3mRFP (dnPDE4D3mRFP) and CHO-dnPDE4A4-GFP (dnPDE4A4-GFP). Histograms indicate the mean percentages of cells in various phases of the cell cycle. (Error bars represent SEM. One-way ANOVA test, \*\*\*p<0.001). .... 171
- Figure 8-7 FACS analysis quantification (mean of 6 independent experiments) for CHO, CHO-dnPDE4D3mRFP (dnPDE4D3mRFP) and CHO-dnPDE4A4-GFP (dnPDE4A4-GFP) upon treatment with forskolin 5 µM. The histogram indicates the average percentages of cells in various phases of the cell cycle. (Error bars represent SEM. One-way ANOVA test, \* p<0.05, \*\* 0.01<p<0.001, \*\*\* p<0.001). .... 172
- Figure 8-8 Top panel: representative (1 out of 6) experiment showing cellular DNA content in untreated CHO cells, CHO cells treated with forskolin, CHO-dnPDE4D3mRFP (dnPDE4D3mRFP) and CHO-dnPDE4A4-GFP (dnPDE4A4-GFP). Gaussian curve around 200 fluorescence emission value corresponds to the 2n content of DNA (G<sub>1</sub>), Gaussian curve around 400 fluorescence emission value corresponds to 4n content of DNA (G<sub>2</sub>/M), values between 200 and 400 correspond to the intermediate content of DNA (S). Bottom panel: quantification of flow cytometry scan analysis (mean of 6 independent experiments). Values indicate the mean percentages of cells in each phases of the cell cycle, as indicated. (Error bars represent SEM. One-way ANOVA test, \*\*\*p<0.001). .... 174

I declare that, except where explicitly stated, the work contained in this dissertation is my own.

Glasgow, Scotland,  
April 2011, Anna Terrin

---

# Abbreviations

---

$\beta$ -AR =  $\beta$ -adrenergic receptor

aa = amino acid

AC = adenylyl cyclases

AKAP = A Kinase anchoring proteins

AKAR3 = A-Kinase activity reporter

AMPA =  $\alpha$ -amino-3-hydroxi-5-methyl-4-isoxazolepropionic

ANOVA = analysis of variance

APC = anaphase-promoting complex

Arf = ADP ribosylation factor

ATP = adenosine triphosphate

bp = base pairs

CaM = calmodulin

cAMP = 3', 5' cyclic adenosine monophosphate

CCD = charged-coupled device

Cdks = cyclin dependent kinases

CFP = cyan fluorescent protein

CFTR = cystic fibrosis trans-membrane conductance regulator

cGMP = 3',5' cyclic guanosine monophosphate

Chk1 = checkpoint kinase 1

CHO = chinese hamster ovary

CBD = cyclic nucleotide binding domains

CNG = Cyclic nucleotide-Gated Channels

cpV = permutant of the YFP variant named Venus

CRE = cAMP response element

CREB = CRE binding protein

CTR = C-terminal region

D/D = docking domain

DAG = diacylglycerol

DEP = Dishevelled, Egl-10, and Pleckstrin

DISC = disrupted in schizophrenia

*E.coli* = Escherichia coli

EGF = epidermal growth factor

EHNA = erythro-9-2-hydroxy-3-nonyl adenine

ER = endoplasmic reticulum

ERK = extracellular regulation kinase

FACS = Flow cytometry scan analysis

FHA1 = forkhead-associated domain 1

FRET = fluorescence resonance energy transfer

FSC = forward scatter

GAP = GTPase-activating protein

GDP = guanosine diphosphate

GEFs = guanine nucleotide exchange factors

GFP = green fluorescent protein

GIT1 = G-protein coupled receptor kinase interacting protein

GPCR = G protein-coupled receptors

GTP = guanosine triphosphate

H-89 = N-[2-[[3-(4-Bromophenyl)-2-propenyl] amino] ethyl]-5-isoquinolinesulfonamide dihydrate dihydrochloride

HBSS = Hank's buffered salt solution

HCN = hyper-polarisation-activated cyclic nucleotide

IBMX = 3-isobutyl-1-methylxantine

IP3 = Inositol-triphosphate

MAP2 = microtubule associate protein 2

mp = myristoylated and palmitoylated sequence

MPF = M-phase Promoting Factor

mRFP = monomeric ref fluorescent protein

MTOC = microtubule organising centre of the cell

NA = numerical aperture

NDEL = nuclear like protein

NES = nuclear export sequence

NLS = nuclear localisation sequence

NMDA = N-methyl-D-aspartic acid

NTR = N-terminal region

OD = optical density

PACT = pericentrin-AKAP450 centrosomal targeting

PCM = pericentriolar material

PDE = phosphodiesterase

PGE<sub>1</sub> = prostaglandin E<sub>1</sub>

PIP3 = Phosphatidylinositol-trisphosphate

PKA = cAMP-dependent protein kinase

PKI = Protein Kinase Inhibitor

Plk = polo-like kinase

PP1 = proteins phosphatase 1

PP2A = protein phosphatase 2A

PPi = inorganic pyrophosphate

RA = Ras-association domain

RACK = receptor for activated protein kinase C

Rb = retinoblastoma

REM = regulatory domain named Ras exchange motif

RT-PCR = Reverse transcription polymerase chain reaction

RyR = ryanodin receptor

sAC = soluble adenylyl cyclase

SEM = standard error of measurement or mean

SSC = side scatter

tmACs = trans-membrane adenylyl cyclases family

UCR= upstream conserved region

YFP = yellow fluorescent protein

# **1** Introduction

---

## **1.1 The “second messenger concept” and the “signal transduction”: a cascade of Nobel Prizes**

In biology “signal transduction” is the process that converts the binding of a specific ligand to a cell-surface receptor into a specific physiological response, by perturbing the concentration of an intracellular molecule. The ligand is usually a hormone, a neurotransmitter or another signal substance that acts as the “first messenger” whereas the intermediate molecule, which triggers a cascade of phosphorylation and de-phosphorylation, is the “second messenger” (Robison et al., 1968) (Sutherland, 1972).

The most studied second messengers are cyclic nucleotides such as 3', 5' cyclic adenosine monophosphate (cAMP) and 3', 5' cyclic guanosine monophosphate (cGMP); Phosphatidylinositol derivatives, such as Phosphatidylinositol-trisphosphate (PIP3), Diacylglycerol (DAG) and Inositol-triphosphate (IP3), controlling the release of intracellular calcium stores; and

Ca<sup>2+</sup>. Among these, cAMP was the first second messenger to be discovered and its signalling pathway has been the most characterised signal transduction cascade (Figure 1-1) (Sutherland, 1972).

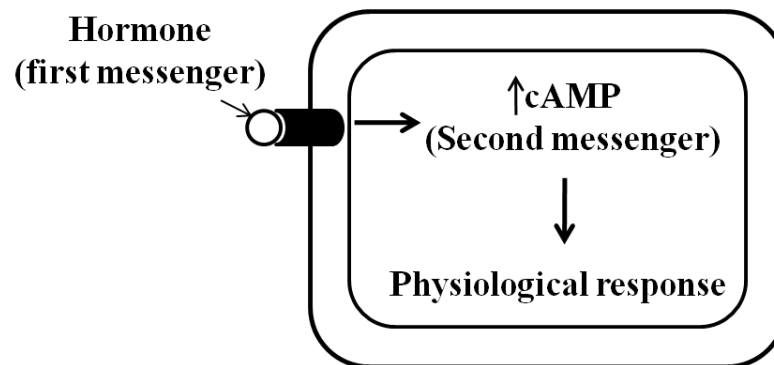


**Figure 1-1 Schematic representation of the “signal transduction” and “second messenger” concept. Adapted from (Sutherland, 1972).**

The concept of a second messenger was elucidated by Earl W. Sutherland with the discovery of 3',5' cyclic adenosine monophosphate (cAMP) as a molecule with an intermediary role in many hormonal functions (Sutherland and Robison, 1966). In 1958 Earl W. Sutherland was investigating the glycogenolytic action of epinephrine and glucagon in extracts of dog liver when he found that epinephrine regulates this reaction by activating a phosphorylase which in turn catalyses the glycogen degradation and the consequent glucose formation. He also observed that the availability of active phosphorylase was mediated by a heat stable factor. Further chemical analysis characterised such a factor as an adenine ribonucleotide the formation of which involves the cyclisation of ATP: now better known as 3',5' cyclic adenosine monophosphate (cAMP).

The discovery of cAMP as intermediate molecule in the degradation of glycogen to glucose raised the question of how hormones can stimulate its production. Sutherland demonstrated that this reaction involved another unknown enzyme which activity required Mg<sup>2+</sup> ions and adenosine triphosphate (ATP). This enzyme was named adenylyl cyclase. Based on this

evidence, Sutherland proposed a “model of signal transduction” in which binding of epinephrine to a specific receptor on the plasma membrane of the cell stimulates adenylyl cyclase leading to cAMP production. cAMP then exerts its effect by activating phosphorylase (Rall and Sutherland, 1958).

Further characterisation of cAMP revealed that it was present not only in liver, but also in heart, skeletal muscle and brain and led to the extension of the signal transduction model to many other hormones. According to Sutherland, hormones do not enter the cell but bind to plasma membrane receptors causing the formation of an intermediary molecule or “second messenger”, which in turn can transduce many cellular processes by the activation of additional signalling cascades. This model met a lot of criticism from the scientific society of that time; however it was then confirmed for many hormones exerting their effect via cAMP.

In 1971 Sutherland won the Nobel Prize for “his discovery concerning the mechanism of the action of the hormones”.

Approximately at the same time as Sutherland isolated cAMP and formulated the second messenger concept, Edwin G. Krebs and Edmond H. Fisher were interested in dissecting the molecular mechanism by which cAMP promotes phosphorylase activation via phosphorylase kinase. It was Donal A. Walsh, a postdoctoral fellow in Krebs’ laboratory, who first discovered the cAMP-dependent protein kinase (PKA) from rabbit skeletal muscle extracts, highlighting for the first time the existence of a protein kinase cascade in which a kinase can phosphorylate and activate another kinase (Walsh et al., 1968). This discovery also promoted further work on the protein phosphorylation process in general that led to Krebs and Fisher winning the Nobel Prize in 1992 for “their discoveries concerning reversible protein phosphorylation as a biological regulatory mechanism”.

Later on, it was shown that PKA is composed of a regulatory subunit to which the cAMP binds and a catalytic subunit inhibited by binding to the regulatory subunit. Binding of cAMP to PKA promotes the release of the active

catalytic subunit and the activation of the cAMP/PKA signalling cascade (Gill and Garren, 1971) (Brostrom et al., 1971).

In the process of elucidation of the hormones/cAMP pathway of signal transduction there was still a missing link between the binding of the hormone to the receptor and the activation of adenylyl cyclase with the consequent cAMP production.

Gilman and co-workers provided evidence to illustrate the adenylyl cyclase activation. First, they noted that the adenylyl cyclase activity required a regulatory protein containing two functional components (now known to be  $\alpha$  and  $\beta\gamma$  subunits of the G-protein, see below). Then, they discovered that such a regulatory protein is a guanine nucleotide-binding protein, capable to activate the adenylyl cyclase. This protein was named G-protein. Finally, they illustrated the mechanism of adenylyl cyclase activation. Schematically, when a hormone activates a specific receptor it triggers the exchange of GTP for GDP in the G-protein, causing a conformational change, which in turn induces the dissociation of the  $G_\alpha$  subunit bearing the GTP from the  $G_{\beta\gamma}$  subunits. The free  $G_\alpha$ -GTP subunit will then binds and activates the adenylyl cyclase. Hydrolysis of the  $G_\alpha$  subunit-bound-GTP in GDP finally promotes the re-association of the G-protein  $\alpha$  and  $\beta\gamma$  subunits (Ross and Gilman, 1977b) (Ross and Gilman, 1977a).

The importance of the G-proteins family discovery, as an essential linker between hundreds different receptors and effectors proteins, awarded Gilman the Nobel Prize in 1994 “for this discovery of G-proteins and the role of these proteins in signal transduction in cells”.

## 1.2 cAMP signalling pathway

cAMP is a small hydrophilic freely diffusible nucleotide responsible for numerous effects and biological functions in a wide variety of systems: from memory formation to cardiac frequency and strength of contraction, lipid

metabolism, differentiation and gene transcription, cell growth and tumour genesis (Francis and Corbin, 1994).

cAMP is generated upon ligand binding to G protein-coupled receptors (GPCR) that induce the release of the  $G_{\alpha s}$  subunit and the consequent activation of the adenylyl cyclases, that in turn catalyses the cyclisation of ATP in 3',5'-cAMP and inorganic pyrophosphate (PPi) (Rall and Sutherland, 1962).

The intracellular level of cAMP depends on the balance between synthesis and degradation, thereby results from the activities of adenylyl cyclases (AC), the only enzymes that can generate cAMP and the phosphodiesterase (PDE), the only proteins capable of degrading cAMP into 5-AMP.

Activation of the cAMP major effector, protein kinase A (PKA), leads to the phosphorylation of a myriad of intracellular targets (membrane receptors, nuclear transcription factors, cytosolic proteins) all of which are responsible for the generation of a specific cellular event.

PKA can bind to A Kinase anchoring proteins (AKAP), which contribute to the specificity as well as the versatility of the cAMP-PKA pathway by tethering PKA to discrete subcellular compartments in close proximity to its substrates.

Since cAMP exerts primary metabolic functions it is clear that a great variety of disorders, such as cardiac hypertrophy, bronchial asthma, diabetes, affective disorders as well as growth of tumours, may be related to alteration of cAMP and its pathway. It is therefore of fundamental importance to study the mechanisms that regulate its formation, functions and compartmentalisation.

## 1.3 cAMP production and degradation

### 1.3.1 Adenylyl cyclase

The adenylyl cyclases (AC) are enzymes that catalyse the cyclisation of adenosine triphosphate (ATP) to generate cAMP and inorganic pyrophosphate (PPi). Since 1989, when the first AC (AC1) was purified, nine other isoforms were isolated in mammals. Nowadays it is possible to identify two basic subfamilies of ACs: the trans-membrane adenylyl cyclases family (tmACs) and a soluble adenylyl cyclase (sAC) (Willoughby and Cooper, 2006) (Kamenetsky et al., 2006).

The first family of ACs to be discovered was the tmACs. This family is encoded by nine distinct genes (type I through type IX) and represents the more widely studied source of cAMP. Membrane-bound AC isoforms are large proteins of approximate 120–140 kDa that share a common secondary structure comprising of an intracellular N-terminus, that retains the regulatory properties of ACs, and two membrane spanning domain (including six trans-membrane helices each) separated by two large cytoplasmatic loop domains: C1 and C2. C1 and C2 domains are the most conserved regions between AC isoforms and their interaction forms the catalytic core of the enzyme. C1 and C2 dimerisation constitutes, in fact, the ATP-binding site. Within these motifs two aspartic acid residues coordinate two catalytic metal ions. These mediate the attachment of the ATP, promoting the cyclisation of the cAMP and the release of PPi (Figure 1-2) (Cooper, 2003).

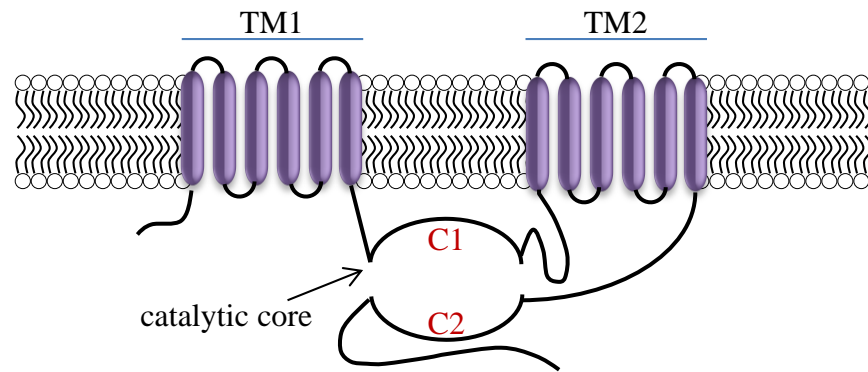


**Figure 1-2 Schematic representation of adenylyl cyclase. TM1 and TM2 are the trans-membrane domains; C1 and C2 are the cytosolic loops that form the catalytic core. Adapted from (Willoughby and Cooper, 2007).**

In spite of this conserved secondary structure, these enzymes are characterised by a different tissue distribution, as well as a different and specific regulation (Table 1).

The major tmACs regulators are GTP-bound G protein subunits ( $G_{\alpha s}$ ,  $G_{\alpha i}$  and  $G_{\beta\gamma}$ ) each of which exerts a type-specific effect on the different ACs isoforms. All the sub-cloned ACs, with exception for sAC, are activated by  $G_{\alpha s}$ .  $G_{\alpha i}$  inhibits almost all the isoforms with exception for AC2, AC4 and AC7.  $G_{\beta\gamma}$  can either activate or inhibit ACs. Thus AC2, AC4 and AC7 are stimulated, AC1 and AC8 are inhibited and AC3, AC5, AC6 and AC9 are insensitive to  $G_{\beta\gamma}$  (Table 1).

Activators of ACs promote the interaction between the two cytosolic domains (C1 and C2) and stimulate catalysis (Tesmer et al., 1997). Accordingly,  $G_{\alpha s}$  helps the catalytic core to bend over the substrate, whereas the  $G_{\alpha i}$  maintains the catalytic domain in an open conformation (Willoughby and Cooper, 2006), thus preventing the formation of the catalytic site and inhibiting the binding of ATP.

	AC1	AC2	AC3	AC4	AC5	AC6	AC7	AC8	AC9
$G_{\alpha s}$	+	+	+	+	+	+	+	+	+
$G_{\alpha i}$	-		-		-	-		-	-
$G_{\beta\gamma}$	-	+		+			+		
$Ca^{2+}$	+		+		-	-		+	-
PKC		+		+	+	-	+		-
					( $\xi$ )	( $\beta\delta\xi$ )	( $\delta$ )		
PKA					-	-			

**Table 1 Adenylyl cyclase regulation system.**

The second major regulator of ACs activity is calcium.  $Ca^{2+}$  affects ACs activity mostly in a calmodulin (CaM)-dependent manner. The mechanism of action proposed indicates that the catalytic core is sterically hindered by the regulatory domains within the enzyme, which contain a CaM binding site. Increase of intracellular  $Ca^{2+}$  and CaM activation induces a conformational change that removes such inhibition, exposing the catalytic site and favouring the ATP binding (Hoeflich and Ikura, 2002). Although AC1, AC3 and AC8 are stimulated by  $Ca^{2+}$ /CaM, supra-micro-molecular concentrations of  $Ca^{2+}$  exert an inhibitory effect on all the ACs isoforms. Only AC5 and AC6 are inhibited by physiological changes of  $Ca^{2+}$  levels (Willoughby and Cooper, 2006).

AC activity can also be modulated by PKC and PKA. For instance PKC activation stimulates the  $G_{\alpha i}$ - and  $Ca^{2+}$ -insensitive ACs: AC2, AC4 and AC7 (Cooper, 2003) (Schallmach et al., 2006) (Tabakoff et al., 2001). In addition, specific isoforms of PKC can also regulate AC5 (Kawabe et al., 1996) (Kawabe et al., 1994) and AC6 (Cheung et al., 2005). PKA-mediated phosphorylation inhibits the activity of AC5 and AC6 (Beazely and Watts, 2006) (Hanoune and Defer, 2001).

A modest positive effect on ACs modulation has also been shown for receptor tyrosine kinase (Tan et al., 2001).

Finally, all the tmACs, with exception for AC9, are stimulated by the plant diterpene forskolin which, as an ACs activator, promotes the C1 and C2 association, resulting in formation of an active catalytic site (Zhang et al., 1997).

A second independent source of cAMP in mammalian cells is the more recently discovered, soluble AC (sAC) (Buck et al., 1999). Despite its name, sAC is not only a soluble protein distributed throughout the cell but it also locates in distinct subcellular compartment such as the nucleus, mitochondria, microtubules and centrioles (Zippin et al., 2003). sAC is uniquely regulated by calcium (Jaiswal and Conti, 2003) and by bicarbonate in a pH-independent manner (Chen et al., 2000); in addition it is insensitive to heterotrimeric G protein regulation ( $G_{\alpha s}$ ,  $G_{\alpha i}$  and  $G_{\beta\gamma}$ ) and forskolin (Zippin et al., 2003). Physiological processes demonstrated to be regulated by sAC include sperm activation (Hess et al., 2005) and TNF activation of granulocytes (Han et al., 2005) (Kamenetsky et al., 2006).

A mechanism of co-localisation/compartmentalisation has been proposed for ACs in order to explain the preserved specificity of ACs activation and the generation of a pool of cAMP close to the appropriate downstream targets. According to this evidence of ACs compartmentalisation part of this co-localisation rest on a residence in lipid raft and an additional part involves scaffolding proteins such AKAP (Willoughby and Cooper, 2007).

### ***1.3.2 Phosphodiesterases***

In 1962, when the concept of second messenger and cAMP/PKA signal transduction pathway were being elucidated, Sutherland and colleagues noticed that cAMP could quantitatively be converted into adenosine 5'-monophosphate when incubated with a purified enzyme from the heart. This specific enzyme, capable of inactivating adenosine 3', 5'-monophosphate, turned out to be a phosphodiesterase, an enzyme that was found to be particularly abundant in brain and heart extracts (Butcher and Sutherland, 1962).

Phosphodiesterase (PDEs) enzymes are a family of related phosphohydrolases that selectively catalyse the hydrolysis of the 3' cyclic phosphate bonds of adenosine and/or guanosine 3', 5 cyclic monophosphate (Figure 1-3).

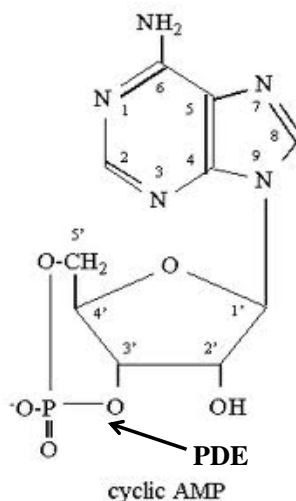


**Figure 1-3 Structural formula of cAMP. Arrow points at the bond hydrolysed by PDE. Adapted from (Bender and Beavo, 2006).**

PDEs represent the only cyclic nucleotide-degrading enzymes and, as such, they are critical regulators of cAMP intracellular homeostasis (Conti, 2000) (Houslay and Adams, 2003). As PDEs are localised to subcellular compartments and recruited into multi-protein signalling complexes, they work together to establish local gradients of cyclic nucleotides. This contributes to the spatial and temporal specificity of cyclic nucleotide signalling by regulating the availability of cAMP to its effectors. For these reasons, PDEs have recently become the focus of studies as potential drugs targets for several diseases including asthma, chronic obstructive pulmonary disease (COPD), heart failure, neurological disorders, erectile dysfunction, as well as cancer therapy (Bender and Beavo, 2006) (Houslay et al., 2005) (Savai et al., 2010).

In mammals, PDE enzymes are subdivided into eleven distinct families based on primary amino acid sequence, kinetics of action, mode of regulation,

and pharmacological properties (Beavo, 1995) (Beavo and Brunton, 2002) (Figure 1-4). PDEs differ also in their substrate specificity, mechanism of action and subcellular location. Of the eleven PDE families only three selectively hydrolyse cAMP (PDEs 4, 7 and 8), three families are selective for cGMP (PDEs 5, 6, and 9), whereas five families hydrolyse both cyclic nucleotides with varying efficiency (PDEs 1, 2, 3, 10 and 11) (Conti and Beavo, 2007).

The different mammalian PDEs share as common structural determinants a catalytic domain, encompassing a region of 270 amino acids, and a regulatory domain, placed between the amino terminus and the catalytic domain.

### Catalytic domain

The functional structure of the catalytic domain, which constitutes the core of the PDE, is highly conserved in all PDEs, despite the fact that sequence of any catalytic domain family exhibits only 25 to 35% amino acid sequence identity with any other. This domain is composed of sixteen alpha helices forming three sub-domains that define a deep pocket where the substrates (cAMP or cGMP) or inhibitors bind. The catalytic core includes two consensus metal binding motifs indispensable for the structure and the catalytic function of PDEs (Francis et al., 2001). Within these motifs the two metal ions, a  $Zn^{2+}$  and an  $Mg^{2+}$ , are coordinated by residues located on each of the three different domains and these residues form part of the signature recognition sequence for cyclic nucleotides PDEs. Several additional amino acids conserved only within a family are probably involved in defining substrate specificity and family-specific sensitivity to different inhibitors. Based on a number of structural studies, an interesting mechanism has recently been proposed to describe the specificity of substrate recognition. In each of the PDEs for which a crystal structure has been solved there seems to be a glutamine present, which stabilises the binding of the purine ring in the binding pocket (Zhang et al., 2004). For appropriate binding of cAMP and cGMP the glutamine residue must be able to rotate freely. For PDEs that can degrade both cyclic nucleotides this rotation is possible, whereas for PDEs that selectively degrade cAMP the

glutamine residue is constrained by neighbouring residues into a specific orientation for cAMP. Vice versa, for PDEs that selectively degrade cGMP the glutamine residue is constrained into the orientation that favours cGMP binding (Zhang et al., 2004).

### Regulatory domain

While the catalytic domain is conserved in almost all the PDEs, the N and C termini always differ markedly. These differences have been hypothesised to confer specificity of expression, specific physiological functions or different ligand affinity. Of the several domains mapped to the N terminus, three are present in multiple PDE families. These include domains for ligand binding, oligomerisation, kinase recognition/phosphorylation, and regions that auto-inhibit the catalytic domain. Docking domains are also present at the N terminus as well as in other regions of the PDE protein (Houslay and Adams, 2003) (Sonnenburg et al., 1995) (Figure 1-4).

Five of the eleven PDE families (PDE2, PDE5, PDE6, PDE10 and PDE11) contain two tandem N-terminal regulatory GAF domains (GAFA and GAFB) (mammalian cAMP and cGMP-specific and -regulated PDE, *Anabaena* adenylyl cyclase, and *E. coli* FhlA transcription factor), involved in dimerisation and cGMP binding (Martinez et al., 2002) (Aravind and Ponting, 1997). UCR1 and UCR2 domains (upstream conserved region) are conserved in the entire four genes composing the PDE4 family. Functionally, the UCR2 conserved domain corresponds to an auto-inhibitory domain that negatively regulates PDE catalytic activity (Jin et al., 1992), while regulatory phosphorylation sites have been mapped in the UCR1 (Sette and Conti, 1996). Although PDE4 isoforms lack GAF domains they appear to exist as oligomeric structures of identical subunits and the dimerisation domain is thought to overlap with the UCR modules (Richter and Conti, 2004) (see section 1.3.2.1). Besides, PDE1 contains two N-terminal Ca<sup>2+</sup>/calmodulin (CaM) binding site; whereas a PAS domain (period, arylhydrocarbon receptor nuclear translocator, and single minded), involved in ligand binding and protein-protein interaction, is contained only within PDE8. No data are available on the oligomerisation state of PDE3, PDE7

and PDE9 although hydrodynamic data suggest that they too exist as dimers (Scapin et al., 2004) (Huai et al., 2004).

Another conserved domain of the N-terminal region is the phosphorylation site. PDE1A, PDE1B and PDE1C can be phosphorylated by PKA and CaM-kinase (CaMKII) and in vitro analysis shows that PKA-mediated phosphorylation decreases the binding and calmodulin-induced activation (Sharma and Wang, 1985) (Florio et al., 1994). PDE2A apparently can be phosphorylated and inhibited by tyrosine kinase (Bentley et al., 2001). PDE3A and PDE3B can be phosphorylated by PKA and PKB, and the PKB-mediated phosphorylation of PDE3B increase the catalytic activity of the enzyme (Zmuda-Trzebiatowska et al., 2006). Similarly, PKA phosphorylation of PDE3A and PDE3B potentiates PDEs activity leading to a decrease in cAMP levels (Rich et al., 2007). In a similar manner, PKA can phosphorylate also long form isoforms of PDE4 (see section 1.3.2.1). PDE5, upon binding of cGMP, undergoes a conformational change that promotes PKG-mediated phosphorylation (Bessay et al., 2007). There are no known regulatory domains on the N-terminus of PDE7 although a consensus for PKA phosphorylation has been mapped in this region (Bender and Beavo, 2006). PKA phosphorylation of PDE10A2 appears to regulate the subcellular distribution between the Golgi apparatus and the cytosol. It is probable that all these different domains regulate PDE catalysis by a common mechanism. The binding of the agonists to the specific site on the N-terminal region produces a change in conformation of the PDE so that the negative constraint to the catalysis exerted by the inhibitory domain is no longer present.

Some PDEs also contain an auto-inhibitory domain. For instance, PDE6, the primary regulator of cGMP in rods and cones photoreceptors of retina, exists as a dimer of  $\alpha$  and  $\beta$  subunits and an N-terminus inhibitory  $\gamma$  subunit. In the dark PDE6 is inactive and cGMP level is on the micro-molar ( $\mu\text{M}$ ) range. Only photo-excitation and the consequent activation of the GPCR lead to the displacement of the  $\gamma$  subunit from the active site of PDE6 thus activating the enzyme (Cote, 2004).

Finally, several targeting sequences have been identified in the N-terminal domain. The three splice variants of PDE2A differ on the first 27 amino acid sequence and these differences seem most likely to account for specific subcellular localisation (Bender and Beavo, 2006). N-terminus domain of PDE3 includes a six-hydrophobic-helices trans-membrane domain, whereas PDE4 and PDE7 include an anchoring domain that enables interaction with AKAPs. PDE9A1 is localised to the nucleus by a pat7 nuclear localisation sequence (Wang et al., 2003) despite the presence of an N-terminal myristoylation domain in its primary sequence.

Several properties of the C-terminal domain have also been described for PDEs, including phosphorylation or prenylation sites; however, there is no unifying concept regarding the function of the PDE C terminus (Conti and Beavo, 2007).

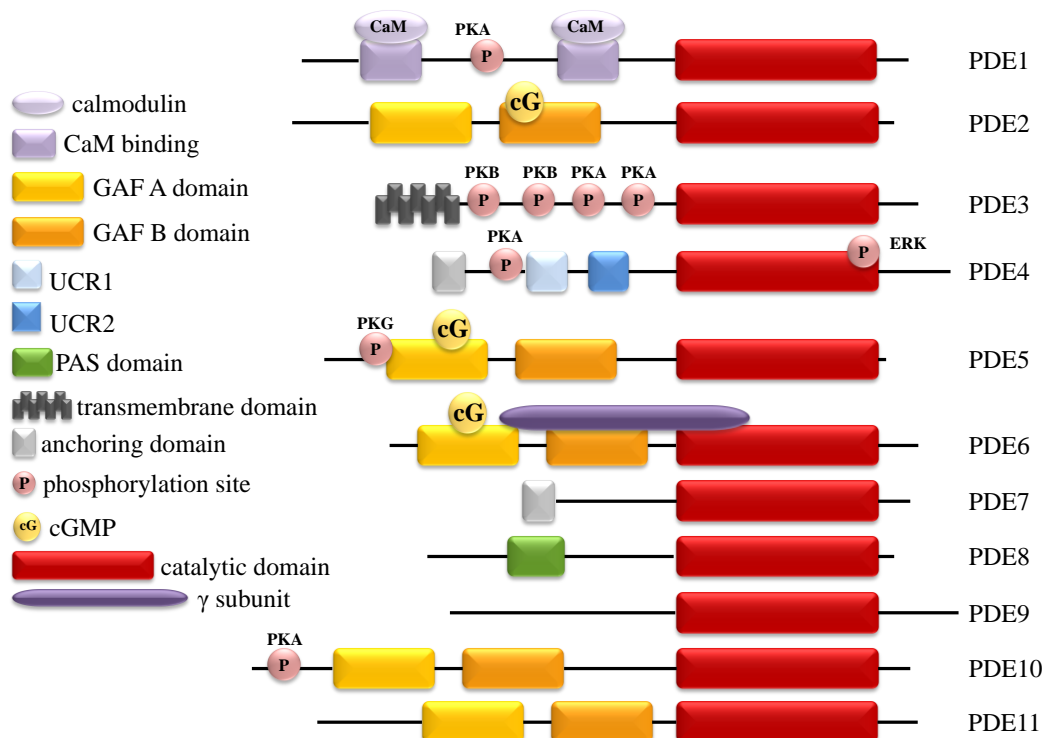


**Figure 1-4 Schematic representation of PDEs families. Adapted from (Conti and Beavo, 2007).**

### 1.3.2.1 PDE4

PDE4 is one of the most studied PDEs families and one of the most highly conserved over evolution being found in *Drosophila melanogaster* and *Caenorhabditis elegans*. PDE4 is expressed in a plethora of tissues and cells type and plays a role in a large number of physiological processes.

The mammalian PDE4 family is encoded by four genes, PDE4A, PDE4B, PDE4C and PDE4D, which give rise to more than twenty distinct PDE4 isoforms by alternative mRNA splicing of the regulatory domain (Figure 1-5). It is important to notice that despite the overwhelming number of isoforms can be associated to a redundancy of functions; it implies unique importance for each individual isoforms.

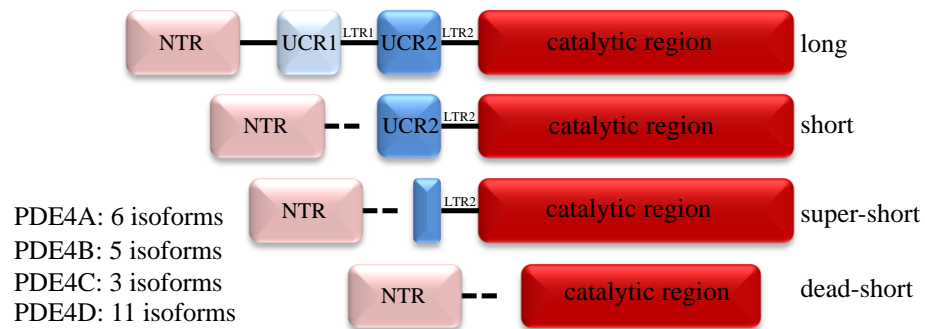


**Figure 1-5 Schematic representation of PDE4 subfamily. Adapted from (McCahill et al., 2008)**

Each PDE4 isoform has a modular structure consisting of an isoform specific N-terminal region (NTR), two regions termed “upstream conserved region” (UCR1 and UCR2), a highly conserved catalytic region domain and a subfamily-specific C-terminal region (CTR) (Bolger et al., 1993).

The catalytic domain is conserved between the eleven PDE families and as such it has been described previously (see section 1.3.2), whereas the C-terminal domain is of unknown functions (Houslay, 1998).

### Regulatory domain

PDE4 isoforms are subject to different regulatory mechanisms, such as phosphorylation (Houslay et al., 2007), ubiquitination (Li et al., 2009) and interaction with other proteins (Bolger et al., 2003a). Regulation is also exerted at the transcriptional level (Vicini and Conti, 1997) (Mayr and Montminy, 2001).

The unique N-terminal region confers specificity to each isoform and promotes the interaction with different binding partners thus favouring targeting to distinct intracellular regions. Different combinations of the UCR1 and UCR2 or the complete absence of them lead to a categorisation of PDE4 as: long forms that contain both UCR1 and UCR2, short forms that lack UCR1, super short forms that not only lack UCR1 but also include a N-terminal truncated UCR2 and “dead short” forms which are both N- and C-terminal truncated and therefore are catalytically inactive (Figure 1-5).

UCR1 and UCR2 domains have a central role in the regulation of PDE4 activity mediated by PKA and ERK phosphorylation. Interaction between UCR1 and UCR2 occurs via electrostatic interaction between the hydrophobic C-terminal of UCR1 and the hydrophilic N-terminal of UCR2 (Houslay, 2001). Truncation studies revealed that UCR2 exerts a constitutive inhibitory effect on PDE activity that can be released by PKA phosphorylation of UCR1 leading to the disruption of UCR1 and UCR2 interaction (Beard et al., 2000). Deletion of UCR2, in fact, results in an increased catalytic activity (Jin et al., 1992) (Lim et al., 1999). However only the long form of PDE4 can be phosphorylated by PKA on the RRESF motif, located at the N-terminal of the UCR1 module (Sette and Conti, 1996). Phosphorylation at this site causes an increase of the catalytic activity of the enzyme promoting a feedback loop mechanism that resets the cAMP concentration to the basal level. In addition the isoform PDE4D3 has a second site for PKA phosphorylation which lies within the NTR domain. It has been proposed that phosphorylation at this site can enhance the affinity of PDE4D3 binding to mAKAP (Dodge-Kafka et al., 2006) or promote the release of the specific PDE4D3 isoform from the nuclear-like protein 1 (NDEL1)

complex (Collins et al., 2008). Thus PKA phosphorylation of PDE4 leads to a dynamic redistribution of PDE4s to different complexes therefore redirecting modulation of cAMP gradients from one specific microdomain to another.

PDE4B, PDE4C and PDE4D can also be regulated by ERK phosphorylation in a single ERK consensus motif, PXSP, within the third subdomain of the catalytic unit (Hoffmann et al., 1999, MacKenzie et al., 2000, Houslay and Adams, 2003, Baillie et al., 2001, Hill et al., 2006). Conversely to PKA, ERK leads to an inhibition of long form PDE4 activity. However this inhibition can be overcome by PKA phosphorylation of the UCR1 by a novel feedback loop mechanism in which the inhibition induced by ERK phosphorylation causes a local increase of cAMP levels, which activates PKA that, in turn, phosphorylates UCR1 to activate the PDE and abolish ERK inhibition (Hoffmann et al., 1999).

Additionally, cAMP can also modulate PDE4 via modulation of transcription of PDE4 genes (Vicini and Conti, 1997, Seybold et al., 1998). This effect is mediated by cAMP response elements (CREs) in the promoter region of PDE genes (D'Sa et al., 2002) (Le Jeune et al., 2002). Activation of PKA results in the phosphorylation of the transcription factor CRE binding protein (CREB), that in turn can bind to the CRE region and promote PDE4 specific gene transcription (Mayr and Montminy, 2001).

#### Targeting and compartmentalisation of PDE4.

PDE4 can be strategically targeted to distinct subcellular compartments through association with other proteins. These protein-protein interactions are mediated mainly, but not exclusively, by the unique N-terminal region of PDE4 isoforms (Houslay and Adams, 2003) (Huston et al., 2006). Thus PDE4A1 associates with the plasma membrane and the Golgi apparatus (Shakur et al., 1993); PDE4A4, PDE4A5 and PDE4D4 interact with members of SRC tyrosyl kinase family (Beard et al., 1999) (O'Connell et al., 1996); PDE4A5 with the immunophilin XAP2 (Bolger et al., 2003b) and PDE4D5 with receptor for activated protein kinase C (RACK1) (Yarwood et al., 1999) and  $\beta$ -arrestin (Perry et al., 2002); PDE4B1 interacts with disrupted in schizophrenia 1

(DISC1) (Millar et al., 2007) and PDE4D3 is sequestered directly to the cardiac ryanodin receptor (RyR2) (Terrenoire et al., 2009) and interact with a variety of AKAPs such as myomegalin (Verde et al., 2001), mAKAP (Dodge et al., 2001), AKAP18 $\delta$  (Stefan et al., 2006) and AKAP450 (Witczak et al., 1999). These and many other evidence of PDE4 sequestration are available in literature (McCahill et al., 2008, Houslay, 2010) and all of them underpin the role of PDEs in defining compartmentalisation of cAMP signalling.

Despite the fact that PDEs can bind different proteins, they seem to be subject to a “scaffold fidelity” rule. Studies on several PDE4 partnerships indicate that a given PDE4 probably binds to no more than one scaffold at a time, highlighting once again the non redundancy of different PDE isoforms (Houslay, 2010).

The wide diversity of PDEs, conserved between species, suggests that different isoforms can play specific roles. This contributes to the spatial and temporal specificity of cyclic nucleotide signalling by regulating the availability of cAMP to its effectors.

## **1.4 cAMP effectors**

### **1.4.1 PKA**

PKA is a hetero-tetramer (Figure 1-6, C)) composed of two catalytic (C) subunits (Figure 1-6, B)) bound non-covalently to a dimer of regulatory (R) subunits (Figure 1-6, A)). The C subunit isoforms ( $C\alpha$ ,  $C\beta$  and  $C\gamma$ ) have identical kinetic and biochemical properties (Buechler and Taylor, 1990) (Taylor et al., 1990). In contrast, the two classes of R subunits (type I: isoforms  $RI\alpha$ ,  $RI\beta$ , and type II: isoforms  $RII\alpha$ ,  $RII\beta$ ) and their corresponding holoenzymes (PKA type I and PKA type II) show different functional and biochemical properties. In particular PKA type-I is more immediately dissociated by cAMP than PKA type-II (showing a  $K_{act}$  of 50-100 nM and 100-200 nM, respectively) (Dostmann et al., 1990) (Cummings et al., 1996). In addition, R subunits are also differentially expressed.  $RII$  expression is tissue-specific and it is predominantly associated

with cellular structures and organelles due to anchoring to A-Kinase Anchoring Proteins (AKAP) (Tasken and Aandahl, 2004) (Theurkauf and Vallee, 1982) (Lohmann et al., 1984) (Sarkar et al., 1984), whereas RI appears to be expressed in most tissues and to be predominantly cytoplasmic. However Dual-AKAPs and selective RI AKAPs have also been identified (Huang et al., 1997b) (Angelo and Rubin, 1998). Binding to AKAP contributes to the specificity as well as to the efficiency of the cAMP-PKA pathway by targeting PKA to discrete subcellular compartments in close proximity to its specific substrates (Theurkauf and Vallee, 1982) (Lohmann et al., 1984). All these features underline the fact that the role of PKA type I and PKA type II in the cells is non redundant, but coordinated to perform a specific biological function.

#### Regulatory subunit

Each R subunit comprises a dimerisation/docking domain (D/D domain), a hinge region, essential for interacting with the C subunit; and two highly conserved cAMP binding domains organised in tandem (Taylor, 1989) (Figure 1-6). The N terminal D/D domain consists of an anti-parallel four helix motif forming a four helix bundle. This region provides the domain for the dimerisation of the two R subunits and the docking surface for high affinity binding to AKAPs (Newlon et al., 1999) (Newlon et al., 2001). Specifically the D/D of RII subunits can be divided into two regions: the first 23 amino acids involved in AKAP binding and the region from amino acid 24 to amino acid 44 which covers the majority of the contacts between the two dimerising subunits. Deletion of the 1-5 sequence in RII abolishes the binding to AKAPs without interfering with the dimerisation (Hausken et al., 1994) (Hausken et al., 1996). The RI subunit dimerises in the same way of RII subunit forming a helix-turn-helix motif, however the dimerisation motif of RI is shifted forward and involves the sequence from amino acid 16 to amino acid 61. In addition, the RI helix bundle has a Y-like shape as opposed to the X-like shape of the corresponding RII motif (Leon et al., 1997) (Banky et al., 1998) (Banky et al., 2000).

The primary function of the regulatory subunit of PKA is to bind to and to inactivate the catalytic subunit in the absence of cAMP (Taylor et al., 1990, Taylor et al., 2008). The hinge region holds this function. It corresponds to the peptide inhibitory site (IS domain) and it represents the region of interaction between the regulatory and catalytic subunits. Despite the fact that they share this common function, the hinge domains differ in RI and RII. In the RII subunit the hinge region contains an auto-phosphorylation site (serine 114) included in an amino acid sequence similar to the consensus sequence found in the substrates for the catalytic subunit (Taylor et al., 1990). Conversely in the RI subunit the serine is replaced by an alanine or a glycine, thus resulting in a pseudo-phosphorylation site (Takio et al., 1984). The auto-phosphorylation of the RII subunit occurs as an intra-molecular event that does not require subunit dissociation (Taylor et al., 1990). In addition, auto-phosphorylation of the regulatory subunit reduces the affinity of the regulatory for the catalytic subunit and therefore lowers the activation threshold of PKA (Taylor et al., 1990) (Taylor et al., 2008).

PKA activation and consequent release of the two catalytic subunits occurs only when four cAMP molecules are bound to the regulatory dimer. Each regulatory subunit consists of two cAMP binding domains (DomainA and DomainB) (Figure 1-6). In the inactive conformation only the domainB is available for cAMP. The engagement of this site induces a conformational change that enhances the cAMP binding to the domainA. Once activated, the catalytic subunit can phosphorylate serine and threonine residues on specific substrate proteins as well as the regulatory subunit itself (Kim et al., 2006) (Figure 1-6).

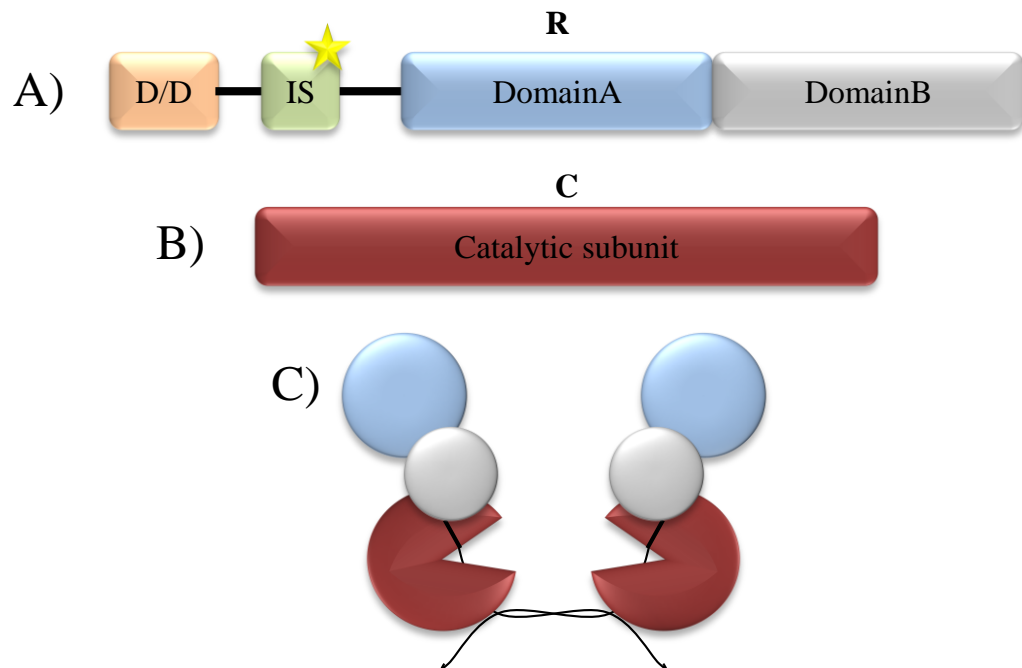


**Figure 1-6** Schematic representation of A) the regulatory and B) the catalytic subunit of PKA. Star in the regulatory subunit A) indicates the pseudo-phosphorylation or the auto-phosphorylation site of R type I and type II respectively. C) Schematic representation of the quaternary structure of PKA.

### 1.4.2 EPAC

Epac proteins were identified in 1998, when evidence hinted towards the existence of PKA-independent mechanisms of cAMP action (de Rooij et al., 1998). In the same period screening for brain proteins containing a cAMP binding domain led to the discovery of Epac proteins (Kawasaki et al., 1998).

Epac is a guanine nucleotide exchange factors (GEFs) for Rap1 and Rap2 (de Rooij et al., 2000). Rap is a small G protein of the Ras family and it cycles from the inactive guanosine diphosphate (GDP) bound state and the active guanosine triphosphate (GTP) bound state. In this reaction Epac catalyses the exchange of the GDP for the GTP whereas the GTPase-activating proteins (GAPs) account for the GTP hydrolysis.

Epac represents an important intracellular effector for cAMP and appears to account for many of its effects from insulin secretion in pancreatic beta cells to cardiac contraction through regulation of calcium channels in cardiomyocytes and permeability of vascular epithelium (Bos et al., 2003).

Most of these processes are also regulated by cAMP/PKA pathway highlighting the cross-talk between these two cAMP pathways.

There are two isoforms of Epac produced by two different genes: Epac1 and Epac2. Each of these consists of an N-terminal regulatory and a C-terminal catalytic region (Figure 1-7). The N-terminal region contains a DEP (Dishevelled, Egl-10, and Pleckstrin) domain responsible for anchoring to the membrane, and one (Epac1) or two (Epac2) cyclic nucleotide binding domains (CBD) homologous to those found in the R subunit of PKA. The function of the extra CBD in Epac2 is not clear since it binds cAMP with low affinity and does not seem to be required for Epac2 regulation by cAMP.

The C-terminal catalytic portion of Epac lodges the CDC25-homology domain (CDC25-HD) characteristic of the exchange factors for Ras family GTPase (GEF domain); and a regulatory domain named Ras exchange motif (REM). An additional Ras-association domain (RA) lies between REM and CDC25-HD domains (de Rooij et al., 1998) (de Rooij et al., 2000) (Figure 1-7). The regulatory domain functions as an auto-inhibitory domain that affects GEF activity by steric hindrance. Such inhibition can be relieved only by cAMP. Crystal structure of active and inactive Epac2 (Rehmann et al., 2008) (Rehmann et al., 2006) revealed that when cAMP is low Epac is folded in an inactive conformation in which the regulatory domain inhibits the Rap association to the catalytic site preventing Rap binding to the CDC25-HD domain (Bos et al., 2003). The increase in cAMP concentration and the occupation of the Epac cAMP-binding domain induces the unfolding of the protein, leading to an open conformation and the exposure of the catalytic domain for the binding of Rap GTPase (Figure 1-7).

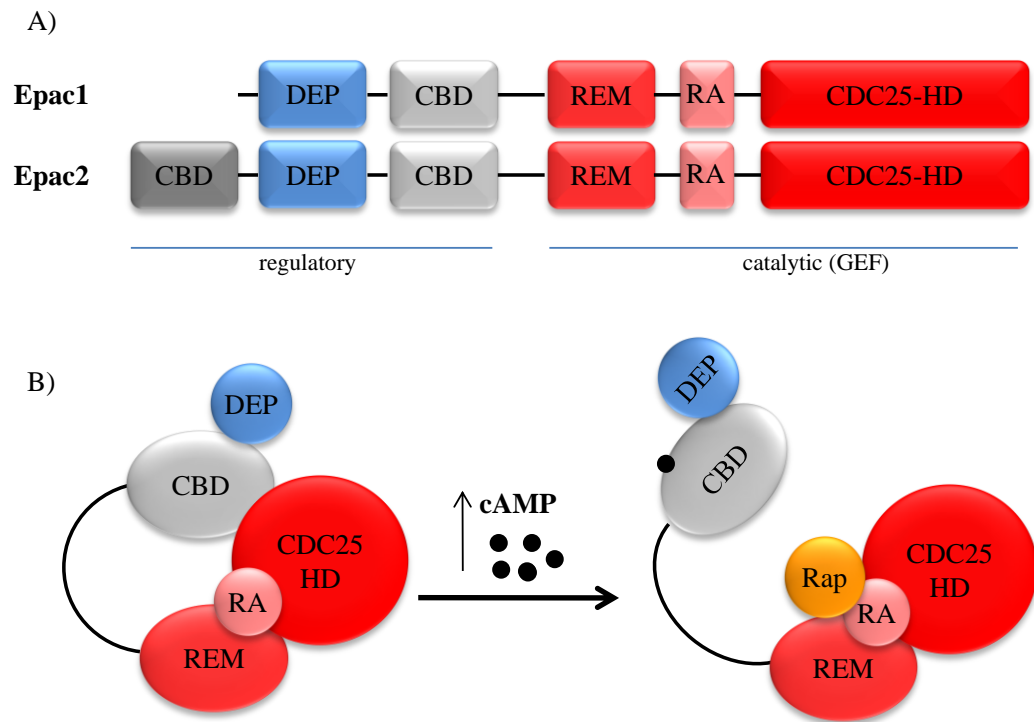


**Figure 1-7 A) Schematic representation of Epac1 and Epac 2 and B) its activation mechanism.**

Epac proteins are ubiquitously expressed inside the cells and like PKA the multiple cellular functions of Epac are regulated by its spatial localisation. Both Epac1 and Epac2 contain sequence mediating binding to the plasma membrane. Epac1 is targeted to the plasma membrane by the DEP domain whereas Epac2 binds via the RA domain, although it has been shown that Epac2 contains an additional membrane targeting sequence at the N-terminal region. In addition, localisation to several other subcellular sites has been described for Epac1. Epac1 can be localised to the nucleus, the nuclear pore complex (Qiao et al., 2002), the centrosome (Wang et al., 2006) as well as microtubules (Sehrawat et al., 2008) and mitochondria (Wang et al., 2006). The specific localisation may link Epac to unique cellular processes.

### **1.4.3 Cyclic nucleotide-Gated Channels (CNG)**

Cyclic nucleotide gate channels are ion channels activated by cAMP and cGMP. They have been originally identified in photoreceptors and olfactory neurons where they play a crucial role in sensory transduction. Although they

have been successively identified in many other tissues such as kidney, endocrine tissue and sperm cells (Kaupp and Seifert, 2002) (Khan et al., 2010) (Bonigk et al., 2009).

The primary functions of the channels are to transduce changes in nucleotides levels into changes of membrane potential and calcium concentration. All the CNG channels characterised so far allow Na<sup>+</sup> and K<sup>+</sup> to flow, but they do not discriminate between them. Also Ca<sup>2+</sup> can flow through the channels even if it acts as a voltage dependent blocker of monovalent cation permeability (Dzeja et al., 1999).

Structurally CNG channels belong to the super-family of pore-loop cation channels (Yu et al., 2005) and they share a common structure with hyperpolarisation-activated cyclic nucleotide (HCN) channels and Eag-like K<sup>+</sup> channels. The family of mammalian CNG channels comprises 6 members (4 subunits A and 2 subunits B) sharing homology of sequence and membrane topology (Figure 1-8). Each member comprises a six trans-membrane domain (S1-S6), a loop (P) between S5 and S6, a PKA/PKG homologous cyclic nucleotide binding domain (CBD) connected allosterically to the channel gate by a C-linker domain and two cytosolic domains at the N and C terminus (Figure 1-8). CNG channels are tetramers with the four subunits aligned around the centrally located pore. In turn the pore is assembled by overlapping of the P-loop and the S6 segment of the four subunits (Higgins et al., 2002). Although subunits A1, A2 and A3 can be functional expressed as homomers, FRET studies strongly suggest that native CNG channels are mainly heterotetramers. (Zheng et al., 2002) (Zheng and Zagotta, 2004).

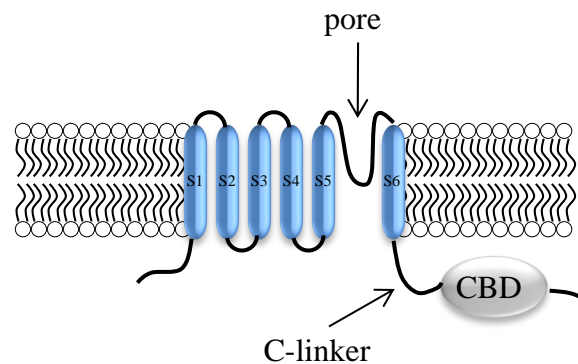


**Figure 1-8 Schematic representation of a CNG channel member. Adapted from (Biel and Michalakis, 2009).**

The mechanism of CNG channels activation comprises two steps: the ligand binding to the CBD and the consequent opening of the channel pore. The binding of the cyclic nucleotide to the channel, in its closed conformation, leads to an allosteric conformational change in which the C-linker domains of the four channel subunits assemble and give rise to a tetrameric gating ring (Taraska and Zagotta, 2007).

Despite the fact that the CNG channels are strictly ligand-gated, exposure to the cyclic nucleotide does not desensitise or inactivate the channels. However, they are regulated by a feedback CaM-mediated mechanism (Bradley et al., 2005, Biel and Michalakis, 2009).

## 1.5 cAMP compartmentalisation

The cAMP/PKA pathway is responsible for a large number of physiological effects and an enormous amount of extracellular signals are converted in appropriate responses via a mechanism that involves concentration changes of the same intracellular molecule, cAMP. In addition, cAMP is a long range-acting second messenger (Kasai and Petersen, 1994) that, after generation, can potentially diffuse and rapidly fill the entire cell, causing the non-selective activation of all the PKA subsets present in the cell. This scenario has raised the question of how specificity is maintained in the cAMP/PKA pathway.

In recent years it has become clear that the concentration gradient of cAMP cannot be the only code used by the cells to transduce information, and that specificity of response is gained with a spatial and temporal patterning of signalling molecules (Kasai and Petersen, 1994) (Hunter, 2000).

The hypothesis of cAMP/PKA compartmentalisation was proposed more than 40 years ago by Brunton and co-workers when they observed that prostaglandin E<sub>1</sub> (PGE<sub>1</sub>) and isoproterenol, a  $\beta$ -adrenergic receptor ( $\beta$ -AR) agonist, caused the activation of different pools of PKA in cardiomyocytes. Although both ligands act on hormone-responsive G protein-coupled receptors to cause consequent AC activation and cAMP elevation, PGE<sub>1</sub> prevalently activates PKA present in the soluble fraction of cardiac myocytes cells lysates, whereas isoproterenol activates PKA present in the particulate fraction of these lysates. Moreover, only isoproterenol shows a positive inotropic effect, whereas the PGE<sub>1</sub>-mediated response in the soluble fraction has no effect on contractility (Brunton et al., 1979) (Steinberg and Brunton, 2001). Based on these observations, it was postulated that differences in the heart response to isoproterenol and to PGE<sub>1</sub> are consequence of activation of cAMP signalling transduction pathways that are confined to distinct intracellular compartments, and that activation of the particulate fraction of PKA is essential for the metabolic and inotropic responses of the heart to elevated cAMP whereas activation of the soluble pool of PKA is not involved in these responses (Keely, 1977) (Keely, 1979) (Hayes et al., 1979) (Hayes and Brunton, 1982) (Hayes et al., 1980) (Byus et al., 1979) (Corbin et al., 1977) (Brunton et al., 1979).

More recently, such a hypothesis has been confirmed by real-time experiments in living cells. Experiments in frog ventricular myocytes (Jurevicius and Fischmeister, 1996), in which Ca<sup>2+</sup> transients were recorded at two physically distant portions of the myocyte, using a whole-cell patch-clamp approach, demonstrated that local application of isoproterenol caused local activation of I<sub>Ca</sub>, whereas local application of forskolin (a non selective AC activator) caused activation of I<sub>Ca</sub> throughout the cell, both at local and at

distant sites. These results support the notion that  $\beta$ -AR-dependent cAMP accumulation and responsiveness are compartmentalised in at least some myocardial cells (Jurevicius and Fischmeister, 1996).

At the same time, several lines of evidence indicated that PDEs may contribute to cAMP compartmentalisation. Pharmacological inhibition of PDEs showed that their activities are localised to prevent the spread of  $\beta$ -adrenergic signals from particulate (membrane) locations to soluble fractions. When PDEs were inhibited, the otherwise local cAMP elevation elicited by a  $\beta$ -adrenergic stimulus became diffused and similar to that seen with forskolin (Fischmeister et al., 2006) (Hohl and Li, 1991). These data suggest that  $\beta$ -AR-stimulated accumulation of cAMP occurs in defined locales in the cell so as to be specifically effective and may originate from a subset of cellular adenylyl cyclases, whereas forskolin generally stimulates most or all available tmACs. The above evidence suggests that there is compartmentalisation of the cAMP signalling pathway, and that this compartmentalisation is subordinate to four postulates: 1) not all cAMP can activate all PKA subsets; 2) not all PKA subsets can phosphorylate all possible targets; 3) not all cAMP can be degraded by all PDEs; 4) there is a spatial relationship between a given receptor-Gs-adenylyl cyclase complex and a specific intracellular compartment (Steinberg and Brunton, 2001).

In the past decade a large number of studies have tried to dissect the crucial role played by both AKAPs and PDEs in cAMP/PKA signalling pathway compartmentalisation, where AKAPs account for the spatial location of the signalling pathway components whereas PDEs assure the shaping of restricted pools of cAMP. The tight cooperation of these two families of proteins provides the means to achieve physical and biochemical compartmentalisation of the cAMP signal transduction pathway.

### 1.5.1 AKAPs and the physical compartmentalisation of PKA pathway

AKAPs are a structurally diverse family of functionally-related proteins that are defined on the basis of their ability to anchor the PKA holoenzyme inside the cell and to co-precipitate catalytic activity (Colledge and Scott, 1999) (Figure 1-9).

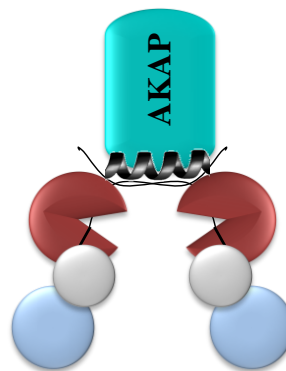


**Figure 1-9 Schematic representation of AKAP-PKA interaction.**

The first AKAP to be isolated was the microtubule associated protein-2 (MAP2), a protein that co-purifies with the PKA holoenzyme when isolated from brain extracts (Lohmann et al., 1984). Since then, a variety of gel overlay, interaction cloning, yeast two-hybrid and proteomic approaches have identified more than fifty AKAPs when splice variants with different cellular targeting are included (Table 2).

Although the majority of identified AKAPs anchor PKA type II (Huang et al., 1997b), a number of PKA type I specific AKAPs have also been characterised. For instance AKAP<sub>CE</sub> (Angelo and Rubin, 1998), myosin VIIa (Kussel-Andermann et al., 2000a) (Kussel-Andermann et al., 2000b) and  $\alpha$ 4 integrins (Lim et al., 2007) show higher affinity for RI than RII subunits. In addition, several AKAPs including D-AKAP1, D-AKAP2 (Huang et al., 1997a), AKAP220, Ezrin, Merlin, PAP7, show dual specificity and can therefore

associate with both RI and RII subunits (Gronholm et al., 2003) (Huang et al., 1997a) (Huang et al., 1997b) (Li et al., 2001) (Liu et al., 2006).

Structurally, each AKAP contains at least two functional domains: a PKA (R subunit) binding motif and a unique subcellular targeting motif. In addition to these two domains, AKAPs include also regions of interaction with different other proteins such as phosphoprotein phosphatases (PP), PDEs and protein kinases (Tasken et al., 2001) (Felicciello et al., 2001).

#### PKA binding motif

The conserved PKA-binding motif consist of 14-18 amino acids arranged to form five turns of an amphipathic helix that exposes a hydrophobic face on one side and charged residues along the other side (Carr et al., 1991).

Surface plasmon resonance experiments suggest that AKAP-RII binding has high affinity whereas AKAP-RI binding has low affinity and faster off-rate; this implies that the AKAP-RI complex is rather dynamic compared with the AKAP-RII complex. The differences at the N-terminus of the two regulatory subunits seem to account for the AKAP-binding specificity (Jarnaess et al., 2008).

Anchoring of PKA type II to AKAPs occurs when the hydrophobic side of the  $\alpha$  helix in the AKAP lies across the four helix bundle formed by the RII docking domain (Newlon et al., 2001). This mechanism of interaction of RII with AKAPs is robust enough to favour the maintenance of the AKAP-PKA complex within the cells. Conversely the extreme N-terminus of RI subunit is believed to be helical and this additional helix collapses on the four helix bundle, causing a steric hindrance for high affinity anchoring to AKAPs. Dual specificity AKAPs have an additional binding motif, RISR (RI specific region) at the N-terminus of the conserved  $\alpha$  helix, which enhances the affinity of AKAPs for RI by providing an additional site of contact for the AKAP-RI interaction and thus stabilising the formation of the anchored complex (Jarnaess et al., 2008).

Other mechanisms that do not involve the amphipathic helix may be responsible for the anchoring of PKA. For instance pericentrin binds the D/D of the regulatory subunit of PKA type II through a 100 amino acid domain that is not predicted to form an amphipathic helix (Diviani et al., 2000), whereas  $\alpha 4$  integrins interact directly with the intact PKA type I holoenzyme through its cytoplasmatic domain (Lim et al., 2007). Interestingly, these AKAPs contain neither the conserved amphipathic helix nor the RISR motif (Jarnaess et al., 2008).

Disruption of the amphipathic helix motif by the introduction of a proline within the helix abolishes AKAPs binding to R subunits both in vivo and in vitro (Carr et al., 1991). Moreover, ectopic expression of peptides designed on the amphipathic helix inhibits PKA interactions with AKAPs. The Ht31 peptide (or Rt31, the rat homologous), derived from AKAP-Lbc, was the first disrupter peptide to be used in competition experiments (Klussmann et al., 2001). Bioinformatics studies allowed the generation of improved versions of this peptide first to a more potent dual specific anchoring disrupter peptide named AKAP-*in silico* (AKAP-IS) (Alto et al., 2003) and successively to a RII and a RI isoform specific anchoring disrupter peptides termed SuperAKAP-IS (Gold et al., 2006) and RIAD (Carlson et al., 2006). Both these peptides were exploited to selectively delineate functional roles of anchored PKA type I and PKA type II (Carlson et al., 2006) (Jarnaess et al., 2008) (Di Benedetto et al., 2008).

### Targeting motif

The AKAP subcellular targeting domain is a unique sequence that directs the AKAP-PKA complex to defined subcellular structures, membrane or organelles (some examples of these are plasma membrane, Golgi apparatus, centrosome, nucleus, mitochondria and cytosol); such a sequence is either a lipid modification targeting motif or a protein-protein interaction domain (Colledge and Scott, 1999) (Beene and Scott, 2007) (Edwards and Scott, 2000). This unique sequence accounts for AKAP-PKA compartmentalisation. Different AKAPs can also be localised to the same subcellular organelle whereas splice

variants of the same AKAPs can be differentially targeted. For example AKAP79/150 binds to the plasma membrane through interaction with phospholipids (Dell'Acqua et al., 1998) whereas  $\alpha$  and  $\beta$  isoforms of AKAP18 anchor to the plasma membrane via a myristoylated and palmitoylated sequence (Trotter et al., 1999). AKAP450 anchors to the centrosome (Witczak et al., 1999) whereas its short splice variant Yotiao is targeted to the post-synaptic membranes (Westphal et al., 1999). Interestingly AKAP450 and pericentrin anchor both to the centrosome through the same conserved domain named pericentrin-AKAP450 centrosomal targeting domain (PACT) (Gillingham and Munro, 2000). Although these two AKAPs share the same targeting domain they are different otherwise, and it is therefore likely that they account for different PKA-mediated phosphorylation pathways.

As for PDEs, the great number of unique AKAPs ensures a great level of specificity and complexity as well as accuracy to each physiological process.

AKAPs were first classified according to their molecular weight on sodium dodecyl sulphate-polyacrylamide gel electrophoresis (SDS Page). However this classification has been considered cumbersome since there are several splice variants of the same AKAP resulting in different molecular weight and other anchoring proteins, such as gravin, that were named before the discovery of their ability to bind PKA. Recently, a gene-based nomenclature system has been introduced (Table 2). In this thesis, I will refer to AKAPs according to the molecular weight based nomenclature.

AKAP (molecular weight-based nomenclature)	AKAP (gene nomenclature)	Tissue	Subcellular localization	Properties and Interacts
S-AKAP84/D-AKAP1/AKAP121/AKAP149	AKAP1	Testis, thyroid, heart, lung, liver, skeletal muscle and kidney	Outer mitochondrial membrane, endoplasmic reticulum, nuclear envelope, sperm midpiece	Dual specific AKAP. Binds laminB, PP1, PDE7A
AKAP-KL	AKAP2	Kidney, lung, thymus and cerebellum	Actin cytoskeleton, apical membrane of epithelial cells	
AKAP110	AKAP3	Testis	Axoneme	Binds G <sub>α13</sub>
AKAP82/FSC1	AKAP4	Testis	Fibrous sheath of sperm tail	Dual-specific AKAP
AKAP75/79/150	AKAP5	Bovine/human/rat orthologous Brain	Plasma membrane, post synaptic density	Binds PKC, calcineurin (PP2), β-AR, SAP97 and PSD95
mAKAP	AKAP6	Heart (mAKAPβ, shorter), skeletal muscle and brain (mAKAPα, longer)	Nuclear membrane	Binds PDE4D3, Epac, MEKK/MEK5/ERK5 and PDK1 (only mAKAPα)
AKAP15/18 α β γ δ	AKAP7	Brain, skeletal muscle, pancreas and heart	Basolateral (α) and apical (β) plasma membrane, cytoplasm (γ), secretory vesicles (δ)	
AKAP95	AKAP8	Heart, liver, skeletal muscle, kidney and pancreas	Nuclear matrix	Binds Eg7/condensin Zinc-finger motif, PDE7A
AKAP350/450/CG-NAP/Yotiao/Hyperion	AKAP9	Brain, pancreas, kidney, heart skeletal muscle, thymus, spleen, placenta, lung, liver and testis	Post-synaptic density, neuromuscular junction, centrosome and Golgi apparatus	Binds PDE4D3, PP1, PP2, PKN, PKCε, CK1δ
D-AKAP2	AKAP10	Liver, lung, spleen and brain		Dual-specific AKAP
AKAP220/hAKAP220	AKAP11	Testis and brain	Vesicles, peroxisomes, centrosome	Dual-specific AKAP. Binds PP1
Gravin	AKAP12	Endothelium	Actin cytoskeleton and cytoplasm	Binds PKC and β-AR
AKAP-Lbc/Ht31/Rt31	AKAP13	Ubiquitous	Cytoplasm	
MAP2B		Ubiquitous	Microtubules	Binds tubulin
Ezrin/AKAP78		Secretory endothelia	Actin cytoskeleton	Dual-specific AKAP
T-AKAP80		Testis	Fibrous sheath of sperm tail	
AKAP80/MAP2D		Ovarian granulosa cells		

AKAP (molecular weight-based nomenclature)	AKAP (gene nomenclature)	Tissue	Subcellular localization	Properties and Interacts
SSeCSK (Src-suppressed C kinase substrate)		Testis and elongating spermatids	Actin remodelling	Gravin-like
Pericentrin		Ubiquitous	Centrosome	Binds dynein and $\gamma$ -tubulin
WAVE-1/Scar		Brain	Actin cytoskeleton	Binds Abl and Wrp
Myosin VIIA		Ubiquitous	Cytoskeleton	Binds RI
PAP7		Steroid-producing cells (adrenal gland and gonads)	Mitochondria	Binds RI
Neurobeachin		Brain	Golgi apparatus	
AKAP28		Primary airway cells	Ciliary axonemes	
Myeloid translocation gene (MTG) 8 and 16b		Lymphocytes	Golgi apparatus	Binds PDE7A
AKAP140		Granulosa cells and meiotic oocytes		Not cloned
AKAP85		Lymphocytes	Golgi apparatus	Not cloned
BIG2 (Brefeldin A-inhibited guanine nucleotide-exchange protein 2)			Cytosol and Golgi apparatus	Binds RI $\alpha$ , RI $\beta$ , RII $\alpha$ and RII $\beta$ through three different PKA binding domains
Rab32			Mitochondria	Binds RI
AKAP <sub>CE</sub>		Caenorhabditis elegans		
DAKAP550		Drosophila	Plasma membrane/cytoplasm	
DAKAP200		Drosophila	Plasma membrane	Binds F-actin and Ca-calmodulin
Nervy		Drosophila	Axons	
AKAP97/radial spoke protein 3 (RSP3)		Chlamydomonas	Flagellar axonemes	

**Table 2 Correlation between the AKAPs molecular weight-based nomenclature and the gene-based nomenclature. Adapted from (Pidoux and Tasken).**

Since the discovery of AKAPs, the evidence of their key role in the organisation of discrete PKA signalling domains has become increasingly clear. Firstly, it was hypothesised that selective activation of targets was due to the specific activation of a subset of PKA located near the intracellular targets themselves. The same hypothesis was consolidated by the finding that components of the cAMP/PKA signal transduction pathway are organised in three dimensional clusters where receptor, effector, targets and regulatory

proteins are specifically associated in macromolecular complexes to maintain localised pools of kinase activity (Feliciello et al., 2001).

The first evidence of a multivalent AKAP complex was reported in 1995 when AKAP79 was shown to be localised in the postsynaptic membrane where it interacts with PKA, protein kinase C (PKC) and the calcium/calmodulin-dependent protein phosphatase (PP2B) (Coghlan et al., 1995) (Klauck et al., 1996). Subsequent studies revealed that the role of this complex is to regulate the phosphorylation and activity of the associated  $\alpha$ -amino-3-hydroxy-5-methyl-4-isoxazolepropionic (AMPA) and N-methyl-D-aspartic acid (NMDA)-type glutamate receptors, as well as L-type  $\text{Ca}^{2+}$  and M-type  $\text{K}^{+}$  channels. As far as the mechanism of regulation of AMPA receptor glutamate receptor 1 (GluR1) is concerned, biochemical and electrophysiological studies indicate that this elaborate molecular architecture ensures that PKA and PP2B preferentially modulate the phosphorylation status of serine 845, a PKA target on the GluR1 subunit of the AMPA channel (Colledge et al., 2000) (Tavalin et al., 2002). AKAP79 holds PP2B in an active state. The functional consequence of this appears to be a reduced activity of the AMPA channel. Activation of PKA by cAMP overcomes this inhibition, leading to an enhancement of the current flowing through the channel (Coghlan et al., 1995). Interestingly AKAP79 anchors and inhibits the catalytic core of PKC. Binding of the calcium/calmodulin complex to AKAP79 releases PKC from the anchoring protein, resulting in activation of the kinase (Faux et al., 1999) (Faux and Scott, 1997). Thus, signalling that proceeds through calcium/calmodulin can lead to the liberation and activation of an anchored pool of PKC at postsynaptic densities. The complexity of this cluster was further appreciated with the finding that  $\beta$ 2-AR co-precipitates with AKAP79 (Fraser et al., 2000). The association of the receptor with PKA to the same AKAP was shown to enhance the phosphorylation of the receptor in an agonist-dependent manner. This phosphorylation favours the switch of the receptor coupling from  $G_s$  to  $G_i$  which in turn results in activation of the MAP kinase cascade (Fraser et al., 2000). Recent biochemical assays and FRET-based analysis of PKA activity (using the FRET based sensor for PKA activity, AKAR, see section 6.1.1) provide

evidence for an additional interaction between AKAP79 and AC5/6 (Bauman et al., 2006). Similarly to the  $\beta$ 2-AR inhibition, direct phosphorylation of AC5 by PKA inhibits AC5 activity and cAMP synthesis in an agonist dependent manner (Bauman et al., 2006).

Another example of such an interaction has been shown for the class C L-type  $\text{Ca}^{2+}$  channel in neurons from hippocampus. This channel assembles in a complex with  $\beta$ 2-AR (Davare et al., 2001) and contains a docking domain for anchoring to the AKAP MAP2B, which in turn binds PKA (Davare et al., 1999). Hormonal stimulation of  $\beta$ -AR receptors leads to an increase of cAMP. The consequent activation of the associated PKA leads to phosphorylation of the channel and regulation of its activity in a highly localised manner (Davare et al., 1999). Thus, the direct physical interaction between PKA-AKAP MAP2B and the channel accounts for a rapid and precise transmission of the signal elicited by the  $\beta$ -AR.

The role of AKAPs in mediating the high levels of specificity and complexity of the cAMP/PKA signal transduction pathway has been widely studied. It is now clear that AKAPs have more complex functions than was originally thought. Beside the primary function of anchoring and targeting PKA in distinct subcellular compartments, AKAPs also act as multi-scaffold proteins, linking upstream activators with their downstream targets and allowing for specificity of transduction as well as for integration and linear relay of multiple signalling pathways (Bauman et al., 2006). AKAPs can also interact with PDEs and protein phosphatases and thus account for coordinated termination of the response. For instance, mAKAP targets PKA and PDE4D3 to the perinuclear region in cardiomyocytes (Dodge et al., 2001) (Kapiloff et al., 2001). This interaction generates a macromolecular complex within which, upon activation by local increases of cAMP, PKA phosphorylates and activates the associated PDE, which in turn reduces cAMP to generate a loop of negative feed-back regulation. In an elegant experiment two different fluorescent PKA activity reporters (AKAR) were modified in order to recruit PKA (AKAR-PKA) or PKA and PDE4DE3 (AKAP-PKA-PDE). By using these reporters, it was possible to

demonstrate that co-anchoring of PDE leads to a brief pulse of PKA activity, whereas in the absence of PDE anchoring, a sustained PKA activity is recorded under the same conditions, demonstrating that recruitment of PDE4D3 terminates the activation of the anchored PKA via a negative feed-back loop mechanism (Figure 1-10) (Dodge-Kafka et al., 2006).

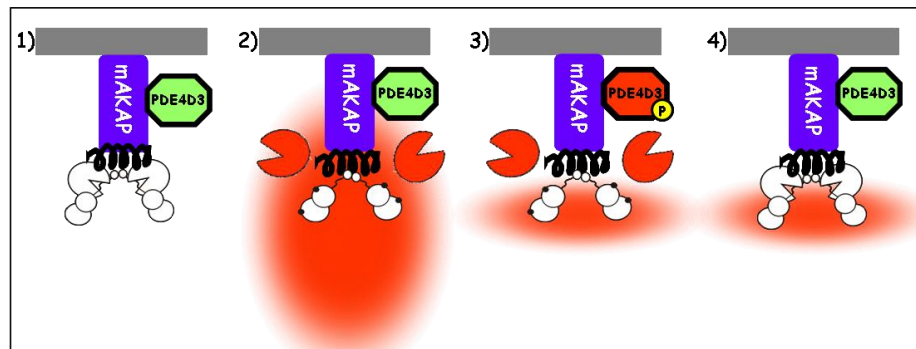


**Figure 1-10 Schematic representation of a negative feedback loop regulation mechanism involving an AKAP-anchored PDE4. 1) mAKAP anchors PKA and PDE4D3 at the perinuclear region of cardiomyocytes. 2) When cAMP increases, PKA is activated and 3) it phosphorylates the associated PDE4D3 4) which in turn degrades cAMP re-establishing the cAMP level below the threshold of PKA activation.**

Anchoring of AC, PKA and PDE to the same AKAP may generate local fluctuations in cAMP and pulses of compartmentalised PKA activity (Dodge-Kafka et al., 2006). Each substrate appears to have a selective anchored subset of PKA and its own local spatio-temporally organised pool of cAMP shaped by anchored PDEs. A rise in the intracellular cAMP level, leads to the activation of PKA and the consequent phosphorylation of PKA targets, including associated PP and PDEs. The activation of both these enzymes promotes the dephosphorylation of the targets and the degradation of the cAMP below the PKA activation threshold thereby promoting re-association of the PKA holoenzyme and rapidly terminating the cAMP response.

It is also important to consider the control exerted by AKAPs on the cAMP/PKA signalling pathway through the dynamic reorganisation of the complexes. For example the binding domain for the RII subunit on Wave1, a

Wiskott-Aldrich syndrome scaffolding protein, overlaps with the actin binding region in a mutually exclusive manner. This might lead to a situation in which binding of PKA is favoured over Wave1 binding to the actin cytoskeleton or vice versa (Westphal et al., 2000).

Phosphorylation of AKAPs represents another way to modify the subcellular location of an AKAP complex. For instance, phosphorylation of AKAP79/150 by PKC abolishes the interaction between the AKAP and the plasma membrane leading to the release of the complex into the soluble fraction of the cells. This might result in relocation of the AKAP79/150-PKA complex to a microdomain where the cAMP concentration is below the activation threshold of the anchored PKA, thereby promoting the re-association of the holoenzyme and rapidly terminate the response (Dell'Acqua et al., 1998).

Finally, recruitment of PKA type I rather than PKA type II to a specific compartmentalised AKAP complex could increase the sensitivity to cAMP of the particular physiological process regulated by the signal complex (Jarnaess et al., 2008) (Di Benedetto et al., 2008).

Taken together all this observation it is clear that these multivalent signal transduction complexes nucleated by AKAPs represent an efficient way to regulate forward and backward steps of a given signalling processes; moreover AKAPs exert a tight control on cAMP levels, via anchored PDEs, thereby modulating PKA activity.

### ***1.5.2 PDEs and the biochemical compartmentalisation of cAMP***

cAMP is generally considered to be freely diffusible in the cytosol, with a diffusion constant of  $220\mu\text{m}^2/\text{sec}$  (Bacskai et al., 1993). This notion is in contrast with the concept of compartmentalisation of the AKAP/PKA/PDE complex as free diffusion of cAMP would result in activation of all PKA subsets, whatever their specific localisation within the cell. In fact, an increasing body

of evidence indicates that diffusion of cAMP can be constrained to prevent the inappropriate activation of effectors.

Four different hypotheses on restriction of cAMP diffusion have been formulated.

First of all the presence of a “physical barrier” has been hypothesised by Rich et al., based on the evidence that the endoplasmic reticulum comes into close contact with the plasma membrane (Finch and Augustine, 1998) (Takechi et al., 1998) (Patterson et al., 1999) (Ma et al., 2000). These authors suggested that the interactions between the ER and the caveole with the cytosolic face of plasma membrane may limit cAMP diffusion from the site of synthesis at the plasma membrane to the cytosolic effectors. PKA localised in the sub-plasma membrane microdomain would be rapidly activated after stimulation of AC, whereas cytosolic pools of PKA would be activated more slowly by persistent stimulation of PKA. Without such restrictions on diffusion cAMP would spread throughout the cell (Rich et al., 2000).

An alternative hypothesis for restricted diffusion of cAMP was proposed by Hall & Hell. These authors hypothesised that AC and PKA might be arranged in such a way that cAMP is “channelled” from the AC to PKA with a mechanism similar to that described for *Salmonella typhimurium* in which indole is channelled from its point of production to the site of tryptophan synthesis along the different subunits of tryptophan synthase  $\alpha_2\beta_2$  multi-enzyme complex (Hyde et al., 1988). Such ‘channelling’ mechanism would dramatically increase the likelihood that newly synthesised cAMP binds to PKA (Hall and Hell, 2001).

Although the above mechanisms may be involved, at least in some circumstances, an increasing body of direct and indirect evidence indicates that the major contributors in limiting diffusion and in shaping cAMP pools are PDEs (Willoughby and Cooper, 2006) (Rochais et al., 2006) (Barnes et al., 2005) (Rich et al., 2001a) (Abrahamsen et al., 2004) (Perry et al., 2002) (Jurevicius et al., 2003). PDEs, being dynamically recruited to defined

subcellular sites via protein-protein interaction and binding to AKAPs, shape asymmetric gradients of cAMP and generate local clouds of the cyclic nucleotides. Zaccolo & Pozzan, using fluorescence energy transfer-based imaging demonstrated that, in cardiomyocytes, stimulation with catecholamines causes a local increase of cAMP, providing the first direct visualisation of microdomains of cAMP (Zaccolo and Pozzan, 2002). When PDEs were inhibited with 3-isobutyl-1-methylxanthine (IBMX), cAMP was found to be free to diffuse and accumulate homogeneously in the cytosol with consequent loss of specificity in the downstream response (Zaccolo and Pozzan, 2002).

A similar observation has been made in airway epithelia cells by patch-clamp recording of chloride currents through the cystic fibrosis transmembrane conductance regulator (CFTR) channels. In these cells PKA is anchored at the apical membrane and is coupled to adenosine A2B receptors and AC. In addition, PDE4 has been shown to be localised in this region. Occupancy of A2R leads to the activation of PKA and the consequent opening of the CFTR chloride channel. However luminal A2B receptor activation does not increase total cellular cAMP levels and cAMP is confined to the apical microdomain that includes CFTR. Only when PDE4 is pharmacologically inhibited the confinement of cAMP signalling is abolished, suggesting that PDEs are critically involved in modulating the spread of cAMP signalling at the apical membrane of airway epithelia (Barnes et al., 2005). According to this model, PDEs create an “enzymatic barrier” to limit cAMP diffusion. Thus, when agonist binds to the receptor, cAMP is produced and PDEs are recruited to prevent its overflow and the phosphorylation of non specific targets. Because PDEs are positively regulated by PKA this spatial diffusion barrier is sensitive and proportional to the levels of local cAMP and the degree of receptor stimulation (Barnes et al., 2005).

Additionally, it has been shown that PDE4D5 can be dynamically engaged by  $\beta$ -arrestin.  $\beta$ -arrestin is a cytosolic protein responsible for the desensitisation of G-protein coupled receptors, including  $\beta_2$ -adrenergic

receptor (Luttrell and Lefkowitz, 2002). When  $\beta_2$ -adrenergic receptor is activated  $\beta$ -arrestin is dynamically recruited to the plasma membrane to prevent receptor coupling to  $G_s$  and promote the switching to  $G_i$ , thereby inhibiting further adenylyl cyclase activation and cAMP production (Luttrell and Lefkowitz, 2002). Interestingly, the gathering of PDE4D5 to the plasma membrane specifically decreases the sub-plasma membrane cAMP concentration in an agonist-dependent manner inhibiting the subsequent PKA-mediated phosphorylation of the  $\beta$ -adrenoreceptor and rapidly terminating the PKA signal cascade (Perry et al., 2002) (Baillie et al., 2003).

In cardiomyocytes the compartmentalisation of each PDEs family, rather than the total enzyme expression level, prevails in determining their effects on intracellular cAMP concentrations (Mongillo et al., 2004). For example it has been demonstrated that the role of PDE2, which represent only 1% of the total amount of PDEs in cardiac cells, is crucial for the control of the cAMP response to  $\beta$ -AR stimulation, as demonstrated by the observation that, in the presence of agonist, PDE2 inhibition releases a very large amount of second messenger (Mongillo et al., 2005).

Based on the above data, a physical or an enzymatic barrier appears to be an adequate model to explain cAMP signalling in cardiomyocytes upon  $\beta$ -AR activation, nevertheless an enzymatic barrier implies the generation of a gradient of cAMP with a higher concentration of the second messenger at the plasma membrane as compared with the bulk cytosol. This model, therefore, fails to explain how cAMP selectively activates a subset of PKA anchored deep inside the cells, far from the site of synthesis, without affecting pools of PKA which are closer to the AC at the plasma membrane. Our previous work in the model cell line HEK293 showed that the nucleus may accumulate higher cAMP levels as compared with the bulk cytosol, demonstrating the existence of multiple, contiguous domains inside the cell each with different cAMP concentrations, irrespective of their distance from the cAMP synthesis site. In those studies we demonstrated that the definition of the boundaries of these multiple microdomains of cAMP relies on the activity of different PDE4

isoforms that are differently localised within the three dimensional matrix of the cell. Thus, at least in the HEK293 cells, localised PDE4s appear to be the crucial mechanism to maintain cAMP compartmentalisation. According to the model we proposed, when cAMP is generated it is able to quickly diffuse into all cellular compartments but it can only accumulate in those compartments where PDE activity is low. In other compartments, in which localised PDEs act as a “sink” to degrade cAMP, the second messenger level is kept low to protect effectors from inappropriate phosphorylation, thus ensuring the specificity of the signal (Terrin et al., 2006). A computational model of the biochemical network in the HEK293 cells showed that local microdomains of cAMP do not require impeded diffusion, thus further supporting the notion that barriers are not required for compartmentalisation (Figure 1-11) (Oliveira et al., 2010).

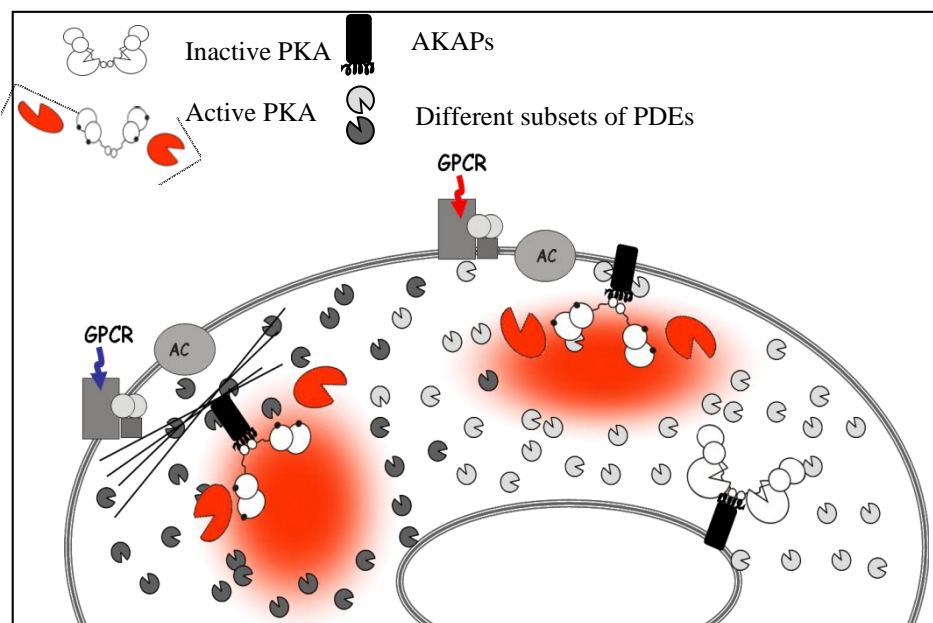


**Figure 1-11 Schematic representation of intracellular cAMP compartmentalisation.** cAMP is locally degraded by different compartmentalised subsets of PDEs that can act either as an enzymatic barrier or as a sink to prevent cAMP free diffusion and to generate spatially restricted pools of cAMP. In this way PDEs prevent the inappropriate activation of PKA. Activation of a specific GPCR generates a specific pool of cAMP whereas the activation of a different GPCR leads to the generation of a different pool of cAMP.

## 1.6 Overview on cAMP detection mechanism

The discovery of cAMP and the consequent delineation of the “second messenger concept” (see section 1.1) (Robison et al., 1968) has been one of the major advances in the cell biology field in the past 50 years. First studies of cAMP pathway immediately revealed that cAMP not only elicits direct response, like enzyme activation, but also it controls farther physiological effects, such as cardiac contractility or gene transcription. We now appreciate that this complex mechanism of transduction of a hormonal dependent perturbation of the plasma membrane into a spatially and temporally specific response via a single second messenger relies on a precise compartmentalisation of all components of the pathway involved. However, the paradigm of compartmentalised cAMP signalling has become clear only recently and a pivotal role in its definition has been played by the development of new tools to locally monitor cAMP fluctuations in intact living cells.

### 1.6.1 Classical approach

For several years the available techniques to monitor cAMP levels were based on the indirect detection using either biochemical or cytochemical methods. The most widely employed method has been a radio-immuno assay (RIA), which measures the concentration of cAMP in cells lysates by using a specific anti-cAMP antibody (Steiner et al., 1969).

RIA is based on the competition between intracellular cAMP and an exogenous radio labelled cAMP pool, used as a tracer, for the binding to the anti-cAMP antibody (Steiner et al., 1969). Due to its sensitivity and reliability, this technique, developed in 1969, is currently one of the most used to detect total cAMP concentration.

Recently, new antibody-based detection methods for cAMP have been introduced. Like RIA, these approaches exploit a cAMP tracer as a competitor for endogenous cAMP and the read-out is a concentration dependent signal decrease. Among these more recent methods the most common are:

Fluorescent polarisation assay (FP) (Kariv et al., 1999), Homogeneous time resolved fluorescence (HTRF) (Prystay et al., 2001) and AlphaScreen (amplified luminescence proximity assay) (Gabriel et al., 2003). For all these methods the improvement compared to RIA consists in the replacement of the radio label with the less toxic fluorescein- and biotin-label for FP and HTRF, respectively.

Additionally a novel bioluminescent-based assay has been developed three years ago. This technique is based on a luciferase/luciferin reaction upon pre-incubation of cells lysates with an exogenous PKA. Increase in cAMP concentration elicits the luciferin/luciferase reaction with consumption of ATP by cAMP-activated PKA and the consequent emission of light (Kumar et al., 2007).

All these methods are high throughput, simple and relatively inexpensive assays; moreover they do not require any sophisticated optical device or other specialised equipment. However, the main limitation of these methods is that they all involve a step in which cells are broken up to release endogenous cAMP. As a consequence any spatial information is completely lost. In addition such type of accumulation assays can only measure cAMP concentration at the steady state or within a time course of minutes. This implies that any cAMP fluctuation within a time scale of seconds will not be appreciated. Finally, these approaches provide information about cAMP dynamics that is averaged over the cell population whereas information at the single cell level may be more physiologically relevant. Clearly these methods are not suited to study the spatial and temporal aspects of cAMP signalling and it was only after the development of a toolkit for real-time detection of cAMP in single living cells that this analysis has become possible (Berrera et al., 2008).

### ***1.6.2 CNG-based sensors***

One approach for real-time detection of cAMP and cGMP exploits the over-expression of an olfactory CNG channel (Rich et al., 2000). Increase in cyclic nucleotides levels leads to the activation of the channels. Thus cAMP and

cGMP changes correlated with changes in  $\text{Ca}^{2+}$  influx that can be monitored by imaging of a fluorescent  $\text{Ca}^{2+}$  indicator (e.g. fura-2) or by patch clamp analysis of  $\text{Ca}^{2+}$  currents. Although the use of the wild type channel allows to monitor cyclic nucleotides dynamics in intact living cells, it presents several limitations: 1) the affinity of the CNG channels is higher for cGMP than cAMP (Rich et al., 2001b); 2) channels can be opened by nitric oxide (Broillet, 2000) and 3) they are negatively regulated by  $\text{Ca}^{2+}$ -calmodulin binding via a feedback loop mechanism (Liu et al., 1994). To overcome this limitations, a mutated and deleted version of the CNG channel,  $\Delta 61-90/\text{C460W}/\text{E583M}$ , was generated (Rich et al., 2001a). The mutant channel is highly sensitive to cAMP and insensitive to calcium regulation, however it still presents some limitations. First, it can monitor cAMP dynamics only at the plasma membrane where it is localised and second, the increased calcium influx can modulate the activity of ACs and calcium sensitive PDEs, thereby potentially leading to a non physiological cAMP change.

### ***1.6.3 GFP and FRET: seeing is believing***

The discovery and cloning of the green fluorescent protein (GFP) from the bioluminescent jellyfish *Aequorea Victoria* in 1992 (Shimomura et al., 1992) (Chalfie et al., 1994) (Tsien, 1992) opened a new era for the direct visualisation of biological processes. GFP became a tool for the *in vivo* study of proteins interactions and imaging of the flow of signalling transduction pathway. The combination of GFP with fluorescence resonance energy transfer further increased the relevance of GFP in biology. Today GFP-FRET based biosensors allow the quantitative study of protein-protein interactions, of protein activity and of small molecule signals, all with high spatial and temporal resolution.

#### **1.6.3.1 Förster resonance energy transfer**

Fluorescence resonance energy transfer (FRET), also called Förster resonance energy transfer, was first described in 1940 by Theodor Förster (Förster, 1948).

FRET is an electro-dynamic phenomenon that occurs between a donor (D) molecule in the excited state and an acceptor (A) molecule in the ground state. The energy transfer between D and A does not involve emission of photons therefore it is defined as energy of resonance.

For FRET to occur, the following requirements must be fulfilled:

1) the emission spectrum of the donor must show a substantial overlap with the absorption spectrum of the acceptor.

2) a long range dipole-dipole interaction between the donor and the acceptor must be established.

3) the distance between the donor and the acceptor must be in the Armstrong range.

In addition, FRET depends on the Quantum yield of the donor ( $Q_D$ ).

The distance at which efficiency of FRET is 50% is called Förster distance and it is typically between 20 and 60 Å. The Förster distance is a constant that depends on the overlap integral of the emission spectrum of the donor and the absorption spectrum of the acceptor, as well as on fluorophores orientation as expressed by the following function:

$$R_0 = 9.78 \times 10^3 (k^2 n^{-4} Q_D J(\lambda))^{1/6}$$

where  $Q_D$  is the quantum yield of the donor in absence of acceptor;  $n$  is the refractive index of the medium and it is typically assumed to be 1.4 for bio-molecules in aqueous solution;  $k^2$  is the factor describing the orientation in space of the fluorophores dipoles and usually is assumed to be equal to 2/3 for randomised rotation of donor and acceptor before energy transfer;  $J$  is the overlap integral of the spectra and it is given by:

$$J = \int_0^{\infty} F_D(\lambda) \varepsilon_A(\lambda) \lambda^4 d\lambda$$

where  $\lambda$  is the wavelength (nm);  $F_D(\lambda)$  is the normalised fluorescence of the donor in the wavelength range of  $\lambda$  to  $\lambda + \Delta\lambda$  (it is dimensionless);  $\varepsilon_A(\lambda)$  is the extinct coefficient of the acceptor at  $\lambda$  and it is typically measured in  $M^{-1} \text{cm}^{-1}$ .

Knowing the distance between donor and acceptor allows to choose the pair of fluorophores with maximum FRET efficiency. Vice versa, from the efficiency of FRET, theoretically it is possible to calculate the distance between the two fluorophores thereby the distance between the interacting proteins.

The rate of energy transfer ( $k_T(r)$ ) from a donor to an acceptor is given by:

$$k_T(r) = \frac{1}{\tau_D} \left( \frac{R_0}{r} \right)^6$$

Where  $\tau_D$  is the lifetime of the donor in absence of the acceptor;  $R_0$  is the Förster distance and  $r$  is the distance between donor and acceptor. When the distance donor to acceptor equals the Förster distance the rate of energy transfer equals the donor lifetime ( $\tau_D$ ) and the transfer efficiency is 50%. If the energy transfer is faster than the decay rate, the energy transfer will be efficient. On the contrary if the energy transfer is slower than the decay rate the energy transfer will be inefficient.

The efficiency of the energy transfer is the ratio between the photons adsorbed by the donor and the energy transferred to the acceptor and it is calculated as:

$$E = \frac{k_T(r)}{\tau_D^{-1} + k_T(r)}$$

That can be easily rearranged to:

$$E = \frac{R_0^6}{R_0^6 + r^6}$$

It is clear that the efficiency of FRET strongly depends on the distance donor to acceptor accordingly to this diagram:

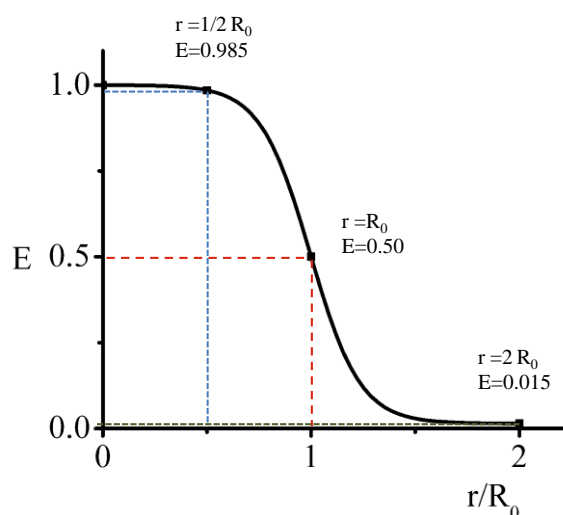


**Figure 1-12 Schematic representation of the dependence of the energy transfer efficiency (E) on distance.  $R_0$  is the Förster distance.**

The efficiency of FRET increases to 100% as the donor to acceptor distance decrease below the  $R_0$ . Conversely FRET efficiency tends to 0% if r doubles the  $R_0$  (Figure 1-12).

A final factor to consider in the analysis of the energy transfer is the orientation of the donor and acceptor's dipoles:  $k^2$ . It is calculated as:

$$k^2 = (\cos\theta_T - \cos\theta_D \cos\theta_A)^2$$

Where  $\theta_T$  is the angle between the emission transition dipole of the donor and the transition absorption dipole of the acceptor;  $\theta_D$  and  $\theta_A$  are the angles between these dipole and the vectors joining the donor and the acceptor. Depending on the orientation of the fluorophores this factor can range between 0 and 4. For head to tail parallel transition dipoles  $K^2=4$ , for parallel dipoles  $K^2=1$  and for perpendicular dipoles  $K^2=0$ , which would result is errors to calculate the distance between the fluorophores (Dale et al., 1979).

### **1.6.3.2 FRET-based cAMP indicators**

The development of FRET-based indicators provides a toolkit to monitor the cAMP/PKA signal transduction pathway by allowing direct visualisation of localised cAMP fluctuations in intact living cell with high resolution in space and in time.

Generally, a cAMP FRET-based indicator requires two essential components:

- 1) a sensor, which may consist of two interacting protein domains or a protein domain undergoing a conformational change upon cAMP binding.
- 2) a donor and an acceptor chromophore fused to the sensor.

Changes in conformation or in the distance of interacting protein partners results in a change in the distance or in the orientation of the two fluorophores, affecting the efficiency of energy transfer. In turn, variation of energy transfer correlates with changes in the ligand concentration.

#### **1.6.3.2.1 *PKA-based sensor***

The first FRET-based sensor that allowed the real-time imaging of cAMP in living cells was FICRhR (Adams et al., 1991). This indicator was based in the microinjection of the fluorescein- and rhodamin-labeled PKA subunits. In the presence of low cAMP concentration in a resting cell, FRET occurs between the

two subunits of the holoenzyme, while a rise in cAMP concentration correlates with a decrease in FRET due to the dissociation of the PKA subunits. Unfortunately this sensor did not find so many applications due to some technical limitations such as: 1) the requirement to microinject a large amount of protein complex ( $\mu\text{M}$ ) (procedure not applicable to all cells type); 2) the aggregation and precipitation of the labelled subunits; and 3) the non-specific interaction of the labelled subunits with cellular structures (Goillard et al., 2001).

The PKA-GFP sensor overcame these limitations (Zaccolo et al., 2000) (Figure 1-13). In this sensor the regulatory (RII $\beta$ ) and the catalytic subunit (C $\alpha$ ) of PKA are fused to the cyan and the yellow mutants of GFP, respectively (Figure 1-13). Being totally genetically encoded, this sensor is introduced into the cells by transfection or infection of the cDNAs encoding for the two chimerical subunits (Warrier et al., 2005), extending the application to most cell types.

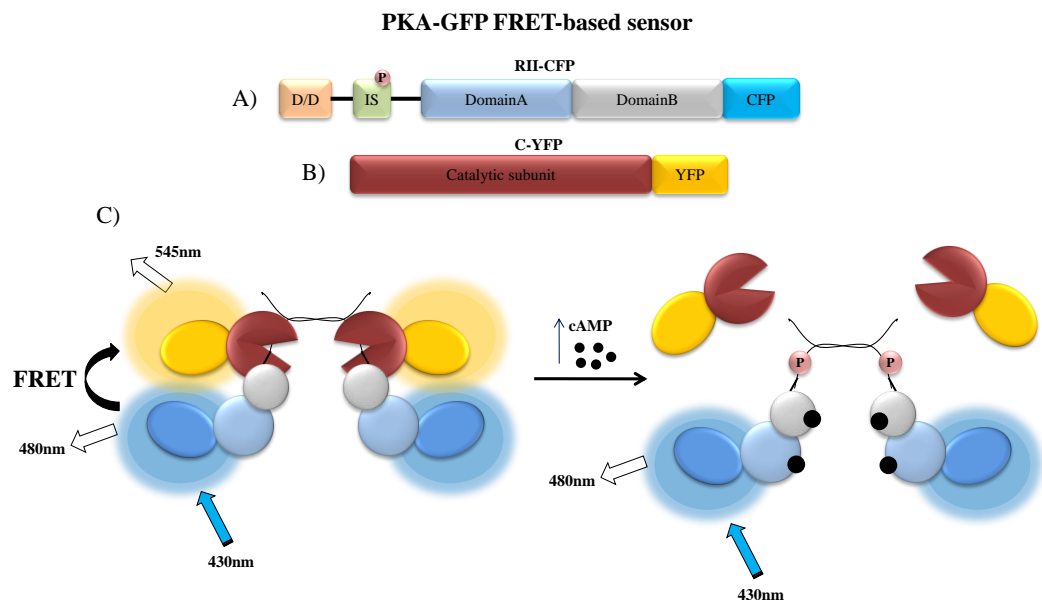


**Figure 1-13 Schematic representation of PKA-GFP FRET based sensor for cAMP and its mechanism of activation.**

Moreover, being the regulatory subunit of the probe the isoform type II $\beta$ , the over-expressed RII-CFP subunit binds, via its D/D domain, to endogenous AKAPs present in the cell, allowing detection of cAMP fluctuations in specific compartments within the cell. Over-expression of the PKA-GFP sensor in cardiomyocytes provides an example of such localisation (Figure 1-14).

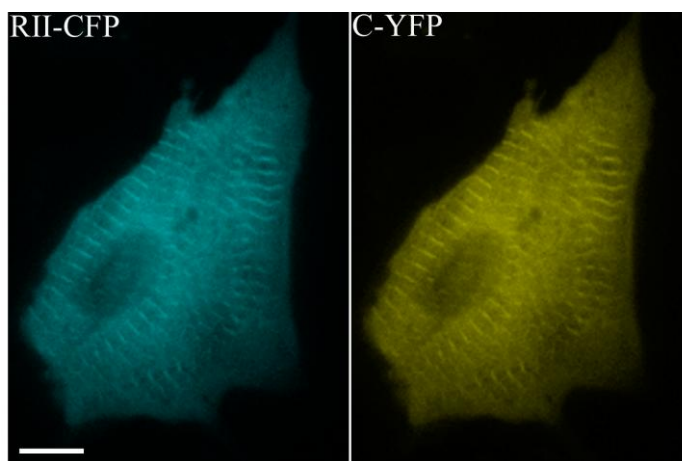


**Figure 1-14 Subcellular localisation of PKA-GFP sensor in neonatal rat ventricular cardiomyocytes. Bar 10 $\mu$ m.**

Different versions of PKA-based sensors have also been developed. In order to improve the dynamic range of the PKA-GFP probe a polypeptide linker of 20 amino acids was introduced between the R subunit and the fluorophore generating a cAMP indicator with doubled FRET efficiency (RII-L20-CFP) (Lissandron et al., 2005). In another case, the R230K mutation was introduced in the R subunit, thus generating a probe with a two orders of magnitude lower affinity for cAMP (Mongillo et al., 2004). Employment of these sensors allowed for the first time direct visualisation of cAMP microdomain in living cardiomyocytes (Zaccolo and Pozzan, 2002), and clarify the role of different PDEs subsets to prevent unrestrained cAMP diffusion (Mongillo et al., 2004) (Mongillo et al., 2006). However, the PKA-GFP sensors show some limitations: 1) co-transfection of two different subunits does not permit to have a control on the stoichiometry of the R and C subunits inside the cell. This can lead to

experimental artefacts due to the preponderance of a fluorophore over the other one; 2) cAMP-dependent dissociation of R and C subunits occurs through a complex cooperative mechanism (Taylor et al., 2005) and the kinetics of FRET change may be slower than the effective kinetics of cAMP changes; 3) the C subunit is catalytically active and this can result in an alteration of cAMP dynamics as a consequence of over-activation of the cAMP/PKA pathway. These reasons, together with the discovery of Epac proteins (de Rooij et al., 1998), contributed to the development of unimolecular FRET based sensors for cAMP.

#### **1.6.3.2.2 *Epac-based sensors***

Upon cAMP activation Epac undergoes a conformational change and this mechanism of activation has been exploited to develop FRET-based sensors (Bos et al., 2003) (Ponsioen et al., 2004).

In 2004, Nikolaev and co-workers developed simple sensors based on the fusion of individual cAMP binding domains of PKA and Epac to cyan and yellow GFP variants. In this way they generated sensors lacking the catalytic activity and the cooperative binding typical of PKA and offering faster speed of activation and capability of measuring cAMP in the physiological range with high temporal resolution (Nikolaev et al., 2004).

Simultaneously, two other groups took advantage of the cAMP binding property of Epac. Using a different approach than Nikolaev, both groups sandwiched the full length Epac1 between the cyan fluorescent protein (CFP) and the yellow fluorescent protein (YFP) generating the ICUE sensor (DiPilato et al., 2004) and the CFP-Epac-YFP sensor (Ponsioen et al., 2004). Despite the improvement compared to the PKA-based sensors, (Adams et al., 1991) (Zaccolo et al., 2000) (Zaccolo and Pozzan, 2000) the CFP-Epac-YFP probe showed localisation to the cytosol and to membranes, in particular to the nuclear envelope and to perinuclear compartments. To generate a soluble version of the probe the DEP domain was deleted (1-148 aa). Moreover, in order to render the indicator catalytically dead, other mutations were

introduced (T781A, F782A) leading to the generation of CFP-Epac ( $\delta$ DEP-CD)-YFP, also called H30 (Ponsioen et al., 2004) (Terrin et al., 2006). Compared to the PKA sensor this probe shows faster activation kinetics, an extended dynamic range but a lower affinity for cAMP. The lower affinity results on one hand in a lower buffering of cytosolic cAMP but on the other hand represents a limitation of application of the probe to systems that show larger changes in cAMP concentration (Ponsioen et al., 2004).

### **1.6.3.2.3 Compartment specific sensors**

The well established concept that cAMP concentration can fluctuate rapidly and non-uniformly within the cell led to the generation of a set of FRET based sensors for cAMP that can be targeted to different compartments within the cell.

The first targetable sensors for cAMP were generated by fusing a specific targeting sequence to the N- or the C-terminus of ICUE. Thus ICUE was targeted to the plasma membrane, mitochondria and the nucleus. The simultaneous transfection of these probes revealed, for the first time, different spatio-temporal cAMP dynamics at the cytosol and at the plasma membrane in response to the activation of  $\beta$ -adrenoreceptors or prostanoid receptors (DiPilato et al., 2004).

Two years later, in order to investigate cAMP compartmentalisation and to assess the role of PDEs in shaping cAMP microdomains in HEK293 cells, we generated the plasma membrane targeted PKA-GFP (mpPKA-GFP). To obtain this sensor a myristoylation/palmitoylation signal from the Lyn kinase was fused to the N terminus of the R subunit. Cells co-transfected with mpR-CFP and C-YFP (mpPKA-GFP) show a localisation of the R and C subunit to the plasma membrane (Figure 1-15) (Terrin et al., 2006).

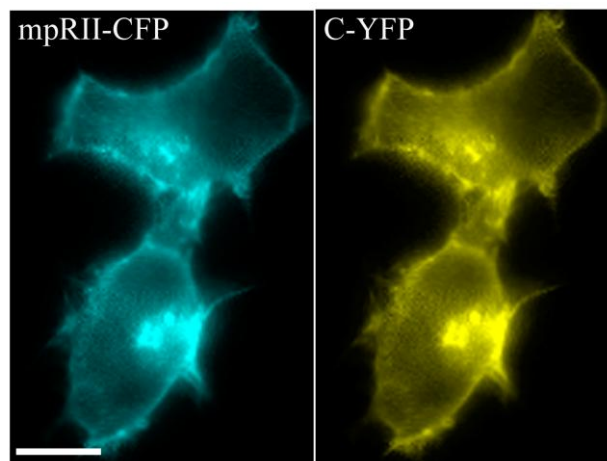


**Figure 1-15** Subcellular localisation of mpPKA-GFP sensor in HEK293 cells. Bar 10 $\mu$ m.

When cAMP binds to the mpPKA-GFP sensor it causes the probe to dissociate and to release of the catalytic subunit away from the regulatory subunit partner. This may result in over-estimation of the FRET response at the plasma membrane. To avoid this possibility, we generated an mpH30 sensor in which the mp sequence was fused to the N-terminus of H30. A further modification was the fusion of the nuclear localisation sequence (nls) to C-terminus of the H30 which targets the sensor to the nucleus (Terrin et al., 2006). All these targeted sensors allowed us to study cAMP dynamics within discrete compartments of the HEK293 cell (membrane, cytosol and nucleus) in response to prostaglandin 1 stimulation, thus describing a new mechanism in which PDEs act as a “sink” to shape contiguous pools of cAMP with different concentrations, independently from their distance from the site of synthesis (Terrin et al., 2006).

In cardiomyocytes, different isoforms of PKA show different subcellular localisation. In particular, PKA type I (containing the isoform RI) is predominantly localised in the cytosol whereas the PKA type II (containing the isoform RII) is mainly associated with the particulate fraction. In order to clarify if these two different isoforms of PKA can be activated by different pools of cAMP in response to the activation of specific receptors, we generated two FRET based reporters targeted to those intracellular sites where endogenous PKA type I and PKA type II isoforms normally localise. To achieve this we fused

the D/D domain of RI or RII to the N terminus of Epac1 (Nikolaev et al., 2004), to generate the sensor RI\_epac and RII\_epac, respectively (Di Benedetto et al., 2008) (Figure 1-16).

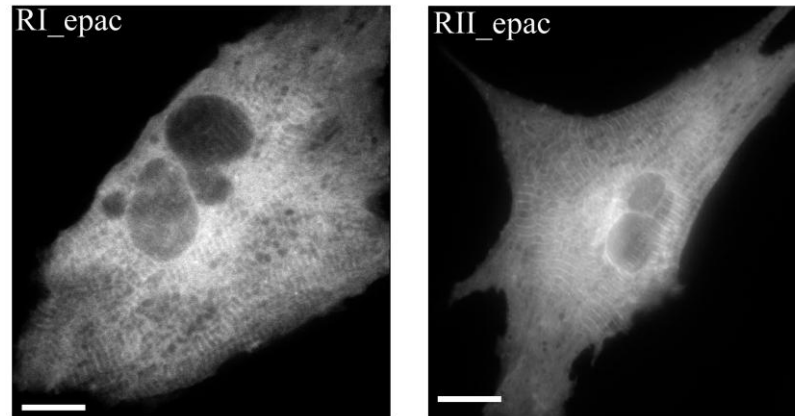


**Figure 1-16 Subcellular localisation of RI\_epac and RII\_epac sensors in neonatal rat ventricular cardiomyocytes. Bars 10 $\mu$ m.**

The sensors show equal sensitivity to cAMP but display a different pattern distribution, with RI\_epac localisation overlaying with the Z and M sarcomeric line and RII\_epac localising to the M line. This different localisation of the probes is due to the binding to specific endogenous AKAPs, as demonstrated by the re-distribution of the sensor to the cytosol when the sensor was co-expressed with AKAP/PKA disruptor peptides (Di Benedetto et al., 2008). The different regulation of cAMP levels in the two compartments also points to a different association of the two PKA isoforms with specific PDEs subsets. Moreover, we showed that stimulation of different GPCR leads to the activation of specific PKA isoforms and, in turn, to specific phosphorylation of downstream targets (Di Benedetto et al., 2008).

## **1.7 A PKA signalling domain localised to the centrosome**

### ***1.7.1 Centrosome structure***

The Centrosome of animal cells is a small organelle of  $\sim 1\text{-}2\ \mu\text{m}$  in diameter usually located at the centre of the cell. It is composed of two barrel-shaped centrioles, orthogonally arranged and linked by a pericentriolar material (PCM), from which the microtubules are nucleated. For this reason it is considered as the major microtubule organising centre of the cell (MTOC).

The PCM is a proteinaceous material containing two subsets of protein complexes defined as matrix and non-matrix proteins and responsible for nucleation, anchoring and stabilisation of the microtubule network. The matrix subset is composed by proteins that link together the proximal minus end of the centrioles pair. The most abundant protein of this group is pericentrin, a protein that has been shown to be involved in all the centrosomal functions (Bornens, 2002); however AKAP450 and ninein are also included in this group (Figure 1-17). These proteins are specifically localised to the centrosome but can also be found in the cytosol, although the size of the cytosolic pool is small. The second subset of the PMC proteins, the non-matrix proteins, is composed by proteins such as  $\gamma$ -tubulin and centrin. These two proteins are classical markers for the centrosome, where they have specific localisation. However 80-90% of the total amount of these proteins is not centrosome-associated. The role of  $\gamma$ -tubulin and centrin in the centrosome is to interact, in a polyglutamylation dependent manner, with the walls of the two centrioles to create a connective bridge between them (Figure 1-17) (Bornens, 2002).

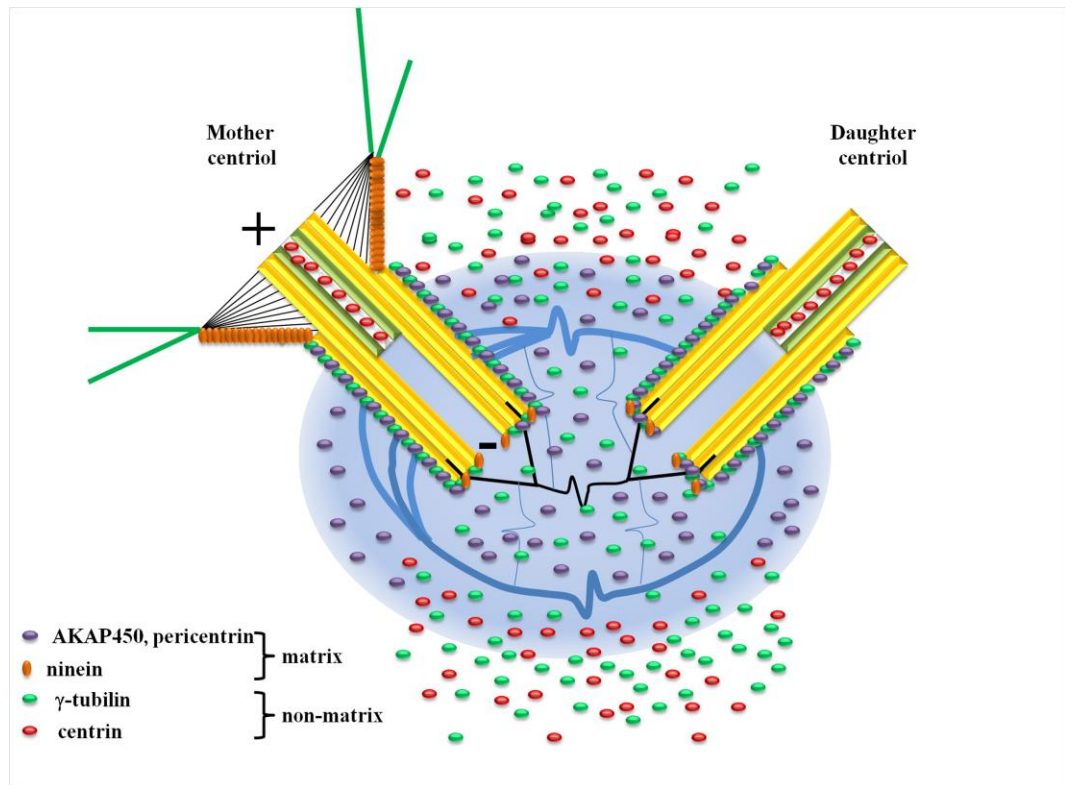


**Figure 1-17 Schematic representation of the centrosome and centrosomal proteins distribution according to their proximal-distal polarity. Adapted from (Bornens, 2002).**

In order to stabilise the interactions and fully assemble the PMC, other proteins cross link these two protein subsets (Bornens, 2002).

Three AKAPs have been identified at the centrosome: the human hAKAP220 (Reinton et al., 2000), pericentrin (Diviani et al., 2000) and AKAP450 (Witczak et al., 1999) (Schmidt et al., 1999) (Takahashi et al., 1999).

### **1.7.1.1 hAKAP220**

Human AKAP220 (hAKAP220) is the homologous of the AKAP220 previously isolated from rat testis extracts and localised to peroxisomes (Lester et al., 1996). hAKAP220, isolated from human testis and spermatocytes, shows high level of similarity with the C-terminal of the AKAP220 of rat although it contains a 727 N-terminal portion that is not present in the rat sequence. Immunofluorescence assays with specific antibodies revealed that hAKAP220 localises in the cytoplasm of premeiotic spermatocytes and to the centrosome of developing post-meiotic germ cells, elongating spermatocytes

and mature sperm. In addition, hAKAP220 seems to be a dual AKAP since it co-precipitates with both type I and type II regulatory subunits of PKA in human testis lysates (Reinton et al., 2000). Binding of PKA to the centrosomal hAKAP220 may have a role in regulating spindle formation and microtubule organisation during spermatogenesis and in post-meiotic germ cells since microtubule stability in somatic cells is influenced by PKA (Lane and Kalderon, 1994); (Gradin et al., 1998).

### **1.7.1.2 Pericentrin**

Pericentrin is a coil-coiled protein, an integral component of the PMC and it is exclusively present at the centrosome (Doxsey et al., 1994). At the centrosome pericentrin interacts with  $\gamma$ -tubulin, centrin, dynein and other proteins of the PMC to assure the proper centrosomal architecture and microtubules nucleation during mitosis and meiosis (Doxsey et al., 1994) (Bornens, 2002) (Dictenberg et al., 1998) (Purohit et al., 1999). The binding of pericentrin to  $\gamma$ -tubulin is required for the correct organisation of microtubule network whereas pericentrin interaction with the motor protein dynein is essential for the transport of  $\gamma$ -tubulin containing complexes along the microtubules from the cytosol to the centrosome (Purohit et al., 1999) (Young et al., 2000) (Doxsey et al., 1994).

Despite this critical role in centrosome organisation, co-immunoprecipitation of pericentrin with catalytic activity of PKA in HEK293 cells showed that pericentrin is also an AKAP. However the interaction between the RII subunit of PKA and pericentrin occurs through an unconventional region of 100 amino acid residues characterised by leucine-repeat sequences (see 1.5.1 section). Interestingly, this 100 amino acid polypeptide does not show the typical amphipathic helix motif presents in all the others AKAPs (Diviani et al., 2000).

The role of centrosomal pericentrin-PKA complex seems to be correlated to the PKA-dependent regulation of dynein-dynactin functions. In fact, it has been shown that impairment of dynein functions results in spindle

defects, such as spindle fragmentation and disorganisation (Purohit et al., 1999) (Diviani and Scott, 2001).

### **1.7.1.3 AKAP450/350/CG-NAP**

The localisation of PKA type II  $\alpha$  and  $\beta$  to the Golgi/centrosome area was demonstrated more than 20 years ago (De Camilli et al., 1986) (Nigg et al., 1985) (Rios et al., 1992) (Keryer et al., 1993). First of all a family of high molecular weight proteins were identified as components of the pericentriolar matrix of human lymphoblastic KE37 cells (Gosti-Testu et al., 1986). A few years later the same research groups, using cell fractioning, immunoprecipitation and immunoblotting assays, showed that both the RII isoforms  $\alpha$  and  $\beta$  localise to the centrosome of human lymphoblasts. Moreover, RII overlay techniques, revealed that the high affinity binding of RII subunit with the centrosome is due to the interaction with a 350 kDa protein which could be phosphorylated by the catalytic subunit of the PKA and that was detectable only in centrosome extracts (Rios et al., 1992) (Keryer et al., 1993). This protein was named AKAP350, based on its molecular weight and the ability to co-precipitate with PKA catalytic activity. Subsequent analysis demonstrated that the previously identified high molecular weight proteins in the PMC of human lymphoblastic cells (Gosti-Testu et al., 1986) were splice variants of the larger AKAP350 protein (Keryer et al., 1993) (Schmidt et al., 1999).

In 1998, two different groups cloned and characterised a cDNA of 12.1 kb (11.7 kb of open reading frame) and encoding a protein of 453 kDa capable of tethering PKA to the centrosome (DDBJ/EMBL/GenBank accession N°AJ131693) (Witczak et al., 1999) (Schmidt et al., 1999). One year later Takahashi and co-workers, in a yeast two hybrid screen using the N-terminal of PKA as bait, identified a novel coiled-coil protein of 450kDa as a PKN interacting protein. They also showed that this protein was localised to the centrosome throughout the cell cycle and to the Golgi in interphase cells so that they named it CG-NAP (centrosome and Golgi localised PKN-associated protein) (Takahashi et al., 1999). We now know that AKAP350, AKAP450 or

CG-NAP represent a family of differently spliced proteins encoded by a single gene sequence localised on the human chromosome 7q21 (Schmidt et al., 1999). From now on I will refer to it as AKAP450 since it is closest to its molecular weight.

At least two splice isoforms of AKAP450 are known: AKAP120, a widely expressed AKAP in rabbit gastric parietal cells (Dransfield et al., 1997) and Yotiao, an AKAP involved in anchoring to the cytoskeleton of NMDA receptor in post-synaptic densities of rat neurons (Lin et al., 1998). Despite splice variants may be differentially distributed among tissues and cells types, AKAP450 contains a coiled coil domain typical of proteins involved in the framework of the perinuclear matrix and was mainly identified anchored to the centrosome (Schmidt et al., 1999) (Takahashi et al., 1999) (Witczak et al., 1999).

The C-terminal domain of AKAP450 accounts for the binding to the centrosome (Gillingham and Munro, 2000). This 90-amino-acid-long domain shares a high degree of homology with the centrosomal targeting domain of pericentrin and for this reason it has been called PACT domain (pericentrin AKAP450 centrosomal targeting). Over-expression of the AKAP450-PACT domain in COS cells results in the displacement of pericentrin, indicating competition for a shared binding site (Gillingham and Munro, 2000). However Keryer and co-workers provided another evidence showing that over-expression of the AKAP450-PACT domain in HeLa cells displaces AKAP450 but not pericentrin, and vice versa, indicating specificity in the targeting of both AKAPs (Keryer et al., 2003b).

It is not clear if AKAP450 can bind to the Golgi apparatus. According to Gillingham and colleagues, AKAP450 can only localise to the centrosome and any Golgi apparatus staining is due to the cross reaction of the antibody used with one of the many coiled-coil proteins localised to these organelles (Gillingham and Munro, 2000). Conversely, Shanks and colleagues reported the presence of a Golgi targeting sequence of 48 amino acids adjacent to the PACT domain (Shanks et al., 2002b).

Further studies showed that in addition to two PKA binding sites, AKAP450 interacts with protein kinase N (PKN), protein phosphatases 1 (PP1) and protein phosphatases 2A (PP2A) (Takahashi et al., 1999), phosphodiesterases 4D3 (PDE4D3) (Tasken et al., 2001), protein kinases C epsilon (PKC $\epsilon$ ) (Takahashi et al., 2000) and the isoform delta of casein kinase I (CKI $\delta$ ).

Moreover it is worth to consider that in lysates from COS1 cells AKAP450 co-immunoprecipitated with the catalytic dead PDE4D3 and PDE4C2, suggesting a possible interaction of PDE4C2 with this specific AKAP in this cell type (McCahill et al., 2005).

PKN is a serine/threonine kinase that associates with and phosphorylates intermediate filament proteins (Mukai, 2003) (Mukai and Ono, 1998). Thus targeting of PKN to AKAP450 may be important for cytoskeleton reorganisation-related events. (Mukai and Ono, 1998) (Mukai, 2003).

Interaction between AKAP450 and the immature non phosphorylated form of PKC $\epsilon$  seems to be required either for the phosphorylation-dependent maturation of PKC $\epsilon$  or for indirectly protect unstable immature PKC $\epsilon$  species (Takahashi et al., 2000). Moreover, it has recently been shown a role of PKC $\epsilon$  for the correct abscission during cytokinesis (Saurin et al., 2008). The correct completion of cytokinesis seems to require the correct assembling of PKC $\epsilon$ -14-3-3 complex during the late stages of mitosis. Absence or inhibition of this functional complex leads to failure of cytokinesis (Saurin et al., 2008).

It has been suggested that the interaction of AKAP450 with PDE4D3 may account for a feedback loop mechanism of negative control of the cAMP/PKA pathway in that specific compartment (Tasken et al., 2001). It has indeed already been shown in other PKA signalling domains, that PDE4D3 allows for tight control of PKA activity by local degradation of cAMP (Dodge et al., 2001).

Finally CKI $\delta$  has been shown to regulate cell cycle progression and its specific inhibition causes a mitotic arrest (Sillibourne et al., 2002). Recent

studies strongly suggest that CKI $\delta$  and PKA physiologically interact within the same compartment. Moreover, PKA mediated phosphorylation of CKI $\delta$  inhibits CKI $\delta$  activity and interferes with normal development of *Xenopus* embryos (Giamas et al., 2007).

The same author identified a region (1382-1515 amino acids) in AKAP450, showing 47% similarity with the centrosomal protein pericentrin (Shanks et al., 2002a), which is responsible for targeting of the chloride intracellular channel (CLIC) family (Shanks et al., 2002a). Although the function of this family of proteins is poorly understood it is well known that all the CLIC isoforms contain a PKA phosphorylation site, hence their anchoring to AKAP450 could regulate their functions and cell distribution (Shanks et al., 2002a).

All these observations suggest that AKAP450 provides a point for integration of distinct signalling pathways that are involved with the cell cycle progression and/or cell proliferation.

### ***1.7.2 Centrosome functions***

The major function of the centrosome is the organisation of microtubules cytoskeleton. In interphase, the centrosome arranges the microtubules astral array involved in crucial cellular functions like trafficking, cell motility, cell adhesion and cell polarity (Azimzadeh and Bornens, 2007). During cell cycle progression the centrosome undergoes a maturation process, involving the accumulation of  $\gamma$ -tubulin and centrin, and culminating with the centrosome duplication at the onset of S phase. The newly synthesised centrosomes are essential for the assembly, organisation and orientation of a bipolar mitotic spindle. Moreover they regulate the fidelity of chromosome segregation and the late events of cytokinesis (Bornens, 2002) (Azimzadeh and Bornens, 2007).

Recent studies indicate that centrosome coordinate cell cycle progression from G<sub>1</sub> to S phase (G<sub>1</sub>-S), from G<sub>2</sub> to M phase (G<sub>2</sub>-M), from

metaphase to anaphase (M-A) and through cytokinesis (Doxsey et al., 2005b) (Doxsey et al., 2005a).

### **1.7.3 The cell cycle and its regulation**

The cell cycle is the process that leads a cell to its division and duplication in two daughter cells.

The cell cycle can be divided into four distinct phases: G<sub>1</sub> phase, S phase, G<sub>2</sub> phase and M phase. The G<sub>1</sub>, S and G<sub>2</sub> phases are collectively known as Interphase, and represent the stage of the cycle in which the cell prepares itself for the following division (Smith and Martin, 1973).

G<sub>1</sub> phase, also called growth phase, is the period from the end of mitosis and the beginning of DNA replication. During this phase the biosynthetic machinery of the cell reaches the maximum activity and all the enzymes required during the following S phase are synthesised. In this stage the cell contains one centrosome with two orthologue centrioles (Smith and Martin, 1973).

S phase starts with the synthesis of DNA and ends when all of the chromosomes have been replicated. While the content of DNA is doubled in this phase the RNA transcription and protein synthesis are completely switched off except for histones production. During this phase the two centrioles of the centrosome replicate (Smith and Martin, 1973).

G<sub>2</sub> phase starts at the end of DNA replication and lasts until the cells enter mitosis. In this period, components of the spindle pole body, such as microtubules, are synthesised. During this phase protein synthesis is again very high and its inhibition will results in a G<sub>2</sub> arrest of the cycle progression. At the end of this phase the two pairs of centrioles start to separate and to become part of the spindle poles body (Smith and Martin, 1973).

M phase or mitosis is the phase during which chromosomes separate and the nucleus divides. Mitosis includes five distinct sub-phases called:

prophase, metaphase, anaphase, telophase, and cytokinesis. During mitosis the chromosomes condense and align on the metaphase plate by attaching to the microtubules of the spindle poles body that in turn pull the sister chromatides to opposite sides of the cell.

During cytokinesis then the cell completes the formation of two daughter cells through the division of the nuclei, cytoplasm, organelles and membranes (Smith and Martin, 1973).

### ***1.7.4 Cell and centrosome coordinating cycles***

Accurate cell division requires the coordinated completion of three cycles: the cell, the centrosome and the nuclear cycles. Regulation of the cell cycle is crucial for the survival of a cell. To this purpose the cell has several control mechanisms to detect genetic damage and to prevent uncontrolled cell division.

Cyclins and cyclin dependent kinases (Cdks) are the two key classes of regulatory molecules which control cell progression through the cell-cycle. Cyclins and Cdks are respectively the regulatory and the catalytic subunit of a large family of heterodimeric serine/threonine protein kinases. In addition cyclins, which are synthesised and degraded during each cell cycle, have no catalytic activity, whereas Cdks, constitutively expressed, are not active unless they are bound to cyclins (Malumbres and Barbacid, 2005).

In  $G_1$  phase, an incoming mitogenic signal induces synthesis of CyclinD and promotes the folding of Cdk4. The active complex Cdk4-CyclinD phosphorylates and inactivates the retinoblastoma (Rb) protein family. The function of the Rb proteins is to repress transcription by binding and modulating the activity of transcription factors. Cdk4-CyclinD complex-dependent phosphorylation of Rb leads to the release of the inhibition exerted by Rb on the transcription factors thereby promoting the transcription of genes such as DNA polymerase, thymidine kinase, chromatin remodelling complexes and also CyclinA and CyclinE, necessary for entry into the following phases. The next activation of the complex Cdk2-CyclinE, during  $G_1$ -S

transition, carries out the irreversible inactivation of the Rb proteins and favours the onset of DNA replication, thereby promoting the exit from G<sub>1</sub> phase and leading the cell into S phase. In addition, Cdk2-CyclinE complex phosphorylates proteins involved in histones modification and centrosome maturation and duplication, as well as its own inhibitor p27, thus promoting its degradation. Once cells enter in S phase CyclinE is rapidly degraded in order to inactivate the Cdk2-CyclinE complex and avoid the re-replication of the DNA (Smith and Martin, 1973).

During S phases CyclinA and B are synthesised and the consequent association of Cdk2-CyclinA promotes the completion and exit from S phase, by phosphorylating numerous substrates such as upstream regulators of CyclinA, transcription factors and protein involved in DNA replication. At this stage CyclinA associates also to Cdk1 (also named cdc2 or p34 kinase). Cdk1-CyclinA shares similar substrates with Cdk2-CyclinA and both promote the S-G<sub>2</sub> transition (Smith and Martin, 1973).

At the beginning of G<sub>2</sub>, CyclinB is synthesised whereas CyclinA is degraded by an ubiquitin-mediated proteolysis process. As a consequence, Cdk1 binds and activates cyclinB, throughout a mechanism involving phosphatase cdc25, the checkpoint kinase 1 (Chk1) and Aurora A kinase (Kramer et al., 2004) (Dutertre et al., 2004). Cdk1-CyclinB complex is also called the M-phase Promoting Factor (MPF) and its activation is essential for the cell to enter mitosis; moreover, in prophase this complex associates with the centrosome and triggers its separation. The MPF regulates chromosomal condensation, fragmentation of the Golgi apparatus, breakdown of the nuclear lamina as well as degradation of the CyclinB for correct exit from mitosis. As for the other cyclins, CyclinB is also degraded upon ubiquitination and subsequent proteolysis. The ubiquitin ligase which promotes degradation of mitotic cyclins is the anaphase-promoting complex (APC) and its activity ensures the correct progression of the cell cycle through the anaphase, telophase and the cytokinesis (Malumbres and Barbacid, 2005).

Centrosome duplication is precisely coordinated with cell cycle progression; however how these two processes are coupled is still matter of study. One possible link can be the use of the same molecular complexes such as Cdks and the anchoring of such complexes to the centrosome. Thus centrosome becomes a scaffold for a network of signalling pathways involved in cellular division. For example, the cell cycle kinase Cdk2, in complex with CyclinE and A, is required to the centrosome for G<sub>1</sub>-S transition and initiation of centrosome duplication (Hinchcliffe et al., 1999) (Lacey et al., 1999). Also mitotic entry (G<sub>2</sub>-M transition) requires centrosome localisation of Cdk1 and its modulator checkpoint kinase 1 (Chk1) (Kramer et al., 2004). In addition, other kinases have been shown to be targeted to the centrosome and to regulate its functions. For example, polo-like kinase (Plk) and Aurora A kinase control centrosome maturation, centrioles duplication (Blagden and Glover, 2003) and recruitment of Cdk1-cyclinB (MPF) to the centrosome before its activation (Dutertre et al., 2004).

As a consequence, perturbations of the centrosome result in the aberration of one or more of these processes leading to the arrest of the cells cycle progression.

#### **1.7.4.1 G<sub>1</sub> arrest**

It has been shown that microsurgical (Hinchcliffe et al., 2001) or laser ablation (Khodjakov and Rieder, 2001) of core centrosome components, such as centrioles, before the completion of S phase, results in cells cycle arrest in G<sub>1</sub> phase. Acentriolar cells form functional mitotic spindle but about 50% of them are not able to exit cytokinesis, generating tetraploid cells. All the population, both the acentriolar and the tetraploid, do not enter S-phase in the following cycle. In a similar manner, ablation of one of the centrioles in pro-metaphase cells results in a daughter cell with a functional centrosome and an acentriolar daughter cell that does not enter the following S-phase (Khodjakov and Rieder, 2001). The same effect results from changes in centrosomal proteins expression level or localisation. An example of this was provided by the over-expression of pericentrin-AKAP450 centrosomal targeting domain (PACT

domain). Displacement of both pericentrin and AKAP450 from the centrosome upon PACT domain over-expression is associated with impaired centrioles duplication and inhibition of cell cycle progression. Cells over-expressing the PACT domain enter mitosis but do not complete cytokinesis, showing arrest in  $G_1$  (Kramer et al., 2004) (Keryer et al., 2003b). Based on this evidence it appears that  $G_1$  arrest arises from alterations in centrosome composition leading to cytokinesis defects. However the pathway linking the centrosomal disruption to the  $G_1$  arrest is currently unknown. A model proposed for this arrest involves CyclinE, the recruitment of which to the centrosome has been shown to be essential for  $G_1$ -S transition (Lacey et al., 1999). Ectopically expression of CyclinE in CHO cells accelerates S phase entry whereas displacement of the CyclinE from the centrosome results in cells population arrest in  $G_1$  (Matsumoto and Maller, 2004). Therefore it is possible that centrosome disruption may affect anchoring of CyclinE to the centrosome, thereby leading to the observed  $G_1$  arrest.

#### **1.7.4.2 $G_2$ arrest (pre-mitotic entry)**

The role of centrosome in  $G_2$ -M transition has been recently correlated to the Cdk1-CyclinB (MPF) activation complex. The activation of this complex, that is the key event for mitosis entry, occurs at the centrosome. It has been shown that Cdk1-CyclinB is activated in late prophase by cytoplasmatic phosphatase cdc25, which in turn is under temporary negative control by centrosome associated checkpoint kinase 1 (Chk1; Cdk1 modulator) (Kramer et al., 2004). With an elegant set of experiments Lukas and colleagues showed that Chk1, anchored to the centrosome, shields Cdk1 from activation during interphase. At the onset of mitosis Chk1 displaces from the centrosome and releases Cdk1 inhibition. Eventually Cdk1 is available for cdc25-dependent activation, leading the cells to enter mitosis at the right moment. To dissect this mechanism, a wild-type and a catalytically dead version of the Chk1 fused to the PACT domain have been generated. The immobilisation of the wild-type Chk1 to the centrosome results in a permanent inhibition of the Cdk1-activation that leads to mitotic failure and formation of polyploid cells. On the

contrary, replacement of the endogenous Chk1 with a catalytically dead version results in a premature Cdk1 activation and a consequent premature mitotic entry (Kramer et al., 2004).

A role in G<sub>2</sub>-M transition is also played by the pericentrin- $\gamma$ -tubulin complex. In fact, uncoupling of pericentrin- $\gamma$ -tubulin interaction or knock-down of pericentrin and the consequent disruption of binding to  $\gamma$ -tubulin, induces arrest at G<sub>2</sub>-M transition. Cells arrested in G<sub>2</sub> then undergo apoptosis. However it is not clear at the moment what is the mechanism responsible for the arrest and if disruption of pericentrin- $\gamma$ -tubulin interaction is responsible for the mislocalisation of other centrosomal molecules involved in the regulation of cell cycle progression (Zimmerman et al., 2004).

### **1.7.4.3 Cytokinesis failure**

Video imaging of cells stably expressing the centrosomal protein centrin tagged to GFP revealed the crucial steps of cytokinesis (Piel et al., 2001). During cytokinesis the mother centriole transiently and quickly migrates to the intracellular bridge near to the midbody. The reason for this repositioning seems to be related to the delivery of membranes and vesicles as well as regulatory components for mitosis exit and cytokinesis ending. Cytokinesis completes with the abscission of the two daughter cells only when the mother centriole moves back to the centre of the cell. This mechanism shows how centrosome is involved also in cytokinesis. It has also been shown that ablation of the centrosome or manipulation of its protein content generates a population of cells that complete the furrow cleavage but do not undergo the abscission, thus remaining attached through a cytoplasmic bridge (Hinchcliffe et al., 2001, Khodjakov and Rieder, 2001, Keryer et al., 2003b). Finally, it is worth mentioning that the correct completion of cytokinesis seems to require the correct assembly of PKC $\epsilon$ -14-3-3 complex during the late stage of mitosis. Absence or inhibition of this functional complex leads to failure of cytokinesis (Saurin et al., 2008). PKC $\epsilon$  binds to AKAP450 at the centrosome.

As described above, cytokinesis failures usually results in a G<sub>1</sub> arrest of the cell population (see section 1.7.4.1).

## 1.8 cAMP and PKA in cell cycle progression

The relationship between cAMP/PKA and cell cycle progression is very controversial and contradictory evidence is present in the literature. cAMP and PKA seem to both activate and inhibit cell proliferation and, despite the overwhelming number of studies, it is not clear what mechanisms may trigger such opposite effects. This is in part due to the numerous targets of PKA so that activation of PKA can trigger both positive and negative signalling pathway for the initiation and progression of the cell cycle. In addition, most of the studies available have been performed on populations of cells that had been synchronised by chemical treatment. Cell synchronisation achieved by these means is known to be difficult to maintain for more than one cycle. Finally, it is important to consider that analysis of cAMP and PKA activity in these studies has always been carried out on cell lysates thereby any relevant information on local differences in cAMP/PKA activity could not be appreciated. Despite such limitations, the emerging picture is that activation of the cAMP/PKA signalling pathway has an anti-mitotic effect.

Studies of the mitogenic role of cAMP and its effect on the inter-conversion of a quiescent population into a cycling population revealed that cAMP alone does not stimulate cells to divide unless the population has already been programmed to undergo cell division (Abell and Monahan, 1973). Accordingly MacManus and Whitfield showed that addition of physiological concentrations of cAMP (between 10 nM and 1  $\mu$ M) to resting thymocytes and lymphocytes cultures stimulates cell entry into mitosis by promoting DNA synthesis. However, an increase in cAMP to a concentration greater than 10  $\mu$ M resulted in inhibition of cell growth (Macmanus and Whitfield, 1969). This finding was further confirmed by many others showing that elevation of cAMP concentration induces either by stimulation of AC, inhibition of PDEs or by addition of cAMP (cAMP or dibutyryl-cAMP), inhibits cells division in many

other mitogen-stimulated cells types, including HeLa cells and 3T3 mouse fibroblasts (Macmanus and Whitfield, 1969) (Ryan and Heidrick, 1968) (Sheppard, 1972). In agreement with these findings, an immediate drop in cAMP level is observed when cells are released from quiescence. It has been shown in fact that proteolytic treatment of 3T3 mouse fibroblasts, growth-arrested for contact inhibition, results in stimulation of proliferation and in a drop in cAMP concentration. The proliferative effect of the protease treatment can be reversed by replenishment of cAMP or dibutyryl cAMP (Burger et al., 1972) (Sheppard, 1972) (Sheppard, 1971). Similarly, the inhibitory effect exerted by cAMP on cell cycle progression is reversible and cell cycle progression can be rescued upon removal of cAMP (Ryan and Heidrick, 1968). Based on this evidence it was possible to conclude that agents that stimulate proliferation in a resting cell population decrease intracellular cAMP level; on the contrary, agents that inhibit cells proliferation induce an increase in intracellular cAMP concentration. Thus cAMP elevation appears to counteract cell growth (Bombik and Burger, 1973).

The involvement of cAMP in regulating cell cycle progression was studied by in vitro analysis of endogenous cAMP concentration in each stage of the cells cycle. Synchronised HeLa and CHO cells revealed that cAMP level fluctuates throughout the cells cycle reaching the highest level in G<sub>1</sub> and the lowest level in mitosis. In agreement with these measurements, early G<sub>1</sub> cells have 50% more cAMP than cells in S phase and mitotic cells have half the amount of cAMP found in S phase cells. Late G<sub>1</sub> cells contain the same amount of cAMP as cells in S phase (Sheppard and Prescott, 1972) (Zeilig et al., 1976).

These reports confirm the inverse correlation between cAMP levels and growth rate. Thus, populations of cells actively dividing will have a higher proportion of cells in S, G<sub>2</sub> and M phase and a lower proportion in G<sub>1</sub> corresponding to a lower amount of total cAMP (Zeilig et al., 1976). Despite the anti-proliferative effect of cAMP analysis of CHO and rat liver cells indicates that the surge of cAMP in late G<sub>1</sub> seems to be necessary for specific PKA type II activation to promote the initiation of DNA synthesis, suggesting a

coordination between cAMP fluctuations and PKA signalling cascade (Boynton and Whitfield, 1980) (Costa et al., 1976a, Costa et al., 1976b) (Costa et al., 1978). Interestingly, lymphoma cells expressing a defective PKA insensitive to cAMP (Daniel et al., 1973) are able to proceed normally through the cell cycle even in the presence of high cAMP concentration, indicating that block of cell cycle in G<sub>1</sub>, in presence of high level of cAMP, is PKA mediated (Coffino et al., 1975).

Further studies on the effects on cell cycle progression induced by experimental elevation of cAMP confirmed previous reports showing that an increase of intracellular cAMP in S phase synchronised cells inhibits cells cycle transition through G<sub>2</sub>/M phase, suggesting the existence of a cAMP-mediated checkpoint for the S-G<sub>2</sub> progression. On the contrary, elevation of cAMP on a mitotic population accelerated cells progression throughout the cycle and the completion of cells division. Finally, inhibition of phosphodiesterases or activation of adenylyl cyclases in a G<sub>1</sub> enriched population results in a prolonged G<sub>1</sub> phase (Zeilig et al., 1976).

Analysis of cell cycle progression in thyroid cells provided evidence that G<sub>1</sub>-S transition requires not only decrease in cAMP concentration but also modification of the PKA localisation. As previously shown for other cell lines evidence shows that the up-regulation of the cAMP/PKA pathway is necessary to induce cell cycle entry and DNA synthesis associated with the translocation of the catalytic subunit into the nucleus. Thus, cells entering in G<sub>1</sub> phase display both nuclear and cytosolic PKA activity. Alteration of PKA activity affects the onset of S phase and shortens the G<sub>1</sub> phase (Feliciello et al., 2000).

Analysis of cAMP level and its effect on cell cycle progression as well as the effect of PKA activation or inhibition led to the conclusion that activation of the cAMP/PKA pathway has an anti-mitotic effect and that PKA is responsible for the maintenance of the highly ordered structure of chromatin during interphase (Lamb et al., 1991). By using rat embryonic fibroblasts it has been shown that inhibition of PKA by injection of PKI (a Protein Kinase A Inhibitor) at any stage of the cycle results in pronounced condensation of chromatin and

disassembling of the microtubule network. Moreover these effects can be rapidly reverted by microinjection of the purified catalytic subunit of PKA (Lamb et al., 1991), meaning that basal activity of PKA is constantly required to preserve interphase state. How PKA activity can account for the uncondensed status of chromatin is still unclear, however the idea is that PKA keeps the nucleosome<sup>1</sup> in an open structural conformation whereas inhibition of PKA may lead to a refolding of the nucleosome (Lamb et al., 1991). Accordingly, reduction of cAMP levels or inhibition of PKA leads to increased chromatin condensation and induces cells entry into mitosis (Lamb et al., 1991). Interestingly, it has recently been shown that activation of cAMP signalling by  $\beta$ -adrenergic, forskolin or 8-Br-cAMP stimulation, significantly reduces the percentage of mitotic Histone H3 phosphorylation in a PKA dependent manner (Wu et al., 1986) (Rodriguez-Collazo et al., 2008b). This reduction correlates kinetically with a pre-mitotic cell cycle arrest and with a rapid decrease of Cdk1-CyclinB kinase (MPF) activity (Rodriguez-Collazo et al., 2008b) (Rodriguez-Collazo et al., 2008a). The sensitivity of this effect to cAMP concentration is interesting since the increase of cAMP to induce a maximal loss on H3 phosphorylation is around 10  $\mu$ M ( $EC_{50}=8.9 \mu$ M) whereas 150  $\mu$ M cAMP is required to induce phosphorylation of the cAMP Response Element Binding Protein (CREB) ( $EC_{50}=144 \mu$ M) (Rodriguez-Collazo et al., 2008a).

Many pieces of other evidence suggest that PKA plays a key role in several interphase processes as well as a direct function in preventing the initiation of mitosis. Thus PKA activity has been associated with the maintenance of the nuclear envelope integrity, through the phosphorylation of lamins A and C (Lamb et al., 1990), as well as the organisation of the cytoskeleton by modulating the integrity of actin filaments (Lamb et al., 1988) and organisation of the microtubule network. Although injection of active catalytic subunit in mouse embryo fibroblasts does not show any effect on the

---

<sup>1</sup> A nucleosome is the fundamental unit of the eukaryotic chromatin. It consists on a DNA segment wound around an histone protein core, like a thread wrapped around a spool.

microtubules organisation, inhibition of PKA by PKI results in very pronounced disassembly of microtubules, even though this does not seem to affect spindle formation (Lamb et al., 1991). This evidence suggests that in living fibroblast the microtubule network is dependent on the presence of an active PKA. Interestingly, PKA localises to the microtubules through the binding with the microtubule-associated protein 2 (MAP2) (a family of cytoskeletal proteins predominantly expressed in neurons involved in the stabilisation of microtubules, see section 1.5.1) and AKAP450.

Similarly, studies in oocytes indicated that cAMP and PKA are negative regulators of maturation. Indeed, a drop in basal cAMP levels has been measured during oocytes maturation of starfish, fish, amphibians and mammals. Maturation can also be induced by injection of phosphodiesterases, the enzymes that degrade cAMP thus reducing its intracellular levels, or by inactivation of PKA via injection of PKI and the regulatory subunit of PKA, thereby inhibiting the catalytic activity of PKA. Furthermore in mammalian oocytes PKI and PKA inhibition result in maturation whereas direct activation of PKA or injection of the catalytic subunit shows inhibitory effects on oocytes maturation. Finally, elevation of cAMP levels inhibits or significantly delays oocytes maturation (Lamb et al., 1991).

Further studies of *Xenopus* oocytes provided evidence that maturation required the release of p34<sup>cdc2</sup> (Cdk1 in mammals) from the indirect PKA inhibitory effect. According to this model PKA would phosphorylate cdc25 in interphase, generating a binding site for a 14-3-3 protein that sequesters cdc25 within the cytoplasm. This would prevent translocation of cdc25 to the nucleus where it functions and would keep cdc25 inactive (Schultz, 2009). At the onset of mitosis a decrease in cAMP level and, consequently, PKA inactivation, would result in release and activation of cdc25 that in turn would de-phosphorylate p34<sup>cdc2</sup> kinase promoting oocytes maturation (Grieco et al., 1994). Hence, inhibition of PKA during interphase prematurely activates p34<sup>cdc2</sup> resulting in a premature interphase-mitosis transition. On the contrary, activation of PKA by 8-Br-cAMP prevents p34<sup>cdc2</sup> activation and prolongs interphase (Grieco et al.,

1994). An interesting consequent finding is that the high level of activity of p34<sup>cdc2</sup> reached at metaphase-anaphase transition is necessary to activate the cAMP/PKA pathway, which in turn is required for the activation of APC and the inactivation of p34<sup>cdc2</sup>, establishing in this way a mechanism of feed-back loop regulation (Grieco et al., 1996).

All these indications suggest that fluctuations of cAMP levels are relevant in controlling cellular proliferation.

# 2

## Aim of the thesis

---

A large body of evidence highlights the importance of a functional centrosome for the completion of the cell cycle from one mitosis to another. There is also evidence indicating that cAMP is involved in regulating the entrance and the progression of a cell through the cell cycle. Based on the knowledge that the cAMP/PKA signalling network is compartmentalised and that a macromolecular complex containing PKA and PDE4D3 is nucleated to the centrosome through binding to AKAP450, it is possible to hypothesise that a cAMP/PKA signalling is selectively regulated. The presence of such a specific signalling domain at the centrosome may be required for tight control of the progression of the cell through the cell cycle.

The aim of my project was to study cAMP dynamics in the centrosomal area, to define the role of PDE4D3 anchored to AKAP450 in shaping a centrosomal pool of cAMP and to investigate the functional involvement of the AKAP450/PKA/PDE4D3 macromolecular complex anchored to the centrosome in the progression of the cell cycle.

# 3

## Materials and Methods

---

### 3.1 Molecular Biology

#### *3.1.1 Generation of competent cells*

This protocol allows preparation of batches of bacteria that yield  $5 \times 10^6$  to  $2 \times 10^7$  of transformed colonies per microgram of DNA.

A single colony of TOP10 *E.coli* from a plate freshly grown overnight at 37°C was picked and transferred to 2 ml of sterile 2xYT broth. The cells were grown overnight at 37°C. The next day the culture was used to inoculate 100 ml of sterile 2xYT broth and incubated at 37°C with vigorous shaking (300 rpm) for about 3 hours or until the OD<sub>600</sub> was 0.3-0.4. Particular care was taken to avoid the number of viable cells exceeding  $10^8$  cells/ml; to this purpose the OD<sub>600</sub> was measured every 20-30 minutes.

The culture was transferred aseptically into a pre-cooled 50 ml tube and left to cool down for 30 minutes on ice. Bacteria were then pelleted by centrifuging the culture at 4000 rpm (1617 rotor type for 15/50 ml tubes, speed max 5000 rpm, max RCF 3875 x g) for 10 minutes at 4°C. The

supernatant was discarded and all traces of media were let drain away. The pellet was re-suspended in 10 ml of ice-cold 100 mM CaCl<sub>2</sub> and incubated in ice for 30 minutes. Bacteria were collected once again by centrifugation at 4000 rpm for 10 minutes at 4°C. The supernatant was discarded and all traces of media were let drain away. Each pellet was re-suspended in 2 ml of ice-cold 100 mM CaCl<sub>2</sub> and 10% glycerol (v/v). Cells were finally dispensed into 100 µl aliquots and snap frozen in liquid nitrogen. Competent cells are stored at -80°C.

### ***3.1.2 Bacterial transformation***

Competent cells were thawed on ice. No more than 50 ng of DNA were added per aliquot of competent cells. The tube was swirled gently to mix (avoiding pipetting) and incubated on ice for 30 minutes. Cells were then heat shocked for not more than 1 minute at 42°C without shaking, placed on ice for 1-2 minutes and, after addition of 400 µl of sterile 2xYT media, incubated at 37°C for 30 minutes. Finally the suspension was spread on a pre-warmed LB plate with the appropriate antibiotic(s) for selection (usually ampicillin or kanamycin) and incubated overnight at 37°C.

### ***3.1.3 DNA extraction and purification***

Generally plasmid DNA was extracted and purified from bacterial cultures using the Hispeed Plasmid Maxi kit from QIAGEN (cat. n°12163, QIAGEN), following the manufacturer's instructions. However, in order to obtain large amounts of ultrapure DNA, an alkaline lysis procedure, followed by equilibrium ultracentrifugation in caesium chloride-ethidium bromide gradients was also utilised. Briefly, 400 ml of cells containing the plasmid of interest were grown overnight at 37°C. The next day the culture was centrifuged at 6000 rpm (1617 rotor type for 15/50 ml tubes, speed max 5000 rpm, max RCF 3875 x g) for 8 minutes. The pellet was re-suspended in a lysozyme and glucose buffer (20 mg lysozyme per ml of glucose buffer: 50 mM glucose, 25 mM Tris-HCl pH 8, 1 mM EDTA) containing 20 mg/ml of RNase A, incubated on ice for 10 minutes and then treated with alkaline detergent (0.2 N NaOH, 1% SDS). Solubilised membranes and proteins were precipitated with

potassium acetate solution (3 M KOAc, pH 5.5). The lysate was then cleared first by filtration of the precipitate through gauze and then by centrifugation at 8000 rpm (1617 rotor type for 15/50 ml tubes, speed max 5000 rpm, max RCF 3875 x g) for 8 minutes. The supernatant containing the DNA was precipitated with 3/5 volume of isopropanol, collected by centrifugation at 10000 rpm (1617 rotor type for 15/50 ml tubes, speed max 5000 rpm, max RCF 3875 x g) for 5 minutes. The pellet was re-suspended in a solution containing 1 gr/ml of caesium chloride and 500 µg/ml of ethidium bromide in Tris-EDTA, loaded into a polyallomer tube and ultra-centrifuged at 57000 rpm (NVT65 rotor type for 13.5 ml tubes, speed max 65,000 rpm, max RCF 402,000 x g) at 20overnight. After ultra-centrifugation the DNA band could be visualised under long wave UV light. Usually, if more than a band is visualised the lower band corresponds to the plasmid DNA whereas the upper band is genomic DNA. The plasmid DNA (lower band) was removed with a 5 ml syringe and dialysed against TE buffer for three hours. Finally the DNA was extracted with phenol-chloroform, precipitated with NaOAc 3N pH 4.8 and cold ethanol and re-suspended in TE 0.1X.

### **3.1.4 mRNA extraction**

Cells (about  $4 \times 10^6$ ) were seeded in a 10 cm tissue culture dish and grown for 48 hours. Total mRNA was extracted with TRIzol® Reagent (cat. n°15596026, Invitrogen). After a wash with D-PBS the cells were lysed with 1 ml of TRIzol® Reagent, directly added into the dish, collected with a scraper and homogenised by passing several times through a 1 ml syringe and a 26 gauge needle. Insoluble material was removed from the homogenate by centrifugation at 12000 rpm in a bench top centrifuge for 10 minutes at 4°C. At this point the pellet contains membranes and high molecular weight DNA, whereas the supernatant contains the RNA. The cleared supernatant was transferred to a new tube, 200 µl of chloroform added, shaken vigorously and incubated for 5 minutes at room temperature. After incubation the sample was centrifuged at 12000 rpm for 15 minutes at 4°C. Following centrifugation, the mixture separated into a lower red, phenol-chloroform phase, an interphase,

and a colourless upper aqueous phase (about 600  $\mu\text{l}$ , 60% of the volume of TRIzol® Reagent used for homogenisation). RNA remains exclusively in the aqueous phase. The aqueous phase was transferred to a fresh tube, 500  $\mu\text{l}$  of isopropanol added and incubated for 10 minutes at room temperature to precipitate RNA. RNA was collected by centrifugation at 12000 rpm for 10 minutes at 4°C. The RNA pellet was washed with 1 ml of 70% EtOH (v/v) in sterile water and centrifuged at 10000 rpm for 10 minutes at 4°C. Finally the RNA was briefly dried under vacuum and re-suspended in RNase-free sterile water

### **3.1.5 Nucleic acid quantification**

DNA and RNA concentration was determined using a PerkinElmer LambdaBio+ Spectrophotometer (cat. n°L7110186) and the Lambert-Beer law which relates the absorption of light ( $A$ ) to the properties of the material through which the light is travelling (extinction coefficient,  $\epsilon$  [ $\text{mol}^{-1} \text{cm}^{-1}$ ]), the concentration of the absorbing species in solution ( $c$ , mol) and the light path length ( $l$  [1 cm]):

$$A = \epsilon lc$$

The nucleic acid absorption peak is at 260 nm and the average  $\epsilon$  for double-stranded DNA is  $0.020 (\mu\text{g}/\text{ml})^{-1} \text{cm}^{-1}$ . Thus, an optical density (or "OD") of 1 corresponds to a concentration of 50  $\mu\text{g}/\text{ml}$  for double-stranded DNA. It is important to consider the dilution factor so that the formula to use will be:

$$\text{DNA concentration } \left( \frac{\mu\text{g}}{\mu\text{l}} \right) = \frac{A_{260} \times 50 \times \text{dilution factor}}{1000}$$

Proteins are the major contaminants of DNA. Since the absorption peak of proteins is at 280 nm the ratio  $A_{260}/A_{280}$  has been used to evaluate the purity of the sample. Pure DNA preparations have an  $A_{260}/A_{280}$  ratio of 1.8.

RNA quantification was performed using the same formula used for DNA.  $\epsilon$  for single strand RNA is  $0.027 \text{ (mg/ml)}^{-1} \text{ cm}^{-1}$ . Moreover pure RNA preparations have an  $A_{260}/A_{280}$  ratio of 2.

### ***3.1.6 cDNA preparation***

An aliquot of total mRNA was reversed transcribed with 1  $\mu\text{l}$  SuperScript™ II RT 2000U/ $\mu\text{l}$  (cat. n°18064022, Invitrogen). Briefly, 1  $\mu\text{g}$  mRNA was mixed with 0.5  $\mu\text{g}$  oligo (dT)<sub>12-18</sub> primer (cat. n°18418, Invitrogen) to a final volume of 10  $\mu\text{l}$  in water and incubated at 70°C for 10 minutes. After incubation the tube was quickly transferred on ice for 10 minutes. A mix containing 1  $\mu\text{l}$  RNAout™ (40 U/ $\mu\text{l}$ , Ribonuclease Inhibitor, cat. n° 10777019, Invitrogen), 1  $\mu\text{l}$  100 mM dNTPs (cat. n° 10297018, Invitrogen) 4  $\mu\text{l}$  5x first strand buffer, 2  $\mu\text{l}$  of 0.1 mM dithiothreitol (DTT) and 1  $\mu\text{l}$  SuperScript™ II was then prepared, added to the tube and brought to a final volume of 20  $\mu\text{l}$  with sterile water. The tube was incubated in a thermocycler at 42°C for 45 minutes. A final incubation step at 70°C for 10 minutes was required to inactivate the reaction.

### ***3.1.7 PCR and DNA purification***

PCR products were precipitated with 2.5 volumes of 95% EtOH (v/v) and 1/10 volume of 3N NaOAc pH 4.8 for 30 minutes at -80°C and a 30 minute spin at 14000 rpm in a bench top centrifuge. The pellet was washed with 70% EtOH (v/v) and re-suspended in an appropriate volume of sterile water.

Digested DNA was separated on an agarose gel, the bands of interest cut out with a sterile scalpel and purified with the QIAquick Gel Extraction kit (cat.

n°28706, QIAGEN) following the manufacturer's instruction. DNA was eluted from the spin column by using 65°C pre-warmed sterile water to promote and increase DNA elution rate.

### **3.1.8 De-phosphorylation reaction**

Digested vectors were incubated with Shrimp alkaline phosphatase (SAP) (cat. n°11758250001, Roche) for 10 minutes at 37°C, according to the manufacturer's instruction, in order to remove the free phosphate group from the 5' end and prevent re-circularisation.

### **3.1.9 Restriction enzymes and Ligation**

All restriction enzymes were purchased from New England Biolabs. Digestion reactions were performed by mixing from 3 to 5 µg of DNA with the required restriction enzymes and the specific buffer solution. The mix are then incubated at 37°C for at least 1h. Each restriction enzyme required a buffer solution that contains the unique mix of cations and other components that aid the enzyme in cutting as efficiently as possible. Moreover they also have different optimal temperatures under which they function. For this reason it is important to follow the manufacturer's instruction.

For ligation reactions T4 DNA ligase (cat. n°M0202, New England Biolabs) or the Rapid DNA Ligation kit (cat. n°11635379001, Roche) were used. Insert and plasmid were quantified on an agarose gel by comparing the band intensity to a known DNA standard and combined at a 1 to 3 plasmid to insert ratio. A reaction containing all components but the insert was always included in the experiment as a negative control.

### **3.1.10 Sub-cloning of RII-CFP in pCDNA3.1/Zeo (+)**

The CFP tagged regulatory subunit (RIIβ) of PKA (Lissandron et al., 2005) was sub-cloned into pCDNA3.1/Zeo (+), which contains the Zeocin™ resistance gene for selection in both *E.coli* and mammalian cells in the presence

of the antibiotic Zeocin™. RII $\beta$ -L20-CFP was inserted in the NheI and XbaI sites of the multiple cloning site of pCDNA3.1/Zeo (+).

### **3.1.11 Sub-cloning of C-YFP in pCDNA3**

The YFP tagged catalytic subunit of PKA was inserted in the HindIII-XbaI sites of the multiple cloning site of pCDNA3. This plasmid contains a gene coding for resistance to Geneticin® (G418 Sulphate, neomycin) for mammalian selection.

### **3.1.12 Generation of RII\_epac**

The RII\_epac sensor was generated by fusion of the dimerisation docking domain of RII $\beta$  (49 aa) to the N-terminus of the Epac1-camps FRET-based sensor (Nikolaev et al., 2004). Between the docking domain and the Epac1-camps sensor a 26 amino-acid linker (A (EAAAK)<sub>5</sub>) has been inserted (Di Benedetto et al., 2008). The functional role of this linker is to prevent steric hindrance between the two hetero-functional domains.

The sensor is cloned into pCDNA3 and thus contains the gene encoding for resistance to Geneticin® (G418 Sulphate, neomycin) for mammalian selection.

### **3.1.13 Generation of RII-RFP**

RII-RFP (Di Benedetto et al., 2008) was constructed by substituting the CFP in the RII $\beta$ -L20-CFP construct with mRFP (monomeric red fluorescent protein) (Lissandron et al., 2005).

### **3.1.14 Generation of SuperAKAP-IS and RIAD**

The constructs containing the cDNA for SuperAKAP-IS and RIAD (Di Benedetto et al., 2008) were generated in the lab by external PCR using the SuperAKAP-IS-GFP and the RIAD-GFP constructs as a template (kindly provided by Prof John D. Scott, Howard Hughes Medical Institute, Department of Pharmacology, University of Washington School of Medicine, Seattle, USA).

### **3.1.15 Generation of AKAP450-2 fragment and mutAKAP450-2 fragment**

The fragment from amino acid 933 to amino acid 1804 encoded by the AKAP450 cDNA (DDBJ/EMBL/GenBank accession N AJ131693) was a kind gift from Prof Kjetil Taskén, (The Biotechnology Centre of Oslo and Centre for Molecular Medicine Norway, Nordic EMBL Partnership, University of Oslo, Oslo, Norway). This fragment was amplified by using the primers: AKAP450-2\_NheI\_frw: 5'-CTAGCTAGCATGGTTGTTGAAAAGGATACA-3' and AKAP450-2\_BamHI\_rev: 5'-CGGGATCCTTACATATCACTTCCAGAATAA-3' and inserted into the NheI-BamHI sites of the multiple cloning site of pcDNA3.1/Hygro (+).

For the mutAKAP450-2 fragment the point mutation S1451P was introduced, using the QuickChange™ Site-directed Mutagenesis Kit (cat. n°200518, Stratagene) as described by the manufacturer with the primers: AKAP450-2\_mut\_frw: 5'-GAAGAAGTAGCTAAGGTTATTGTGCCAATGAGTATAGCATTTGC-3' and AKAP450-2\_mut\_rev: 5'-CTTCTTCATCGATTCCAATAACACGGTTACTCATATCGTAAACG-3'.

### **3.1.16 Generation of $\Delta$ PKA-GFP**

The fragment from amino acid 50 to amino acid 419 of RII $\beta$  was amplified by PCR and substituted for the full length RII $\beta$  of the RII $\beta$ -L20-CFP construct (Lissandron et al., 2005).

### **3.1.17 AKAP79 and AKAP149**

These plasmids were kindly provided by Prof Kjetil Taskén, (The Biotechnology Centre of Oslo and Centre for Molecular Medicine Norway, Nordic EMBL Partnership, University of Oslo, Oslo, Norway).

### **3.1.18 Generation of the Rt31 fragment**

Rt31 in pGEX4T3 was a kind gift from Dr Enno Klussmann, (Leibniz Institute for Molecular Pharmacology, Berlin, Germany). The fragment from

amino acid 1 to amino acid 940 was amplified by using the following pair of primers: Rt31\_2-19\_frw: 5'-CCGGAATTCATGGCACGAGAAACAACGCGA-3' and Rt31\_1659-1678\_rev: 5'-CGCCGCTCGAGTTACCTGTTTAACTTTGACGTCTG-3'; and inserted into the EcoRI-XhoI sites of the multiple cloning sites of pIRES.

### **3.1.19 Generation of RII\_AKAR3 and GIT1\_AKAR3**

The pcDNA3-AKAR3 sensor was kindly provided by Prof Jin Zhang, (Department of Pharmacology and Molecular Sciences, John Hopkins University School of Medicine, Baltimore, USA). RII\_AKAR3 was generated by inserting the docking domain of RII $\beta$  (1-49aa) in the HindIII site of the multiple cloning site of pcDNA3, in frame with the N-terminus of the original AKAR3.

The fragment from amino acid 1 to amino acid 119 of GIT1 in pXJ40GST (kind gift from Prof Edward Manser and Dr Zhao S. Zhuoshen, GSK-IMCB Group, Institute of Molecular and Cell Biology, Singapore) was amplified using the primers: GIT1\_BamHI\_frw\_long: 5'-CGCGGATCCATGTCCCAGGAAGGGGCCG-3' and GIT1\_BamHI\_rev\_long: 5'-GCGGGATCCAAGCTTGTGCACAAACGCCAGC-3' and inserted into the BamHI site of the multiple cloning site of pcDNA3, in frame with the N-terminus of the original AKAR3.

### **3.1.20 Generation of mutRII-CFP**

The regulatory subunit of the RII $\beta$ -L20-CFP construct was mutated by introducing the mutation S114A using the QuickChange™ Site-directed Mutagenesis Kit (cat. n°200518, Stratagene) as described by the manufacturer with the primers: RII-P sense 5'-CCGGTTCACAAGGCGTGCCGCGGTATGTGCAGAAGCTTATAATCC-3' and RII-P antisense: 5'-GGATTATAAGCTTCTGCACATACCGCGGCACGCCTTGTGAACCGG-3'.

### **3.1.21 Generation of dnPDE4D3mRFP**

The constructs for dnPDE4D3 was kindly provided by Prof Miles Houslay, (Neuroscience and Molecular Pharmacology, Wolfson Link & Davidson Buildings, University of Glasgow, Glasgow, UK). dnPDE4D3 contains

the mutation D484A that render it catalytically inactive (McCahill et al., 2005). The insert was amplified by PCR using the primers: PDE4D3\_BstXI\_frw: 5'-CACTAGTCCAGTGTGGTGGATGATGCACGTGAATAATTTTCC-3' and PDE4D3\_BstXI\_REV: 5'-GCAGAATTCCACTGTGCTGGCGTGTTCAGGAGAACGATCATCT-3' and sub-cloned into the BstXI site of the multiple cloning site of pcDNA3.1/Hygro (+). The monomeric red fluorescent protein was then inserted into the XhoI-XbaI restriction sites of the multiple cloning sites of pcDNA3.1/Hygro (+), in frame with the C-terminus of dnPDE4D3.

### **3.1.22 *dnPDE4A4-GFP***

dnPDE4A4 in pCDNA3 was a kind gift from Prof Miles Houslay (Neuroscience and Molecular Pharmacology, Wolfson Link & Davidson Buildings, University of Glasgow, Glasgow, UK). dnPDE4A4 contains the mutation D591A that render it catalytically inactive (McCahill et al., 2005).

## **3.2 Cell Biology**

### **3.2.1 *Cell culture and transfection***

#### **3.2.1.1 CHO cells**

CHO-K1 cells from Hamster Chinese ovary (Puck et al., 1958) are characterised by an epithelia morphology and adherent growth mode.

Cells were grown in Ham's F-12 medium (cat. n°21765-029, Invitrogen) supplemented with FBS (cat. n°10270106, Invitrogen) 10% v/v, 2 mM L-glutamine (cat. n°25030-024, Invitrogen), 100 U/ml penicillin and 100 µg/ml streptomycin (cat. n°P07081, SIGMA) at 37°C in a humidified atmosphere containing 5% CO<sub>2</sub>.

#### **3.2.1.2 SH-SY5Y cells**

SH-SY5Y cells from human neuroblastoma (Biedler et al., 1978) are characterised by a neuroblast morphology and adherent growth mode.

SH-SY5Y is a thrice cloned sub-line of the SK-S-SH line derived from bone marrow biopsy (Biedler et al., 1973).

Cells were grown in Ham's F-12:EMEM (cat. n°42430-025, Invitrogen) (1:1) supplemented with FBS 10% (v/v), 2 mM L-glutamine, non essential amino acids (cat. n°11140-035, Invitrogen) 1% (v/v), 100 U/ml penicillin and 100 µg/ml streptomycin at 37°C in a humidified atmosphere containing 5% CO<sub>2</sub>.

### **3.2.1.3 Thawing of cells**

Cells were thawed in a water bath at 37°C and added drop wise to 5 ml of pre-warmed medium, spun for 5 minutes at 1200 rpm (TTH-750 rotor type, speed max 4600 rpm, max RCF 4,570), re-suspended in fresh medium and seeded in a 75 cm<sup>2</sup> flask containing 10 ml of the appropriate medium.

### **3.2.1.4 Freezing of cells**

Cells were trypsinised (trypsin-EDTA 0.05%, cat. n°25300-054, Invitrogen), spun for 5 minutes at 1200 rpm (TTH-750 rotor type, speed max 4600 rpm, max RCF 4,570), re-suspended in 3 volumes of FBS and 1 volume of freezing solution (DMEM, glucose 12% (w/v) and DMSO 40% (v/v)) added drop wise. Cells were then dispensed into 2 ml cryo vials and transferred to -80°C for 24h. Cells were then stored in liquid nitrogen tank.

### **3.2.1.5 Cell transfection**

Approximately 3x10<sup>5</sup> cells/well were plated on a 6-well plate in complete medium and grown for 24 hours. The transfection mix was prepared as follows: 6 µl/well of TransIT®-LT1 Reagent (cat. n°M2300, Mirus) was added drop wise to 100 µl/well of serum-free DMEM and incubated for 5 minutes at room temperature. After incubation 2-4 µg of DNA and/or 125 pmol of small interference RNA were added to the diluted TransIT®-LT1 Reagent and incubated for 15 minutes at room temperature. The TransIT®-LT1 Reagent-DNA complex was finally added drop wise to the cells. Experiments were performed 24-48 hours after transfection.

## **3.2.2 Stable clone selection**

### **3.2.2.1 Antibiotics**

Zeocine™ (cat. n°450003, Invitrogen), Geneticin® (G418 Sulphate, neomycin) (cat. n°V7983, Promega) and Hygromycin B (cat. n°10 843 555 001, Roche).

### **3.2.2.2 Dose-response curve**

#### Zeocine™

To test the sensitivity of CHO cells to Zeocine™, a dose-response curve has been performed, as natural resistance to antibiotics varies among cells lines. Approximately  $3 \times 10^4$  cells/well were plated and grown for 24 hours in a 24 well plate. After 24 hours the medium was removed and replaced with medium containing increasing concentrations of Zeocine™ (0, 50, 100, 200, 400, 600, 800 and 1000  $\mu\text{g/ml}$ ). Every concentration was tested in duplicate. After 12 days of treatment a concentration of 300  $\mu\text{g/ml}$  of Zeocin™ was selected as the minimum amount of antibiotic required for selection of stable clones.

#### Geneticin® (G418 Sulphate, neomycin)

Approximately  $3 \times 10^4$  cells/well of CHO cells stably expressing RII-CFP were plated in a 24 wells plate. After 24 hours of incubation medium was replaced with media containing increasing concentration of Geneticin® (G418 Sulphate, neomycin) (0, 100, 200, 300, 400, 500, 600, 700, 800, 900, 1000 and 1100  $\mu\text{g/ml}$ ). After 12 days of incubation a concentration of 800  $\mu\text{g/ml}$  was determined as the minimum amount of antibiotic necessary to select against untransfected cells.

#### Hygromycin B

Approximately  $3 \times 10^4$  cells/well of CHO cells were plated in a 24 well plate. After 24 hours of incubation medium was replaced with medium containing increasing concentration of Hygromycin B (0, 100, 200, 300, 400, 500, 600, 700, 800, 900, 1000 and 1100  $\mu\text{g/ml}$ ). After 12 days of incubation a

concentration of 700 µg/ml was determined as the minimum amount of antibiotic necessary to select against untransfected cells.

### **3.2.2.3 Stable clone selection**

#### **3.2.2.3.1 *CHO stably expressing PKA-GFP***

Two 3 cm tissue culture dishes were seeded with approximately  $10^5$  CHO cells per dish. 24 hours later one of the two dishes was transfected (see section 3.2.1.5) with pcDNA3.1/Zeo(+)-RII-CFP subunit. The following day medium in both dishes was replaced with medium containing 300 µg/ml of Zeocine™ and plates were incubated for an additional 12 days. During this period medium was replaced every 2 days with fresh medium. After 12 days non-transfected CHO cells had died whereas the transfected cells were starting to form foci. Colonies were then picked with a 200 µl tip, limit diluted (dilution 1 to 7 cells to well ratio), transferred into 96 well plates and grown until confluent. A single clone expressing high levels of RII-CFP was selected according to the brightness of the cells under an epifluorescence microscope upon excitation at 430 nm.

Approximately  $10^5$  of CHO cells stably over-expressing RII-CFP subunit were plated in two 3 cm tissue culture dishes. After 24 hours one of the two dishes was transfected with pcDNA3 C-YFP. Selection with 800 µg/ml of Geneticin® (G418 Sulphate, neomycin) was carried out analogous to the Zeocine™ selection. After limited dilution™ in a 96 well plate cells stably expressing both RII-CFP and C-YFP subunit were selected at the microscope upon direct excitation of CFP and YFP at 430 nm and 500 nm respectively.

Where necessary a further limited dilution has been performed.

#### **3.2.2.3.2 *CHO-RII\_epac and SH-SY5Y-RII\_epac***

As described for the selection of CHO cells stably expressing PKA-GFP, approximately  $10^5$  of CHO or SH-SY5Y cells were plated and transfected after 24 hours with the RII\_epac sensor. The following day medium was replaced with fresh medium containing 800 µg/ml or 500 µg/ml (Jang and Juhn, 2001)

of Geneticin® (G418 Sulphate, neomycin) for CHO and SH-SY5Y cells respectively. A control sample of untransfected cells was included in each experiment. After 12 days of treatment cells were limit diluted and transferred to a 96 plate. Cells stably expressing the RII\_epac sensor were selected at the microscope according to their brightness upon direct excitation of CFP and YFP at 430 and 500 nm, respectively.

### **3.2.2.3.3 CHO-dnPDE4D3mRFP and CHO-dnPDE4A4-GFP**

Approximately  $10^5$  of CHO cells were plated and transfected after 24 hours with dnPDE4D3mRFP or dnPDE4A4-GFP. The following day medium was replaced with fresh medium containing 700 µg/ml of Hygromycin B or 800 µg/ml of Geneticin® (G418 Sulphate, neomycin) for cells transfected with the dnPDE4D3mRFP or with the dnPDE4A4-GFP respectively. A control sample of untransfected cells was included for each antibiotic used. After 12 days of treatment cells were limit diluted and transferred to a 96 plate. Cells stably expressing the dnPDE4D3mRFP or the dnPDE4A4-GFP were selected at the microscope according to their brightness upon direct excitation of RFP at 568 nm or GFP at 500 nm.

A further verification of the clones was carried out by retro-transcription (see section 3.1.6) of total RNA extracted (see section 3.1.4) from the CHO-dnPDE4D3mRFP cells and amplification of the coding regions of dnPDE4D3mRFP using specific primers annealing on the D484A mutation (McCahill et al., 2005). Primers used are the following: PDE4D3frw911: 5'-GGTAACCGGCCCTTGACTG-3' and PDE4D3frw1510\_wild\_asp: 5'-GGTTCTTCAGAATATGGTGCAGAT-3' for the PDE4D3 wild type amplification; and PDE4D3frw911: 5'-GGTAACCGGCCCTTGACTG-3' with PDE4D3frw1510\_mut\_ala: 5'-GGTTCTTCAGAATATGGTGCAGCA-3' for dnPDE4D3 amplification.

## **3.2.3 PDE4D knock-down**

Knock down of PDE4D was achieved by using a small interfering RNA oligonucleotide targeting the PDE4D gene (125nM final concentration)

(sequence: GAACUUGCCUUGAUGUACA, Thermo scientific Dharmacon) as previously described (Lynch et al., 2005). CHO cells were transfected using TransIT®-LT1 Reagent following the supplier's instructions (see section 3.2.1.5). Control experiments were carried out using siGLO® Red transfection indicator (125 nM) (cat. n°D-001630-02-20, Thermo scientific Dharmacon).

### 3.3 FRET based analysis of cAMP

Fluorescence resonance energy transfer occurs when two chromophores, a donor and an acceptor, with the appropriate distance, orientation and spectral properties are close enough for resonance energy transfer from the donor to the acceptor upon direct excitation of the donor (see section 1.6.3.2).

Generally a FRET-based sensor for cAMP consists of a cAMP binding domain, which undergoes conformational changes upon cAMP binding, genetically fused to cyan fluorescence protein and yellow fluorescent protein. When cAMP concentration is low the two fluorophores are close enough for FRET to occur. Excitation of CFP (430 nm) results in the transfer of part of its excited-state energy to YFP that can in turn emit at its own emission wavelength (545 nm). Both CFP and YFP emission are collected.

As far as the FRET-based sensors for cAMP used for this research are concerned the mechanism of activation is the following. When the intracellular cAMP concentration increases, the activation of the sensor and the subsequent conformational change will affect the distance and the orientation of the two fluorophores thereby decreasing the efficiency of energy transfer. In this situation YFP is too far to be excited and only CFP emission (480 nm) can be detected upon CFP excitation. Changes in FRET correlate with changes in cAMP concentration.

FRET changes are measured as changes in the ratio between 480 nm/545 nm upon excitation at 430 nm and expressed as the percentage of

increase of 480 nm/545 nm emission over the basal value of 480 nm/545 nm emission at the beginning of the experiment.

### **3.3.1 Imaging set up**

A system for FRET imaging of cAMP in cultured live cells comprises of a wide field fluorescence microscope, a light source for excitation of CFP, a beam splitter or a filter wheel for simultaneous collection of CFP and YFP emission signals separately onto a digital camera and a computer to store the acquired images and to analyse the data.

The characteristics of the FRET imaging system I used for the experiments presented here are as follows:

Microscope: Olympus IX81 inverted microscope.

In principle, both inverted and upright microscopes can be used for FRET imaging. Generally an inverted microscope is more flexible, since it allows to easily access to the sample for compound addition as well as insertion of manipulators or microelectrodes.

Light source: Xenon Mercury mixed gas arc burner Intense peaks at 365, 405, 436, 546, and 577 nm (MT-ARC/HG LG2076, Ushio).

Generally excitation light must fall into the spectral window where CFP is excited selectively. The appropriate spectral range of excitation is between 430 and 440 nm and such excitation can be obtained either with a monochromatic source or with a conventional mercury or xenon bulb. While monochromators can be tuned to the appropriate excitation wavelength, mercury or xenon bulbs need to be coupled to an appropriate long band-pass filter in excitation. Filter manufacturers (Chroma, Omega optical) provide filter sets with exciter, dichroic and emitter that are optimised for FRET measurements with CFP and YFP.

Excitation Filters: CFP: excitation filter ET436/20x, dichroic mirror T455LP, (Chroma Technology). The filter ET436/20x transmits all

wavelengths above 436 nm to the dichroic mirror that reflects wavelength below 455 nm to the sample therefore exciting CFP at 430 nm. This dichroic also transmits wavelength longer than 455 nm to the beam splitter, thereby allowing emission of CFP at 480 nm and YFP at 545 nm to be separated. YFP: excitation filter ET500/30x, dichroic mirror T515LP (Chroma Technology).

Emission Filters: CFP: emission filter ET480/40m; YFP: emission filter ET535/30m beam splitter: dichroic mirror 505DCLP, YFP emission 545 nm, CFP emission 480 nm (all from Chroma Technology).

A beam splitter is an optical device that allows simultaneous collection of CFP and YFP emission images on the two halves of the chip of the digital camera. This device mounts a dichroic filter and two band-pass filters, within a single apparatus and is commercially available (Micro imager, Optical Insight). When light emitted by the samples reaches the dichroic filter it is split into two beams. Wavelengths shorter than 505 nm, including CFP emission at 480 nm, are reflected towards the CFP emission filter whereas wavelength longer than 505 nm, including YFP emission at 545 nm, are transmitted and directed to the YFP filter.

Alternatively, different solutions can be adopted to collect CFP and YFP emission separately. One possibility is to use a motorised, software controlled filter wheel that contains emission filters for CFP and YFP. In this case, each time point of the FRET measure is composed of two sequential pulses of excitation and acquisition of two sequential images, each with a different emission filter. Such a solution is flexible, since the same setup can mount several filters and can be used to image other fluorescent indicators and probes. On the other hand, CFP and YFP emission images will necessarily be collected with a delay, depending on the time required for the wheel to switch between the two. This problem is often negligible, but it might introduce artefacts in case the sample or the focal plane move during the lag time between the acquisition of the CFP and YFP images. Also, the total time required for the acquisition of each time point is doubled leading to increased photo-damage and hindering imaging at fast acquisition rates.

Albeit very expensive, another possible strategy is to equip the microscope with a dichroic filter to separate CFP from YFP emission channels that are then collected with two separate digital cameras.

*Objective:* PlanApoN 60X/1.42 oil  $\infty$ /0.17/FN26.5

High NA optics allows to collect emission light efficiently with high resolution.

*Camera:* ORCA AG (model C4742-80-12AG, Hamamatsu Photonics K.K., Made in Japan) and HAMAMATSU camera controller.

A high sensitivity cooled charge-coupled-device (CCD) camera is usually preferred.

*Image acquisition and analysis:* All the devices of the imaging system, such as the shutter on the excitation beam path, the motorised filter wheel (if present), and the digital camera must be software-controlled.

Several commercial software packages are available and generally they allow image acquisition and offline image analysis and data processing. Image analysis can also be optimally performed with freely available open source software programmes (i.e. ImageJ, National Institutes of Health; Bethesda) (Evellin et al., 2004), (Mongillo et al., 2005), (Berrera et al., 2008).

### **3.3.2 FRET experiment**

CHO and SH-SY5Y cells stably or transiently expressing a FRET-based cAMP sensor were used to monitor the basal intracellular cAMP concentration and changes in cAMP concentration upon addition of cAMP raising agents.

#### **3.3.2.1 Procedure**

A FRET experiment consists basically of three steps:

1. Sample preparation
2. Data acquisition

### 3. Data analysis

#### **3.3.2.2 Sample preparation**

48 hours before FRET analysis cells are seeded on a 24 mm cover-slip at 30% confluence.

24 hours later cells will reach 60% of confluence and are ready to be transfected with the appropriate cAMP FRET-based sensor (see section 3.2.1.5).

Cells were imaged 24 hours after transfection. The cover-slip is mounted in ring metal slide holders sealed at the bottom that allow addition of stimuli directly to the bath (Figure 3-1). CHO cells were maintained in D-PBS solution (cat. n°14190-094, Invitrogen) at room temperature (20-22°C) whereas experiments on SH-SY5Y cells were performed in Hank's buffered salt solution (HBSS: 137 mM NaCl, 5mM KCl, 0.6mM Na<sub>2</sub>HPO<sub>4</sub>, 5.5mM glucose, 20 mM HEPES, 1.4 mM CaCl, pH 7.4) at room temperature (20-22°C).



**Figure 3-1 Representation of the slide holder used for live fluorescence imaging experiments.**

#### **3.3.2.3 Data acquisition**

Before starting the actual time-course experiment a standard protocol for all series of experiments has to be designed with respect to exposure time, frequency of acquisition, number of acquisitions and camera binning.

### **3.3.2.3.1 Exposure Time**

This is the time during which the sample is illuminated and the camera acquires CFP and YFP signals. Optimal exposure time depends on the expression levels of fluorophores as well as the characteristics of the lamp, the optics and the camera. Usually the exposure time is between 50 and 300 ms according to the brightness of the sample to be imaged. A good rule of thumb is to aim at generating images with signal to noise ratio  $>3$ . Experiments in this thesis have been acquired with a 200 ms exposure time.

### **3.3.2.3.2 Setting the Time course and Number of Acquisitions**

The frequency of acquisition corresponds to the time between two consecutive acquisitions. Normally it is between 2 and 60 seconds and depends on the sensor characteristics and the kinetics expected. Shorter intervals have to be used for rapid and transient responses. During this interval the shutter controlling the incident light has to be closed to avoid photo-damaging of cells and photo-bleaching of the fluorophores. For the experiments presented here the frequency of acquisition was 10 sec.

### **3.3.2.3.3 Camera Binning**

Camera binning is the process through which a CCD (charged-coupled device) camera clocks multiple pixel charges into a single larger super-pixel. This super-pixel represents the area of all individual pixels contributing to the charge. A binning of 1x1 means that each individual pixel is used as such whereas a binning of 2x2 means that an area of 4 adjacent pixels is combined into one larger pixel, and so on. This process can improve the signal to noise ratio at the expense of spatial resolution. For example, in the case of 2x2 binning there is a four-fold increase in signal (the four single pixel contributions), a two-fold loss in resolution and a two-fold improvement in signal-to-noise ratio.

Experiments in this thesis have been acquired with binning 1x1.

At this point it is possible to run the actual experiment and record the time-course.

During the experiments the chosen cell is excited at 430 nm (CFP excitation wavelength, donor) and the emission of CFP (480 nm) and YFP (545 nm, acceptor) are collected by the camera on the two halves of the camera chip.

Most packages of software allow the live display of the mean fluorescence intensity of each channel as well as the ratio (480 nm/545 nm) changes. Following these kinetics it is possible to estimate when the ratio signal is stable (normally after about 20 acquisitions). Once the signal is stabilised it is possible to add the stimulus to the cells in order to perturb the intracellular cAMP concentration. Further stimuli can be added to the cell every time a new plateau has been reached.

#### **3.3.2.4 Data analysis**

After data acquisition, the collected images are software-processed.

Our set up is equipped with a beam-splitter. This means that the FRET experiment is stored as a stack of images combining the information for CFP and YFP fluorescence intensity changes.

The first step of the analysis is to split and align CFP and YFP images, in order to obtain two distinct and super-imposable movies (one each intensity channel).

The second step is to draw regions of interest (ROIs) on the background and in the cells (different cell compartments can be analysed by drawing different ROIs) (Figure 3-2). Figure 3-2 shows how cytosol and centrosome within the same cell have been analysed for FRET changes in the experiments presented in this thesis.

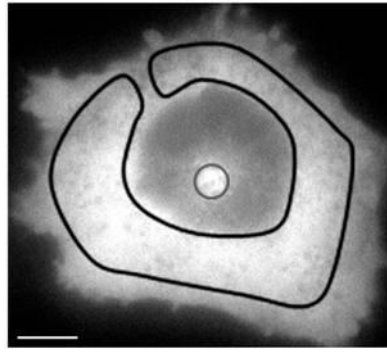


**Figure 3-2** CHO cell stably expressing the PKA-GFP sensors. Black line represents a typical region of interest (ROI) drawn on the cytosol; grey line represents a typical region of interest (ROI) drawn around the centrosome. Bar 10  $\mu\text{m}$ .

At this point mean intensities values are calculated for each ROI from both stacks (CFP and YFP). Numerical values, exported in excel, are processed in this way:

1. The background noise is subtracted (mean intensity value of the ROI drawn on the background) from each mean intensity value of the ROIs drawn inside the cell, both for CFP and YFP intensity. This operation serves to remove the out-of-the-cell fluorescence and the intrinsic electronic noise of the camera, reducing artefacts and increasing the dynamic range of the measurement.

2. The ratio (R) between CFP and YFP mean intensity values is calculated for each frame. The value of each pixel in the ratio movie corresponds to the CFP/YFP ratio in the corresponding pixels of the raw images. Such a ratio-metric movie is normally displayed in pseudo-colour, according to a user-defined lookup table that assigns a different colour to each ratio value.

3. The kinetic of the ratio is plotted and the FRET change is calculated as follows:

$$\% \frac{\Delta R}{R_{(t_0)}} = \frac{R_{(t_1)} - R_{(t_0)}}{R_{(t_0)}} \times 1000$$

Where  $R_{(t_0)}$  corresponds to the basal FRET level and mathematically is the average of all ratio values before the addition of the stimulus; whereas  $R_{(t_1)}$  is the average of the five data points after the plateau is reached for the corresponding stimulus.

Ratio-metric calculation helps to correct for focus changes and for unequal distribution of the probe, as well as for bleaching of the fluorophores occurring during the time course experiment. However, FRET changes can be considered reliable only when donor and acceptor emission kinetics are divergent, i.e. an increase in CFP emission must be accompanied by a decrease in YFP emission.

A fundamental problem of wide-field fluorescent microscopy is the partial overlapping of excitation and emission spectra. As a consequence the FRET signal will always be affected by direct excitation of the YFP acceptor at the donor CFP excitation wavelength and by CFP emission into the YFP channel.

When static FRET (i.e. basal FRET ratio) instead of dynamic FRET changes have to be assessed it is possible to generate a correction curve to clean up the signal and increase the differences. Direct excitation of YFP at the CFP excitation wavelength can be quantified by the ratio between emission at 545 nm upon excitation at 430 nm and 500 nm of cells over-expressing YFP only. The “bleed-through” of CFP emission into the YFP channel instead can be estimated as the ratio between YFP and CFP emission channel intensity in cells expressing CFP only, on excitation of CFP. In our system about 50% of CFP emission bleeds through into the YFP channel.

In this thesis numerical values of the basal FRET ratio measured in the cytosol ( $R_{0\text{cyt}}$ ) and at the centrosome ( $R_{0\text{centr}}$ ), and presented in chapter 4, were

expressed as normalised as respect to the cytosol basal FRET ratio value ( $R_{0\text{cyt}}$ ). Thus the plotted values are:

$$\frac{R_0}{R_{0\text{cyt}}}$$

### **3.3.2.5 Statistics**

Data are presented as mean  $\pm$  standard error (SEM). Two tailed paired and un-paired Student's t-tests were used to determine significance between groups. One-way ANOVA test was used to compare means from multiple samples. Number of replicates and the type of Student's t-test used are indicated in the text. Asterisks are used to indicate levels of significance based on p-values: \*  $p < 0.05$ ; \*\*  $0.05 < p < 0.01$ ; \*\*\*  $p < 0.001$ .

### **3.3.3 *Stimuli and reagent***

Forskolin (cat. n°F6886), Rolipram (cat. n°R6526), Cilostamide (cat. n°C7971), EHNA (cat. n°E114), H-89 (cat. n°B1427) were purchased from SIGMA. Caliculyn A (cat. n 1336) was purchased from TOCRIS.

## **3.4 Biochemistry**

### **3.4.1 *Western Blotting***

#### **3.4.1.1 SDS-PAGE (sodium dodecyl sulphate Polyacrylamide gel electrophoresis)**

##### **3.4.1.1.1 *Sample preparation***

CHO cells or PKA-GFP stable clones were seeded on 10 cm tissue culture dishes, treated as indicated and washed twice with ice cold D-PBS before cell lyses.

Cell lysates were prepared in lysis buffer containing 25 mM Hepes, pH 7.5, 2.5 mM EDTA, 50 mM NaCl, 30 mM sodium pyrophosphate, 10% (v/v)

glycerol and 1% (v/v) Triton X-100 (cat. n°106K0177, SIGMA) and Complete™ EDTA-free protease inhibitor cocktail tablets (cat. n°11836170001, Roche). Protein concentration was quantified using the Bradford Protein Assay (cat. n 500-0006, Biorad) (Nguewa et al., 2011). Equal amounts of protein were mixed with lithium dodecyl sulphate sample buffer (LDS, NuPAGE LDS cat. n°NP00084, Invitrogen) and 1, 4-Diothiothreitol (DTT, 100mM) and boiled at 75°C for 10 minutes.

#### **3.4.1.1.2 Gel electrophoresis and immuno-blotting**

Proteins were separated by gradient gel electrophoresis on NuPAGE Novex 4-12% Bis-Tris gels, 1 mm thickness (cat. n°NP0321BOX, Invitrogen), and transferred to Polyvinylidene fluoride (PVDF) membranes (Millipore).

Membranes were then blocked either with Protein-Free T20 (TBS) Blocking Buffer (cat. n°37571, Thermo Scientific) or 5% (w/v) skimmed milk in TBS-T for 1 hour at room temperature.

#### **3.4.1.1.3 Primary Antibodies**

The following antibodies were used to probe the membranes: Purified Mouse Anti-PKA<sub>R11β</sub> (cat. n°610625, BD Transduction Laboratories™), Purified Mouse Anti-PKA<sub>R11β</sub> (pS114) (cat. n°612550, BD Transduction Laboratories™), goat pan-PDE4D (kind gift from Prof Miles Houslay, Neuroscience and Molecular Pharmacology, Wolfson Link & Davidson Buildings, University of Glasgow, Glasgow, UK) and goat Anti  $\gamma$ -tubulin (C-20) (cat. n°sc-7396, Santa Cruz). Primary antibodies were diluted to the appropriate concentration either in TBS-Tween (cat. n°P7949, SIGMA) or in 1% skimmed milk (w/v) in TBS-T and incubated overnight at 4°C.

#### **3.4.1.1.4 Secondary Antibodies**

The species specific secondary antibodies were HRP conjugated.

Secondary antibodies were diluted to the appropriate concentration either in TBS-Tween or in 1% skimmed milk (w/v) in TBS-T and incubated for 1 hour at room temperature.

### **3.4.1.2 Detection and quantification**

Western blots were detected on X-ray film following enhanced chemiluminescent (ECL) reaction (cat. n°P34080, Pierce Protein Research Products). After image scanning, intensity quantification of the bands was performed using ImageJ software (National Institutes of Health, Bethesda). Results, representing the mean of at least three independent experiments, were normalised to the amount of the structure protein  $\gamma$ -tubulin. This practice ensures correction for the amount of total protein on the membrane in case of loading errors or incomplete protein transfers.

## **3.4.2 *Immunostaining and Confocal Imaging***

CHO cells stably expressing PKA-GFP sensor was washed three times with ice cold D-PBS. The centrosome was exposed by treatment with PHEM solution (45 mM Pipes, 45 mM HEPES, 10 mM EGTA, 5 mM MgCl<sub>2</sub>, 1 mM PMSF and 0.1% (v/v) Triton X-100, pH 6.9) for 30 seconds at room temperature. Cells were then fixed with ice cold methanol for 5 minutes at -20°C, washed twice in PBS and saturated in 3% BSA for 30 minutes at room temperature. Primary antibodies were diluted in 3% BSA and incubated over night in a wet chamber. CTR453 (a kind gift from Dr Guy Keryer Institut Curie, Orsay F-91405, France), a centrosome specific monoclonal antibody raised in mouse was used at a 1:5 dilution, rabbit anti-PDE4D3 (kind gift from Prof Miles Houslay, Neuroscience and Molecular Pharmacology, Wolfson Link & Davidson Buildings, University of Glasgow, Glasgow, UK) was used at a 1:500 dilution and goat anti  $\gamma$ -tubulin (C-20) (cat. n°sc-7396, Santa Cruz) was used at 1:2000. Goat anti-mouse AlexaFluor® 568 (cat. n°A11004, Invitrogen), goat anti-rabbit AlexaFluor® 568 (cat. n°A11011, Invitrogen) and donkey anti-goat AlexaFluor® 488 (cat. n°A11055, Invitrogen) were used as secondary antibodies. Control cells were stained for the secondary antibody only.

Confocal images were acquired with a Nikon Eclipse TE300 inverted microscope equipped with a spinning disk confocal system (Ultraview LCI; PerkinElmer), a 60×1.4 NA PlanApo objective (Nikon) and an Orca ER 12-bit CCD camera (Hamamatsu Photonics, Hamamatsu City, Japan). Cells were excited using the 568 nm laser line of a 643 series Argon-Krypton-Laser Melles Griot (643-Ryb-A02; Melles Griot) for imaging of the AlexaFluor568 fluorophore and the 405 nm line of a diode laser (iFlex2000; Point Source) for imaging CFP. The emission filters were 607/45 for the red emission and 480/30 for the cyan emission, respectively.

### **3.5 Flow cytometry scan analysis of cell cycle distribution of a cell population using Propidium Iodide**

This assay exploits the properties of Propidium iodide (PI), a water soluble DNA intercalator, to bind and dye DNA after cell permeabilisation. After staining, cells are analysed on a flow cytometer. The amount of dye correlates with the amount of DNA inside the cell and the relative content of DNA indicates the distribution of a cell population throughout the cell cycle. The content of nuclear DNA changes throughout the cell cycle. Cells in the  $G_0/G_1$  phases of the cell cycle are diploid and have a DNA content of  $2n$ . Cells within the  $G_2/M$  phases have a DNA content of  $4n$ , while S-phase cells have DNA content greater than  $2n$  and less than  $4n$ . Accordingly, cells in  $G_2/M$  will have twice the fluorescence intensity of cells in  $G_1$  and cells in S will have fluorescence values between the  $G_1$  and  $G_2/M$  population. The resulting histogram will show two Gaussian curves, for the  $G_1$  and  $G_2/M$  population respectively, overlapped and connected by the area representing the S-phase population.

Approximately  $10^6$  of cells were grown with or without  $5 \mu\text{M}$  forskolin in a T75 flask for 48 hours. After 48 hours exponentially growing cells were trypsinised, washed twice with D-PBS, and re-suspended in  $300 \mu\text{l}$  of D-PBS.  $700 \mu\text{l}$  of ice-cold 70% (v/v) EtOH/PBS was added drop-wise and the samples

were incubated at 4°C for 1 hour. After incubation cells were spun down (TTH-750 rotor type, speed max 4600 rpm, max RCF 4,570), washed with 1 ml of D-PBS and then re-suspended in 250 µl of D-PBS containing 5 µl of 10 mg/ml RNAaseA (Ribonuclease A cat. n°R6513, SIGMA) and incubated for 1 hours at 37°C. Finally samples were stained with 5 µl of 1 mg/ml of PI (Propidium iodide cat. n°P4864) and kept in the dark at 4°C until analysis.

Flow cytometry scan analysis (FACS) has been done by using a FACSCalibur flow cytometer (Becton Dickinson). 10<sup>4</sup> cells in the FCS/SSC gate were scanned for each sample. No more than 400 events per seconds were collected. The plot of the width versus the area of the pulse (FL2-A versus FL2-W dot plot) was used to discriminate the single cell population from aggregate and debris subpopulations. Single cells will have a similar pulse width whereas doublets will show a larger width of the pulse and thus can be easily distinguished from the single cell region.

Data collected have been analysed with FlowJo software and compute with "Dean-Jett-Fox" model.

# 4

## **The centrosome is a subcellular domain characterised by low basal cAMP levels**

---

### Background:

3',5 cyclic adenosine monophosphate (cAMP) is a ubiquitous cyclic nucleotide that has been described as the first second messenger (Rall and Sutherland, 1958), (Ashman et al., 1963). cAMP is responsible for a large number of cellular effects and regulates multiple biological functions including, among others, learning and memory, immune response, insulin secretion, cardiac frequency and strength of contraction, ion channel conductivity, synaptic release of neurotransmitters, cell growth, cell differentiation and gene transcription (Friedman, 1976), (Abel and Nguyen, 2008) (Colledge et al., 2000) (Serezani et al., 2008) (Rall and Sutherland, 1959). The intracellular level of cAMP depends on the activities of two families of enzymes: adenylyl cyclases (ACs), the only enzymes that generate cAMP and phosphodiesterases (PDEs), proteins capable of degrading cAMP into 5'-AMP. The principal effector of cAMP is the cAMP-dependent protein kinase (PKA), which can

phosphorylate hundreds of cellular targets. Such targets may be localised at the plasma membrane or other internal membranes, may be soluble in the cytosol or localised in the nucleus and the PKA-mediated phosphorylation of these diverse targets is responsible for an array of different cellular functions. In other words, an enormous amount of information is encoded into the changes of one single intracellular signal, cAMP. This scenario has raised the question of how specificity is achieved in the cAMP/PKA signalling pathway. A simple concentration gradient of the second messenger does not appear to be adequate to account for the specificity and diversity of the intracellular transduction events that depend on cAMP. Recent studies have uncovered a sophisticated array of regulatory mechanisms that allow for a tight control of signalling both in time and space and the notion of spatio-temporal compartmentalisation of cAMP is now well accepted (Steinberg and Brunton, 2001).

A critical role in the spatial control of the cAMP/PKA signal transduction events is played by A-Kinase Anchoring Proteins (AKAPs), which, by anchoring PKA, PDEs and other specific signalling enzymes in distinct subcellular domains, nucleate macromolecular signalling complexes that may generate spatially restricted pools of cAMP. For example it has been shown that in cardiomyocytes mAKAP anchors PDE4D3 and PKA in the perinuclear region. This organisation results in a negative feed-back loop mechanism in which an increase in cAMP activates the mAKAP-anchored PKA; in turn, active PKA phosphorylates and activates the mAKAP-anchored PDE4D3 which then degrades cAMP more efficiently. Such a feedback loop has profound effects on the local functions of PKA as it generates local fluctuations in cAMP and pulses of compartmentalised PKA activity (Dodge-Kafka et al., 2005).

The centrosome is a small non-membranous organelle whose primary role is to nucleate and organise the microtubules network (Doxsey, 1998), (Abal et al., 2002), (Bornens, 2002). Three AKAPs have been identified at the centrosome: hAKAP220 (Michel and Scott, 2002), pericentrin (Diviani et al., 2000), and AKAP450 (Witczak et al., 1999). The existence of multiple AKAPs

that anchor PKA to the centrosome suggests that the cAMP/PKA signals may have an important role in the regulation of centrosomal functions and that specific, local control of such signal may be critical for correct activity. In addition, the apparent redundancy of PKA anchoring to the centrosome may reflect the necessity to achieve a high level of compartmentalisation of PKA activity at this site (Diviani and Scott, 2001).

Pericentrin is a component of the pericentriolar matrix and forms a centrosomal macromolecular complex with  $\gamma$ -tubulin (Dictenberg et al., 1998) and dynein (Purohit et al., 1999). Pericentrin and AKAP450 share a high degree of homology and a common centrosomal-targeting region, named PACT domain (Gillingham and Munro, 2000). Interestingly two opposite evidence have been shown upon over-expression of the AKAP450-PACT domain. In one case over-expression of AKAP450-PACT domain displaces pericentrin indicating competition between pericentrin and AKAP450 for a shared binding site (Gillingham and Munro, 2000), in another case over-expression of specific AKAP450-PACT domain displaces AKAP450 but not pericentrin, indicating a specificity in the targeting of both AKAPs (Keryer et al., 2003b).

While the role of pericentrin has been correlated to the correct microtubule nucleation in interphase and spindle formation in mitosis (Purohit et al., 1999) (Young et al., 2000) (Doxsey et al., 1994), the role of AKAP450 at the centrosome is largely unknown and no information is available on the dynamics of cAMP in this subcellular compartment, on the mechanisms that regulate activation of the PKA subsets anchored to AKAP450 and/or on the role of PDE4D3 localised at this site.

Hypothesis:

The leading hypothesis of my research project is that the centrosomal subcellular compartment represents a domain where cAMP dynamics are uniquely regulated. Based on this hypothesis the first aim of my work was the analysis of cAMP levels in the centrosomal area in intact, unstimulated cells.

Experimental procedure:

- 1) Generation of two different stable clones expressing the genetically encoded FRET based sensors PKA-GFP (Zaccolo and Pozzan, 2000) or RII\_epac (Di Benedetto et al., 2008).
- 2) Validation of the localisation of the sensors PKA-GFP and RII\_epac to endogenous centrosomal AKAPs.
- 3) Analysis of cAMP levels in the centrosomal region and comparison with cAMP levels in the bulk cytosol using FRET-based imaging.
- 4) Analysis of the role of centrosomal PDE4D3 in determining basal cAMP levels in the centrosomal area.

## 4.1 Results

### ***4.1.1 Generation of a CHO clone stably expressing a FRET sensor based on PKA (PKA-GFP)***

Chinese hamster Ovary (CHO) cells (see section 3.2.1.1) were selected as the experimental model due to their morphology that allows to easily inspect the centrosome at the epifluorescence microscope. In order to analyse cAMP levels in the centrosomal region of intact and non-synchronised cells I performed real-time imaging of cAMP using a FRET biosensor based on PKA (Zaccolo and Pozzan, 2000). The sensor was stably expressed in CHO cells. One of the most important advantages of FRET-based real-time imaging of cAMP is that it allows to monitor local cAMP signals in intact living cells. Recently a large number of FRET based sensors for cAMP have been developed that are either cytosolic or targeted to specific subcellular compartments, providing a varied toolkit for real-time study of cAMP dynamics (see section 1.6.3.2). The choice to use the PKA-GFP sensor was based on two considerations. First of all this reporter can naturally anchor to endogenous AKAPs, allowing the direct visualisation of cAMP levels in the microenvironment surrounding AKAPs;

second, the PKA-GFP sensor is catalytically active and thereby offers the possibility to further investigate specific mechanism related to PKA activation at the centrosome.

The PKA-GFP probe comprises the regulatory (RII) and the catalytic (C) subunits of PKA genetically fused to the cyan (CFP) and the yellow mutants (YFP) of the green fluorescent protein (GFP), respectively (see section 1.6.3.2.1). When the intracellular concentration of cAMP is low the two subunits in the inactive PKA holoenzyme are close enough for FRET to occur. When the cAMP concentration rises, two cAMP molecules bind to each regulatory subunit promoting the release of the catalytic subunits and a concomitant decrease in FRET. FRET changes therefore correlate with changes in intracellular cAMP concentration (see section 1.6.3.2.1) (Zaccolo and Pozzan, 2000).

In order to generate a stable clone expressing both the regulatory subunit and the catalytic subunit of PKA-GFP the RII-CFP subunit (Lissandron et al., 2005) was sub-cloned into the vector pCDNA3.1/Zeo (+), that allows stable expression in mammalian cells using Zeocine™ as a selective antibiotic (Drocourt et al., 1990), (Mulsant et al., 1988). As natural resistance to antibiotics varies among cells lines it was necessary to test the sensitivity of CHO cells to Zeocine™. To this end I determined a dose-response curve for Zeocine™ from which the concentration of 300 µg/ml of Zeocin™ resulted to be the lowest concentration required for untransfected CHO cells to die. Using the pCDNA3.1/Zeo(+)RII-CFP subunit and the Zeocine™ concentration determined by the dose-response curve, a stable clone in CHO cells was established (see section 3.2.2.2). I further used these cells for the selection of a stable clone over-expressing also the C-YFP subunit. The C-YFP subunit was inserted in the pCDNA3 vector, which contains the gene coding for resistance to Geneticin® (G418 Sulphate, neomycin). As described in the material and methods (see section 3.2.2.2), I performed a dose-response curve by using cells stably expressing RII-CFP. After treating the cells for 12 days with media containing increasing concentration of Geneticin® the concentration of 800 µg/ml was

determined as the minimum amount of antibiotic necessary to select against cells not expressing the C-YFP protein. The resultant clone stably express both subunits of the PKA-GFP sensor (Figure 4-1)(Vaasa et al., 2010).

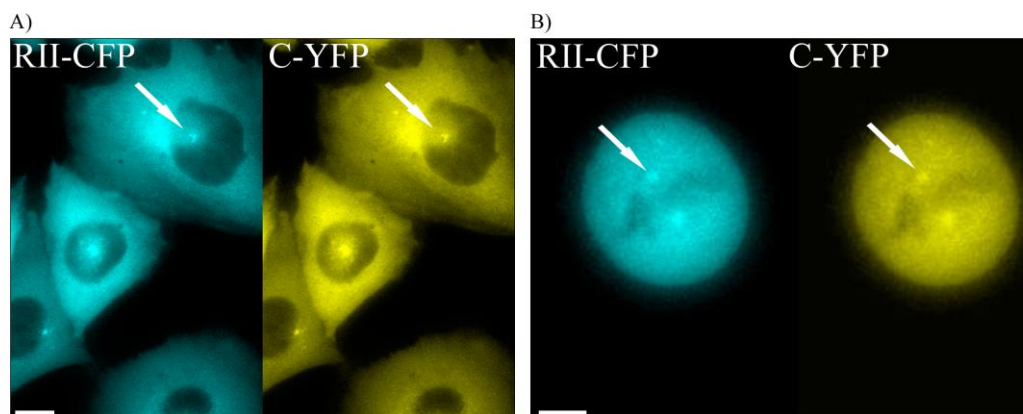


**Figure 4-1** CHO stably expressing the PKA-GFP sensor. The two panels show the signal generated by the RII-CFP (left panel) and C-YFP (right panel) subunit in interphase cells A) and mitotic cells B). The arrows point to the centrosome A) and centrioles B). The region of the cell in which the fluorescent signal of the probe is excluded is the nucleus in interphase cells A) and the metaphasic plate in mitotic cells B). Bars 10 $\mu$ m.

### ***4.1.2 The PKA-GFP FRET sensor localises to the centrosome in CHO cells via binding to endogenous AKAPs***

Fluorescence microscopy analysis revealed that interphase CHO cells stably expressing the PKA-GFP sensor exhibited a clear localisation of the probe in proximity to the nucleus, suggestive of localisation to the centrosome. In a number of cells it was possible to clearly recognise two orthogonally arranged structures that could represent the two centrioles (Figure 4-2 ).

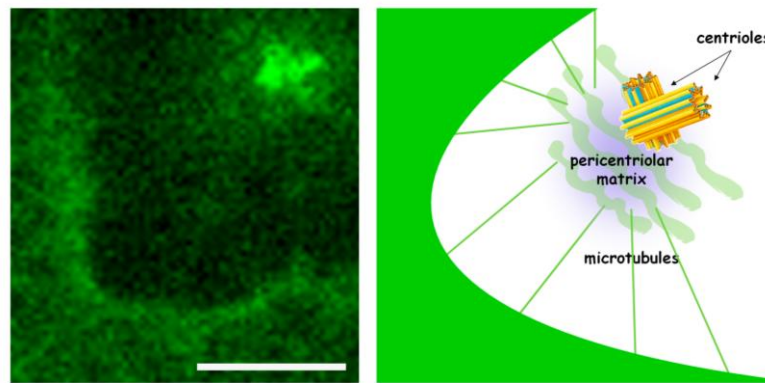


**Figure 4-2** Detail of a CHO cell stably expressing the PKA-GFP sensor (left panel) and imaged at the confocal microscope. The cell shows a clear localisation of the sensor in correspondence of a perinuclear structure in which it is possible to recognise two elements organised orthogonally to each other. Bar 10 $\mu$ m; and schematic representation of a centrosome (right panel).

In mitotic cells, the sensor clearly localises in two separate spots positioned on the opposite sides of the metaphasic plate, recognisable as a central area in which the fluorescent signal of the probe is excluded due to the presence of the condensed and aligned chromosomes (Figure 4-1, B).

To assess if the localisation of the sensor corresponds to the centrosomal area I performed an immunostaining using an antibody for  $\gamma$ -tubulin as a centrosome-specific marker. In the same cells the localisation of AKAP450 was assessed by using CTR453, an antibody that specifically recognised AKAP450 (Keryer et al., 2003a), (Bailly et al., 1989). As shown in Figure 4-3, PKA-GFP clearly co-localises with both  $\gamma$ -tubulin and AKAP450 (Figure 4-3).

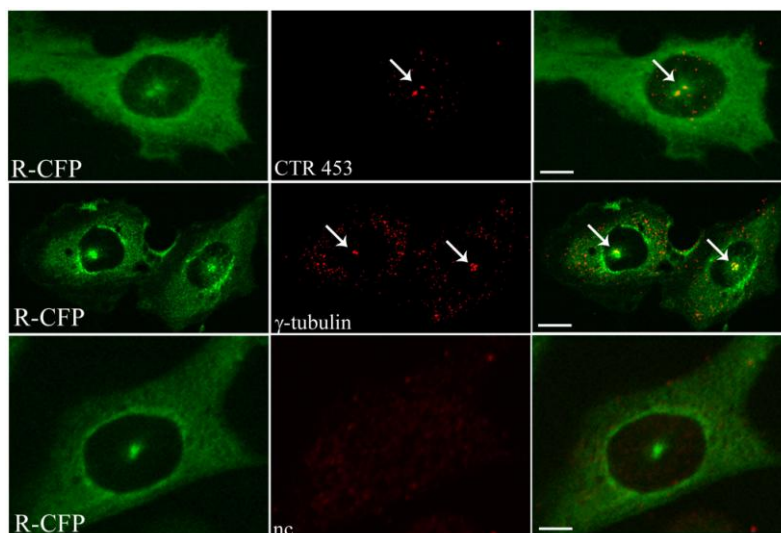


**Figure 4-3** Immunostaining of CHO cells stably expressing the PKA-GFP FRET sensor. Images show co-localisation of RII-CFP with CTR453 (antibody specific for AKAP450), top panel; and with  $\gamma$ -tubulin (specific marker for centrosome) middle panel. Secondary antibody (nc) control in the bottom panel. The signal from the C-YFP component of the sensor is not shown. Bars 10 $\mu$ m.

Next, I set out to establish if the observed localisation of the PKA-GFP sensor to the centrosome was due to anchoring of the GFP-tagged PKA to the endogenous centrosomal AKAPs. To this end “green fluorescent protein”-tagged versions of the AKAP-competing peptides RIAD (Carlson et al., 2006) and SuperAKAP-IS (Gold et al., 2006) were used. These peptides have been shown to compete selectively with the binding to endogenous AKAPs of regulatory subunit type I (RI) and type II (RII), respectively. In particular, the RIAD peptide was shown to have more than 1000-fold selectivity for RI over RII (Carlson et al., 2006) whereas the peptide SuperAKAP-IS was shown to be 10000-fold more selective for the RII isoform relative to RI (Gold et al., 2006). Due to the spectral overlap between GFP signal from the tagged competing peptides and the signal from the tagged sensor subunits this experiment was performed using a red fluorescent protein (RFP)-tagged version of the RII subunit that had been previously generated in our laboratory (see section 3.1.13) (Di Benedetto et al., 2008). RII-RFP was co-expressed in CHO cells in combination with either SuperAKAP-IS-GFP or RIAD-GFP. As shown in Figure 4-4, cells over-expressing both SuperAKAP-IS and RII-RFP, show no localisation of RII-RFP to the centrosome (Figure 4-4, top panel, cell in the left

end side), whereas a cell in the same field expressing only RII-RFP and not SuperAKAP-IS-GFP clearly shows a centrosomal localisation of RII-RFP (Figure 4-4, top panel, cell on the right). On the contrary over-expression of RIAD did not affect the localisation of RII-RFP to the centrosome (Figure 4-4, bottom panels).

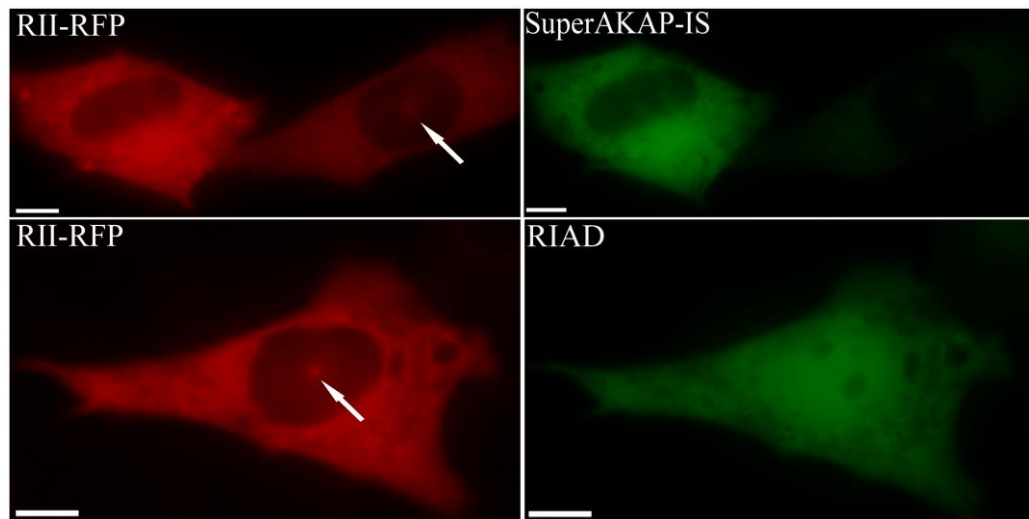


**Figure 4-4** CHO cells over-expressing RII-RFP (upper and lower panel on the left) in combination with SuperAKAP-IS-GFP (right upper panel) or RIAD-GFP (right lower panel). The arrows point to the centrosome. Bars 10 $\mu$ m.

These findings indicate that the specific localisation of the PKA-GFP sensor is due to the binding of the RII subunit to the endogenous AKAPs, as previously shown in cardiomyocytes (Zaccolo and Pozzan, 2002). The fact that SuperAKAP-IS, and not RIAD, compete for the binding of the sensor to the centrosome confirms that the localisation is specific and possibly mediated by centrosomal AKAPs. Interestingly both AKAP450 and pericentrin have been described as RII-specific AKAPs.

### ***4.1.3 A microdomain with low cAMP concentration at the centrosome***

Expression of the PKA-GFP FRET indicator in CHO cells offers the possibility to examine the relative level of cAMP in the centrosomal area compared to the bulk cytosol. As explained in detail in the Material and

Methods (see section 3.3), the FRET signal is expressed as the ratio of the CFP emission intensity over the YFP emission intensity (CFP/YFP) upon excitation of the cell at 430 nm. A pseudo-colour image of the cell expressing the FRET reporter can be generated by calculating, pixel by pixel, the value of the CFP/YFP emission intensity and by assigning to each pixel a colour according to a pre-defined colour scale. In the example below and throughout my thesis, red indicates high cAMP and green/blue indicates low cAMP. Figure 4-5 shows a representative example of a pseudo-colour image of a resting CHO cell stably expressing the PKA-GFP reporter. As evident from the differences in colour, the cAMP level at the centrosome is lower than the average cAMP level in the bulk cytosol (blue/green colour in the area corresponding to the centrosome compared to the yellow/red colour in the area corresponding to the cytosol, see section 3.3.2.4 and Figure 3-2 for details of how the analysis was performed).

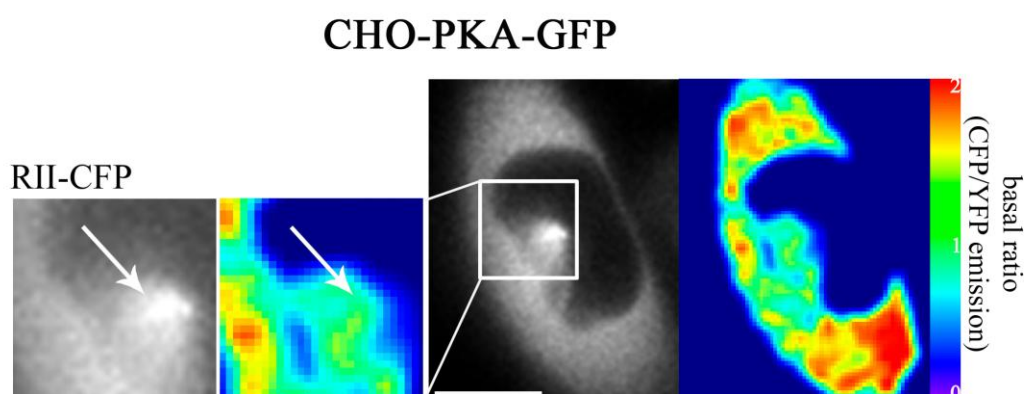


**Figure 4-5** RII-CFP signal and pseudo-colour image of a CHO cell stably expressing the PKA-GFP sensor. The signal generated by the C-YFP component of the PKA-GFP sensor is not shown. On the left, a higher magnification of the cell area delimited by the white box is shown. Bar 10 $\mu$ m.

Statistical analysis of all the observed cells revealed a difference in basal ratio (CFP/YFP emission) between cytosol and centrosome of about 2.04%, with a centrosomal ratio expressed as normalised value with respect to the cytosol of  $R_0/R_{0\text{cyt}}=0.980\pm 0.004$  (mean $\pm$ SEM; n=34) (see section 3.3.2.4 for

analysis details) (Figure 4-6). Paired T-test analysis shows that the difference in the ratio values detected in the two subcellular compartments is statistically significant ( $p < 0.001$ ).

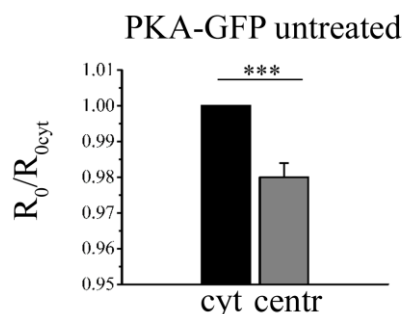


**Figure 4-6 Summary of the CFP/YFP ratio values recorder in the bulk cytosol and in the centrosome of cells stably expressing the PKA-GFP sensor. Data are normalised to the ratio value in the cytosol. (Error bar represents SEM. Two tailed; paired t-test, \*\*\*  $p < 0.001$ ).**

#### ***4.1.4 Generation and characterisation of a stable clone expressing the RII\_epac cAMP sensor.***

The C-YFP component of the PKA-GFP sensor is catalytically active hence there is a possibility that over-expression of this sensor may lead to an increased phosphorylation of PKA targets, including PDEs responsible for cAMP degradation, thereby affecting the cAMP dynamics under investigation. To exclude the possibility that the lower cAMP level detected at the centrosome of resting CHO cells may be an artefact due to the over-expression of the catalytically active PKA-GFP sensor and not to a physiological condition of the cell I set out to monitor centrosomal cAMP levels using the sensor RII\_epac (Figure 4-7) (Di Benedetto et al., 2008). RII\_epac is a FRET-based unimolecular sensor for cAMP based on Epac1-camps (Nikolaev et al., 2004) which has been modified in our laboratory by fusing the dimerisation/docking domain (D/D) of the RII $\beta$  subunit of PKA to the N-terminus (see section 3.1.12). This sensor is therefore capable of anchoring to endogenous AKAPs, similarly to the RII-CFP subunit, but is devoid of any catalytic activity (Figure 4-7) (Di Benedetto et al., 2008).

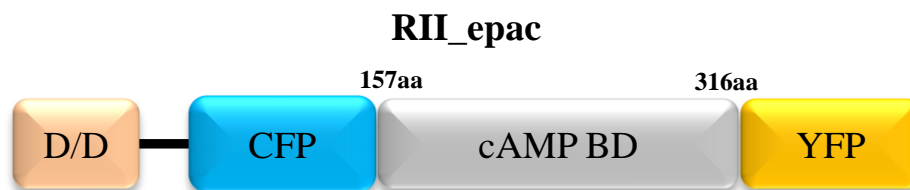


**Figure 4-7 Schematic representation of RII\_epac sensor. D/D=PKA-RII $\beta$  dimerization docking domain; CFP=cyan variant of the green fluorescent protein (GFP); cAMP BD=cAMP binding domain of Epac1; YFP=yellow variant of the green fluorescent protein.**

In order to select cells stably expressing RII\_epac, the sensor was cloned into pcDNA3 vector containing the gene coding for Geneticin® (G418 Sulphate, neomycin) resistance. CHO cells were transfected with RII\_epac and cultured in medium containing the amount of antibiotic established by the antibiotic dose-response curve for Geneticin® (see section 3.2.2.2 and 3.2.2.3.2). As expected, upon inspection at the fluorescence microscope, these cells showed a clear localisation of the probe to the centrosome of interphase cells (Figure 4-8).

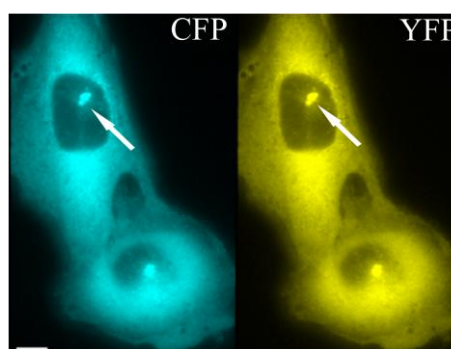


**Figure 4-8 CHO stably expressing the RII\_epac sensor. The two panels show the signal generated by the CFP (left panel) and YFP (right panel) emission. The arrows point to the centrosome. Bar 10 $\mu$ m.**

Next, I used this stable cell line to monitor cAMP levels in the cytosol and at the centrosome within the same cell. Similar to what I found with the PKA-GFP sensor, FRET analysis of CHO cells stably expressing the RII\_epac sensor showed a lower CFP/YFP ratio value at the centrosome compared with the

cytosol. The centrosomal ratio expressed as normalised value with respect to the cytosol was  $R_0/R_{0\text{cyt}}=0.961\pm 0.006$ , corresponding to a 4.17% difference between the two compartments ( $n=31$ ;  $p<0.001$ ) (Figure 4-9).

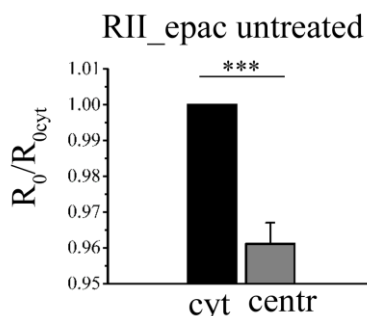


**Figure 4-9 Summary of the differences of basal CFP/YFP ratio between the cytosol and the centrosome of CHO cells stably expressing RII\_epac sensor. Data are normalised to the ratio value in the cytosol. (Error bar represents SEM. Two tailed; paired t-test, \*\*\*  $p<0.001$ ).**

These data confirmed that the centrosome of CHO cells is a microdomain with low cAMP level compared with the bulk cytosol.

#### ***4.1.5 Low cAMP centrosomal microdomain in SH-SY5Y***

In order to establish whether a microdomain with low cAMP is a feature exclusively found in CHO cells or rather it is present at the centrosome of other cell lines, the neuroblastoma cell line SH-SY5Y (see section 3.2.1.2) was employed.

As a first step I established a SH-SY5Y stable clone over-expressing the RII\_epac sensor (see section 3.2.2.3.2). In order to select cells stably expressing the cAMP indicator, SH-SY5Y cells were transfected with RII\_epac and grown in EMEM/F-12 supplemented with 500  $\mu\text{g/ml}$  of Geneticin® (G418 Sulphate, neomycin). When SH-SY5Y cells stably expressing the sensor were inspected at the fluorescence microscope, they showed, similarly to CHO cells, a centrosomal sub-localisation of the RII\_epac sensor, confirming anchoring of the sensor to endogenous AKAPs (Figure 4-10).

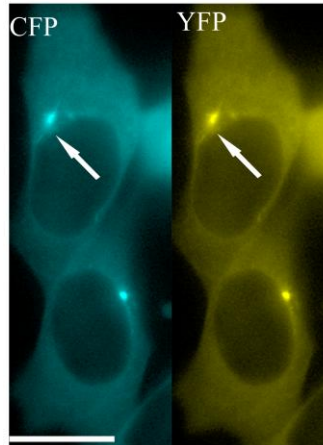


**Figure 4-10** SH-SY5Y stably expressing the RII\_epac sensor. The two panels show the signal generated by the CFP (left panel) and YFP (right panel) emission. The arrows point to the centrosome. Bar 10 $\mu$ m.

As shown in Figure 4-11, FRET based analysis of SH-SY5Y cells stably expressing the RII\_epac sensor revealed the presence of a microdomain with lower cAMP concentration at the centrosome as compared with the cytosol. The difference in basal ratio (CFP/YFP emission) between the two compartments resulted to be highly significant (6.10%,  $p < 0.001$ ;  $n = 12$ ), with a centrosomal ratio expressed as normalised value with respect to the cytosol of  $R_0/R_{0\text{cyt}} = 0.942 \pm 0.013$ .

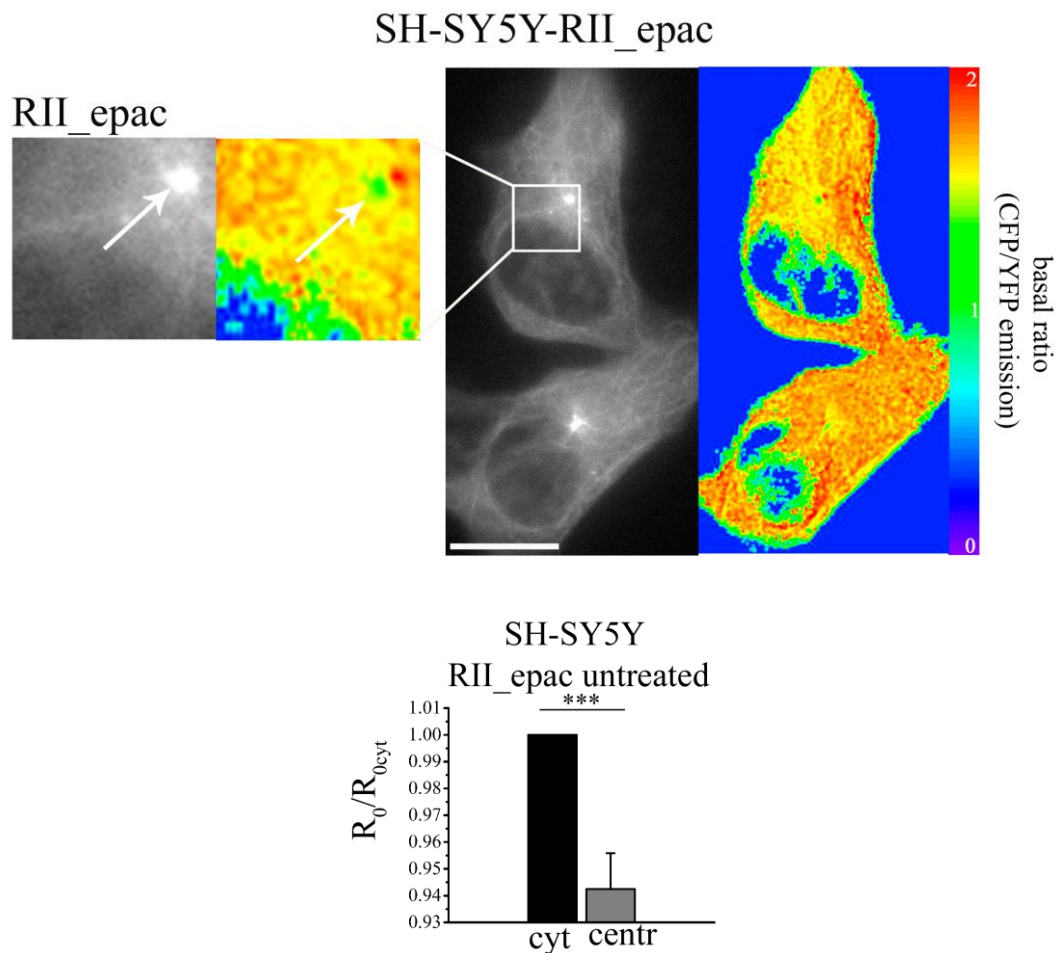


**Figure 4-11** Top panel: CFP signal and pseudo-colour image of SH-SY5Y cells stably expressing RII\_epac. The box shows the magnification of the centrosome region. Bar 10 $\mu\text{m}$ . Bottom panel: summary of the differences of basal CFP/YFP ratio values in the cytosol and in the centrosome of SH-SY5Y cells stably expressing RII\_epac sensor. Data are normalised to the CFP/YFP value in the cytosol. (Error bar represents SEM. Two tailed; paired t-test, \*\*\*  $p < 0.001$ ).

## 4.1.6 Role of PDE4D3 in the regulation of cAMP levels at the centrosome

### 4.1.6.1 PDE4D3 localises to the centrosome in CHO cells

It had been previously shown that PDE4D3 localises to the centrosome via binding to AKAP450 (Tasken et al., 2001). I therefore hypothesised that PDE4D3 may be responsible for maintaining the observed low basal level of cAMP at this site. To test this hypothesis, I sought to confirm by immunocytochemistry that PDE4D3 localises to the centrosome in CHO cells. As shown in Figure 4-12, an antibody specific for PDE4D3 decorates the centrosome and co-localises with  $\gamma$ -tubulin, a specific marker for this organelle.

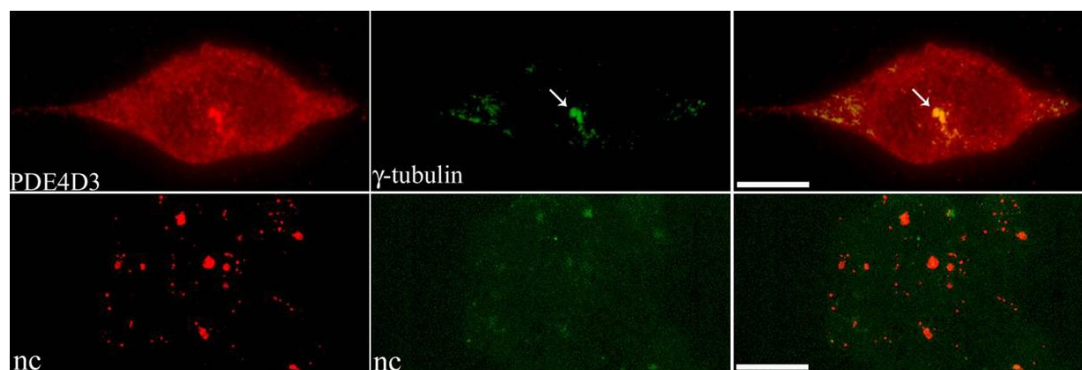


**Figure 4-12** Subcellular localisation of PDE4D3 in CHO cells. Images show co-localisation of PDE4D3, top left panel, with  $\gamma$ -tubulin (specific antibody for centrosome) middle panel. Secondary antibody control in the bottom panels. Bars 10 $\mu$ m.

#### **4.1.6.2 Selective inhibition of PDE4 abolishes the microdomain with low cAMP at the centrosome**

To further test PDE4D3 involvement in maintaining a centrosomal microdomain with low cAMP, I selectively inhibited all PDE4 isoforms with 10  $\mu$ M rolipram in CHO cells lines stably expressing either the PKA-GFP sensor or the RII\_epac sensor (Figure 4-13). In both cases I found that inhibition of PDE4, while increasing the cAMP concentration in both compartments (see Fig 4-18), completely abolishes the observed difference in FRET signal between centrosome and cytosol (centrosomal ratio expressed as normalised value with respect to the cytosol was  $R_0/R_{0\text{cyt}}=0.997\pm 0.005$  [n=44]; p=0.661 when probing with the PKA-GFP sensor and  $R_0/R_{0\text{cyt}}=0.990\pm 0.005$  [n=13]; p=0.078 when probing with RII\_epac sensor).

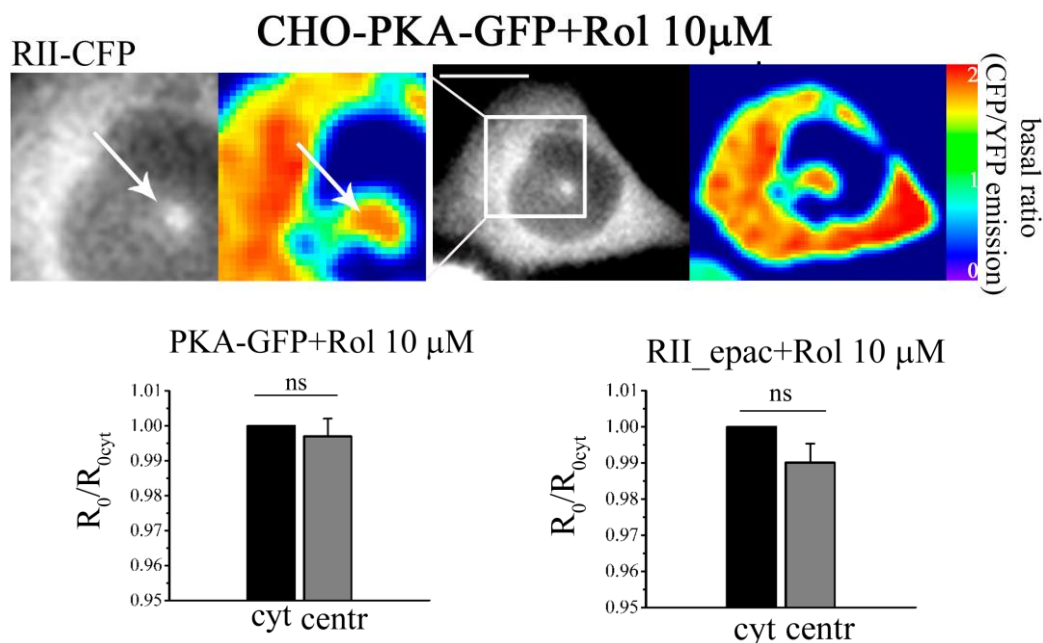


**Figure 4-13** Top panel: RII-CFP signal and pseudo-colour image of a CHO cell stably expressing PKA-GFP and treated with 10  $\mu$ M rolipram. The box shows the magnification of the centrosome region. Bar 10 $\mu$ m. Bottom panel: summary of the basal CFP/YFP ratio values in the cytosol and in the centrosome of cells stably expressing either PKA-GFP or RII\_epac sensor, as indicated, and treated with rolipram. Data are normalised to the CFP/YFP value in the cytosol (Error bars represent SEM. Two tailed; paired t-test).

As a control, cells stably expressing the PKA-GFP sensor were treated with the selective PDE2 inhibitor EHNA (erythro-9-(2-hydroxy-3-nonyl) adenine), and with the selective PDE3 inhibitor cilostamide. 10  $\mu$ M EHNA and 10  $\mu$ M cilostamide did not affect the cAMP gradient between cytosol and centrosome and the difference in the CFP/YFP emission ratio value between the two compartments was maintained at 1.95% upon PDE2 inhibition and at 1.64% upon PDE3 inhibition. Specifically, centrosomal ratio expressed as normalised value with respect to the cytosol was  $R_0/R_{0cyt}=0.981\pm 0.004$  [n=46]  $p<0.001$  in the presence of EHNA and  $R_0/R_{0cyt}=0.984\pm 0.004$  [n=39],  $p<0.001$  in the presence of cilostamide (Figure 4-14).

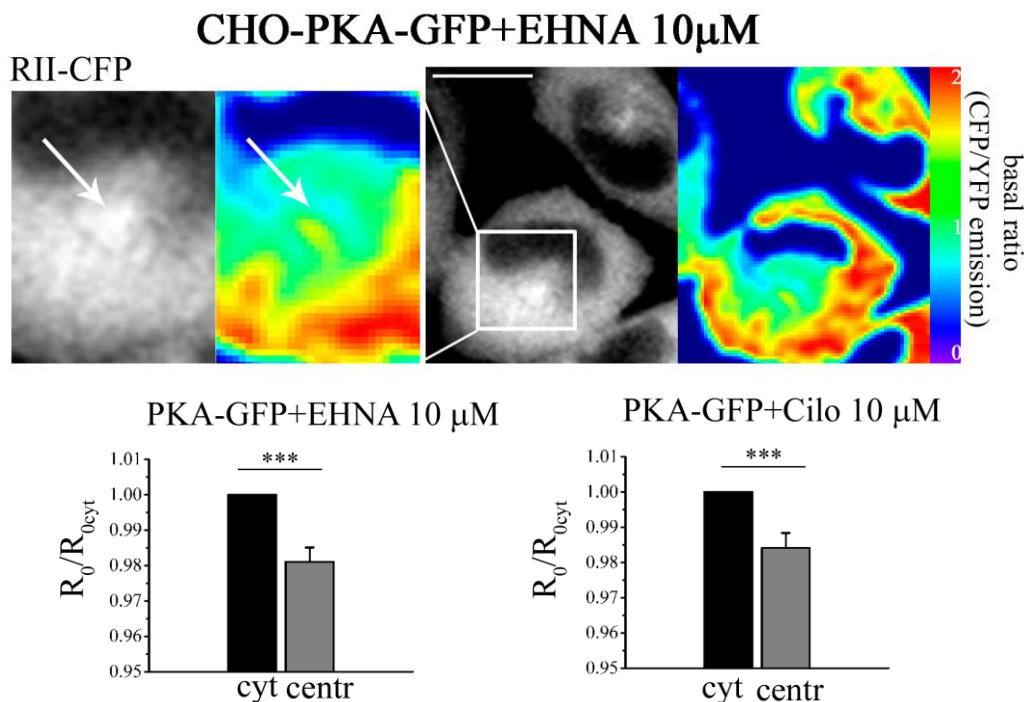


**Figure 4-14** Top panel: RII-CFP signal and pseudo-colour image of a CHO cell stably expressing PKA-GFP and treated with 10  $\mu$ M EHNA. The box shows the magnification of the centrosome region. Bar 10 $\mu$ m. Bottom panel: summary of the differences of basal CFP/YFP ratio value in the cytosol and at the centrosome of cells stably expressing PKA-GFP and treated, as indicated, with EHNA 10  $\mu$ M or cilostamide (cilo) 10  $\mu$ M. Data are normalised to the CFP/YFP value in the cytosol (Error bars represent SEM. Two tailed; paired t-test, \*\*\*  $p < 0.001$ ).

#### **4.1.6.3 PDE4D selective knock-down abolishes the difference in cAMP between cytosol and centrosome**

To further confirm the involvement of PDE4D3 in shaping a centrosomal microdomain with low cAMP I performed a knock-down experiment in which PDE4D was genetically ablated by over-expression of a small interfering RNA oligonucleotide (siRNA). CHO cells were co-transfected with the PKA-GFP sensor and either a siRNA oligonucleotide for PDE4D (Lynch et al., 2005) or the control siRNA oligonucleotide, siGLO®.

The efficiency of endogenous PDE4D knock-down was determined by western blot analysis. Lysates from cells over-expressing either the siRNA for PDE4D or the control siGLO® were separated by SDS-PAGE and probed with a specific antibody against PDE4D, as illustrated in Figure 4-15. PDE4D sub-family-specific siRNA-mediated knock-down results in a very significant

reduction in the level of PDE4D expression, whereas no effect on PDE4D expression level was detected in cells treated with the control siGLO® (Figure 4-15).

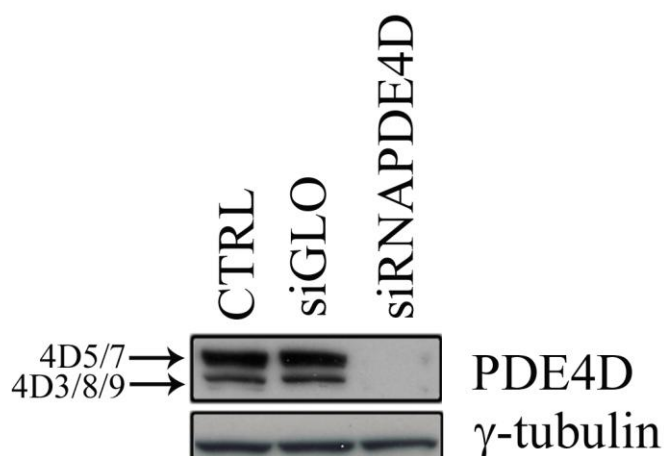


**Figure 4-15** Western blot of PDE4D and  $\gamma$ -tubulin obtained from cells treated as follows: untreated CHO (CTRL), CHO over-expressing the control siGLO® (siGLO) and CHO over-expressing the small RNA interference of PDE4D (siRNAPDE4D).

Pseudo-colour images of CHO cells over-expressing siRNA for PDE4D show that the selective knock-down of the PDE4D completely abolishes the differences in the basal CFP/YFP ratio between cytosol and centrosome ( $R_0/R_{0\text{cyt}}=0.994\pm 0.005$  [n=40] at the centrosome;  $p=0.219$ ). On the contrary, in cells transfected with siGLO®, such a difference is maintained with a basal ratio in the cytosol 1.43% higher than at the centrosome ( $R_0/R_{0\text{cyt}}=0.986\pm 0.003$  [n=40] at the centrosome;  $p<0.001$ ) (Figure 4-16).

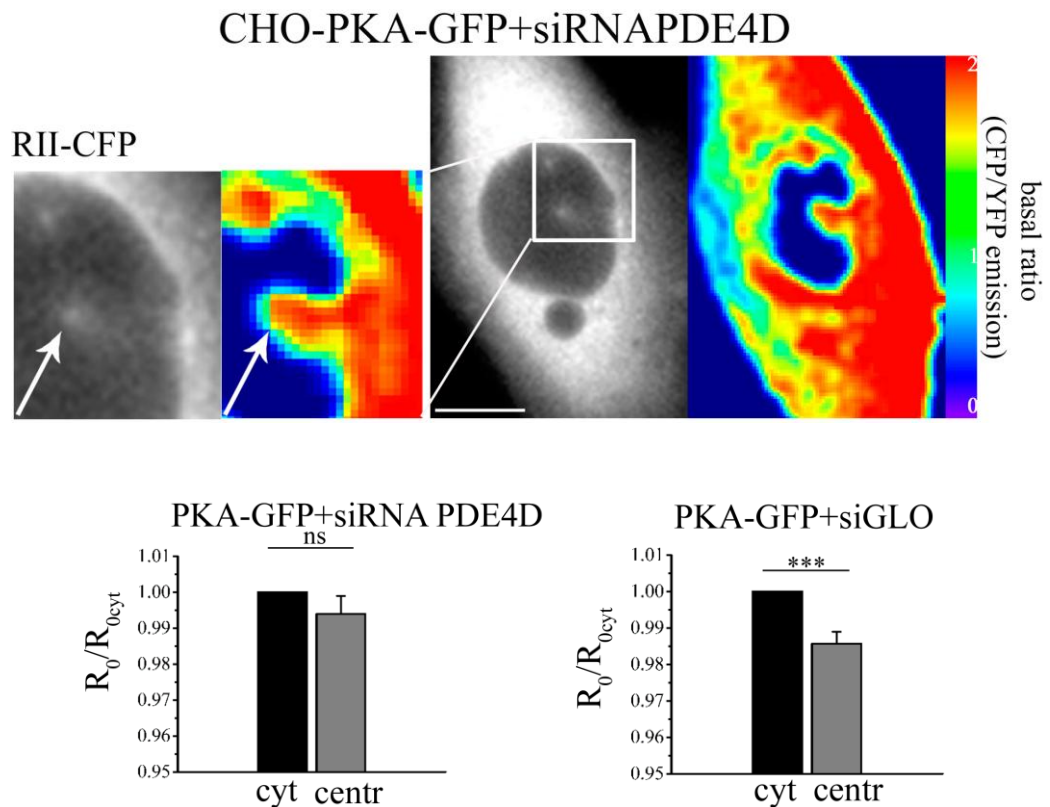


**Figure 4-16** Top panel: RII-CFP signal and pseudo-colour image of a CHO cell co-expressing PKA-GFP and siRNA for PDE4D. The box shows the magnification of the centrosome region. Bar 10 $\mu$ m. Bottom panel: summary of the differences of basal CFP/YFP ratio value in the cytosol and at the centrosome of cells expressing either siRNA for PDE4D or the control siGLO®, as indicated. Data are normalised to the CFP/YFP value in the cytosol. (Error bars represent SEM. Two tailed; paired t-test, \*\*\*  $p < 0.001$  with siGLO®).

#### **4.1.6.4 PDE4D3 displacement abolishes the low cAMP compartment at the centrosome**

To further confirm that anchoring of PDE4D3 to the centrosome is necessary to maintain a low local concentration of cAMP, the effect of displacing PDE4D3 from its intracellular anchor sites, by over-expressing a dominant negative variant of PDE4D3 (dnPDE4D3) (McCahill et al., 2005), was tested. In this context, a dominant negative PDE is an enzyme containing a point mutation in the catalytic site that abolishes the enzymatic activity (Baillie et al., 2003). The over-expression of such a protein results in the displacement of the cognate, endogenous, active counterpart and in its replacement with the catalytically dead version of the same enzymes. The consequence of this is to abolish any effect due to the specific localisation of the enzyme. Co-transfection

of the PKA-GFP sensor in combination with the dnPDE4D3, in CHO cells, completely abolished the difference in cAMP concentration between the cytosol and the centrosome, with  $R_0/R_{0\text{cyt}}=0.993\pm 0.006$  [n=31],  $p=0.270$ . As a control, over-expression of a catalytically inactive PDE4A4 (dnPDE4A4) did not affect the difference in ratio between the cytosol and the centrosome with a ratio value in the cytosol 1.63% higher than at the centrosome ( $R_0/R_{0\text{cyt}}=0.984\pm 0.006$  [n=21];  $p<0.012$ ) (Figure 4-17).

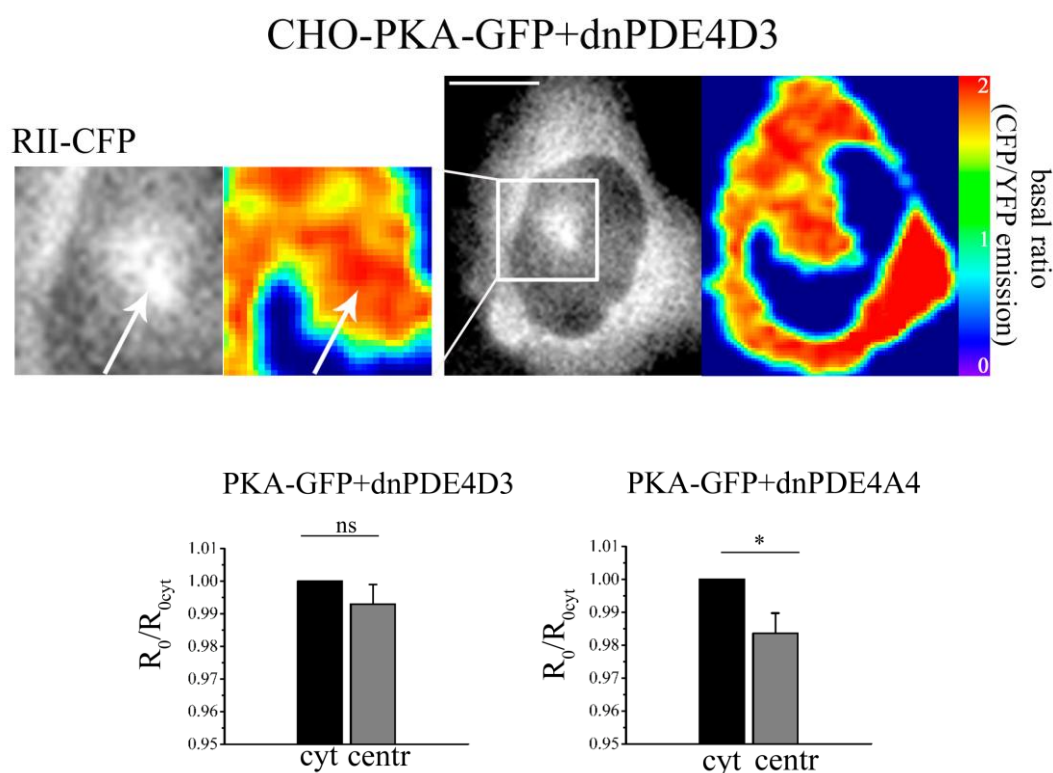


**Figure 4-17** Top panel: RII-CFP signal and pseudo-colour image of a CHO cell co-expressing PKA-GFP and dnPDE4D3. The box shows the magnification of the centrosome region. Bar 10 $\mu\text{m}$ . Bottom panel: summary of the differences of basal CFP/YFP ratio values in the cytosol and at the centrosome of cells expressing either dnPDE4D3 or the control dnPDE4A4, as indicated. Data are normalised to the CFP/YFP value in the cytosol. (Error bars represent SEM. Two tailed; paired t-test, \*  $p<0.5$ ).

Collectively, the above evidence strongly indicates that PDE4D3 is responsible for maintaining at the centrosome a level of cAMP that is lower than in the bulk cytosol (Figure 4-18).

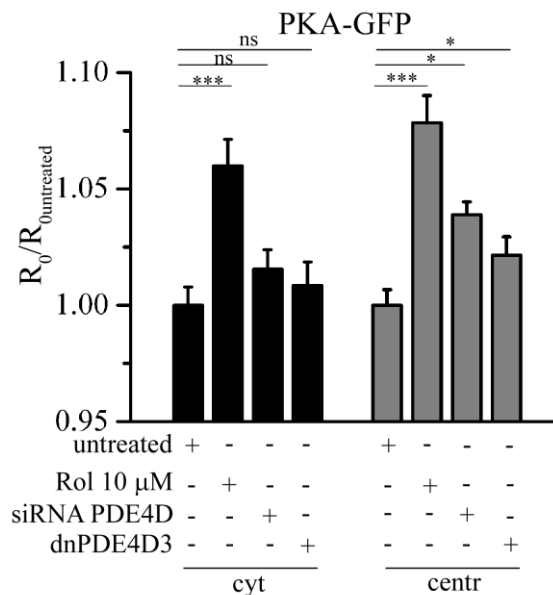


**Figure 4-18 Comparison between the effect of rolipram, siRNA for PDE4D and dnPDE4D3 on cytosolic (cyt) and centrosomal (centr) ratio increase compared to untreated control. (Error bars represent SEM. Two tailed; un-paired t-test; \*\*\*  $p < 0.001$ , \*  $p < 0.05$ )**

## 4.2 Discussion

The centrosome is an organelle which contains all the machinery required for cAMP signal transduction. Hence it is very interesting to study if a localised pool of cAMP could be uniquely regulated at this site and what are the mechanisms that may selectively control the cAMP/PKA pathway in this compartment.

In order to study cAMP dynamics in intact and non-synchronised cells I generated stable clones over-expressing the FRET based sensors and performed real-time imaging of cAMP using PKA-GFP (Zaccolo and Pozzan, 2000) (Figure 4-1) and RII\_epac (Di Benedetto et al., 2008) (Figure 4-8). Using these stable clones I was able to show that the PKA holoenzyme is anchored to the centrosome through specific binding to endogenous RII-specific AKAPs (Figure 4-3), as this specific anchoring could be abolished by over-expression of the competing peptide SuperAKAP-IS (Figure 4-4).

Subsequent FRET-based analysis of these cells revealed that the centrosome is a domain with a low cAMP concentration compared with the

cytosol (Figure 4-5 and Figure 4-6). Moreover, this special subcellular domain is not a peculiarity of CHO cells but it can be found in different cellular models, as for example in human neuroblastoma cells (Figure 4-10).

It has been shown that AKAP450 nucleates a cAMP/PKA signalling complex to the centrosome by simultaneously anchoring PKA and PDE4D3 (Tasken et al., 2001). Thus, I investigated the role of PDE4D3 bound to the centrosomal AKAP450 in regulating the local concentration of cAMP at the centrosome. Indeed, selective inhibition of PDE4 with rolipram completely dissipates the gradient of cAMP between centrosome and cytosol (Figure 4-13). On the contrary, selective inhibition of different PDE families, such as PDE2 or PDE3, does not affect the centrosomal low cAMP microdomain, suggesting that these two subfamilies of PDEs are not involved in the centrosomal cAMP compartmentalisation (Figure 4-14). Further evidence that PDE4D is responsible for the lower cAMP concentration at the centrosomal subcellular compartment is provided by experiments in which PDE4D was selective knocked-down, which also showed abolishment of the difference in cAMP concentration between the two compartments (Figure 4-16). Finally, displacement of PDE4D3 confirmed that the localisation of this specific isoform to the centrosome is required to shape the centrosomal pool of cAMP (Figure 4-17). It has been previously shown in our laboratory and by other groups that anchored PDEs act as a “sink” draining cAMP and contributing to shape asymmetric gradients of cAMP (Terrin et al., 2006). Based on the data presented in this chapter, it can be hypothesised that PDE4D3 is active at resting levels of cAMP and its activity may prevent the inappropriate activation of PKA. In addition it is important to note that this mechanism is not cell specific but can be extended to other cell lines, indicating that a specific cAMP-dependent regulatory mechanism is taking place at the centrosome and this warrants further investigation.

# 5 Anchoring of PKA to AKAP450 lowers PKA activation threshold

---

## *Background:*

In the first chapter I demonstrated that the centrosome is a subcellular compartment in which, in resting and unstimulated cells, the level of cAMP is lower than the level of cAMP in the bulk cytosol. In addition, I provided evidence that the centrosomal PDE4D3 is necessary to maintain such a gradient of cAMP. The presence at the centrosome of PKA and PDE4D3 anchored to AKAP450, together with evidence for a low cAMP microdomain in this compartment, suggest that the centrosome may represent a signalling domain in which cAMP dynamics in response to extracellular inputs are uniquely regulated.

## *Hypothesis:*

Based on these observations the guiding hypothesis of this chapter is that cAMP raising agents generate a cAMP response at the centrosome that is different from the cAMP response in the bulk cytosol.

Experimental procedure:

- 1) FRET-based analysis of cAMP levels in CHO clones stably expressing either the PKA-GFP or the RII\_epac sensor and treated with forskolin.
- 2) Comparison of FRET changes in the cytosol and at the centrosome upon forskolin stimulation.
- 3) Study of the role of AKAP450 in the activation of centrosomal PKA.

## 5.1 Results

### ***5.1.1 Upon forskolin stimulation the PKA-GFP sensor responds with a larger FRET change at the centrosome than in the cytosol***

To investigate the cAMP response at the centrosome, CHO cells stably expressing PKA-GFP were treated with 25  $\mu$ M forskolin, a direct activator of adenylyl cyclases, and FRET changes at the centrosome and in the cytosol were monitored by time-lapse fluorescence microscopy. As shown in Figure 5-1, the FRET change recorded at the centrosome resulted to be significantly higher ( $p < 0.001$ ) than the FRET change detected in the bulk cytosol of the same cell, with  $\Delta R/R_0 = 12.198 \pm 0.662\%$  and  $\Delta R/R_0 = 14.334 \pm 0.910\%$  in the cytosol and at the centrosome, respectively ([n=35]). Figure 5-1 shows the plots of the normalised average kinetics of FRET changes recorded in the two compartments for the entire set of analysed cells (see section 3.3.2.4 and Figure 3-2 for analysis details).

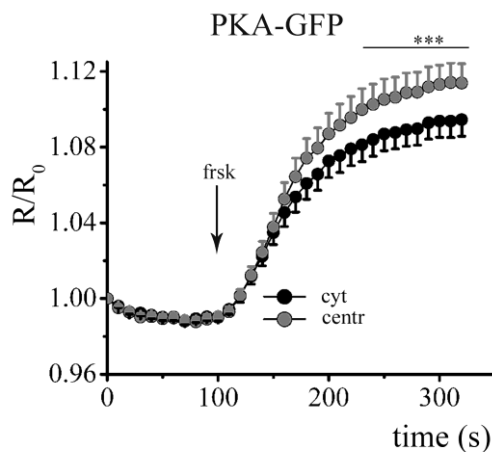


**Figure 5-1** Normalised average kinetics of FRET change detected in response to 25  $\mu\text{M}$  forskolin (frsk) and recorded in the cytosol (cyt; black circles) and at the centrosome (centr; grey circles) in CHO cells stably expressing PKA-GFP. (Error bar represents SEM. Two tailed; un-paired t-test, \*\*\*  $p < 0.001$ ).

One possible explanation for these results is that the higher FRET increase detected at the centrosome may be due to a higher cAMP increase in this region compared to the cAMP increase in the bulk cytosol. The so-called 'soluble' AC (sAC), has been described as being associated to the centrosome (see section 1.3.1) (Zippin et al., 2003). However, it should be noted that sAC is the only AC isoform that is not directly activated by forskolin (Zippin et al., 2003). To verify that the larger FRET change detected by PKA-GFP at the centrosome upon forskolin stimulation was due to a larger cAMP signal generated in this compartment, I took advantage of a different FRET reporter, the unimolecular sensor RII\_epac. CHO cells stably expressing RII\_epac were challenged with forskolin and FRET changes were recorded at the centrosome and in the bulk cytosol. Interestingly, 25  $\mu\text{M}$  forskolin generated an equal FRET change in the two compartments, with  $\Delta R/R_0 = 10.605 \pm 0.475\%$  and  $\Delta R/R_0 = 10.622 \pm 0.728\%$  in the cytosol and at the centrosome, respectively ([ $n=31$ ];  $p=0.97$ ), as indicated by the normalised average kinetic for the entire set of analysed cells (Figure 5-2).

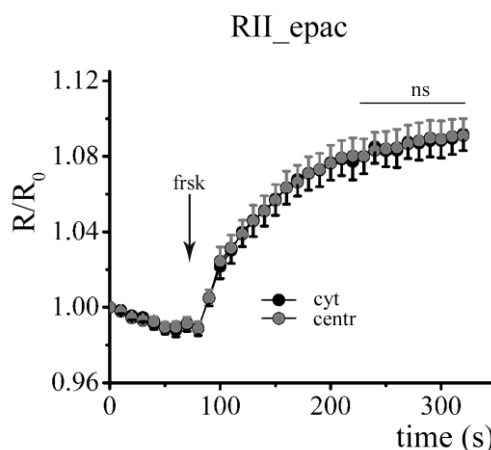


**Figure 5-2 Normalised average kinetics of FRET change induced by 25  $\mu$ M forskolin (frsk) in CHO cells stably expressing RII\_epac and recorded in the cytosol (cyt; black circles) and at the centrosome (centr; grey circles). (Error bar represents SEM. Two tailed; un-paired t-test).**

These data indicate that treatment with forskolin leads to a comparable increase in cAMP at the centrosome and in the cytosol. Consequently, the higher FRET change observed at the centrosome with the PKA-GFP sensor must be explained by another phenomenon.

### ***5.1.2 PKA anchored to AKAP450 shows increased sensitivity to cAMP***

An alternative explanation for the observed larger FRET change detected at the centrosome by the PKA-GFP sensor upon forskolin stimulation is that anchoring of PKA to the centrosomal AKAPs modifies the sensitivity of PKA to cAMP. To investigate this possibility, a fragment of AKAP450 (933-1804aa) (see section 3.1.15) (Witczak et al., 1999) designated AKAP450-2 and including the amphipathic helix (amino acidic sequence: LEEEVAKVIVSMSIAFA) responsible for PKA anchoring, was sub-cloned into pcDNA3.1/Hygro (Figure 5-3).

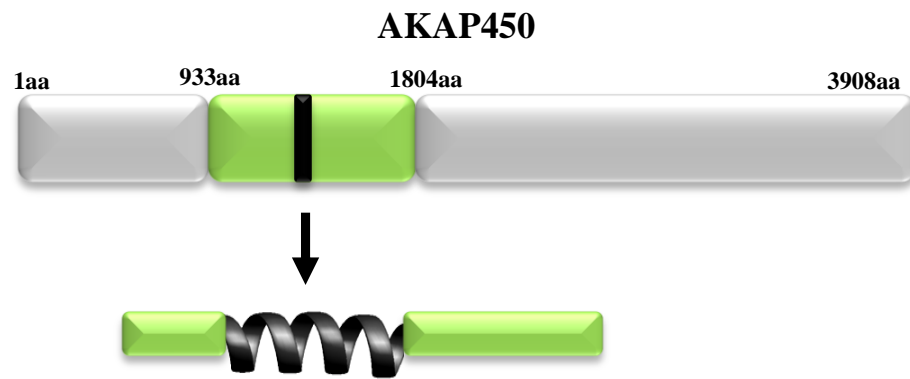


**Figure 5-3 Schematic representation of AKAP450 and AKAP450-2 fragment.**

This fragment lacks the C-terminal domain responsible for targeting of AKAP450 to the centrosome (PACT domain: pericentrin-AKAP450 centrosomal targeting domain). As a consequence, the AKAP450-2 fragment, when expressed in cells, shows a cytosolic distribution (Figure 5-3). CHO cells were co-transfected with PKA-GFP and the AKAP450-2 fragment and FRET changes upon forskolin stimulation were recorded by time-lapse fluorescence microscopy. The rationale for this experiment was that the AKAP450-2 fragment and the PKA-GFP sensor would interact in the cytosol, in the same way as endogenous PKA and AKAP450 interact at the centrosome (Figure 5-4, A)). As shown in Figure 5-4, B), CHO cells co-expressing the AKAP450-2 fragment and the PKA-GFP reporter showed a significantly higher ( $p < 0.05$ ) FRET increase upon stimulation with 25  $\mu$ M forskolin ( $\Delta R/R_0 = 11.115 \pm 0.975\%$  [n=22] compared with CHO cells expressing the PKA-GFP sensor alone ( $\Delta R/R_0 = 14.077 \pm 0.898\%$  [n=20])).

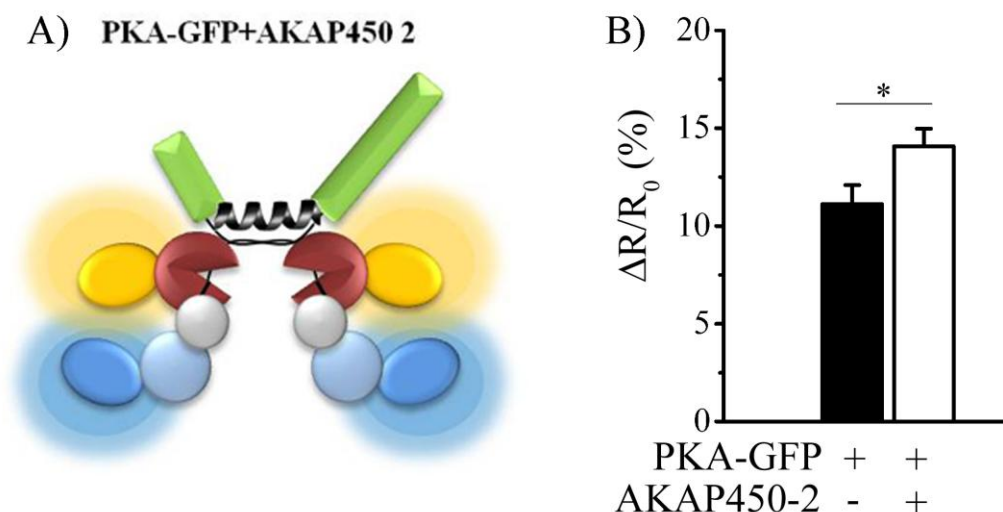


**Figure 5-4 Effect of PKA-GFP binding to AKAP450-2 fragment. A) Schematic representation of PKA-GFP and AKAP450-2 fragment interaction; B) Summary of FRET changes induced by 25  $\mu$ M forskolin in the presence or absence of the AKAP450-2 fragment. (Error bar represents SEM. Two tailed; un-paired t-test, \*  $p < 0.05$ ).**

Next, CHO cells over-expressing PKA-GFP, in the presence or absence of AKAP450-2, were challenged with increasing concentrations of forskolin (Figure 5-5 and Figure 5-6). From the analysis of this experiment it emerges that over-expression of AKAP450-2 fragment increases the number of cells responding to low concentrations of forskolin. Specifically, the percentage of cells co-expressing PKA-GFP and AKAP450-2 and showing a response to concentrations of forskolin between 0.2-1  $\mu$ M was almost double than the percentage of cells expressing PKA-GFP alone and responding to this range of forskolin concentration (Figure 5-5).

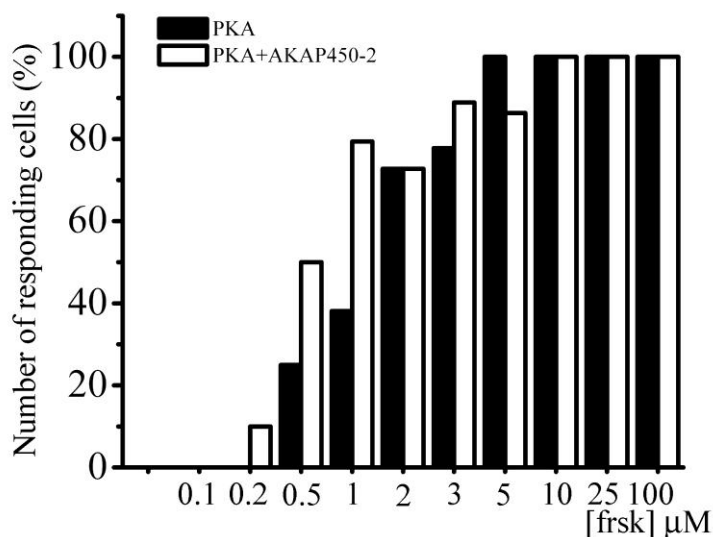


**Figure 5-5 Percentage of cells responding to increasing concentration of forskolin. Open and full bars represent CHO cells expressing PKA-GFP in the presence or absence of the AKAP450-2 fragment, respectively. [n<10].**

These experiments also clearly showed that in the presence of the AKAP450-2 fragment the dose-response curve to forskolin is shifted to the left, indicating an increased sensitivity of the PKA-GFP sensor to cAMP. Analysis of the curve fitted to the experimental points allowed to determine a reduction of the  $EC_{50}$  value by a factor of 2 ( $EC_{50}=2.23$  and  $1.03$  in the absence and in the presence of AKAP450-2, respectively) (Figure 5-6). These findings indicate that a lower concentration of cAMP is sufficient to dissociate the PKA holoenzyme when PKA is bound to AKAP450.

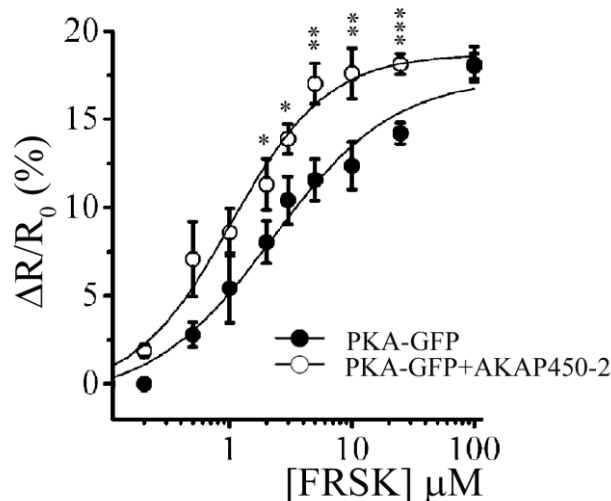


**Figure 5-6 Dose-response curve. FRET change induced by increasing concentration of forskolin in CHO cells expressing PKA-GFP in the presence of absence of AKAP450-2 [n<10]. (Error bars represent SEM. Two tailed; un-paired t-test, \* p<0.05, \*\* 0.01<p<0.001, \*\*\* p<0.001).**

To further confirm that the increased sensitivity of PKA-GFP to cAMP was the consequence of the interaction of the sensor with AKAP450, the amplitude of FRET change detected by PKA-GFP sensor was measured in the presence of SuperAKAP-IS (see section 3.1.14), a disrupting peptide that selectively competes for the binding of PKA type II to AKAPs (see section 4.1.2) (Gold et al., 2006). Upon challenge with 25 μM forskolin, CHO cells over-expressing the PKA-GFP sensor in combination with the AKAP450-2 fragment and SuperAKAP-IS showed a FRET change equal to the FRET change measured in CHO cells expressing the PKA-GFP sensor alone ( $\Delta R/R_0=13.422\pm 0.774\%$  [n=18] with PKA-GFP,  $\Delta R/R_0=15.563\pm 0.561\%$  [n=24] with PKA-GFP plus AKAP450-2 fragment; and  $\Delta R/R_0=13.074\pm 0.709\%$  [n=24] with PKA-GFP plus AKAP450-2 plus SuperAKAP-IS; PKA-GFP versus PKA-GFP plus AKAP450-2 p<0.05; PKA-GFP plus AKAP450-2 versus PKA-GFP plus AKAP450-2 plus SuperIS 0.01<p<0.001, Figure 5-7).

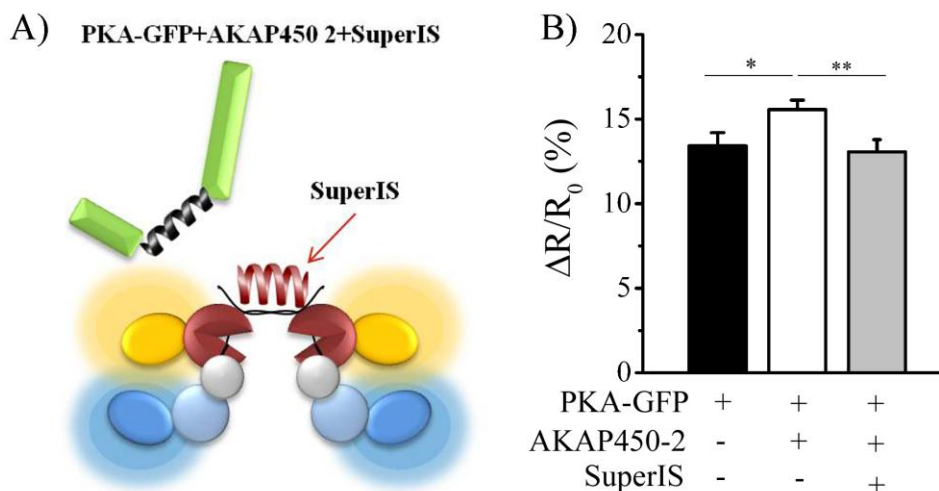


**Figure 5-7 Effect of disrupting PKA-GFP/AKAP450-2 interaction with SuperAKAP-IS (SuperIS). A) Schematic representation of PKA-GFP, AKAP450-2 and SuperAKAP-IS interaction (SuperIS, red helix); B) Summary of FRET change induced by 25  $\mu$ M forskolin in the presence or absence of AKAP450-2 fragment and SuperAKAP-IS. (Error bars represent SEM. Two tailed; un-paired t-test, \*  $p < 0.05$ , \*\*  $0.01 < p < 0.001$ ).**

Similarly, AKAP450-2 had no effect on the FRET change detected by a deletion mutant of the PKA-GFP sensor,  $\Delta$ PKA-GFP, in which the regulatory subunit,  $\Delta$ R<sub>II</sub>-CFP, lacks the dimerisation/docking domain (see section 3.1.16) (Zaccolo, 2002) and therefore cannot bind to AKAPs. As shown in Figure 5-8 cells expressing either  $\Delta$ PKA-GFP alone or  $\Delta$ PKA-GFP in combination with the AKAP450-2 fragment showed the same amplitude of response to forskolin stimulation ( $\Delta R/R_0 = 13.605 \pm 0.607\%$  [n=25] with  $\Delta$ PKA-GFP and  $\Delta R/R_0 = 13.927 \pm 0.768\%$  [n=23] with  $\Delta$ PKA-GFP plus AKAP450-2 fragment;  $p = 0.74$ ; Figure 5-8).

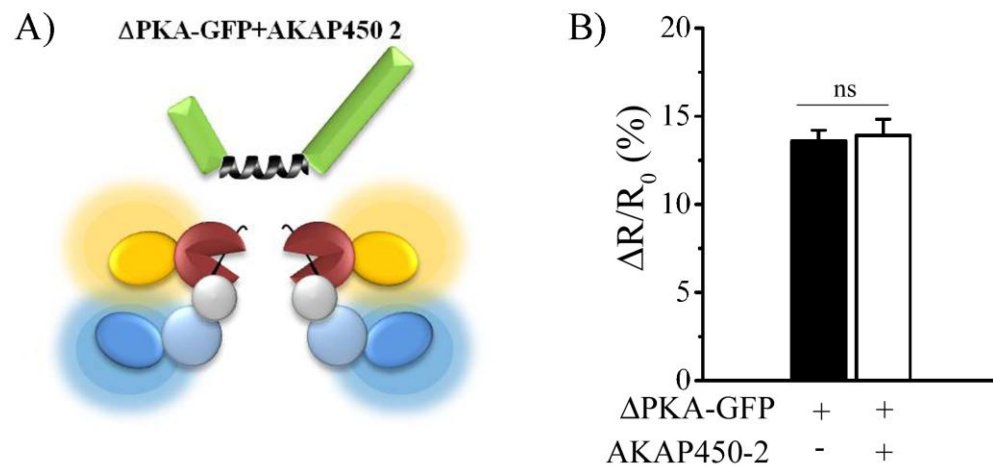


**Figure 5-8 Effect of AKAP450-2 on  $\Delta$ PKA-GFP. A) Schematic representation of AKAP450-2 fragment and  $\Delta$ PKA-GFP; B) Summary of FRET change induced by 25  $\mu$ M forskolin in the presence or absence of AKAP450-2 fragment on  $\Delta$ PKA-GFP. (Error bar represents SEM. Two tailed un-paired t-test).**

A comparable result was obtained when, together with PKA-GFP, a mutant of AKAP450-2 fragment (mutAKAP450-2 fragment, see section 3.1.15) was co-expressed in which the point mutation S1451P was introduced in the amphipathic helix responsible for the interaction of the regulatory subunit of PKA (mutated amino acidic sequence: LEEEVAKVIVPMSIAFA). The introduction of a proline residue in this sequence results in the disruption of the helix and, as a consequence, abolishes the ability of the AKAP fragment to bind to PKA (Carr et al., 1991) (Feliciello et al., 2001), (Alto et al., 2003). In agreement with the previous findings, over-expression of mutAKAP450-2 in CHO cells did not affect the FRET change detected by the PKA-GFP sensor upon forskolin stimulation compared with cells that did not over-express the mutant fragment ( $\Delta R/R_0=12.726\pm 1.450\%$  [n=14] with PKA-GFP,  $\Delta R/R_0=16.518\pm 0.969\%$  [n=26] with PKA-GFP plus AKAP450-2 fragment; and  $\Delta R/R_0=12.938\pm 1.310\%$  [n=19] with PKA-GFP plus mutAKAP450-2 fragment; PKA-GFP versus PKA-GFP plus AKAP450-2 and PKA-GFP plus AKAP450-2 versus PKA-GFP plus mutAKAP450-2;  $p<0.05$ ; Figure 5-9).

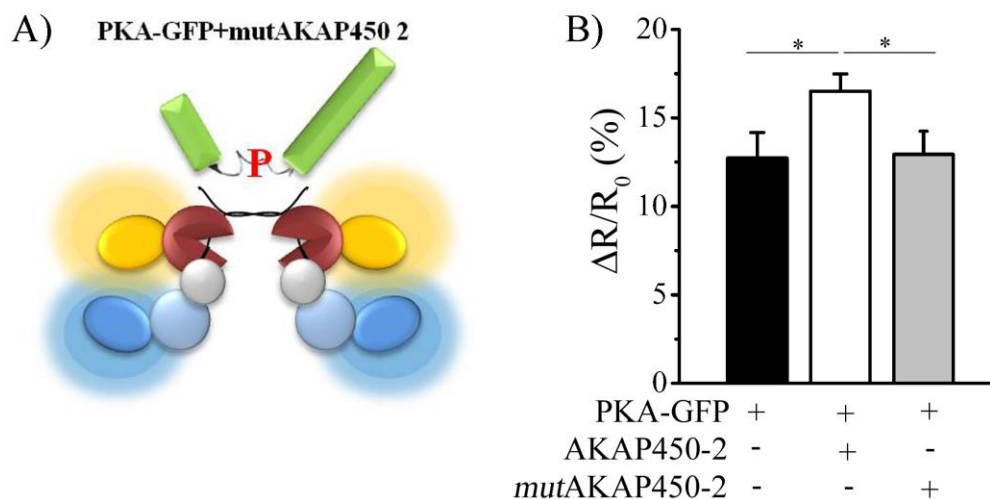


**Figure 5-9 Effect of PKA-GFP binding to mutAKAP450-2 fragment compared to the binding to the AKAP450-2 (wild type). A) Schematic representation of PKA-GFP and mutAKAP450 2; B) Summary of FRET change induced by 25  $\mu$ M forskolin in the presence or absence of the AKAP450-2 and mutAKAP450-2 fragments. (Error bars represent SEM. Two tailed; un-paired t-test, \*  $p < 0.05$ ).**

As a further control, the AKAP450-2 fragment was over-expressed in cells over-expressing the RII\_Epac sensor. As shown Figure 5-10, CHO cells transiently expressing RII\_epac alone and challenged with forskolin showed the same FRET increase as cells expressing RII\_epac plus the AKAP450-2 fragment ( $\Delta R/R_0 = 9.684 \pm 0.467\%$  [n=34] for RII\_epac and  $\Delta R/R_0 = 10.346 \pm 0.483\%$  [n=41] for RII\_epac plus AKAP450-2 fragment;  $p = 0.33$ ; Figure 5-10).

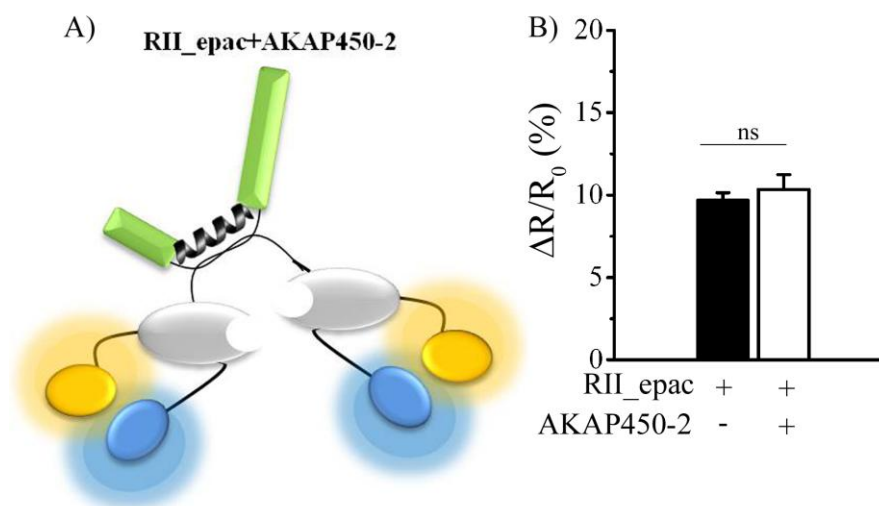


**Figure 5-10** Effect of RII\_epac binding to AKAP450-2 fragment. A) Schematic representation of RII\_epac/AKAP450-2 fragment interaction; B) Summary of FRET change induced by 25  $\mu$ M forskolin in the presence or absence of the AKAP450-2 fragment. (Error bar represents SEM. Two tailed un-paired t-test).

These data indicate that the larger FRET change detected by the PKA-GFP sensor in the presence of AKAP450-2 is specific for the PKA-based probe.

Taken together these data indicate that binding of PKA to AKAP450 lowers the activation constant of PKA for cAMP and strongly indicate that the larger FRET change detected at the centrosome compared to the bulk cytosol is the consequence of PKA being anchored to AKAP450 in this locale.

### ***5.1.3 The increased sensitivity to cAMP of AKAP-anchored PKA is specific for the PKA/AKAP450 interaction***

The next question I asked was whether the observed increased sensitivity to cAMP displayed by the PKA-GFP sensor anchored to AKAP450 was specifically due to the binding to AKAP450 or if it was also occurring when PKA was bound to other AKAPs. To answer this question I investigated the effect on cAMP sensitivity of three other AKAP fragments containing the amphipathic helix responsible for the anchoring of PKA (see section 3.1.17 and 3.1.19). Specifically, CHO cells expressing PKA-GFP were co-transfected with either the soluble AKAP Rt31 (see section 3.1.18) (Klussmann et al., 2001) or

with two membrane targeted AKAPs: AKAP79 (Herberg et al., 2000) and AKAP149 (see section 3.1.17) (Carlson et al., 2003). In all cases FRET changes elicited by application of 25  $\mu$ M forskolin were recorded by time-lapse fluorescence microscopy.

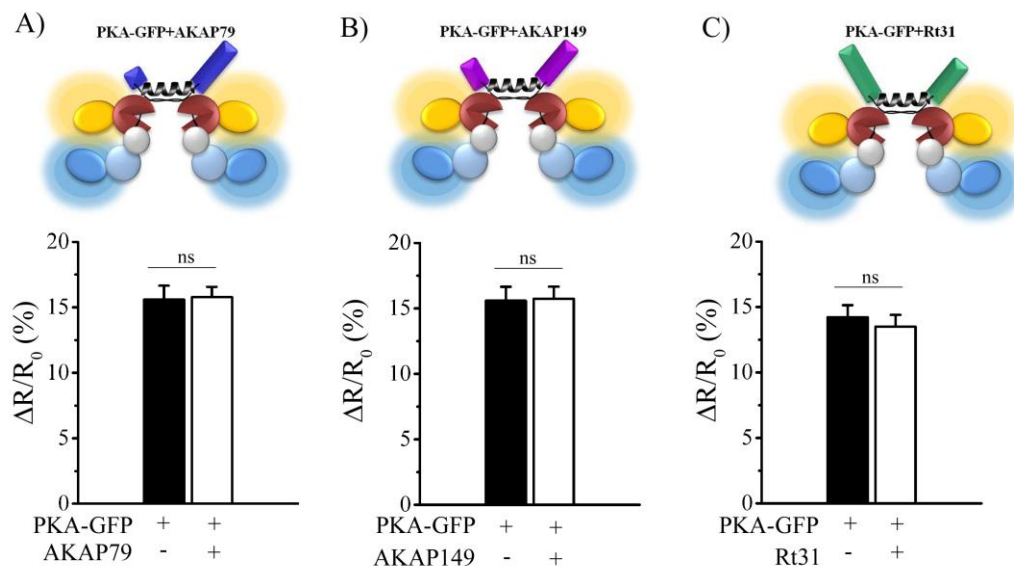


**Figure 5-11** Effect of PKA-GFP interaction with AKAP79, AKAP149 and Rt31 fragments on the sensitivity of PKA-GFP to cAMP. A) Schematic representation of PKA-GFP anchored to AKAP79 fragment (top) and summary of FRET change induced by 25  $\mu$ M forskolin in the presence or in the absence of the AKAP79 fragment (bottom); B) Schematic representation of PKA-GFP anchored to AKAP149 fragment (top) and summary of FRET change induced by 25  $\mu$ M forskolin in the presence or absence of the AKAP149 fragment (bottom); C) Schematic representation of PKA-GFP anchored to Rt31 fragment (top) and summary of FRET change induced by 25  $\mu$ M forskolin in the presence or absence of the Rt31 fragments (bottom). (Error bars represent SEM. Two tailed; un-paired t-test).

As shown in Figure 5-11, none of these AKAP fragments had an effect on the FRET change detected by the PKA-GFP sensor upon forskolin stimulation ( $\Delta R/R_0=14.222\pm 0.913\%$  [n=17] with PKA-GFP and  $\Delta R/R_0=13.506\pm 0.832\%$  [n=27] with PKA-GFP plus Rt31 fragment; p=0.57;  $\Delta R/R_0=15.583\pm 1.073\%$  [n=24] with PKA-GFP and  $\Delta R/R_0=15.778\pm 0.785\%$  [n=38] with PKA-GFP plus AKAP79 fragment; p=0.88;  $\Delta R/R_0=15.583\pm 1.073\%$  [n=24] with PKA-GFP and  $\Delta R/R_0=15.740\pm 0.924\%$  [n=43] with PKA-GFP plus AKAP149 fragment; p=0.91; Figure 5-11).

Taken together these results show that anchoring of PKA to AKAP450 results in a higher sensitivity of PKA to cAMP. This effect seems to be dependent on and specific for the binding of PKA to AKAP450. The increased sensitivity of PKA to cAMP can be estimated to be about two-fold (Figure 5-6) and points to a specific function of the centrosomal AKAP450 to lower the activation threshold of PKA in this area.

## 5.2 Discussion

The main result of this chapter is that, upon forskolin stimulation, CHO cells stably expressing a PKA-GFP sensor show a higher FRET change at the centrosome than in the cytosol (Figure 5-1). Since FRET changes correlate with cAMP increase these data suggest that forskolin leads to a higher cAMP level in the centrosomal region compared with the cytosol. A possible explanation for these findings is that a source of cAMP is present at the centrosome. Although it has been shown that a soluble isoform of AC (sAC) can be present at the centrosome, it is unlikely that sACs could be responsible for the enhanced activation of the centrosomal PKA-GFP. In fact, only bicarbonate is able to elicit a cAMP increase in nuclear extracts containing sAC, whereas forskolin does not produce any significant change in the same extracts (Zippin et al., 2003). However, to completely exclude the hypothesis of a higher cAMP increase at the centrosome than in the cytosol following forskolin stimulation, I monitored FRET changes at the centrosome and in the cytosol in cells stably expressing the unimolecular sensor for cAMP: RII\_epac. The idea was that if the cAMP increase is different between the two compartments I should detect such a difference independently from the molecular structure of the sensor used. Interestingly, upon forskolin stimulation the RII\_epac sensor detected equal FRET changes in the two compartments. This finding allows to exclude that forskolin induces a higher cAMP level at the centrosome (Figure 5-2).

To explain the higher FRET change detected at the centrosome upon forskolin stimulation when probed with the PKA-GFP sensor, I hypothesised that the interaction between AKAP450 and PKA could modify the sensitivity of

the anchored PKA to cAMP (Figure 5-4). Supporting this hypothesis, I provided evidence that binding of PKA to AKAP450 in CHO cells lowers the activation threshold of PKA upon forskolin stimulation (Figure 5-4 and Figure 5-6). Not only did cells over-expressing AKAP450 show a larger response to the same concentration of forskolin (Figure 5-4 and Figure 5-6), but also the number of cells responding to low concentrations of forskolin increased when PKA was co-expressed with this specific AKAP (Figure 5-5). Suppression of PKA-AKAP interaction through the over-expression of a SuperAKAP-IS disrupting peptide or deletion of the PKA dimerisation/docking domain (Figure 5-7 and Figure 5-8), as well as disruption of the AKAP450-amphipathic helix, abolished the increased sensitivity of PKA to cAMP, re-establishing the same activation threshold of soluble PKA (Figure 5-9). These findings strongly indicate that it is indeed the binding of PKA to AKAP450-2 that is responsible for increasing the sensitivity of the enzyme to cAMP. The fact that AKAP450-2 does not show any effect on the RII<sub>epac</sub> sensitivity to cAMP indicates that AKAP450-2 fragment affects specifically PKA (Figure 5-10). Finally, over-expression of three different AKAPs fragments (Rt31, AKAP79, AKAP149) revealed that none of those modified PKA-GFP FRET change upon forskolin stimulation, demonstrating that this effect is specific for the binding of PKA to AKAP450 (Figure 5-11).

It should be noted that the results presented here also allow to exclude the possibility that the higher FRET changes observed at the centrosome are due to an artefact related to the biochemical nature of the PKA-GFP sensor. When measuring FRET changes in response to a specific stimulus a region of interest (ROI) is selected and the FRET change is calculated as the ratio between CFP and YFP emission in that area. Since the PKA-GFP sensor is bimolecular and the activation of the sensor results in the release of the catalytic subunit from the regulatory subunit, one needs to consider the possibility that the higher FRET change detected at the centrosome may be due to a decreasing amount of C-YFP within the ROI that is being analysed. This problem relates only to the analysis of small compartments such as the centrosome, as when analysing the entire cell the signal from all R-CFP and all

C-YFP subunits present in the cell is averaged to calculate the CFP/YFP change. Based on the observation that over-expression of PKA together with the AKAP450-2 fragment showed in the cytosol FRET changes comparable to FRET changes detected at the centrosome of CHO stably expressing PKA-GFP (Figure 5-1 and Figure 5-4), I can exclude that the results obtained with the bimolecular PKA-GFP-based sensor are due to such an artefact.

The role of AKAPs in mediating the high levels of specificity and complexity of the cAMP/PKA signal transduction pathway has been widely studied (Beene and Scott, 2007) (Pidoux and Tasken). Beside the most important function of scaffolding protein, there is evidence that AKAPs can indirectly affect cAMP signalling pathway in several other ways (Wong and Scott, 2004) (Tasken and Aandahl, 2004). For instance, by recruiting PKA type I rather than PKA type II to a specific subcellular compartment, AKAPs can increase the sensitivity to cAMP of a particular process, as PKA type I can more easily be dissociated by cAMP than PKA type II (Jarnaess et al., 2008). Moreover, upon specific phosphorylation, AKAPs can associate or dissociate from different subcellular compartments (Westphal et al., 2000) (Dell'Acqua et al., 1998), as well as recruit or release components to and from the complex they nucleates. For instance, surface plasmon resonance spectroscopy showed that auto-phosphorylation of PKA type II modifies PKA affinity for Ht31, mAKAP and AKAP15/18 (Zakhary et al., 2000a) (Zakhary et al., 2000b). In another example, cAMP elevation and PKA mediated phosphorylation of PDE4D3 increases the affinity of PDE4D3 for mAKAP, suggesting that activation of mAKAP-anchored PKA enhances the recruitment of PDE4D3 and allow for a quicker signal termination (Carlisle Michel et al., 2004). This evidence supports a role for AKAPs in the modulation of the cAMP/PKA signal transduction pathway by moving the complex where cAMP concentration is below the PKA-activation threshold or by favouring cAMP degradation, rapidly terminating the response and promoting the re-association of the PKA holoenzyme (see section 1.5.1). However a direct modulation of PKA sensitivity to cAMP as a consequence of PKA interaction with an AKAP had

never been shown before, and represent therefore a novel mechanism through which cAMP/PKA signalling can be modulated.

In summary, the data presented here indicate that PKA anchored to AKAP450 can be activated by concentrations of cAMP that do not affect soluble PKA or other subsets of PKA anchored to different AKAPs. These data show, for the first time, that anchoring of PKA to an AKAP can locally modify the sensitivity of PKA to cAMP. This is a completely new mechanism of local regulation of the cAMP/PKA pathway that is achieved by lowering the activation threshold of the effectors without affecting the concentration level of the second messenger itself. The ability to modify PKA activation through binding to PKA also constitutes a completely new function for AKAPs.

# 6 Study of PKA activity at the centrosome

---

## Background:

In the previous chapters I investigated the role of the centrosomal AKAP450 and PDE4D3 in modulating cAMP signalling at the centrosome. By using a FRET based approach I could demonstrate that PDE4D3 activity is required to maintain cAMP at low concentration at the centrosome. In addition, I showed that binding of PKA to the centrosomal AKAP450 modulates PKA sensitivity to cAMP by lowering PKA activation threshold.

## Hypothesis:

Based on the previous results, the guiding hypothesis of this chapter is that, at a given cAMP concentration, the activity of the PKA subset anchored to AKAP450 is higher than the activity of cytosolic PKA.

## Experimental procedure:

- 1) FRET based analysis of PKA activity by using an **A-Kinase activity reporter (AKAR3)** (Allen and Zhang, 2006).

- 2) FRET based analysis of PKA activity upon binding to AKAP450.
- 3) Comparison of PKA activity in the cytosol and at the centrosome within the same cell by using different centrosome-targeted versions of the AKAR3 sensor.

## 6.1 Results

### 6.1.1 AKAR3 as a sensor to measure PKA activity

AKAR3 is a FRET-based sensor that allows to monitor PKA activity in real-time with high resolution in space and time (Allen and Zhang, 2006) (Zhang et al., 2005) (Herbst et al., 2009). It is based on a substrate sequence for PKA (LRRATLVD) and the phosphothreonine binding domain forkhead-associated domain 1 (FHA1) sandwiched between CFP and a circular permutant of the YFP variant named Venus (cpV). When the PKA activity is low the two fluorophores are too far for FRET to occur. Activated PKA phosphorylates the PKA substrate sequence in AKAR3 resulting in binding of the FHA1 domain to phosphothreonine. The consequent conformational change results in a reduction of the distance between the donor and the acceptor fluorophores leading to a FRET increase (Figure 6-1). Therefore, FRET changes correlate with changes in PKA activity.

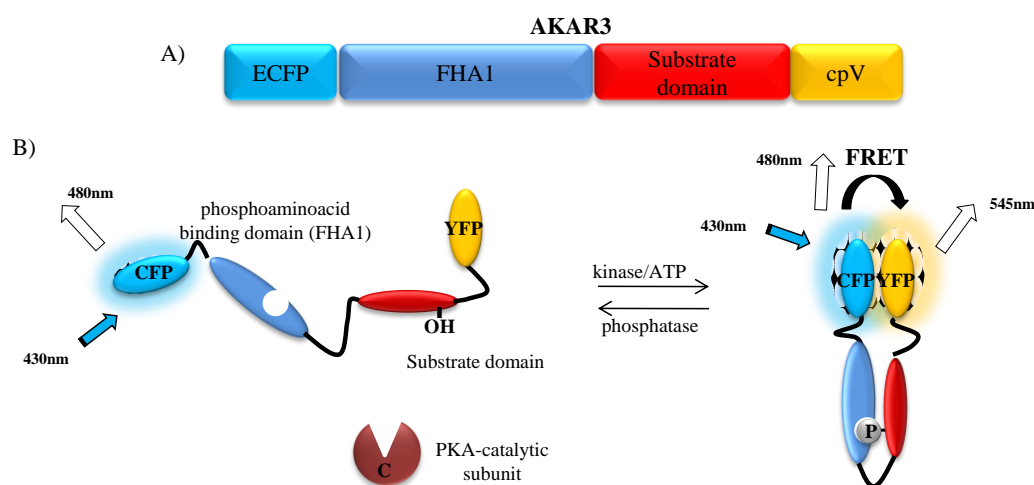


**Figure 6-1 Schematic representation of AKAR3 reporter and its mechanism of function.**

In order to validate AKAR3 as a reporter of PKA activity I first challenged CHO cells over-expressing AKAR3 with 25  $\mu\text{M}$  forskolin. As shown in Figure 6-2 forskolin generated a FRET change of  $\sim 10\%$ , indicating that the sensor can monitor activity of endogenous PKA ( $\Delta R/R_0 = 10.0934 \pm 0.672\%$  [ $n=56$ ]).

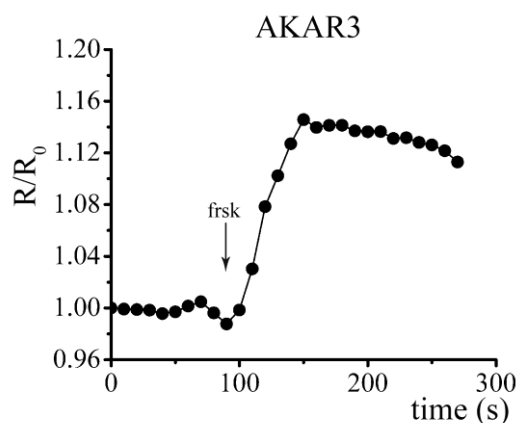


**Figure 6-2 Representative kinetics of FRET change induced by 25  $\mu\text{M}$  forskolin (frsk) in CHO cells expressing AKAR3 reporter.**

Next, I tested the specificity of the sensor for PKA activity by incubating AKAR3 expressing CHO cells with the PKA inhibitor H-89 (N-[2-[[3-(4-Bromophenyl)-2-propenyl] amino] ethyl]-5-isoquinolinesulfonamide dihydrate dihydrochloride, 10  $\mu\text{M}$ ). As shown in Figure 6-3 pre-treatment with H-89 almost completely abolished the FRET change detected by AKAR3 to forskolin treatment, further confirming that the sensor measures PKA-dependent activity.

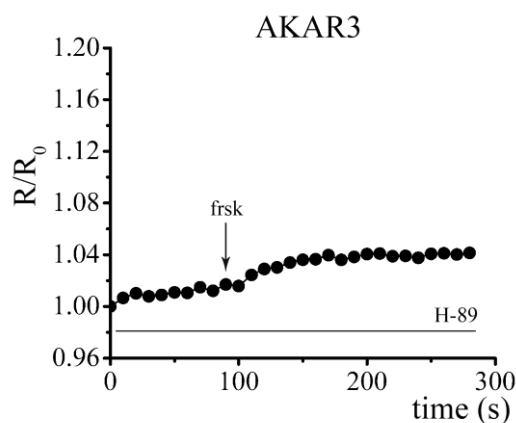


**Figure 6-3** Representative kinetics of FRET change induced by 25  $\mu\text{M}$  forskolin (frsk) in CHO cells expressing AKAR3 and pre-treated with 10  $\mu\text{M}$  H-89.

### ***6.1.2 Binding of PKA to AKAP450-2 increases PKA activity***

The next step was to assess whether binding of PKA to AKAP450, by affecting PKA sensitivity to cAMP, would also increase PKA activity in response to a given concentration of second messenger. In the experiments described below the PKA-activity reporter was co-expressed with AKAP450-2 and FRET changes were monitored upon forskolin stimulation. The rationale here is that anchoring of endogenous PKA to the over-expressed cytosolic AKAP450-2 fragment should increase PKA sensitivity to cAMP leading to an increase in the PKA activity detected by AKAR3. CHO cells over-expressing AKAR3 and the AKAP450-2 fragment were challenged with 25  $\mu\text{M}$  forskolin and the FRET change recorded was compared with the FRET change detected in cells over-expressing AKAR3 alone. As shown in Figure 6-4, over-expression of AKAP450-2 resulted in a significantly higher FRET response ( $0.01 < p < 0.001$ ) compared with control cells not expressing the AKAP450-2. The FRET change detected was  $\Delta R/R_0 = 10.093 \pm 0.672\%$ , [n=56] for AKAR3 and  $\Delta R/R_0 = 13.577 \pm 1.059\%$ , [n=53] for AKAR3 plus AKAP450-2 fragment.

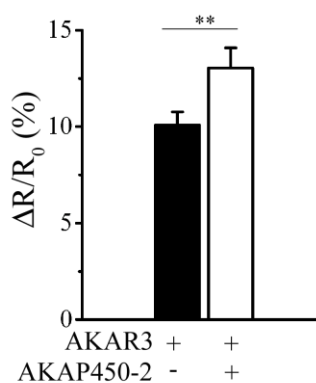


**Figure 6-4 Effect of over-expression of AKAP450-2 on endogenous PKA activity. Error bar represents SEM. Two tailed; un-paired t-test, \*\* 0.01<p<0.001).**

On the contrary, no difference in PKA activity was recorded in CHO cells over-expressing AKAR3 in combination with a fragment of AKAP79 (see section 3.1.17) ( $\Delta R/R_0=15.811\pm 1.860\%$ , [n=16] with AKAR3 and  $\Delta R/R_0=14.773\pm 2.043\%$ , [n=14] with AKAR3 plus AKAP79 fragment; p=0.69) (Figure 6-5).

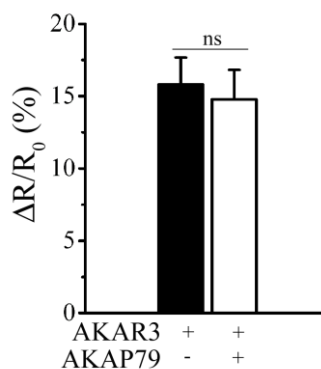


**Figure 6-5 Effect of over-expression of AKAP79 on endogenous PKA activity. (Error bar represents SEM. Two tailed; un-paired t-test).**

These results confirm that anchoring of PKA to AKAP450 increases the sensitivity of PKA to cAMP resulting in increased PKA activity at a given cAMP level.

### 6.1.3 Generation of targeted AKAR3 sensors to monitor centrosomal PKA activity

The purpose of the following experiment was to directly monitor the local activity in response to a given cAMP level of a PKA subset anchored to AKAP450 at the centrosome. To this end I generated two centrosome-targeted variants of the AKAR3 reporter (Figure 6-6). For one of these constructs, the RII\_AKAR3 sensor (Stangherlin et al., 2011), I genetically fused the D/D of the RII $\beta$  subunit (aa 1-49) to the N-terminus of AKAR3 in order to target the probe to endogenous AKAPs, including AKAP450 (see section 3.1.19). For the second construct, I fused the GIT1 sequence (aa 1-119) to the N-terminus of the AKAR3 reporter. GIT1 is a G-protein coupled receptor kinase interacting protein and a GTPase-activating protein (GAP) for the ADP ribosylation factor (ArfGAP protein) (see section 3.1.19) (Premont et al., 1998). It has previously been shown that GIT1 is concentrated at the centrosome during all stages of the cell cycle and the N-terminus domain of this protein (aa 1-119) has been shown to be responsible for centrosomal targeting (Zhao et al., 2005).



**Figure 6-6 Schematic representations of centrosome-targeted AKAR3 reporters: A) RII\_AKAR3 and B) GIT1\_AKAR3.**

As illustrated in Figure 6-7 both these sensors showed a clear localisation to the centrosome in CHO cells.

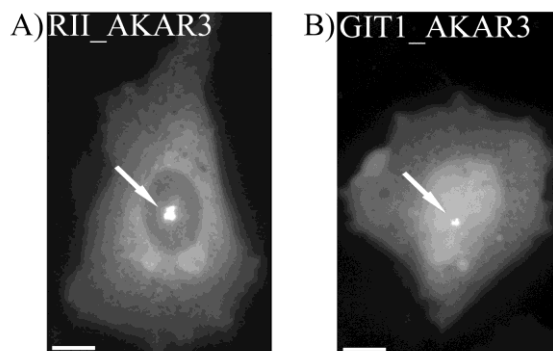


**Figure 6-7** Subcellular localisation of RII\_AKAR3 and GIT1\_AKAR3 in CHO cells. The arrows point to the centrosome. Bars 10 $\mu$ m.

CHO cells transfected either with RII\_AKAR3 or with GIT1\_AKAR3 and challenged with 25  $\mu$ M forskolin generated a FRET change (averaged over the entire cell) of  $19.570 \pm 0.798\%$  ( $n=50$ ) and  $15.306 \pm 1.692\%$  ( $n=22$ ) respectively, both at the centrosome and in the cytosol, indicating that the engineering of the sensors did not affect their capability to generate a FRET change in response to PKA-mediated phosphorylation (Figure 6-8).

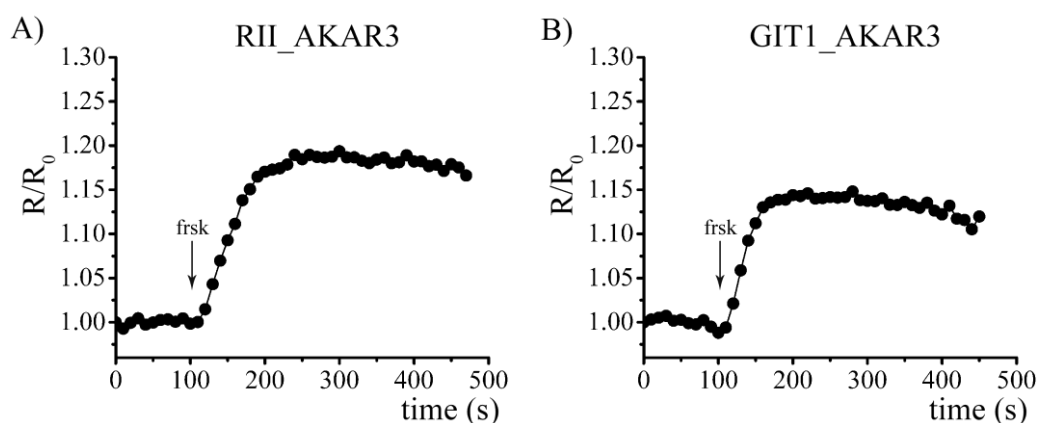


**Figure 6-8** Representative kinetics of FRET change generated by 25  $\mu$ M forskolin (frsk) in CHO cells expressing A) RII\_AKAR3 sensor or B) GIT1\_AKAR3 sensor.

Subsequently, I compared the FRET changes elicited by 25  $\mu$ M forskolin at the centrosome and in the cytosol of CHO cells over-expressing either RII\_AKAR3 or GIT1\_AKAR3 (Figure 6-9).

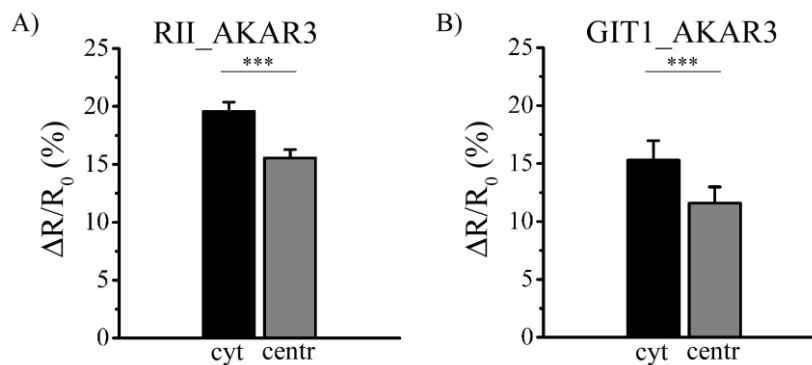


**Figure 6-9 Effect of 25  $\mu$ M forskolin on endogenous cytosolic and centrosomal PKA activity. Summary of FRET changes recorded in the cytosol (cyt) and at the centrosome (centr) of CHO cells expressing A) RII\_AKAR3 or B) GIT1\_AKAR3 sensor. (Error bars represent SEM. Two tailed; paired t-test, \*\*\*  $p < 0.001$ ).**

Surprisingly, both sensors showed a significantly higher FRET response in the cytosol compared to the centrosome ( $\Delta R/R_0 = 19.570 \pm 0.798\%$ , in the cytosol and  $\Delta R/R_0 = 15.550 \pm 0.727\%$  at the centrosome with RII\_AKAR3, [n=50];  $p < 0.001$  and  $\Delta R/R_0 = 15.306 \pm 1.609\%$ , in the cytosol and  $\Delta R/R_0 = 11.586 \pm 1.404\%$  at the centrosome with GIT1\_AKAR3, [n=22];  $p < 0.001$ ; Figure 6-9). These data do not seem to support the hypothesis of an increased PKA activity at the centrosome as a consequence of PKA binding to AKAP450. Moreover they are contradictory to the previous results obtained upon the binding of the endogenous PKA to the AKAP450-2 fragment in the cytosol.

In Takahashi et al. it was shown that AKAP450 targets two phosphatases, proteins phosphatase 1 (PP1) and protein phosphatase 2A (PP2A) to the centrosome (Takahashi et al., 1999). A possible explanation for the above results could be that the centrosome-targeted sensors, RII\_AKAR3 and GIT1\_AKAR3, are rapidly de-phosphorylated by these two phosphatases thus masking the hypothesised higher PKA activity at the centrosome. Based on this consideration, CHO cells over-expressing AKAR3, RII\_AKAR3 or the GIT1\_AKAR3 were pre-treated with 20 nM calyculin A, a potent and selective cell-permeable inhibitor of PP1 and PP2A. Figure 6-10 shows that calyculin A is

effective in inhibiting phosphatase activity in the cell as shown by the significantly higher FRET change detected by AKAR3 in the presence of the inhibitor ( $\Delta R/R_0=11.745\pm 0.696\%$ , and  $\Delta R/R_0=18.709\pm 1.460\%$  in the presence or absence of calyculin A, [n>24];  $p<0.001$ , values are averages over the entire cell).

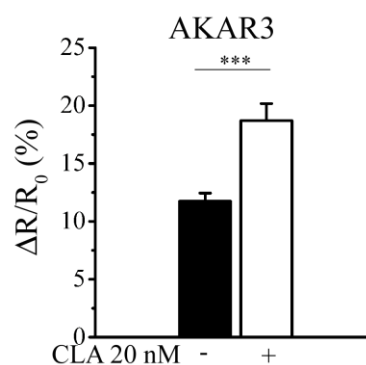


**Figure 6-10** Effect of 25  $\mu\text{M}$  forskolin on endogenous PKA activity in the presence of the PP1 and PP2A inhibitor calyculin A. Summary of FRET changes induced by 25  $\mu\text{M}$  forskolin in CHO cells expressing AKAR3 and in the absence or in the presence of 20 nM calyculin A (CLA). (Error bar represents SEM. Two tailed; un-paired t-test, \*\*\*  $p<0.001$ ).

However, the comparison between centrosome and cytosol in the presence of calyculin A revealed that PKA activity was still significantly lower at the centrosome than in the cytosol, either when FRET changes were detected with RII\_AKAR3 or GIT1\_AKAR3 ( $\Delta R/R_0=22.661\pm 2.917\%$ , in the cytosol and  $\Delta R/R_0=188.19\pm 2.088\%$  at the centrosome with RII\_AKAR3, [n=15];  $p<0.05$  and  $\Delta R/R_0=19.705\pm 2.234\%$ , in the cytosol and  $\Delta R/R_0=16.561\pm 2.315\%$  at the centrosome with GIT1\_AKAR3, [n=14];  $0.01<p<0.00$ ; Figure 6-11).

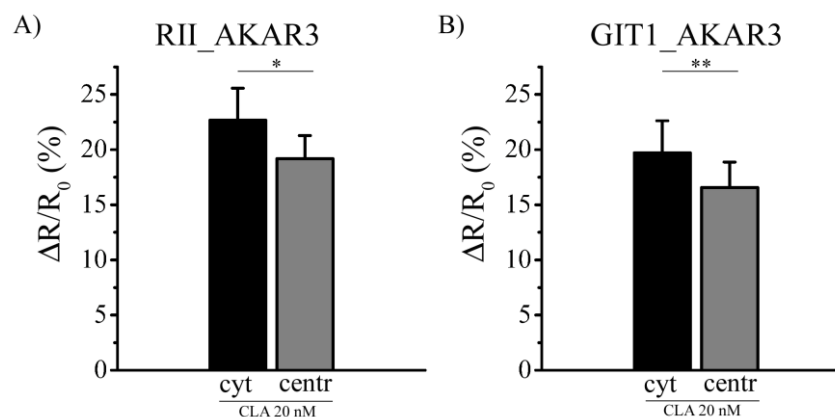


**Figure 6-11** Effect of 25  $\mu\text{M}$  forskolin on endogenous cytosolic and centrosomal PKA activity after inhibition of PP1 and PP2A. Summary of FRET changes recorded in the cytosol (cyt) and at the centrosome (centr) of CHO cells expressing A) RII\_AKAR3 or B) GIT1\_AKAR3 sensor and pre-treated with 20 nM calyculin A (CLA). (Error bars represent SEM. Two tailed; paired t-test, \*  $p < 0.01$ , \*\*  $0.01 < p < 0.001$ ).

One possible explanation for these results is that application of 20 nM calyculin A and 25  $\mu\text{M}$  of forskolin results in the saturation of the centrosomal anchored sensors. If this were the case, every difference in PKA activity between the two compartments would be masked. In an attempt to overcome this problem I stimulated CHO cells expressing the centrosome-targeted PKA activity reporter with 100 nM forskolin in the presence or in absence of the phosphatase inhibitor calyculin A (Figure 6-12).

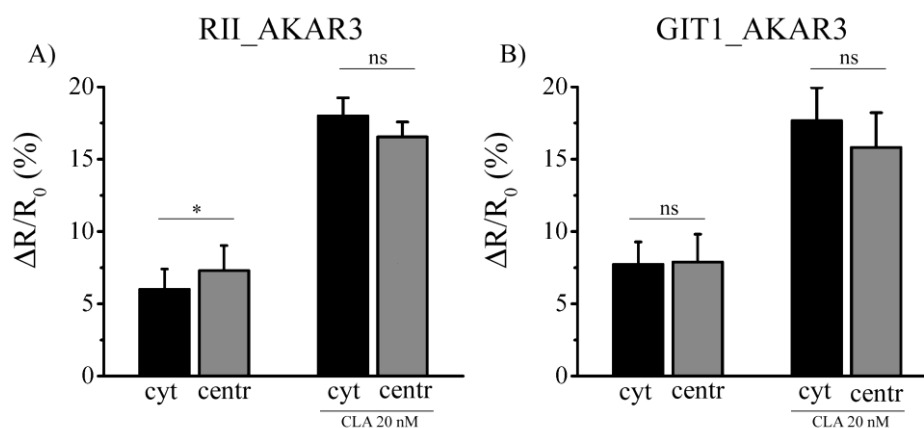


**Figure 6-12** Effect of 100 nM forskolin on endogenous cytosolic and centrosomal PKA activity with or without inhibition of PP1 and PP2A. Summary of FRET changes recorded in the cytosol (cyt) and at the centrosome (centr) of CHO cells expressing A) RII\_AKAR3 or B) GIT1\_AKAR3 sensor and pre-treated with or without 20 nM calyculin A (CLA). (Error bars represent SEM. Two tailed; paired t-test, \*  $p < 0.05$ ).

Results obtained are shown in Figure 6-12. When I probed with RII\_AKAR3 (Figure 6-12; A), left panel), in the absence of calyculin A, the FRET change is significantly higher ( $p < 0.05$ ) at the centrosome than in the cytosol, in response to 100 nM of forskolin ( $\Delta R/R_0 = 6.005 \pm 1.399\%$ , in the cytosol and  $\Delta R/R_0 = 7.303 \pm 1.727\%$  at the centrosome for RII\_AKAR3, [n=12]); however these data were not confirmed by the inhibition of the phosphatases. Pre-treatment with calyculin A did not affect centrosomal-PKA activity and resulted in a trend towards a lower PKA activity at the centrosome than in the cytosol ( $\Delta R/R_0 = 18.000 \pm 1.246\%$ , in the cytosol and  $\Delta R/R_0 = 16.544 \pm 1.034\%$  at the centrosome for RII\_AKAR plus calyculin A, [n=18];  $p = 0.16$ ).

When I probed PKA activity with GIT1\_AKAR3 (Figure 6-12; B), right panel), in the absence of calyculin A, FRET response did not show any significant difference between the two compartments ( $\Delta R/R_0 = 7.732 \pm 1.555\%$ , in the cytosol and  $\Delta R/R_0 = 7.896 \pm 1.917\%$  at the centrosome for GIT1\_AKAR3, [n=5];  $p = 0.89$ ). However, pre-treatment with calyculin A resulted in a trend toward lower PKA activity at the centrosome than in the cytosol (not significant) ( $\Delta R/R_0 = 17.675 \pm 2.280\%$ , in the cytosol and  $\Delta R/R_0 = 15.822 \pm 2.399\%$  at the centrosome for GIT1\_AKAR3 plus calyculin A, [n=14];  $p = 0.09$ ).

## 6.2 Discussion

In this chapter I set out to study the activity of the centrosomal, AKAP450-anchored, PKA by using the FRET based sensor AKAR3 (Figure 6-1). As a first step, the cellular responses of AKAR3 were shown to be specific for PKA since in the presence of H-89 (a specific PKA inhibitor) the sensor did not show any response upon forskolin stimulation (Figure 6-2 and Figure 6-3).

Then, I provided evidence that endogenous PKA, upon binding to the AKAP450-2 fragment in the cytosol, shows increased activity (Figure 6-4), whereas the binding of endogenous PKA to a different AKAP fragment does not affect PKA activity (Figure 6-5). These data suggest, once again, that AKAP450 is not only a scaffolding protein which anchors PKA to the centrosome, but also acts as a modulator of the cAMP/PKA pathway enhancing PKA sensitivity to cAMP. It is possible that anchoring of PKA to AKAP450 raises PKA sensitivity and activity in a location in which would be difficult to selectively increase cAMP concentration. It has been shown that ERK can inhibit PDE4D3 upon phosphorylation (MacKenzie et al., 2000). Thus a possible scenario would be that the constitutively active PDE4D3 anchored to the centrosome is inactivated by ERK phosphorylation, allowing centrosomal cAMP levels to rise independently from adenylyl cyclases activation.

An important advantage of genetically encoded FRET reporters is that they can be targeted to different locations via various localisation signals. This approach provides a tool to monitor PKA activity in distinct subcellular compartments within the same cell and can reveal differences in PKA signalling between the site of cAMP synthesis at the plasma membrane and other regions where the signal is propagating to. This has been previously demonstrated by a study using AKAR3 sensors specifically targeted to the plasma membrane (pm-AKAR3, pm= palmitoylated and myristoylated sequence), to the cytosol (AKAR3-NES, NES=nuclear export sequence) and to the nucleus (AKAR3-NLS NLS=nuclear localisation sequence) (Allen and Zhang, 2006). Based on this studies, I generated two different centrosome-targeted

sensors by fusing the D/D of the RII $\beta$  subunit (1-49aa) or the N-terminus of GIT1 (1-119aa) to AKAR3 (Figure 6-6 and Figure 6-7). Targeting of AKAR3 to the centrosome, however, did not detect the expected higher PKA activity upon forskolin stimulation (Figure 6-9). One possible explanation for these results is that phosphatases anchored to the centrosome could be responsible for a rapid de-phosphorylation of the sensor thereby masking a higher AKAR3 activation at the centrosome. Although pre-treatment of cells with calyculin A did increase the FRET change monitored by the AKAR3 reporter (Figure 6-10), it failed to invert the difference in PKA activity between the two compartments (Figure 6-11 and Figure 6-12).

Another possible explanation for these findings is that targeting of AKAR3 to the centrosome is affecting the PKA signalling complex in such a small compartment. In fact, the over-expression of RII\_AKAR3 and its anchoring to the endogenous AKAPs might lead to the displacement of the endogenous PKA subsets from their original anchoring site. If the endogenous PKA anchored to AKAP450 is displaced by the over-expressed RII\_AKAR3 there would be reduced endogenous PKA at this site and therefore I would not be able to monitor a higher activity of the AKAP450-anchored PKA.

As far as the anchoring of the over-expressed GIT1\_AKAR3 is concerned, this may occur on other centrosomal location and may not involve AKAP450/PKA/PDE4D3 molecular complex. This may explain why no higher activity of centrosomal PKA is detected in this case.

# 7

## **Anchoring of PKA to AKAP450 favours auto-phosphorylation of the PKA regulatory subunit**

---

### *Background*

So far I have provided evidence that AKAP450, by anchoring PKA and PDE4D3, nucleates a multi-protein complex at the centrosome within which cAMP/PKA signalling is tightly regulated. On the one hand, PDE4D3 maintains cAMP at a lower concentration in the centrosome as compared to the bulk cytosol; on the other hand, anchoring of PKA to AKAP450 appears to increase the sensitivity of PKA to cAMP.

In this chapter I aim at elucidating the mechanism responsible for the higher sensitivity to cAMP of the PKA subset bound to AKAP450.

It is well established that the RII $\beta$  subunit of PKA can undergo auto-phosphorylation at Ser114. Phosphorylation at this site reduces the affinity of the regulatory subunit for the catalytic subunit by almost one order of magnitude thereby lowering the activation constant of PKA (Rangel-Aldao and

Rosen, 1977). Moreover, auto-phosphorylation of PKA occurs as an intramolecular event and does not require PKA dissociation (Rangel-Aldao and Rosen, 1976b).

Hypothesis:

The guiding hypothesis of the studies presented in this chapter is that anchoring of PKA to AKAP450 favours auto-phosphorylation of the RII subunit at S114, thus decreasing the activation threshold of PKA.

Experimental procedure:

- 1) Analysis of the phosphorylation level at S114 in the RII $\beta$  subunit using western blot analysis in the presence or in the absence of the AKAP450-2 fragment.
- 2) Analysis of FRET changes detected using a PKA-GFP sensor including a non-phosphorylatable R subunit (mutRII-CFP, containing the mutation S114A).
- 3) Generation of a CHO cell line stably expressing the mutPKA-GFP sensor and comparison of the FRET signal in the cytosol and at the centrosome upon forskolin stimulation.

## 7.1 Results

### ***7.1.1 Anchoring of PKA to AKAP450 enhances auto-phosphorylation of the RII subunit***

To assess if auto-phosphorylation of the RII $\beta$  subunit is involved in the observed increased sensitivity to cAMP of AKAP450-bound PKA, the level of phosphorylation at S114 of the RII-CFP component of the PKA-GFP sensor was determined by SDS-PAGE analysis. Lysates from CHO cells over-expressing the PKA-GFP sensor, in the presence or in the absence of the AKAP450-2 fragment, were probed with a RII antibody and with a phospho S114-specific antibody. Western blot analysis revealed a band at ~80kDa, corresponding to the molecular weight of the recombinant RII subunit tagged with CFP. A band at ~53kDa, corresponding to the endogenous RII subunit, was also detected.

Clearly, over-expression of AKAP450 led to an increase of the phosphorylation level of both the endogenous and the over-expressed RII-CFP subunits. A quantitative analysis of the bands intensities confirmed that the auto-phosphorylation level of RII subunits is indeed significantly increased (~50% increase) when PKA is co-expressed with AKAP450-2. These data indicate that anchoring of PKA-GFP to AKAP450-2 fragment promotes the auto-phosphorylation of PKA RII $\beta$  subunit (Figure 7-1).

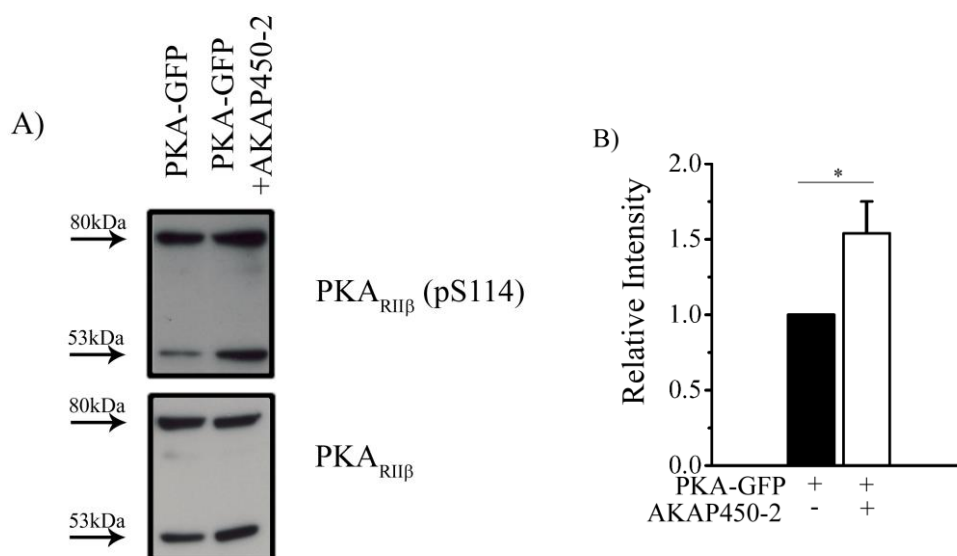


**Figure 7-1 Effect of over-expression of AKAP450-2 on endogenous PKA RII $\beta$ -subunit auto-phosphorylation. A) Representative western blot of total RII $\beta$  and phospho-RII $\beta$ . B) Western Blot quantification (mean of 5 separate experiments). (Error bar represents SEM. Two tailed; paired t-test, \*  $p < 0.05$ ).**

### ***7.1.2 Generation of a non-phosphorylatable mutant of the PKA-GFP sensor (mutPKA-GFP)***

To further assess if the auto-phosphorylation site of the RII $\beta$  subunit is involved in the mechanism that increases the cAMP-sensitivity of AKAP450-bound PKA, I generated a non-phosphorylatable mutant of the regulatory subunit (mutRII-CFP) by introducing the point mutation S114A, (see section 1.4.1, 3.1.20) (Figure 7-2) (Rodriguez-Vilarrupla et al., 2005), (Wehrens et al., 2006), (Taylor et al., 1990).

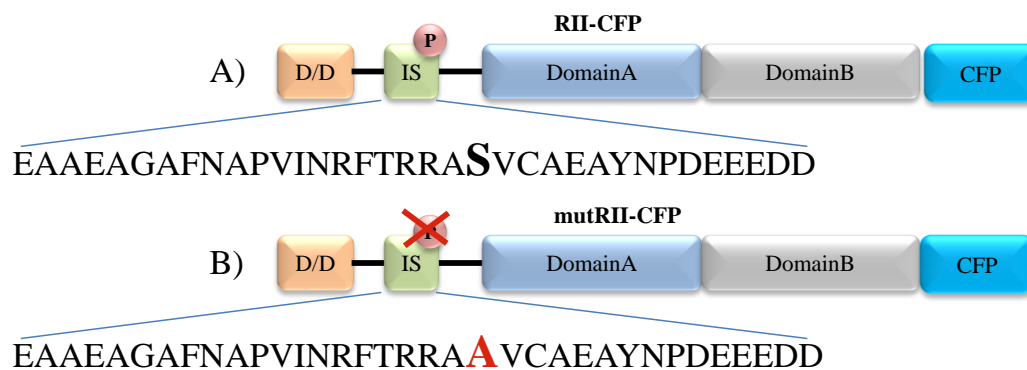


**Figure 7-2 Schematic representation of A) RII-CFP and B) mutRII-CFP subunit with the substitution S114A. D/D=PKA-RII $\beta$  dimerisation docking/domain; IS=inhibitory site (or auto-phosphorylation site); DomainA=cAMP binding domain A; DomainB=cAMP binding domain B; CFP=cyan variant of the green fluorescent protein (GFP).**

First of all I wanted to confirm that the mutant sensor (mutRII-CFP+C-YFP) could not be auto-phosphorylated. CHO lysates from cells expressing mutPKA-GFP were probed with the phospho-S114 specific antibody and compared with lysates from cells expressing the PKA-GFP (wild type) sensor (Figure 7-3).

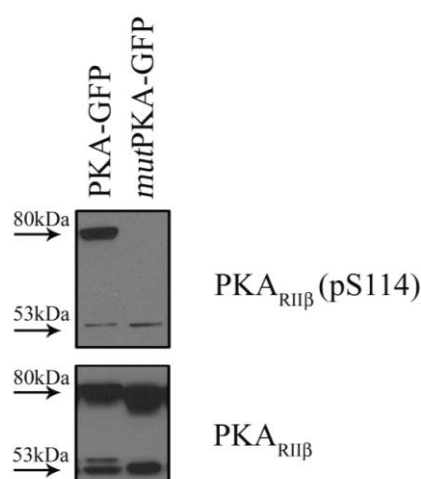


**Figure 7-3 Western blot showing auto-phosphorylation of PKA-GFP and mutPKA-GFP. The PKA<sub>RII $\beta$</sub>  (pS114) antibody recognised only the auto-phosphorylation of the endogenous PKA in lysates from CHO cells over-expressing the mutPKA-CFP.**

Western blot analysis, using the anti-phospho S114 antibody, revealed in both cell lysates a band at  $\sim 53$ kDa corresponding to the endogenous phospho-RII $\beta$  subunit, whereas only cells over-expressing the PKA-GFP (wild type) also showed a band at  $\sim 80$ kDa, corresponding to the molecular weight of the RII-CFP (Figure 7-3); thereby confirming that the point mutation completely abolishes auto-phosphorylation of the RII $\beta$  subunit.

Next, I tested the ability of mutPKA-GFP to detect FRET changes upon forskolin stimulation. CHO cells over-expressing mutPKA-GFP or PKA-GFP (wild type) were challenged with 25  $\mu$ M forskolin. The mutPKA-GFP showed a significantly lower FRET change than PKA-GFP ( $\Delta R/R_0 = 12.401 \pm 0.834\%$  [n=38] with PKA-GFP and  $\Delta R/R_0 = 9.746 \pm 0.643\%$  [n=46] with mutPKA-GFP;  $p < 0.05$ , Figure 7-4) (Rangel-Aldao and Rosen, 1976a).

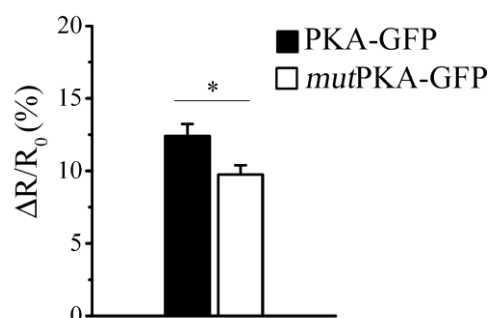


**Figure 7-4 Comparison between PKA-GFP (wild type) and mutPKA-GFP FRET sensors. Summary of FRET changes induced by 25  $\mu$ M forskolin in CHO cells over-expressing PKA-GFP or mutPKA-GFP. (Error bar represents SEM. Two tailed; unpaired t-test, \*  $p < 0.05$ )**

### ***7.1.3 mutPKA-GFP anchored to AKAP450-2 does not show increased sensitivity to cAMP***

In order to test whether anchoring to AKAP450 might affect auto-phosphorylation of PKA thus lowering its activation threshold, I looked at the effect of over-expressing AKAP450-2 fragment on the FRET changes detected by the mutPKA-GFP sensor. When FRET changes were measured in the bulk cytosol of CHO cells over-expressing mutPKA-GFP in combination with

AKAP450-2, the response to 25  $\mu$ M forskolin stimulation detected was of the same amplitude as in cells that did not express the AKAP450-2 fragment ( $\Delta R/R_0=9.745\pm 0.643\%$  [n=46] and  $\Delta R/R_0=10.715\pm 0.720\%$  [n=28] in the presence or absence of the AKAP450-2 fragment, respectively; p=0.33; Figure 7-5).

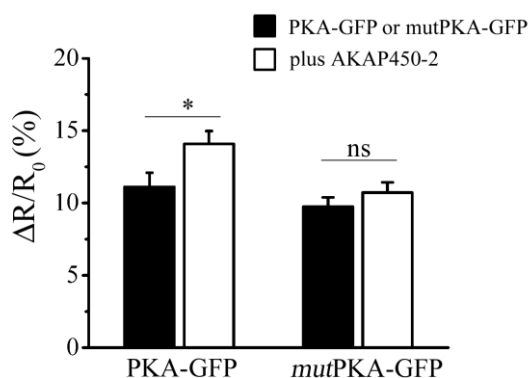


**Figure 7-5 Effect of AKAP450-2 on the FRET change detected by PKA-GFP and mutPKA-GFP. Summary of FRET changes induced by 25  $\mu$ M forskolin and detected by PKA-GFP (wild type) and mutPKA-GFP in the presence (white columns) or absence (black columns) of the AKAP450-2 fragment. (Error bars represent SEM. Two tailed; unpaired t-test, \* p<0.05).**

These results differ from those obtained when over-expressing PKA-GFP in combination with AKAP450-2 ( $\Delta R/R_0=11.115\pm 0.975\%$  [n=22] and  $\Delta R/R_0=14.077\pm 0.890\%$  [n=20] in the presence or absence of AKAP450-2 fragment, respectively; p<0.05; Figure 7-5) and indicate that the S114A mutation abolishes the ability of the AKAP450-2 fragment to affect the activation threshold of PKA.

#### ***7.1.4 Generation of a stable clone over-expressing mutPKA-GFP***

To further address the role of the auto-phosphorylation site in the PKA regulatory subunit in determining increased PKA sensitivity to cAMP of centrosomal PKA, I established a CHO clone stably expressing the mutPKA-GFP

sensor. The mutRII-CFP contains an intact docking domain and therefore the mutant sensor can, and does, anchor to the centrosome (Figure 7-6).

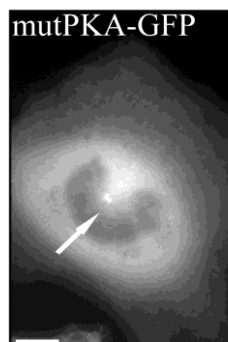


**Figure 7-6 Subcellular localisation of mutPKA-GFP in CHO cells. The centrosome is indicated by the arrow. Bar 10  $\mu$ m.**

Cells stably expressing mutPKA-GFP were challenged with forskolin and the FRET changes were monitored both in the cytosol and at the centrosome. As shown in Figure 7-7 there was no significant difference in the FRET change detected by the mutPKA-GFP sensor at the centrosome and in cytosol (Figure 7-7, white bars). Thus, introduction of the S114A mutation completely abolished the difference in cAMP sensitivity recorded in two compartments by the PKA-GFP sensor (Figure 7-7, black bars), confirming that auto-phosphorylation of RII $\beta$  at S114 is required to increase the sensitivity to cAMP of the AKAP450-anchored PKA subset at the centrosome (PKA-GFP (black columns):  $\Delta R/R_0 = 12.198 \pm 0.662\%$  and  $\Delta R/R_0 = 14.334 \pm 0.910\%$  [n=35] in the cytosol and at the centrosome, respectively;  $p < 0.001$ , mutPKA-GFP (white columns):  $\Delta R/R_0 = 10.196 \pm 1.036\%$  [n=16] and  $\Delta R/R_0 = 10.662 \pm 1.358\%$  [n=16] in the cytosol and at the centrosome, respectively;  $p = 0.61$ ; Figure 7-7).

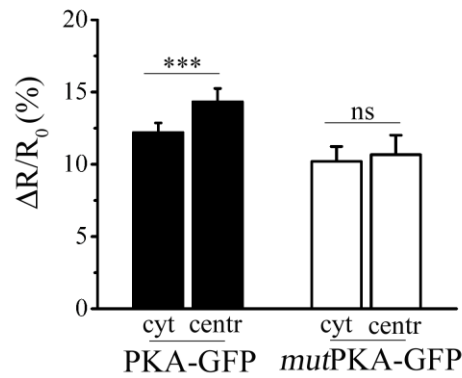


**Figure 7-7** Effect of 25  $\mu$ M forskolin on the FRET change detected in the cytosol (cyt) and at the centrosome (centr) by mutPKA-GFP and PKA-GFP. (Error bars represent SEM. Two tailed; paired t-test, \*\*\*  $p < 0.001$ ).

## 7.2 Discussion

In this set of experiments I set out to investigate if the auto-phosphorylation site in the PKA regulatory subunit may be involved in the mechanism responsible for the higher sensitivity to cAMP shown by the AKAP450-bound PKA subset. By western blot analysis I provided evidence that anchoring of PKA to AKAP450 results in increased auto-phosphorylation of the PKA regulatory subunit (Figure 7-1). Mutation of the auto-phosphorylation site in the RII $\beta$  subunit by introducing an alanine residue in position 114 (S114A mutation) prevented AKAP450 from affecting the PKA activation threshold (Figure 7-5), although it did not interfere with the ability of the sensor to generate a FRET change upon forskolin stimulation (Figure 7-4). In addition, FRET-based analysis of CHO cells stably expressing mutPKA-GFP revealed a comparable FRET change generated by sensor at the centrosome and in the cytosol (Figure 7-7). These results strongly support the hypothesis that the auto-phosphorylation site in the PKA regulatory subunit is involved in the mechanism that leads to lowering of the PKA activation threshold. How the binding of PKA to AKAP450 can promote auto-phosphorylation of the RII subunit is still unclear and requires further investigation.

# 8 Displacement of centrosomal PDE4D3 from AKAP450 results in altered cell cycle progression

---

## Background:

The centrosome is a small non-membranous organelle representing the major microtubules-organising centre of the cell. It consists of a pair of centrioles surrounded by a pericentriolar matrix composed of pericentrin and  $\gamma$ -tubulin, from which microtubules are nucleated (Doxsey, 1998) (Bornens, 2002). The primary function of the centrosome is the nucleation and organisation of microtubules. In interphase cells the centrosome has a key role in establishing the cytoplasmic microtubules network for motor protein based transport and positioning of organelles and vesicles. During the progression of the cell cycle the centrosome undergoes duplication and at this stage it is essential for the formation and orientation of a bipolar mitotic spindle, for the fidelity of chromosome segregation and correct exit from mitosis (Bornens, 2002) (Azimzadeh and Bornens, 2007).

A large body of evidence suggests that the centrosome is essential for the regulation of the cell cycle progression by acting as a scaffold protein for a network of signalling pathways which in turn trigger cellular division (see section 1.7.4) (Hinchcliffe et al., 1999) (Lacey et al., 1999) (Kramer et al., 2004). Thus manipulation of the centrosome has often been shown to result in cell cycle aberrations or cell cycle arrest. For example, centrosomal ablation as well as silencing of centrosomal components results in impairment of cytokinesis with consequent arrest of the cell population in G<sub>1</sub> phase (Kramer et al., 2004). Interestingly, it has been shown that displacement of endogenous AKAP450, by over-expression of the PACT domain (pericentrin-AKAP450 centrosomal targeting), results in impaired centrioles duplication. As a consequence of this, cells enter mitosis but do not complete cytokinesis (Keryer et al., 2003b). Similarly, manipulation of other subsets of centrosomal proteins, such as Chk1 or pericentrin, results in an arrest of the cell cycle in G<sub>2</sub> phase (Kramer et al., 2004) (Zimmerman et al., 2004).

It has also been shown that cAMP and cellular growth rate are inversely correlated and that the cAMP/PKA signal transduction pathway acts as a negative regulator of cell entrance in mitosis (Zeilig et al., 1976) (Lamb et al., 1991). Total cAMP levels and PKA activity fluctuate throughout cell cycle progression reaching the highest level in G<sub>1</sub> and the lowest level in mitotic phase (see section 1.8) (Sheppard and Prescott, 1972) (Zeilig et al., 1976). Accordingly, experimental manipulation of cAMP level or PKA activity results in the arrest of the cell cycle. Thus, elevation of cAMP results in arrest of the cell population in G<sub>1</sub> whereas inhibition of PKA results in a rapid chromatin condensation and cells entry in mitosis (Zeilig et al., 1976) (Lamb et al., 1991).

In the previous chapters I have shown the importance of the AKAP450/PKA/PDE4D3 complex anchored to the centrosome for fine regulation of centrosomal cAMP levels. While PDE4D3 ensures a cAMP basal concentration at the centrosome lower than in the cytosol, AKAP450 increases PKA sensitivity to cAMP by lowering its activation threshold via a mechanism involving the auto-phosphorylation site of PKA.

Based on these findings it is possible to envisage that the local centrosomal modulation of the cAMP/PKA pathway activity is critical for the correct regulation of cell cycle progression.

Hypothesis:

The guiding hypothesis of the experiment described in this result chapter is that the centrosomal AKAP450/PKA/PDE4D3 complex plays a role in the control of cell cycle progression.

Experimental procedure:

- 1) Generation of a CHO cell line stably expressing the dominant negative variant of PDE4D3 (McCahill et al., 2005) genetically fused to the red fluorescent protein (dnPDE4D3mRFP).
- 2) Generation of a CHO cell line stably expressing the dominant negative variant of PDE4A4 (McCahill et al., 2005) genetically fused to the green fluorescent protein (dnPDE4A4-GFP).
- 3) Assessment, by flow cytometry scan analysis, of cell cycle progression of non-synchronised cells lines stably expressing the dnPDE4D3mRFP compared with control CHO cells and CHO cells stably expressing the dnPDE4A4-GFP, before and after forskolin treatment.

## 8.1 Results

### ***8.1.1 Generation of a CHO cell line stably expressing the dominant negative variant of PDE4D3***

In order to investigate the functional relevance of the centrosomal AKAP450/PKA/PDE4D3 complex, within which PKA activation and cAMP level are tightly and uniquely regulated, I set up to study how manipulation of this complex may affect cell cycle progression. As a first step for such investigation, the catalytically dead PDE4D3 variant (dnPDE4D3) (McCahill et al., 2005) was genetically fused to the monomeric red fluorescent protein (mRFP) and this

construct was used to establish a CHO cell line stably over-expressing the transgene dnPDE4D3mRFP (see section 3.1.21 and 3.2.2.3.3).

Establishing the dnPDE4D3mRFP stable clone proved difficult when compared with the generation and maintenance of all the other stable clones developed for this project (see section 4.1.1, 4.1.4, 4.1.5 and 7.1.4). After a month of culture with medium containing the proper amount of antibiotic (700 $\mu$ g of Higromycin B, see section 3.2.2.2) western blot analysis of lysates from dnPDE4D3mRFP expressing cells probed with a specific antibody against PDE4D did not show any band corresponding to the molecular weight of PDE4D3mRFP (about 120 kDa) (Figure 8-1, “Old clone dn4D3”). This finding indicates that the selected cells had lost the transgene after this period in culture. A newly established CHO cells line over-expressing the dnPDE4D3mRFP was analysed for transgene expression after 15 days in selection medium. Western blot analysis showed in Figure 8-1, confirms that the “New clone dn4D3” expresses the dnPDE4D3mRFP.

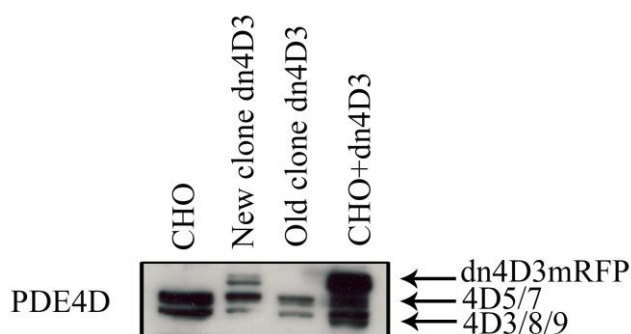


**Figure 8-1** Western blot of cell lysates from CHO cells, CHO lines (“Old clone dn4D3” and “New clone dnPDE4D3mRFP”) stably expressing the dnPDE4D3 tagged to mRFP and CHO cells transiently transfected with the dnPDE4D3mRFP (CHO+dn4D3) probed with an antibody directed to PDE4D. “Old clone dn4D3” is the first clone selected, in which it is not possible to detect the dnPDE4D3mRFP; “New clone dnPDE4D3mRFP” is the newly selected clone in which it is possible to detect the PDE4D3, the PDE4D5 and the PDE4D3mRFP as well as these PDEs isoforms appear in lysate from CHO cells transiently transfected with dnPDE4D3mRFP. Lysates from CHO cells and from the “Old clone dn4D3” show only the bands for the endogenous PDE4D3 and PDE4D5.

To further confirm the presence of the dnPDE4D3mRFP in the newly selected CHO clone, total mRNA was extracted and retro-transcribed (see

section 3.1.4, 3.1.6 and 3.2.2.3.3), and specific oligonucleotides annealing on the nucleotide sequence encoding for the mutation (D484A) were used to amplify a 650 bp band from the cDNA of the dnPDE4D3mRFP (Figure 8-2). As shown in Figure 8-2, the entire set of samples analysed show an amplification band corresponding to the wild type isoform of PDE4D3. Conversely only cDNA from “New clone dn4D3” and from CHO cells transiently expressing the dnPDE4D3mRFP yield a band when primers annealing on D484A mutation were used, confirming that only these two samples over-express the dominant negative variant of the PDE4D3.

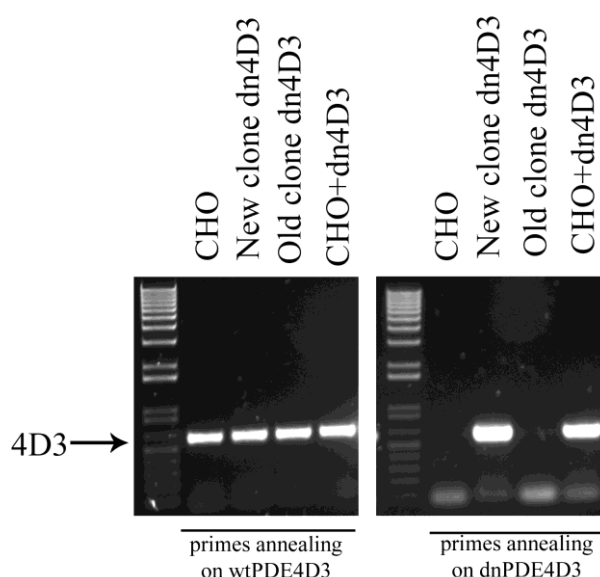


**Figure 8-2** RT-PCR analysis of PDE4D3 wild type and dominant negative variant in CHO cells, CHO lines stably expressing the dnPDE4D3 tagged to mRFP, “Old clone dn4D3” and “New clone dn4D3” respectively, and CHO cells transiently transfected with the dnPDE4D3mRFP. The 650 bp band expected from the wild type isoform of the PDE4D3 is detectable in the entire set of samples analysed (left panel), whereas only the “New clone dn4D3” and CHO cells transiently expressing the dnPDE4D3mRFP show amplification of the dominant negative variant of PDE4D3.

Next, to test whether the dominant negative variant of the PDE4D3 localises within the cell in the specific subcellular locales where the wild type is normally anchored I performed a fluorescence microscopy analysis of the dnPDE4D3mRFP stably expressing cells. Figure 8-3 shows an example of a “New clone dn4D3” cell in which it is possible to recognise the localisation of

the recombinant protein in proximity of the nucleus, typical of a localisation to the centrosome (Figure 8-3).

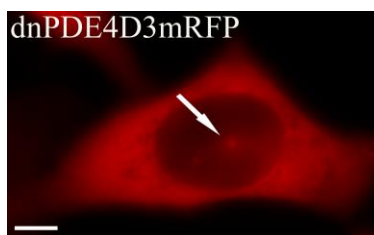


**Figure 8-3** Fluorescence microscopy image of a “New clone dn4D3” cell. Image show the subcellular localisation of the recombinant protein. Arrow points to the centrosome. Bar 10 $\mu$ m.

In order to confirm the centrosomal localisation of the catalytic inactive PDE4D3 isoform I used RII-CFP as a centrosomal marker. To this end, I transfected CHO cells stably expressing the dnPDE4D3 (“New clone dn4D3”) with a plasmid carrying the coding sequence for RII-CFP. Image of the co-localisation of dnPDE4D3mRFP and RII-CFP is shown in Figure 8-4.

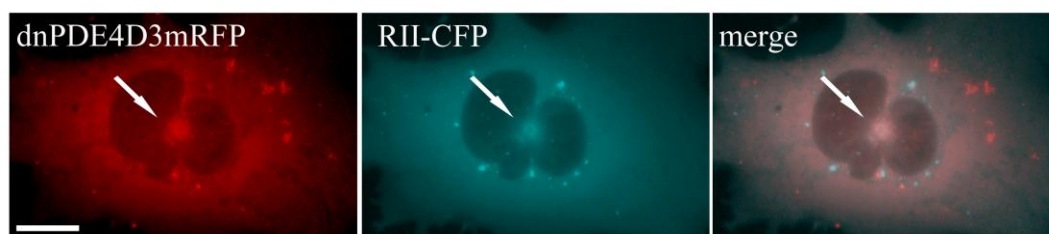


**Figure 8-4** Subcellular localisation of dnPDE4D3mRFP in CHO cells. Images show co-localisation of dnPDE4D3mRFP (left panel) with RII-CFP (middle panel); arrows point to the centrosome. Bar 10 $\mu$ m.

As shown in Figure 8-4 the dominant negative variant of the PDE4D3 co-localises with the RII-CFP at the centrosome, as previously shown for the endogenous PDE4D3 (Figure 4-12). This specific localisation suggests that the mutant dnPDE4D3 is displacing the endogenous active PDE4D3.

### ***8.1.2 Generation of a CHO cell line stably expressing the dominant negative variant of PDE4A4***

As a control, I generated a CHO line stably expressing the dominant negative variant of the PDE4A4 (see section 3.1.22 and 3.2.2.3.3) (McCahill et al., 2005).

As shown in Figure 8-5 fluorescent microscopy analysis of cells stably expressing dnPDE4A4-GFP shows a clear cytosolic distribution and no specific centrosomal localisation in CHO cells.

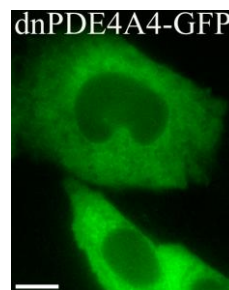
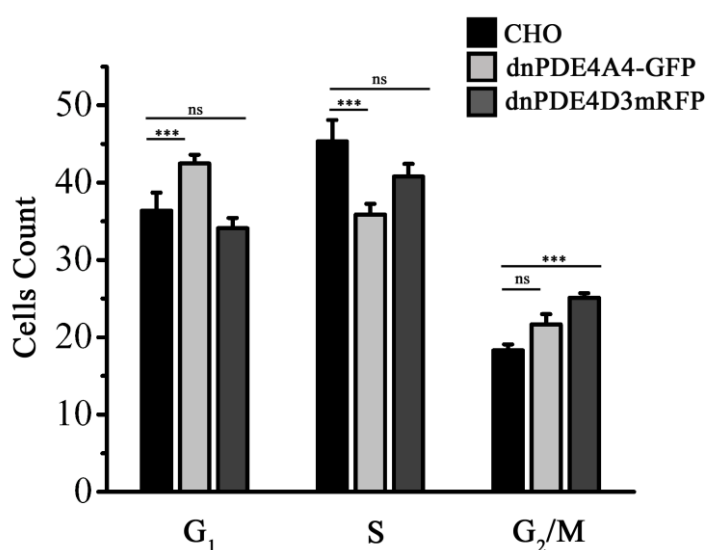


**Figure 8-5** CHO stably expressing the dnPDE4A4-GFP. Bar 10 $\mu$ m.

### ***8.1.3 Flow cytometry scan analysis of cell cycle progression***

In order to investigate whether PDE4D3 anchored to the centrosome plays a role in the control of cell cycle progression I took advantage of the CHO cell clone stably expressing the dnPDE4D3mRFP and I analysed, at the flow cytometer, the distribution of the cell population among the different phases of the cell cycle. Non-synchronised control CHO cells, CHO cells stably expressing dnPDE4D3mRFP (“New clone dn4D3”) or dnPDE4A4-GFP were seeded at low density and let to grow for 48 hours. After two days in culture cells were harvested, fixed with EtOH 70% (v/v) stained with propidium iodide (PI) and analysed (see section 3.5).

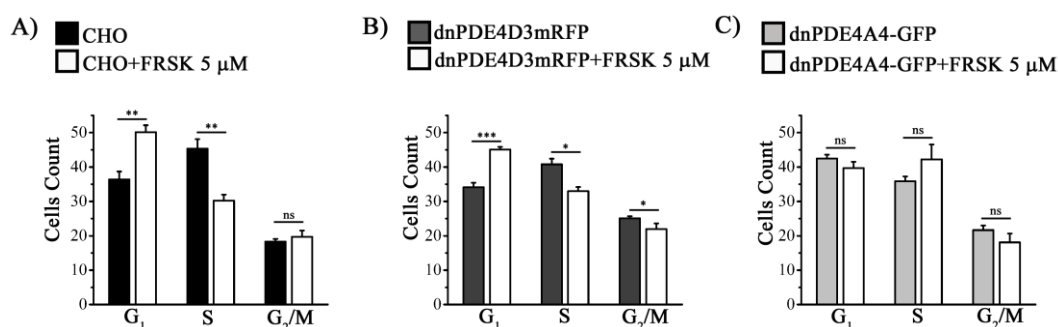
As shown in Figure 8-6 CHO cells stably expressing dnPDE4D3mRFP showed a significant higher proportion of cells in G<sub>2</sub>/M, whereas CHO cells stably expressing dnPDE4A4-GFP showed a significant higher proportion of cells arrested in G<sub>1</sub> as compared with control CHO cells (CHO: G<sub>1</sub>=36.374±2.321%, S=45.334±2.759%, G<sub>2</sub>/M=19.293±0.785%; CHO-dnPDE4A4-GFP: G<sub>1</sub>=42.470±1.136%, S=35.876±1.390%, G<sub>2</sub>/M=21.655±1.350%; CHO-dnPDE4D3mRFP: G<sub>1</sub>=34.106±1.331%, S=40.790±1.645%, G<sub>2</sub>/M=25.104±0.589% [n=6]; \*\*\*p<0.001; Figure 8-6).



**Figure 8-6** Quantification of flow cytometry scan analysis (mean of 6 independent experiments) for CHO, CHO-dnPDE4D3mRFP (dnPDE4D3mRFP) and CHO-dnPDE4A4-GFP (dnPDE4A4-GFP). Histograms indicate the mean percentages of cells in various phases of the cell cycle. (Error bars represent SEM. One-way ANOVA test, \*\*\*p<0.001).

It has been shown that experimental elevation of cAMP concentration induced either by stimulation of AC, inhibition of PDEs or by addition of cAMP (cAMP or dibutyryl-cAMP), inhibits cells division in many cell line models, exerting a counteracting effect on cell proliferation (see section 1.8) (Macmanus and Whitfield, 1969) (Ryan and Heidrick, 1968) (Sheppard, 1972). To test the effect of total cAMP elevation in CHO, CHO-dnPDE4D3mRFP and CHO-dnPDE4A4-GFP cells, flow cytometry scan analysis was performed after treatment with 5  $\mu$ M forskolin for 48 hours. As shown in Figure 8-7 upon forskolin stimulation, and in agreement with published evidence, CHO cells and

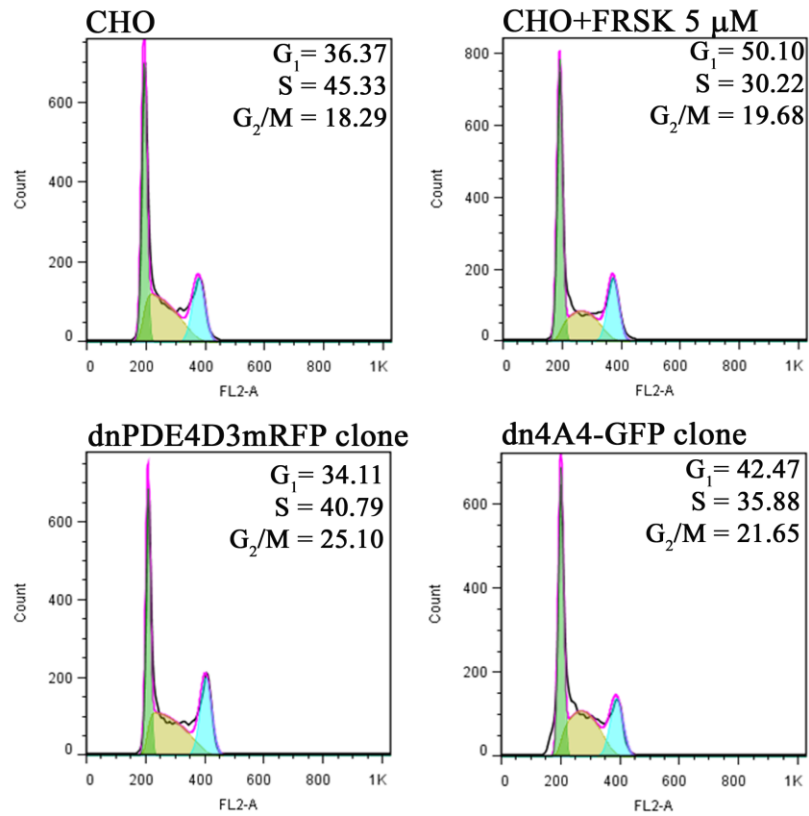
CHO-dnPDE4D3mRFP population show a significant higher fraction of cells in G<sub>1</sub> phase and a significant lower fraction in S phase (white bars) as compared to untreated cells, suggestive of an arrest of the cell cycle progression (Figure 8-7, A); CHO black bars: G<sub>1</sub>=36.374±2.321%, S=45.334±2.759%, G<sub>2</sub>/M=19.293±0.785%; CHO+FRSK white bars: G<sub>1</sub>=50.103±2.051%, S=30.221±1.757%, G<sub>2</sub>/M=19.676±1.872% [n<3]; and B) CHO-dnPDE4D3mRFP dark grey bars: G<sub>1</sub>=34.106±1.331%, S=40.790±1.645%, G<sub>2</sub>/M=25.104±0.589%; CHO-dnPDE4D3mRFP+FRSK white bars: G<sub>1</sub>=40.074±0.818%, S=32.995±1.195%, G<sub>2</sub>/M=21.931±1.697% [n<3]). Conversely forskolin seems do not have any effect on CHO-dnPDE4A4 population (Figure 8-7, C) CHO-dnPDE4A4-GFP light gray bars: G<sub>1</sub>=42.470±1.136%, S=35.876±1.390%, G<sub>2</sub>/M=21.655±1.350%; CHO-dnPDE4A4-GFP+FRSK white bars: G<sub>1</sub>=39.709±1.819%, S=42.202±4.326%, G<sub>2</sub>/M=18.090±2.584% [n<3]).



**Figure 8-7 FACS analysis quantification (mean of 6 independent experiments) for CHO, CHO-dnPDE4D3mRFP (dnPDE4D3mRFP) and CHO-dnPDE4A4-GFP (dnPDE4A4-GFP) upon treatment with forskolin 5 μM. The histogram indicates the average percentages of cells in various phases of the cell cycle. (Error bars represent SEM. One-way ANOVA test, \* p<0.05, \*\* 0.01<p<0.001, \*\*\* p<0.001).**

Interestingly, a direct comparison of CHO cells, CHO plus forskolin, CHO-dnPDE4D3mRFP and CHO-dnPDE4A4-GFP confirmed that CHO-dnPDE4A4-GFP cells progress through the cell cycle with a similar trend as CHO cells treated with forskolin (Figure 8-8). This indicates that displacement of PDE4A4 affect the cell cycle progression in a similar manner as total cAMP elevation, resulting in an arrest of the cell cycle progression in G<sub>1</sub> and a significant lower amount of cells entering the S phase.

On the contrary, the G<sub>2</sub>/M arrest detected in CHO-dnPDE4D3mRFP cells indicates that tight regulation of centrosomal level of cAMP is essential for the correct progression through G<sub>2</sub>/M and completion of the cell cycle (Figure 8-8).



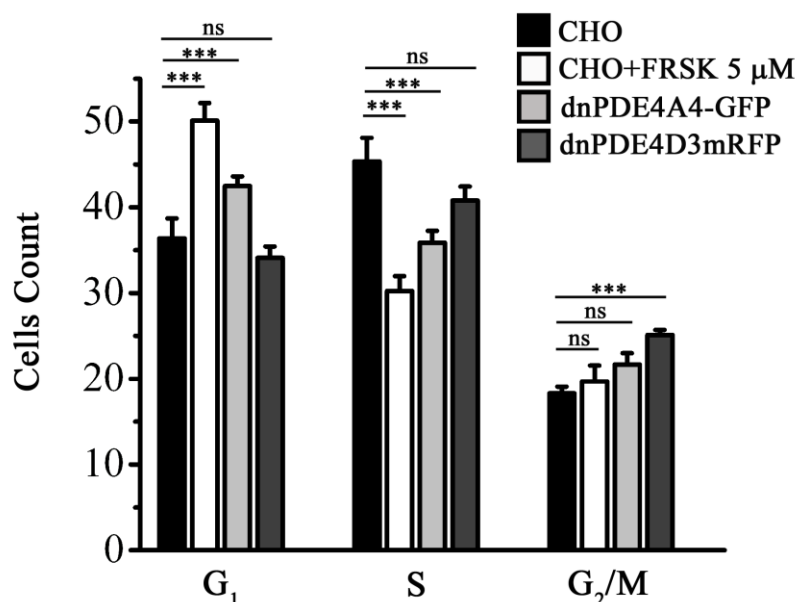


**Figure 8-8 Top panel:** representative (1 out of 6) experiment showing cellular DNA content in untreated CHO cells, CHO cells treated with forskolin, CHO-dnPDE4D3mRFP (dnPDE4D3mRFP) and CHO-dnPDE4A4-GFP (dnPDE4A4-GFP). Gaussian curve around 200 fluorescence emission value corresponds to the 2n content of DNA (G<sub>1</sub>), Gaussian curve around 400 fluorescence emission value corresponds to the 4n content of DNA (G<sub>2</sub>/M), values between 200 and 400 correspond to the intermediate content of DNA (S). **Bottom panel:** quantification of flow cytometry scan analysis (mean of 6 independent experiments). Values indicate the mean percentages of cells in each phases of the cell cycle, as indicated. (Error bars represent SEM. One-way ANOVA test, \*\*\*p<0.001).

## 8.2 Discussion

The aim of this chapter was to study the functional role of the AKAP450/PKA/PDE4D3 macromolecular complex present at the centrosome in the regulation of cell cycle progression. To this purpose, I generated a CHO cell line stably expressing the catalytically dead variant of PDE4D3. Fluorescent microscopy analysis of this cell line confirmed that dnPDE4D3 binds to the same anchor sites where the endogenous active counterpart PDE4D3 is normally localised (Figure 4-12 and Figure 8-4). Moreover, co-localisation with RII-CFP to the centrosome indicates that dnPDE4D3 binds to AKAP450, as previously shown for PDE4D3 (Figure 8-4). As shown in section 4.1.6.4 and Figure 4-17, displacement of the centrosomal wild-type PDE4D3 results in the increase of the basal cAMP level at the centrosome and in the abolishment of the difference in cAMP concentration between centrosome and cytosol. Based

on these findings, I asked if local elevation of centrosomal cAMP concentration secondary to displacement of centrosomal PDE4D3 may have an effect on cell cycle progression. Flow cytometry scan analysis of CHO stably expressing the dnPDE4D3 showed a higher percentage of cells in G<sub>2</sub>/M as compared with control CHO cells. As a control, I tested the effect of displacement of a PDE that does not show any centrosomal localisation and that does not modified the low level of cAMP at the centrosome, when its catalytically dead variant is over-expressed in CHO cells (see section 4.1.6.4 and Figure 4-7). To this end, I generated a CHO cell line stably expressing the catalytically dead variant of PDE4A4. In this case, flow cytometry scan analysis of CHO-dnPDE4A4-GFP showed a higher proportion of cells in G<sub>1</sub> as compared with CHO cells; however arrest of cell cycle progression in G<sub>1</sub> has already been well documented following experimental elevation of total intracellular cAMP or PKA activity (Macmanus and Whitfield, 1969) (Ryan and Heidrick, 1968) (Sheppard, 1972) (Lamb et al., 1991). Pre-treatment of CHO-dnPDE4D3mRFP, CHO-dnPDE4A4-GFP and CHO control cells with forskolin results, indeed, in a cell cycle arrest in G<sub>1</sub> at the expenses of S phase both for CHO and CHO-dnPDE4D3mRFP cells; whereas forskolin does not have any effect on cell cycle progression of CHO-dnPDE4A4-GFP population. This data suggests that displacement of PDE4A4 induces an increase in cAMP which exerts an effect on the cell cycle progression similar to that induced by forskolin treatment. On the contrary, cell cycle arrest in G<sub>2</sub>/M shown by CHO-dnPDE4D3mRFP population may result from the specific cAMP elevation at the centrosome.

Arrest of cell cycle in G<sub>2</sub>/M phase has previously been shown to be associated with manipulation of the centrosome. Activation of Cdk1-CyclinB (MPF) occurs at the centrosome at the onset of mitosis. During interphase Cdk1 is kept inactive by the action of its modulator Chk1. At the beginning of mitosis, Chk1 dissociates from the centrosome releasing Cdk1 available for activation. Interestingly, fusion of the PACT domain (pericentrin AKAP450 centrosome targeting domain) to Chk1, leads to the immobilisation of the wild type Chk1 to the centrosome and to a permanent inhibition of Cdk1 activation. As a consequence, asynchronous cell populations undergo mitotic failure and

formation of polyploidy cells (Kramer et al., 2004). In a similar way, it has been shown that over-expression of a GFP tagged-PACT domain results in a higher percentage of cells showing a DNA content of 4n upon flow cytometry scan analysis. Further investigation revealed that the G<sub>2</sub> sub-cellular fraction is characterised by polyploidy cells, suggesting a defect of cytokinesis (Keryer et al., 2003b). Interestingly, in both studies, the approach used was over-expression of the PACT domain which results in the displacement of the AKAP450/PKA/PDE4D3 complex from the centrosome. The fact that I observe the same functional outcome (arrest in G<sub>2</sub>/M) when displacing PDE4D3 alone, as described in experiments in which the entire AKAP450/PKA/PDE4D3 complex was removed from the centrosome, suggests that PDE4D3 may be the key regulator for the control of these mitotic events.

“Mitotic catastrophe” is the primary mechanism of cells death in a number of tumour cell lines, following treatment with chemotherapeutic agents, and its major function is to eliminate damaged cells from the cell population. It is characterised by delay of mitosis, chromosome segregation and cytokinesis failure and leads to the accumulation of polynucleated and large non-viable cells (Roninson et al., 2001). Eventually cells die. “Mitotic catastrophe” has been linked to G<sub>2</sub>/M arrest and centrosome disruption (Roninson et al., 2001). Therefore it is possible that the difficulties I found in maintaining the CHO-dnPDE4D3mRFP stably expressing cells may be caused by a counteractive selection imposed by the G<sub>2</sub>/M arrest and the consequent “mitotic catastrophe” response. It would be of interest to follow up these studies by investigating the G<sub>2</sub>/M arrested subcellular fraction in the CHO-dnPDE4D3mRFP stable clone to define what specific mechanism is misregulated by over-activation of the centrosomal AKAP450-anchored PKA upon displacement of PDE4D3. If the consequence of PDE4D3 displacement is ‘mitotic catastrophe’ I expect that the sub-fraction of cells arrested in G<sub>2</sub>/M is represented predominantly by polynucleated cells. Moreover I expect a progressive loss of expression of the catalytically dead PDE4D3mRFP tagged in the “New clone dn4D3” clone, as previously happened for the first CHO-dnPDE4D3 clone selected (Old clone dn4D3).

# 9

## Conclusion and future perspectives

---

In this thesis I investigated cAMP signalling at the centrosome using real-time FRET-based imaging in living, non-synchronised CHO cells.

In the first part of my project I focused on the analysis of centrosomal cAMP in cells in resting conditions. The major finding of this part of my work is that the centrosome is a subcellular domain characterised by a cAMP concentration that is lower than the average cAMP concentration in the bulk cytosol. My studies revealed that the AKAP450-associated PDE4D3 plays a key role in regulating the cAMP level within the centrosomal microdomain. This is compatible with a mechanism whereby PDE4D3 protects AKAP450-anchored PKA from inappropriate activation. Moreover, this specific microdomain of low cAMP seems to be present not only at the centrosome of CHO cells but also at the centrosome of other cell lines, suggesting that this may be a general feature of cAMP compartmentalisation, possibly playing a specific role in the control of centrosomal associated events.

In the second part of my project I focused on centrosomal cAMP dynamics following treatment of cells with the cAMP raising agent forskolin.

The major finding of this part of my work is that specific anchoring of PKA to AKAP450 increases the sensitivity of PKA to cAMP. As a consequence, AKAP450-anchored PKA shows a lower activation threshold than soluble PKA or other subsets of PKA bound to different AKAPs. This conclusion is strengthened by the observation that anchoring of endogenous PKA subsets to a cytosolic fragment of AKAP450, which includes the PKA binding site, results in increased PKA activity.

Given the co-localisation of PKA and PDE4D3 to the centrosome and the ability of PKA to phosphorylate and increase PDE4D3 activity (Sette and Conti, 1996), it is possible that a negative feedback loop mechanism is present at the centrosome. A low level of cAMP selectively activates the PKA subset anchored to AKAP450. PKA, in turn, phosphorylates and activates PDE4D3 anchored to the same complex and this maintains a lower level of cAMP in this compartment. A way to further investigate if this mechanism is in place would be to generate a CHO cell line stably expressing a PDE4D3 mutated in the PKA phosphorylation site, such that PDE4D3 activity cannot be regulated by PKA-mediated phosphorylation. If a feedback loop mechanism is indeed present in this compartment, the centrosomal low cAMP micro-compartment would be abolished in the presence of such a mutant.

The data presented here show, for the first time, that anchoring of PKA type II to an AKAP can locally modify the sensitivity of a specific event to cAMP. This represents a completely new mechanism of PKA regulation that is effected by lowering the kinase activation threshold rather than by increasing the level of the second messenger itself. This novel mechanism introduces a further level of complexity to the already sophisticated regulation of the cAMP/PKA pathway and it defines a novel function for AKAPs. Although my results show that this mechanism does not apply for the interaction of PKA with Ht31, AKAP79 and AKAP149, I cannot exclude that a similar mechanism may function for other AKAP/PKA complexes. It would be interesting to explore if anchoring of a PKA to an AKAP can increase the activation threshold of the anchored PKA, thereby lowering its sensitivity to cAMP.

I subsequently investigated the mechanism responsible for the increased sensitivity to cAMP of AKAP450-bound PKA. My results strongly indicate that the auto-phosphorylation site of the PKA RII subunit is involved in this mechanism. It has been previously shown that auto-phosphorylation of PKA, which occurs as an intra-molecular event, promotes PKA dissociation by lowering its activation constant. It is possible that anchoring of PKA to AKAP450 promotes a conformation of the PKA regulatory subunit which favours the auto-phosphorylation of the holoenzyme.

To summarise the results of my work, I propose here a model in which PDE4D3 acts to maintain a low level of cAMP at the centrosome and inhibits the inappropriate activation of the PKA subset anchored to AKAP450. This specific subset of PKA, characterised by a lower activation constant, can be activate by an amount of cAMP that cannot affect other subsets of PKA anchored in different subcellular compartments. Given the fact that it has been shown that ERK can phosphorylate and inactivated PDE4D3 (see section 1.3.2 and 1.3.2.1) (Hoffmann et al., 1999) (MacKenzie et al., 2000), an interesting possibility is that in a specific phase of the cell cycle the centrosomal PDE4D3 is inactivated by ERK phosphorylation. The consequent local increase of cAMP level may then be sufficient to activate the AKAP450-anchored PKA but not sufficient to activate other subsets of PKA. Interestingly, this mechanism would not require adenylyl cyclase activation and new synthesis of cAMP. Activation of centrosomal PKA may then regulate critical events involved in the progression of the cell cycle. Eventually PKA would phosphorylate and activate the associated PDE4D3, thereby relieving it from ERK inhibition and re-establishing a cAMP level that is below the activation threshold of the AKAP450-tethered PKA. This mechanism would provide a time-specific feedback regulatory mechanism whereby ERK inhibition of PDE4D3 would allow centrosomal cAMP level to rise at the right moment of the cell cycle progression. In this scenario PDE4D3 would act as a “gate” for PKA activation.

To further investigate if ERK dependent phosphorylation of PDE4D3 is a mechanism responsible for activation of PKA anchored to AKAP450 one

possibility would be to perform FRET-based analysis of CHO cells stably expressing the PKA-GFP sensor upon treatment with an ERK specific activator, such as the epidermal growth factor (EGF). If the hypothesis illustrated above is true ERK phosphorylation would inhibit PDE4D3, leading to a local rise of cAMP level. As a consequence the difference in cAMP concentration between centrosome and cytosol would be expected to be abolished.

In the last part of my project I investigated the role of the AKAP450/PKA/PDE4D3 complex in the control of cell cycle progression. My findings show that displacement of endogenous PDE4D3 from the centrosome abolishes the difference in cAMP concentration between centrosome and cytosol, previously detected in cells in resting condition, and this is concomitant with an arrest of the cell cycle progression in G<sub>2</sub>/M. Interestingly, these results are in agreement with previous reports in which the AKAP450/PKA/PDE4D3 complex was displaced by over-expression of the PACT domain of AKAP450 (Keryer et al., 2003b, Kramer et al., 2004) suggesting that not only the AKAP450/PKA/PDE4D3 complex is essential for correct cell cycle progression, but also strongly indicating that PDE4D3 may be the complex component playing a key role in this.

Various alterations leading to activation or inactivation of key components of the cAMP signalling pathway are observed in tumorigenesis. It has been shown that cells from different tumour models, such as chronic lymphocytic leukaemia and carcinoma, show an over-expression of PDEs and a consequent decrease of cAMP level (Marko et al., 1998, Zhang et al., 2008). Interestingly, treatment with chemotherapeutic agents, including PDEs inhibitors (i.e. caffeine and pentoxifylline), leads to a phenomenon defined as “mitotic catastrophe” that is characterised by aberrant mitosis, G<sub>2</sub>/M arrest, formation of polynucleated cells and, ultimately, cell death (Roninson et al., 2001). Therefore it would be of particular interest to investigate whether the G<sub>2</sub>/M arrest induced by displacement of the PDE4D3 isoform is due to a “mitotic catastrophe”, as it may be suggested by the observation that cells over-expressing the recombinant catalytically dead PDE4D3 mRFP tagged appear to

lose expression of the transgene (see section 8.1.1). An experiment that could help investigating this would be to estimate the percentage of polynucleated cells in the G<sub>2</sub>/M sub-fraction of cells expressing the catalytically dead version of PDE4D3. If this number results significantly increased compared to control cells, then the centrosomal PDE4D3 would become a potentially interesting target for anticancer therapy. In this context, it is worth considering that the development of specific PDEs inhibitors, allowing the activation of PKA subsets with specific and restricted outcomes, has recently gained crucial importance as anticancer therapy (Savai et al., 2010).

Elucidation of the mechanisms responsible for cAMP compartmentalisation in the microenvironment surrounding specific macromolecular complexes and the physiological role of PDEs in this is essential to understand whether molecular aberrations disrupting these complexes can be linked to disease states. The studies presented here reveal an additional level of regulation in the cAMP/PKA signalling pathway in which anchoring of PKA to an AKAP increases the enzyme sensitivity to its activator. These findings may be relevant for the development of new therapeutics.

# 10

## References

---

- ABAL, M., PIEL, M., BOUCKSON-CASTAING, V., MOGENSEN, M., SIBARITA, J. B. & BORNENS, M. 2002. Microtubule release from the centrosome in migrating cells. *J Cell Biol*, 159, 731-7.
- ABEL, T. & NGUYEN, P. V. 2008. Regulation of hippocampus-dependent memory by cyclic AMP-dependent protein kinase. *Prog Brain Res*, 169, 97-115.
- ABELL, C. W. & MONAHAN, T. M. 1973. The role of adenosine 3',5'-cyclic monophosphate in the regulation of mammalian cell division. *J Cell Biol*, 59, 549-58.
- ABRAHAMSEN, H., BAILLIE, G., NGAI, J., VANG, T., NIKA, K., RUPPELT, A., MUSTELIN, T., ZACCOLO, M., HOUSLAY, M. & TASKEN, K. 2004. TCR- and CD28-mediated recruitment of phosphodiesterase 4 to lipid rafts potentiates TCR signaling. *J Immunol*, 173, 4847-58.
- ADAMS, S. R., HAROOTUNIAN, A. T., BUECHLER, Y. J., TAYLOR, S. S. & TSIEN, R. Y. 1991. Fluorescence ratio imaging of cyclic AMP in single cells. *Nature*, 349, 694-7.
- ALLEN, M. D. & ZHANG, J. 2006. Subcellular dynamics of protein kinase A activity visualized by FRET-based reporters. *Biochem Biophys Res Commun*, 348, 716-21.
- ALTO, N. M., SODERLING, S. H., HOSHI, N., LANGEBERG, L. K., FAYOS, R., JENNINGS, P. A. & SCOTT, J. D. 2003. Bioinformatic design of A-kinase anchoring protein-in silico: a potent and selective peptide antagonist of type II protein kinase A anchoring. *Proc Natl Acad Sci U S A*, 100, 4445-50.
- ANGELO, R. & RUBIN, C. S. 1998. Molecular characterization of an anchor protein (AKAPCE) that binds the RI subunit (RCE) of type I protein kinase A from *Caenorhabditis elegans*. *J Biol Chem*, 273, 14633-43.
- ARAVIND, L. & PONTING, C. P. 1997. The GAF domain: an evolutionary link between diverse phototransducing proteins. *Trends Biochem Sci*, 22, 458-9.

- ASHMAN, D. F., LIPTON, R., MELICOW, M. M. & PRICE, T. D. 1963. Isolation of adenosine 3', 5'-monophosphate and guanosine 3', 5'-monophosphate from rat urine. *Biochem Biophys Res Commun*, 11, 330-4.
- AZIMZADEH, J. & BORNENS, M. 2007. Structure and duplication of the centrosome. *J Cell Sci*, 120, 2139-42.
- BACSKAI, B. J., HOCHNER, B., MAHAUT-SMITH, M., ADAMS, S. R., KAANG, B. K., KANDEL, E. R. & TSIEN, R. Y. 1993. Spatially resolved dynamics of cAMP and protein kinase A subunits in *Aplysia* sensory neurons. *Science*, 260, 222-6.
- BAILLIE, G., MACKENZIE, S. J. & HOUSLAY, M. D. 2001. Phorbol 12-myristate 13-acetate triggers the protein kinase A-mediated phosphorylation and activation of the PDE4D5 cAMP phosphodiesterase in human aortic smooth muscle cells through a route involving extracellular signal regulated kinase (ERK). *Mol Pharmacol*, 60, 1100-11.
- BAILLIE, G. S., SOOD, A., MCPHEE, I., GALL, I., PERRY, S. J., LEFKOWITZ, R. J. & HOUSLAY, M. D. 2003. beta-Arrestin-mediated PDE4 cAMP phosphodiesterase recruitment regulates beta-adrenoceptor switching from Gs to Gi. *Proc Natl Acad Sci U S A*, 100, 940-5.
- BAILLY, E., DOREE, M., NURSE, P. & BORNENS, M. 1989. p34cdc2 is located in both nucleus and cytoplasm; part is centrosomally associated at G2/M and enters vesicles at anaphase. *Embo J*, 8, 3985-95.
- BANKY, P., HUANG, L. J. & TAYLOR, S. S. 1998. Dimerization/docking domain of the type Ialpha regulatory subunit of cAMP-dependent protein kinase. Requirements for dimerization and docking are distinct but overlapping. *J Biol Chem*, 273, 35048-55.
- BANKY, P., NEWLON, M. G., ROY, M., GARROD, S., TAYLOR, S. S. & JENNINGS, P. A. 2000. Isoform-specific differences between the type Ialpha and IIalpha cyclic AMP-dependent protein kinase anchoring domains revealed by solution NMR. *J Biol Chem*, 275, 35146-52.
- BARNES, A. P., LIVERA, G., HUANG, P., SUN, C., O'NEAL, W. K., CONTI, M., STUTTS, M. J. & MILGRAM, S. L. 2005. Phosphodiesterase 4D forms a cAMP diffusion barrier at the apical membrane of the airway epithelium. *J Biol Chem*, 280, 7997-8003.
- BAUMAN, A. L., SOUGHAYER, J., NGUYEN, B. T., WILLOUGHBY, D., CARNEGIE, G. K., WONG, W., HOSHI, N., LANGEBOG, L. K., COOPER, D. M., DESSAUER, C. W. & SCOTT, J. D. 2006. Dynamic regulation of cAMP synthesis through anchored PKA-adenylyl cyclase V/VI complexes. *Mol Cell*, 23, 925-31.
- BEARD, M. B., O'CONNELL, J. C., BOLGER, G. B. & HOUSLAY, M. D. 1999. The unique N-terminal domain of the cAMP phosphodiesterase PDE4D4 allows for interaction with specific SH3 domains. *FEBS Lett*, 460, 173-7.
- BEARD, M. B., OLSEN, A. E., JONES, R. E., ERDOGAN, S., HOUSLAY, M. D. & BOLGER, G. B. 2000. UCR1 and UCR2 domains unique to the cAMP-specific phosphodiesterase family form a discrete module via electrostatic interactions. *J Biol Chem*, 275, 10349-58.
- BEAVO, J. A. 1995. Cyclic nucleotide phosphodiesterases: functional implications of multiple isoforms. *Physiol Rev*, 75, 725-48.
- BEAVO, J. A. & BRUNTON, L. L. 2002. Cyclic nucleotide research -- still expanding after half a century. *Nat Rev Mol Cell Biol*, 3, 710-8.
- BEAZELY, M. A. & WATTS, V. J. 2006. Regulatory properties of adenylyl cyclases type 5 and 6: A progress report. *Eur J Pharmacol*, 535, 1-12.
- BEENE, D. L. & SCOTT, J. D. 2007. A-kinase anchoring proteins take shape. *Curr Opin Cell Biol*, 19, 192-8.
- BENDER, A. T. & BEAVO, J. A. 2006. Cyclic nucleotide phosphodiesterases: molecular regulation to clinical use. *Pharmacol Rev*, 58, 488-520.

- BENTLEY, J. K., JULIFS, D. M. & UHLER, M. D. 2001. Nerve growth factor inhibits PC12 cell PDE 2 phosphodiesterase activity and increases PDE 2 binding to phosphoproteins. *J Neurochem*, 76, 1252-63.
- BERRERA, M., DODONI, G., MONTERISI, S., PERTEGATO, V., ZAMPARO, I. & ZACCOLO, M. 2008. A toolkit for real-time detection of cAMP: insights into compartmentalized signaling. *Handb Exp Pharmacol*, 285-98.
- BESSAY, E. P., ZORAGHI, R., BLOUNT, M. A., GRIMES, K. A., BEASLEY, A., FRANCIS, S. H. & CORBIN, J. D. 2007. Phosphorylation of phosphodiesterase-5 is promoted by a conformational change induced by sildenafil, vardenafil, or tadalafil. *Front Biosci*, 12, 1899-910.
- BIEDLER, J. L., HELSON, L. & SPENGLER, B. A. 1973. Morphology and growth, tumorigenicity, and cytogenetics of human neuroblastoma cells in continuous culture. *Cancer Res*, 33, 2643-52.
- BIEDLER, J. L., ROFFLER-TARLOV, S., SCHACHNER, M. & FREEDMAN, L. S. 1978. Multiple neurotransmitter synthesis by human neuroblastoma cell lines and clones. *Cancer Res*, 38, 3751-7.
- BIEL, M. & MICHALAKIS, S. 2009. Cyclic nucleotide-gated channels. *Handb Exp Pharmacol*, 111-36.
- BLAGDEN, S. P. & GLOVER, D. M. 2003. Polar expeditions--provisioning the centrosome for mitosis. *Nat Cell Biol*, 5, 505-11.
- BOLGER, G., MICHAELI, T., MARTINS, T., ST JOHN, T., STEINER, B., RODGERS, L., RIGGS, M., WIGLER, M. & FERGUSON, K. 1993. A family of human phosphodiesterases homologous to the dunce learning and memory gene product of *Drosophila melanogaster* are potential targets for antidepressant drugs. *Mol Cell Biol*, 13, 6558-71.
- BOLGER, G. B., MCCAHILL, A., HUSTON, E., CHEUNG, Y. F., MCSORLEY, T., BAILLIE, G. S. & HOUSLAY, M. D. 2003a. The unique amino-terminal region of the PDE4D5 cAMP phosphodiesterase isoform confers preferential interaction with beta-arrestins. *J Biol Chem*, 278, 49230-8.
- BOLGER, G. B., PEDEN, A. H., STEELE, M. R., MACKENZIE, C., MCEWAN, D. G., WALLACE, D. A., HUSTON, E., BAILLIE, G. S. & HOUSLAY, M. D. 2003b. Attenuation of the activity of the cAMP-specific phosphodiesterase PDE4A5 by interaction with the immunophilin XAP2. *J Biol Chem*, 278, 33351-63.
- BOMBIK, B. M. & BURGER, M. M. 1973. c-AMP and the cell cycle: inhibition of growth stimulation. *Exp Cell Res*, 80, 88-94.
- BONIGK, W., LOOGEN, A., SEIFERT, R., KASHIKAR, N., KLEMM, C., KRAUSE, E., HAGEN, V., KREMMER, E., STRUNKER, T. & KAUPP, U. B. 2009. An atypical CNG channel activated by a single cGMP molecule controls sperm chemotaxis. *Sci Signal*, 2, ra68.
- BORNENS, M. 2002. Centrosome composition and microtubule anchoring mechanisms. *Curr Opin Cell Biol*, 14, 25-34.
- BOS, J. L., DE BRUYN, K., ENSERINK, J., KUIPERIJ, B., RANGARAJAN, S., REHMANN, H., RIEDL, J., DE ROOIJ, J., VAN MANSFELD, F. & ZWARTKRUIS, F. 2003. The role of Rap1 in integrin-mediated cell adhesion. *Biochem Soc Trans*, 31, 83-6.
- BOYNTON, A. L. & WHITFIELD, J. F. 1980. A possible involvement of type II cAMP-dependent protein kinase in the initiation of DNA synthesis by rat liver cells. *Exp Cell Res*, 126, 477-81.
- BRADLEY, J., REISERT, J. & FRINGS, S. 2005. Regulation of cyclic nucleotide-gated channels. *Curr Opin Neurobiol*, 15, 343-9.
- BROILLET, M. C. 2000. A single intracellular cysteine residue is responsible for the activation of the olfactory cyclic nucleotide-gated channel by NO. *J Biol Chem*, 275, 15135-41.

- BROSTROM, C. O., CORBIN, J. D., KING, C. A. & KREBS, E. G. 1971. Interaction of the subunits of adenosine 3':5'-cyclic monophosphate-dependent protein kinase of muscle. *Proc Natl Acad Sci U S A*, 68, 2444-7.
- BRUNTON, L. L., HAYES, J. S. & MAYER, S. E. 1979. Hormonally specific phosphorylation of cardiac troponin I and activation of glycogen phosphorylase. *Nature*, 280, 78-80.
- BUCK, J., SINCLAIR, M. L., SCHAPAL, L., CANN, M. J. & LEVIN, L. R. 1999. Cytosolic adenylyl cyclase defines a unique signaling molecule in mammals. *Proc Natl Acad Sci U S A*, 96, 79-84.
- BUECHLER, J. A. & TAYLOR, S. S. 1990. Differential labeling of the catalytic subunit of cAMP-dependent protein kinase with a water-soluble carbodiimide: identification of carboxyl groups protected by MgATP and inhibitor peptides. *Biochemistry*, 29, 1937-43.
- BURGER, M. M., BOMBIK, B. M., BRECKENRIDGE, B. M. & SHEPPARD, J. R. 1972. Growth control and cyclic alterations of cyclic AMP in the cell cycle. *Nat New Biol*, 239, 161-3.
- BUTCHER, R. W. & SUTHERLAND, E. W. 1962. Adenosine 3',5'-phosphate in biological materials. I. Purification and properties of cyclic 3',5'-nucleotide phosphodiesterase and use of this enzyme to characterize adenosine 3',5'-phosphate in human urine. *J Biol Chem*, 237, 1244-50.
- BYUS, C. V., HAYES, J. S., BRENDDEL, K. & RUSSELL, D. H. 1979. Regulation of glycogenolysis in isolated rat hepatocytes by the specific activation of type I cyclic AMP-dependent protein kinase. *Mol Pharmacol*, 16, 941-9.
- CARLISLE MICHEL, J. J., DODGE, K. L., WONG, W., MAYER, N. C., LANGEBERG, L. K. & SCOTT, J. D. 2004. PKA-phosphorylation of PDE4D3 facilitates recruitment of the mAKAP signalling complex. *Biochem J*, 381, 587-92.
- CARLSON, C. R., LYGREN, B., BERGE, T., HOSHI, N., WONG, W., TASKEN, K. & SCOTT, J. D. 2006. Delineation of type I protein kinase A-selective signaling events using an RI anchoring disruptor. *J Biol Chem*, 281, 21535-45.
- CARLSON, C. R., RUPPELT, A. & TASKEN, K. 2003. A kinase anchoring protein (AKAP) interaction and dimerization of the RIalpha and RIIbeta regulatory subunits of protein kinase a in vivo by the yeast two hybrid system. *J Mol Biol*, 327, 609-18.
- CARR, D. W., STOFKO-HAHN, R. E., FRASER, I. D., BISHOP, S. M., ACOTT, T. S., BRENNAN, R. G. & SCOTT, J. D. 1991. Interaction of the regulatory subunit (RII) of cAMP-dependent protein kinase with RII-anchoring proteins occurs through an amphipathic helix binding motif. *J Biol Chem*, 266, 14188-92.
- CHALFIE, M., TU, Y., EUSKIRCHEN, G., WARD, W. W. & PRASHER, D. C. 1994. Green fluorescent protein as a marker for gene expression. *Science*, 263, 802-5.
- CHEN, Y., CANN, M. J., LITVIN, T. N., IOURGENKO, V., SINCLAIR, M. L., LEVIN, L. R. & BUCK, J. 2000. Soluble adenylyl cyclase as an evolutionarily conserved bicarbonate sensor. *Science*, 289, 625-8.
- CHEUNG, R., ERCLIK, M. S. & MITCHELL, J. 2005. 1,25-dihydroxyvitamin D(3) stimulated protein kinase C phosphorylation of type VI adenylyl cyclase inhibits parathyroid hormone signal transduction in rat osteoblastic UMR 106-01 cells. *J Cell Biochem*, 94, 1017-27.
- COFFINO, P., GRAY, J. W. & TOMKINS, G. M. 1975. Cyclic AMP, a nonessential regulator of the cell cycle. *Proc Natl Acad Sci U S A*, 72, 878-82.
- COGHLAN, V. M., PERRINO, B. A., HOWARD, M., LANGEBERG, L. K., HICKS, J. B., GALLATIN, W. M. & SCOTT, J. D. 1995. Association of protein kinase A and protein phosphatase 2B with a common anchoring protein. *Science*, 267, 108-11.

- COLLEDGE, M., DEAN, R. A., SCOTT, G. K., LANGEBERG, L. K., HUGANIR, R. L. & SCOTT, J. D. 2000. Targeting of PKA to glutamate receptors through a MAGUK-AKAP complex. *Neuron*, 27, 107-19.
- COLLEDGE, M. & SCOTT, J. D. 1999. AKAPs: from structure to function. *Trends Cell Biol*, 9, 216-21.
- COLLINS, D. M., MURDOCH, H., DUNLOP, A. J., CHARYCH, E., BAILLIE, G. S., WANG, Q., HERBERG, F. W., BRANDON, N., PRINZ, A. & HOUSLAY, M. D. 2008. Ndel1 alters its conformation by sequestering cAMP-specific phosphodiesterase-4D3 (PDE4D3) in a manner that is dynamically regulated through Protein Kinase A (PKA). *Cell Signal*, 20, 2356-69.
- CONTI, M. 2000. Phosphodiesterases and cyclic nucleotide signaling in endocrine cells. *Mol Endocrinol*, 14, 1317-27.
- CONTI, M. & BEAVO, J. 2007. Biochemistry and physiology of cyclic nucleotide phosphodiesterases: essential components in cyclic nucleotide signaling. *Annu Rev Biochem*, 76, 481-511.
- COOPER, D. M. 2003. Regulation and organization of adenylyl cyclases and cAMP. *Biochem J*, 375, 517-29.
- CORBIN, J. D., SUGDEN, P. H., LINCOLN, T. M. & KEELY, S. L. 1977. Compartmentalization of adenosine 3':5'-monophosphate and adenosine 3':5'-monophosphate-dependent protein kinase in heart tissue. *J Biol Chem*, 252, 3854-61.
- COSTA, M., GERNER, E. W. & RUSSELL, D. H. 1976a. Cell cycle-specific activity of type I and type II cyclic adenosine 3':5'-monophosphate-dependent protein kinases in Chinese hamster ovary cells. *J Biol Chem*, 251, 3313-9.
- COSTA, M., GERNER, E. W. & RUSSELL, D. H. 1976b. G1 specific increases in cyclic AMP levels and protein kinase activity in Chinese hamster ovary cells. *Biochim Biophys Acta*, 425, 246-55.
- COSTA, M., GERNER, E. W. & RUSSELL, D. H. 1978. Cyclic AMP levels and types I and II cyclic AMP-dependent protein kinase activity in synchronized cells and in quiescent cultures stimulated to proliferate. *Biochim Biophys Acta*, 538, 1-10.
- COTE, R. H. 2004. Characteristics of photoreceptor PDE (PDE6): similarities and differences to PDE5. *Int J Impot Res*, 16 Suppl 1, S28-33.
- CUMMINGS, D. E., BRANDON, E. P., PLANAS, J. V., MOTAMED, K., IDZERDA, R. L. & MCKNIGHT, G. S. 1996. Genetically lean mice result from targeted disruption of the RII beta subunit of protein kinase A. *Nature*, 382, 622-6.
- D'SA, C., TOLBERT, L. M., CONTI, M. & DUMAN, R. S. 2002. Regulation of cAMP-specific phosphodiesterases type 4B and 4D (PDE4) splice variants by cAMP signaling in primary cortical neurons. *J Neurochem*, 81, 745-57.
- DALE, R. E., EISINGER, J. & BLUMBERG, W. E. 1979. The orientational freedom of molecular probes. The orientation factor in intramolecular energy transfer. *Biophys J*, 26, 161-93.
- DANIEL, V., LITWACK, G. & TOMKINS, G. M. 1973. Induction of cytolysis of cultured lymphoma cells by adenosine 3':5'-cyclic monophosphate and the isolation of resistant variants. *Proc Natl Acad Sci USA*, 70, 76-9.
- DAVARE, M. A., AVDONIN, V., HALL, D. D., PEDEN, E. M., BURETTE, A., WEINBERG, R. J., HORNE, M. C., HOSHI, T. & HELL, J. W. 2001. A beta2 adrenergic receptor signaling complex assembled with the Ca<sup>2+</sup> channel Cav1.2. *Science*, 293, 98-101.
- DAVARE, M. A., DONG, F., RUBIN, C. S. & HELL, J. W. 1999. The A-kinase anchor protein MAP2B and cAMP-dependent protein kinase are associated with class C L-type calcium channels in neurons. *J Biol Chem*, 274, 30280-7.

- DE CAMILLI, P., MORETTI, M., DONINI, S. D., WALTER, U. & LOHMANN, S. M. 1986. Heterogeneous distribution of the cAMP receptor protein RII in the nervous system: evidence for its intracellular accumulation on microtubules, microtubule-organizing centers, and in the area of the Golgi complex. *J Cell Biol*, 103, 189-203.
- DE ROOIJ, J., REHMANN, H., VAN TRIEST, M., COOL, R. H., WITTINGHOFER, A. & BOS, J. L. 2000. Mechanism of regulation of the Epac family of cAMP-dependent RapGEFs. *J Biol Chem*, 275, 20829-36.
- DE ROOIJ, J., ZWARTKRUIS, F. J., VERHEIJEN, M. H., COOL, R. H., NIJMAN, S. M., WITTINGHOFER, A. & BOS, J. L. 1998. Epac is a Rap1 guanine-nucleotide-exchange factor directly activated by cyclic AMP. *Nature*, 396, 474-7.
- DELL'ACQUA, M. L., FAUX, M. C., THORBURN, J., THORBURN, A. & SCOTT, J. D. 1998. Membrane-targeting sequences on AKAP79 bind phosphatidylinositol-4, 5-bisphosphate. *EMBO J*, 17, 2246-60.
- DI BENEDETTO, G., ZOCCARATO, A., LISSANDRON, V., TERRIN, A., LI, X., HOUSLAY, M. D., BAILLIE, G. S. & ZACCOLO, M. 2008. Protein kinase A type I and type II define distinct intracellular signaling compartments. *Circ Res*, 103, 836-44.
- DICTENBERG, J. B., ZIMMERMAN, W., SPARKS, C. A., YOUNG, A., VIDAIR, C., ZHENG, Y., CARRINGTON, W., FAY, F. S. & DOXSEY, S. J. 1998. Pericentrin and gamma-tubulin form a protein complex and are organized into a novel lattice at the centrosome. *J Cell Biol*, 141, 163-74.
- DIPILATO, L. M., CHENG, X. & ZHANG, J. 2004. Fluorescent indicators of cAMP and Epac activation reveal differential dynamics of cAMP signaling within discrete subcellular compartments. *Proc Natl Acad Sci U S A*, 101, 16513-8.
- DIVIANI, D., LANGEBERG, L. K., DOXSEY, S. J. & SCOTT, J. D. 2000. Pericentrin anchors protein kinase A at the centrosome through a newly identified RII-binding domain. *Curr Biol*, 10, 417-20.
- DIVIANI, D. & SCOTT, J. D. 2001. AKAP signaling complexes at the cytoskeleton. *J Cell Sci*, 114, 1431-7.
- DODGE-KAFKA, K. L., LANGEBERG, L. & SCOTT, J. D. 2006. Compartmentation of cyclic nucleotide signaling in the heart: the role of A-kinase anchoring proteins. *Circ Res*, 98, 993-1001.
- DODGE-KAFKA, K. L., SOUGHAYER, J., PARE, G. C., CARLISLE MICHEL, J. J., LANGEBERG, L. K., KAPILOFF, M. S. & SCOTT, J. D. 2005. The protein kinase A anchoring protein mAKAP coordinates two integrated cAMP effector pathways. *Nature*, 437, 574-8.
- DODGE, K. L., KHOUANGSATHIENE, S., KAPILOFF, M. S., MOUTON, R., HILL, E. V., HOUSLAY, M. D., LANGEBERG, L. K. & SCOTT, J. D. 2001. mAKAP assembles a protein kinase A/PDE4 phosphodiesterase cAMP signaling module. *Embo J*, 20, 1921-30.
- DOSTMANN, W. R., TAYLOR, S. S., GENIESER, H. G., JASTORFF, B., DOSKELAND, S. O. & OGREID, D. 1990. Probing the cyclic nucleotide binding sites of cAMP-dependent protein kinases I and II with analogs of adenosine 3',5'-cyclic phosphorothioates. *J Biol Chem*, 265, 10484-91.
- DOXSEY, S. 1998. The centrosome--a tiny organelle with big potential. *Nat Genet*, 20, 104-6.
- DOXSEY, S., MCCOLLUM, D. & THEURKAUF, W. 2005a. Centrosomes in cellular regulation. *Annu Rev Cell Dev Biol*, 21, 411-34.
- DOXSEY, S., ZIMMERMAN, W. & MIKULE, K. 2005b. Centrosome control of the cell cycle. *Trends Cell Biol*, 15, 303-11.

- DOXSEY, S. J., STEIN, P., EVANS, L., CALARCO, P. D. & KIRSCHNER, M. 1994. Pericentrin, a highly conserved centrosome protein involved in microtubule organization. *Cell*, 76, 639-50.
- DRANSFIELD, D. T., YEH, J. L., BRADFORD, A. J. & GOLDENRING, J. R. 1997. Identification and characterization of a novel A-kinase-anchoring protein (AKAP120) from rabbit gastric parietal cells. *Biochem J*, 322 ( Pt 3), 801-8.
- DROCOURT, D., CALMELS, T., REYNES, J. P., BARON, M. & TIRABY, G. 1990. Cassettes of the *Streptoalloteichus hindustanus* ble gene for transformation of lower and higher eukaryotes to phleomycin resistance. *Nucleic Acids Res*, 18, 4009.
- DUTERTRE, S., CAZALES, M., QUARANTA, M., FROMENT, C., TRABUT, V., DOZIER, C., MIREY, G., BOUCHE, J. P., THEIS-FEBVRE, N., SCHMITT, E., MONSARRAT, B., PRIGENT, C. & DUCOMMUN, B. 2004. Phosphorylation of CDC25B by Aurora-A at the centrosome contributes to the G2-M transition. *J Cell Sci*, 117, 2523-31.
- DZEJA, C., HAGEN, V., KAUPP, U. B. & FRINGS, S. 1999. Ca<sup>2+</sup> permeation in cyclic nucleotide-gated channels. *EMBO J*, 18, 131-44.
- EDWARDS, A. S. & SCOTT, J. D. 2000. A-kinase anchoring proteins: protein kinase A and beyond. *Curr Opin Cell Biol*, 12, 217-21.
- EVELLIN, S., MONGILLO, M., TERRIN, A., LISSANDRON, V. & ZACCOLO, M. 2004. Measuring dynamic changes in cAMP using fluorescence resonance energy transfer. *Methods Mol Biol*, 284, 259-70.
- FAUX, M. C., ROLLINS, E. N., EDWARDS, A. S., LANGEBERG, L. K., NEWTON, A. C. & SCOTT, J. D. 1999. Mechanism of A-kinase-anchoring protein 79 (AKAP79) and protein kinase C interaction. *Biochem J*, 343 Pt 2, 443-52.
- FAUX, M. C. & SCOTT, J. D. 1997. Regulation of the AKAP79-protein kinase C interaction by Ca<sup>2+</sup>/Calmodulin. *J Biol Chem*, 272, 17038-44.
- FELICIELLO, A., GALLO, A., MELE, E., PORCELLINI, A., TRONCONE, G., GARBI, C., GOTTESMAN, M. E. & AVVEDIMENTO, E. V. 2000. The localization and activity of cAMP-dependent protein kinase affect cell cycle progression in thyroid cells. *J Biol Chem*, 275, 303-11.
- FELICIELLO, A., GOTTESMAN, M. E. & AVVEDIMENTO, E. V. 2001. The biological functions of A-kinase anchor proteins. *J Mol Biol*, 308, 99-114.
- FINCH, E. A. & AUGUSTINE, G. J. 1998. Local calcium signalling by inositol-1,4,5-trisphosphate in Purkinje cell dendrites. *Nature*, 396, 753-6.
- FISCHMEISTER, R., CASTRO, L. R., ABI-GERGES, A., ROCHAIS, F., JUREVICIUS, J., LEROY, J. & VANDECASTEELE, G. 2006. Compartmentation of cyclic nucleotide signaling in the heart: the role of cyclic nucleotide phosphodiesterases. *Circ Res*, 99, 816-28.
- FLORIO, V. A., SONNENBURG, W. K., JOHNSON, R., KWAK, K. S., JENSEN, G. S., WALSH, K. A. & BEAVO, J. A. 1994. Phosphorylation of the 61-kDa calmodulin-stimulated cyclic nucleotide phosphodiesterase at serine 120 reduces its affinity for calmodulin. *Biochemistry*, 33, 8948-54.
- FÖRSTER, T. 1948. Zwischenmolekulare Energiewanderung und Fluoreszenz. *Annalen der Physik*, 437, 55-75.
- FRANCIS, S. H. & CORBIN, J. D. 1994. Structure and function of cyclic nucleotide-dependent protein kinases. *Annu Rev Physiol*, 56, 237-72.
- FRANCIS, S. H., TURKO, I. V. & CORBIN, J. D. 2001. Cyclic nucleotide phosphodiesterases: relating structure and function. *Prog Nucleic Acid Res Mol Biol*, 65, 1-52.
- FRASER, I. D., CONG, M., KIM, J., ROLLINS, E. N., DAAKA, Y., LEFKOWITZ, R. J. & SCOTT, J. D. 2000. Assembly of an A kinase-anchoring protein-beta(2)-adrenergic receptor complex facilitates receptor phosphorylation and signaling. *Curr Biol*, 10, 409-12.

- FRIEDMAN, D. L. 1976. Role of cyclic nucleotides in cell growth and differentiation. *Physiol Rev*, 56, 652-708.
- GABRIEL, D., VERNIER, M., PFEIFER, M. J., DASEN, B., TENAILLON, L. & BOUHELAL, R. 2003. High throughput screening technologies for direct cyclic AMP measurement. *Assay Drug Dev Technol*, 1, 291-303.
- GIAMAS, G., HIRNER, H., SHOSHIASHVILI, L., GROTHEY, A., GESSERT, S., KUHL, M., HENNE-BRUNS, D., VORGIAS, C. E. & KNIPPSCHILD, U. 2007. Phosphorylation of CK1delta: identification of Ser370 as the major phosphorylation site targeted by PKA in vitro and in vivo. *Biochem J*, 406, 389-98.
- GILL, G. N. & GARREN, L. D. 1971. Role of the receptor in the mechanism of action of adenosine 3':5'-cyclic monophosphate. *Proc Natl Acad Sci U S A*, 68, 786-90.
- GILLINGHAM, A. K. & MUNRO, S. 2000. The PACT domain, a conserved centrosomal targeting motif in the coiled-coil proteins AKAP450 and pericentrin. *EMBO Rep*, 1, 524-9.
- GOAILLARD, J. M., VINCENT, P. V. & FISCHMEISTER, R. 2001. Simultaneous measurements of intracellular cAMP and L-type Ca<sup>2+</sup> current in single frog ventricular myocytes. *J Physiol*, 530, 79-91.
- GOLD, M. G., LYGREN, B., DOKURNO, P., HOSHI, N., MCCONNACHIE, G., TASKEN, K., CARLSON, C. R., SCOTT, J. D. & BARFORD, D. 2006. Molecular basis of AKAP specificity for PKA regulatory subunits. *Mol Cell*, 24, 383-95.
- GOSTI-TESTU, F., MARTY, M. C., BERGES, J., MAUNOURY, R. & BORNENS, M. 1986. Identification of centrosomal proteins in a human lymphoblastic cell line. *EMBO J*, 5, 2545-50.
- GRADIN, H. M., LARSSON, N., MARKLUND, U. & GULLBERG, M. 1998. Regulation of microtubule dynamics by extracellular signals: cAMP-dependent protein kinase switches off the activity of oncoprotein 18 in intact cells. *J Cell Biol*, 140, 131-41.
- GRIECO, D., AVVEDIMENTO, E. V. & GOTTESMAN, M. E. 1994. A role for cAMP-dependent protein kinase in early embryonic divisions. *Proc Natl Acad Sci U S A*, 91, 9896-900.
- GRIECO, D., PORCELLINI, A., AVVEDIMENTO, E. V. & GOTTESMAN, M. E. 1996. Requirement for cAMP-PKA pathway activation by M phase-promoting factor in the transition from mitosis to interphase. *Science*, 271, 1718-23.
- GRONHOLM, M., VOSSEBEIN, L., CARLSON, C. R., KUJA-PANULA, J., TEESALU, T., ALFTHAN, K., VAHERI, A., RAUVALA, H., HERBERG, F. W., TASKEN, K. & CARPEN, O. 2003. Merlin links to the cAMP neuronal signaling pathway by anchoring the R1beta subunit of protein kinase A. *J Biol Chem*, 278, 41167-72.
- HALL, D. D. & HELL, J. W. 2001. The fourth Dimension in Cellular Signaling. *Science*, 293, 2204-5.
- HAN, H., STESSIN, A., ROBERTS, J., HESS, K., GAUTAM, N., KAMENETSKY, M., LOU, O., HYDE, E., NATHAN, N., MULLER, W. A., BUCK, J., LEVIN, L. R. & NATHAN, C. 2005. Calcium-sensing soluble adenylyl cyclase mediates TNF signal transduction in human neutrophils. *J Exp Med*, 202, 353-61.
- HANOUNE, J. & DEFER, N. 2001. Regulation and role of adenylyl cyclase isoforms. *Annu Rev Pharmacol Toxicol*, 41, 145-74.
- HAUSKEN, Z. E., COGHLAN, V. M., HASTINGS, C. A., REIMANN, E. M. & SCOTT, J. D. 1994. Type II regulatory subunit (RII) of the cAMP-dependent protein kinase interaction with A-kinase anchor proteins requires isoleucines 3 and 5. *J Biol Chem*, 269, 24245-51.
- HAUSKEN, Z. E., DELL'ACQUA, M. L., COGHLAN, V. M. & SCOTT, J. D. 1996. Mutational analysis of the A-kinase anchoring protein (AKAP)-binding site on RII.

- Classification Of side chain determinants for anchoring and isoform selective association with AKAPs. *J Biol Chem*, 271, 29016-22.
- HAYES, J. S. & BRUNTON, L. L. 1982. Functional compartments in cyclic nucleotide action. *J Cyclic Nucleotide Res*, 8, 1-16.
- HAYES, J. S., BRUNTON, L. L., BROWN, J. H., REESE, J. B. & MAYER, S. E. 1979. Hormonally specific expression of cardiac protein kinase activity. *Proc Natl Acad Sci U S A*, 76, 1570-4.
- HAYES, J. S., BRUNTON, L. L. & MAYER, S. E. 1980. Selective activation of particulate cAMP-dependent protein kinase by isoproterenol and prostaglandin E1. *J Biol Chem*, 255, 5113-9.
- HERBERG, F. W., MALESZKA, A., EIDE, T., VOSSEBEIN, L. & TASKEN, K. 2000. Analysis of A-kinase anchoring protein (AKAP) interaction with protein kinase A (PKA) regulatory subunits: PKA isoform specificity in AKAP binding. *J Mol Biol*, 298, 329-39.
- HERBST, K. J., NI, Q. & ZHANG, J. 2009. Dynamic visualization of signal transduction in living cells: from second messengers to kinases. *IUBMB Life*, 61, 902-8.
- HESS, K. C., JONES, B. H., MARQUEZ, B., CHEN, Y., ORD, T. S., KAMENETSKY, M., MIYAMOTO, C., ZIPPIN, J. H., KOPF, G. S., SUAREZ, S. S., LEVIN, L. R., WILLIAMS, C. J., BUCK, J. & MOSS, S. B. 2005. The "soluble" adenylyl cyclase in sperm mediates multiple signaling events required for fertilization. *Dev Cell*, 9, 249-59.
- HIGGINS, M. K., WEITZ, D., WARNE, T., SCHERTLER, G. F. & KAUPP, U. B. 2002. Molecular architecture of a retinal cGMP-gated channel: the arrangement of the cytoplasmic domains. *EMBO J*, 21, 2087-94.
- HILL, E. V., SHEPPARD, C. L., CHEUNG, Y. F., GALL, I., KRAUSE, E. & HOUSLAY, M. D. 2006. Oxidative stress employs phosphatidylinositol 3-kinase and ERK signalling pathways to activate cAMP phosphodiesterase-4D3 (PDE4D3) through multi-site phosphorylation at Ser239 and Ser579. *Cell Signal*, 18, 2056-69.
- HINCHCLIFFE, E. H., LI, C., THOMPSON, E. A., MALLER, J. L. & SLUDER, G. 1999. Requirement of Cdk2-cyclin E activity for repeated centrosome reproduction in *Xenopus* egg extracts. *Science*, 283, 851-4.
- HINCHCLIFFE, E. H., MILLER, F. J., CHAM, M., KHODJAKOV, A. & SLUDER, G. 2001. Requirement of a centrosomal activity for cell cycle progression through G1 into S phase. *Science*, 291, 1547-50.
- HOEFLICH, K. P. & IKURA, M. 2002. Calmodulin in action: diversity in target recognition and activation mechanisms. *Cell*, 108, 739-42.
- HOFFMANN, R., BAILLIE, G. S., MACKENZIE, S. J., YARWOOD, S. J. & HOUSLAY, M. D. 1999. The MAP kinase ERK2 inhibits the cyclic AMP-specific phosphodiesterase HSPDE4D3 by phosphorylating it at Ser579. *Embo J*, 18, 893-903.
- HOHL, C. M. & LI, Q. A. 1991. Compartmentation of cAMP in adult canine ventricular myocytes. Relation to single-cell free Ca<sup>2+</sup> transients. *Circ Res*, 69, 1369-79.
- HOUSLAY, M. D. 1998. Adaptation in cyclic AMP signalling processes: a central role for cyclic AMP phosphodiesterases. *Semin Cell Dev Biol*, 9, 161-7.
- HOUSLAY, M. D. 2001. PDE4 cAMP-specific phosphodiesterases. *Prog Nucleic Acid Res Mol Biol*, 69, 249-315.
- HOUSLAY, M. D. 2010. Underpinning compartmentalised cAMP signalling through targeted cAMP breakdown. *Trends Biochem Sci*, 35, 91-100.
- HOUSLAY, M. D. & ADAMS, D. R. 2003. PDE4 cAMP phosphodiesterases: modular enzymes that orchestrate signalling cross-talk, desensitization and compartmentalization. *Biochem J*, 370, 1-18.

- HOUSLAY, M. D., BAILLIE, G. S. & MAURICE, D. H. 2007. cAMP-Specific phosphodiesterase-4 enzymes in the cardiovascular system: a molecular toolbox for generating compartmentalized cAMP signaling. *Circ Res*, 100, 950-66.
- HOUSLAY, M. D., SCHAFER, P. & ZHANG, K. Y. 2005. Keynote review: phosphodiesterase-4 as a therapeutic target. *Drug Discov Today*, 10, 1503-19.
- HUAI, Q., WANG, H., ZHANG, W., COLMAN, R. W., ROBINSON, H. & KE, H. 2004. Crystal structure of phosphodiesterase 9 shows orientation variation of inhibitor 3-isobutyl-1-methylxanthine binding. *Proc Natl Acad Sci U S A*, 101, 9624-9.
- HUANG, L. J., DURICK, K., WEINER, J. A., CHUN, J. & TAYLOR, S. S. 1997a. D-AKAP2, a novel protein kinase A anchoring protein with a putative RGS domain. *Proc Natl Acad Sci U S A*, 94, 11184-9.
- HUANG, L. J., DURICK, K., WEINER, J. A., CHUN, J. & TAYLOR, S. S. 1997b. Identification of a novel protein kinase A anchoring protein that binds both type I and type II regulatory subunits. *J Biol Chem*, 272, 8057-64.
- HUNTER, T. 2000. Signaling--2000 and beyond. *Cell*, 100, 113-27.
- HUSTON, E., HOUSLAY, T. M., BAILLIE, G. S. & HOUSLAY, M. D. 2006. cAMP phosphodiesterase-4A1 (PDE4A1) has provided the paradigm for the intracellular targeting of phosphodiesterases, a process that underpins compartmentalized cAMP signalling. *Biochem Soc Trans*, 34, 504-9.
- HYDE, C. C., AHMED, S. A., PADLAN, E. A., MILES, E. W. & DAVIES, D. R. 1988. Three-dimensional structure of the tryptophan synthase alpha 2 beta 2 multienzyme complex from *Salmonella typhimurium*. *J Biol Chem*, 263, 17857-71.
- JAISWAL, B. S. & CONTI, M. 2003. Calcium regulation of the soluble adenylyl cyclase expressed in mammalian spermatozoa. *Proc Natl Acad Sci U S A*, 100, 10676-81.
- JANG, I. S. & JUHNN, Y. S. 2001. Adaptation of cAMP signaling system in SH-SY5Y neuroblastoma cells following expression of a constitutively active stimulatory G protein alpha, Q227L Galpha. *Exp Mol Med*, 33, 37-45.
- JARNAESS, E., RUPPELT, A., STOKKA, A. J., LYGREN, B., SCOTT, J. D. & TASKEN, K. 2008. Dual specificity A-kinase anchoring proteins (AKAPs) contain an additional binding region that enhances targeting of protein kinase A type I. *J Biol Chem*, 283, 33708-18.
- JIN, S. L., SWINNEN, J. V. & CONTI, M. 1992. Characterization of the structure of a low Km, rolipram-sensitive cAMP phosphodiesterase. Mapping of the catalytic domain. *J Biol Chem*, 267, 18929-39.
- JUREVICIUS, J. & FISCHMEISTER, R. 1996. Acetylcholine inhibits Ca<sup>2+</sup> current by acting exclusively at a site proximal to adenylyl cyclase in frog cardiac myocytes. *J Physiol*, 491 ( Pt 3), 669-75.
- JUREVICIUS, J., SKEBERDIS, V. A. & FISCHMEISTER, R. 2003. Role of cyclic nucleotide phosphodiesterase isoforms in cAMP compartmentation following beta<sub>2</sub>-adrenergic stimulation of I<sub>Ca,L</sub> in frog ventricular myocytes. *J Physiol*, 551, 239-52.
- KAMENETSKY, M., MIDDELHAUFE, S., BANK, E. M., LEVIN, L. R., BUCK, J. & STEEGBORN, C. 2006. Molecular details of cAMP generation in mammalian cells: a tale of two systems. *J Mol Biol*, 362, 623-39.
- KAPILOFF, M. S., JACKSON, N. & AIRHART, N. 2001. mA<sub>1</sub>AKAP and the ryanodine receptor are part of a multi-component signaling complex on the cardiomyocyte nuclear envelope. *J Cell Sci*, 114, 3167-76.
- KARIV, I. I., STEVENS, M. E., BEHRENS, D. L. & OLDENBURG, K. R. 1999. High Throughput Quantitation of cAMP Production Mediated by Activation of Seven Transmembrane Domain Receptors. *J Biomol Screen*, 4, 27-32.

- KASAI, H. & PETERSEN, O. H. 1994. Spatial dynamics of second messengers: IP3 and cAMP as long-range and associative messengers. *Trends Neurosci*, 17, 95-101.
- KAUPP, U. B. & SEIFERT, R. 2002. Cyclic nucleotide-gated ion channels. *Physiol Rev*, 82, 769-824.
- KAWABE, J., EBINA, T., TOYA, Y., OKA, N., SCHWENCKE, C., DUZIC, E. & ISHIKAWA, Y. 1996. Regulation of type V adenylyl cyclase by PMA-sensitive and -insensitive protein kinase C isoenzymes in intact cells. *FEBS Lett*, 384, 273-6.
- KAWABE, J., IWAMI, G., EBINA, T., OHNO, S., KATADA, T., UEDA, Y., HOMCY, C. J. & ISHIKAWA, Y. 1994. Differential activation of adenylyl cyclase by protein kinase C isoenzymes. *J Biol Chem*, 269, 16554-8.
- KAWASAKI, H., SPRINGETT, G. M., MOCHIZUKI, N., TOKI, S., NAKAYA, M., MATSUDA, M., HOUSMAN, D. E. & GRAYBIEL, A. M. 1998. A family of cAMP-binding proteins that directly activate Rap1. *Science*, 282, 2275-9.
- KEELY, S. L. 1977. Activation of cAMP-dependent protein kinase without a corresponding increase in phosphorylase activity. *Res Commun Chem Pathol Pharmacol*, 18, 283-90.
- KEELY, S. L. 1979. Prostaglandin E1 activation of heart cAMP-dependent protein kinase: apparent dissociation of protein kinase activation from increases in phosphorylase activity and contractile force. *Mol Pharmacol*, 15, 235-45.
- KERYER, G., DI FIORE, B., CELATI, C., LECHTRECK, K. F., MOGENSEN, M., DELOUVEE, A., LAVIA, P., BORNENS, M. & TASSIN, A. M. 2003a. Part of Ran is associated with AKAP450 at the centrosome: involvement in microtubule-organizing activity. *Mol Biol Cell*, 14, 4260-71.
- KERYER, G., RIOS, R. M., LANDMARK, B. F., SKALHEGG, B., LOHMANN, S. M. & BORNENS, M. 1993. A high-affinity binding protein for the regulatory subunit of cAMP-dependent protein kinase II in the centrosome of human cells. *Exp Cell Res*, 204, 230-40.
- KERYER, G., WITCZAK, O., DELOUVEE, A., KEMMNER, W. A., ROUILLARD, D., TASKEN, K. & BORNENS, M. 2003b. Dissociating the centrosomal matrix protein AKAP450 from centrioles impairs centriole duplication and cell cycle progression. *Mol Biol Cell*, 14, 2436-46.
- KHAN, S., PERRY, C., TETREAULT, M. L., HENRY, D., TRIMMER, J. S., ZIMMERMAN, A. L. & MATTHEWS, G. 2010. A novel cyclic nucleotide-gated ion channel enriched in synaptic terminals of isotocin neurons in zebrafish brain and pituitary. *Neuroscience*, 165, 79-89.
- KHODJAKOV, A. & RIEDER, C. L. 2001. Centrosomes enhance the fidelity of cytokinesis in vertebrates and are required for cell cycle progression. *J Cell Biol*, 153, 237-42.
- KIM, C., VIGIL, D., ANAND, G. & TAYLOR, S. S. 2006. Structure and dynamics of PKA signaling proteins. *Eur J Cell Biol*, 85, 651-4.
- KLAUCK, T. M., FAUX, M. C., LABUDDA, K., LANGEBERG, L. K., JAKEN, S. & SCOTT, J. D. 1996. Coordination of three signaling enzymes by AKAP79, a mammalian scaffold protein. *Science*, 271, 1589-92.
- KLUSSMANN, E., EDEMIR, B., PEPPERLE, B., TAMMA, G., HENN, V., KLAUSCHENZ, E., HUNDSRUCKER, C., MARIC, K. & ROSENTHAL, W. 2001. Ht31: the first protein kinase A anchoring protein to integrate protein kinase A and Rho signaling. *FEBS Lett*, 507, 264-8.
- KRAMER, A., MAILAND, N., LUKAS, C., SYLJUASEN, R. G., WILKINSON, C. J., NIGG, E. A., BARTEK, J. & LUKAS, J. 2004. Centrosome-associated Chk1 prevents premature activation of cyclin-B-Cdk1 kinase. *Nat Cell Biol*, 6, 884-91.

- KUMAR, M., HSIAO, K., VIDUGIRIENE, J. & GOUELI, S. A. 2007. A bioluminescent-based, HTS-compatible assay to monitor G-protein-coupled receptor modulation of cellular cyclic AMP. *Assay Drug Dev Technol*, 5, 237-45.
- KUSSEL-ANDERMANN, P., EL-AMRAOUI, A., SAFIEDDINE, S., HARDELIN, J. P., NOUAILLE, S., CAMONIS, J. & PETIT, C. 2000a. Unconventional myosin VIIA is a novel A-kinase-anchoring protein. *J Biol Chem*, 275, 29654-9.
- KUSSEL-ANDERMANN, P., EL-AMRAOUI, A., SAFIEDDINE, S., NOUAILLE, S., PERFETTINI, I., LECUIT, M., COSSART, P., WOLFRUM, U. & PETIT, C. 2000b. Vezatin, a novel transmembrane protein, bridges myosin VIIA to the cadherin-catenins complex. *Embo J*, 19, 6020-9.
- LACEY, K. R., JACKSON, P. K. & STEARNS, T. 1999. Cyclin-dependent kinase control of centrosome duplication. *Proc Natl Acad Sci U S A*, 96, 2817-22.
- LAMB, N. J., CAVADORE, J. C., LABBE, J. C., MAURER, R. A. & FERNANDEZ, A. 1991. Inhibition of cAMP-dependent protein kinase plays a key role in the induction of mitosis and nuclear envelope breakdown in mammalian cells. *Embo J*, 10, 1523-33.
- LAMB, N. J., FERNANDEZ, A., CONTI, M. A., ADELSTEIN, R., GLASS, D. B., WELCH, W. J. & FERAMISCO, J. R. 1988. Regulation of actin microfilament integrity in living nonmuscle cells by the cAMP-dependent protein kinase and the myosin light chain kinase. *J Cell Biol*, 106, 1955-71.
- LAMB, N. J., FERNANDEZ, A., WATRIN, A., LABBE, J. C. & CAVADORE, J. C. 1990. Microinjection of p34cdc2 kinase induces marked changes in cell shape, cytoskeletal organization, and chromatin structure in mammalian fibroblasts. *Cell*, 60, 151-65.
- LANE, M. E. & KALDERON, D. 1994. RNA localization along the anteroposterior axis of the *Drosophila* oocyte requires PKA-mediated signal transduction to direct normal microtubule organization. *Genes Dev*, 8, 2986-95.
- LE JEUNE, I. R., SHEPHERD, M., VAN HEEKE, G., HOUSLAY, M. D. & HALL, I. P. 2002. Cyclic AMP-dependent transcriptional up-regulation of phosphodiesterase 4D5 in human airway smooth muscle cells. Identification and characterization of a novel PDE4D5 promoter. *J Biol Chem*, 277, 35980-9.
- LEON, D. A., HERBERG, F. W., BANKY, P. & TAYLOR, S. S. 1997. A stable alpha-helical domain at the N terminus of the RIalpha subunits of cAMP-dependent protein kinase is a novel dimerization/docking motif. *J Biol Chem*, 272, 28431-7.
- LESTER, L. B., COGHLAN, V. M., NAUERT, B. & SCOTT, J. D. 1996. Cloning and characterization of a novel A-kinase anchoring protein. AKAP 220, association with testicular peroxisomes. *J Biol Chem*, 271, 9460-5.
- LI, H., DEGENHARDT, B., TOBIN, D., YAO, Z. X., TASKEN, K. & PAPADOPOULOS, V. 2001. Identification, localization, and function in steroidogenesis of PAP7: a peripheral-type benzodiazepine receptor- and PKA (RIalpha)-associated protein. *Mol Endocrinol*, 15, 2211-28.
- LI, X., BAILLIE, G. S. & HOUSLAY, M. D. 2009. Mdm2 directs the ubiquitination of beta-arrestin-sequestered cAMP phosphodiesterase-4D5. *J Biol Chem*, 284, 16170-82.
- LIM, C. J., HAN, J., YOUSEFI, N., MA, Y., AMIEUX, P. S., MCKNIGHT, G. S., TAYLOR, S. S. & GINSBERG, M. H. 2007. Alpha4 integrins are type I cAMP-dependent protein kinase-anchoring proteins. *Nat Cell Biol*, 9, 415-21.
- LIM, J., PAHLKE, G. & CONTI, M. 1999. Activation of the cAMP-specific phosphodiesterase PDE4D3 by phosphorylation. Identification and function of an inhibitory domain. *J Biol Chem*, 274, 19677-85.

- LIN, J. W., WYSZYNSKI, M., MADHAVAN, R., SEALOCK, R., KIM, J. U. & SHENG, M. 1998. Yotiao, a novel protein of neuromuscular junction and brain that interacts with specific splice variants of NMDA receptor subunit NR1. *J Neurosci*, 18, 2017-27.
- LISSANDRON, V., TERRIN, A., COLLINI, M., D'ALFONSO, L., CHIRICO, G., PANTANO, S. & ZACCOLO, M. 2005. Improvement of a FRET-based indicator for cAMP by linker design and stabilization of donor-acceptor interaction. *J Mol Biol*, 354, 546-55.
- LIU, J., RONE, M. B. & PAPADOPOULOS, V. 2006. Protein-protein interactions mediate mitochondrial cholesterol transport and steroid biosynthesis. *J Biol Chem*, 281, 38879-93.
- LIU, M., CHEN, T. Y., AHAMED, B., LI, J. & YAU, K. W. 1994. Calcium-calmodulin modulation of the olfactory cyclic nucleotide-gated cation channel. *Science*, 266, 1348-54.
- LOHMANN, S. M., DECAMILLI, P., EINIG, I. & WALTER, U. 1984. High-affinity binding of the regulatory subunit (RII) of cAMP-dependent protein kinase to microtubule-associated and other cellular proteins. *Proc Natl Acad Sci U S A*, 81, 6723-7.
- LUTTRELL, L. M. & LEFKOWITZ, R. J. 2002. The role of beta-arrestins in the termination and transduction of G-protein-coupled receptor signals. *J Cell Sci*, 115, 455-65.
- LYNCH, M. J., BAILLIE, G. S., MOHAMED, A., LI, X., MAISONNEUVE, C., KLUSSMANN, E., VAN HEEKE, G. & HOUSLAY, M. D. 2005. RNA silencing identifies PDE4D5 as the functionally relevant cAMP phosphodiesterase interacting with beta arrestin to control the protein kinase A/AKAP79-mediated switching of the beta2-adrenergic receptor to activation of ERK in HEK293B2 cells. *J Biol Chem*, 280, 33178-89.
- MA, H. T., PATTERSON, R. L., VAN ROSSUM, D. B., BIRNBAUMER, L., MIKOSHIBA, K. & GILL, D. L. 2000. Requirement of the inositol trisphosphate receptor for activation of store-operated Ca<sup>2+</sup> channels. *Science*, 287, 1647-51.
- MACKENZIE, S. J., BAILLIE, G. S., MCPHEE, I., BOLGER, G. B. & HOUSLAY, M. D. 2000. ERK2 mitogen-activated protein kinase binding, phosphorylation, and regulation of the PDE4D cAMP-specific phosphodiesterases. The involvement of COOH-terminal docking sites and NH<sub>2</sub>-terminal UCR regions. *J Biol Chem*, 275, 16609-17.
- MACMANUS, J. P. & WHITFIELD, J. F. 1969. Stimulation of DNA synthesis and mitotic activity of thymic lymphocytes by cyclic adenosine 3'5'-monophosphate. *Exp Cell Res*, 58, 188-91.
- MALUMBRES, M. & BARBACID, M. 2005. Mammalian cyclin-dependent kinases. *Trends Biochem Sci*, 30, 630-41.
- MARKO, D., ROMANAKIS, K., ZANKL, H., FURSTENBERGER, G., STEINBAUER, B. & EISENBRAND, G. 1998. Induction of apoptosis by an inhibitor of cAMP-specific PDE in malignant murine carcinoma cells overexpressing PDE activity in comparison to their nonmalignant counterparts. *Cell Biochem Biophys*, 28, 75-101.
- MARTINEZ, S. E., WU, A. Y., GLAVAS, N. A., TANG, X. B., TURLEY, S., HOL, W. G. & BEAVO, J. A. 2002. The two GAF domains in phosphodiesterase 2A have distinct roles in dimerization and in cGMP binding. *Proc Natl Acad Sci U S A*, 99, 13260-5.
- MATSUMOTO, Y. & MALLER, J. L. 2004. A centrosomal localization signal in cyclin E required for Cdk2-independent S phase entry. *Science*, 306, 885-8.
- MAYR, B. & MONTMINY, M. 2001. Transcriptional regulation by the phosphorylation-dependent factor CREB. *Nat Rev Mol Cell Biol*, 2, 599-609.

- MCCA HILL, A., MCSORLEY, T., HUSTON, E., HILL, E. V., LYNCH, M. J., GALL, I., KERYER, G., LYGREN, B., TASKEN, K., VAN HEEKE, G. & HOUSLAY, M. D. 2005. In resting COS1 cells a dominant negative approach shows that specific, anchored PDE4 cAMP phosphodiesterase isoforms gate the activation, by basal cyclic AMP production, of AKAP-tethered protein kinase A type II located in the centrosomal region. *Cell Signal*, 17, 1158-73.
- MCCA HILL, A. C., HUSTON, E., LI, X. & HOUSLAY, M. D. 2008. PDE4 associates with different scaffolding proteins: modulating interactions as treatment for certain diseases. *Handb Exp Pharmacol*, 125-66.
- MICHEL, J. J. & SCOTT, J. D. 2002. AKAP mediated signal transduction. *Annu Rev Pharmacol Toxicol*, 42, 235-57.
- MILLAR, J. K., MACKIE, S., CLAPCOTE, S. J., MURDOCH, H., PICKARD, B. S., CHRISTIE, S., MUIR, W. J., BLACKWOOD, D. H., RODER, J. C., HOUSLAY, M. D. & PORTEOUS, D. J. 2007. Disrupted in schizophrenia 1 and phosphodiesterase 4B: towards an understanding of psychiatric illness. *J Physiol*, 584, 401-5.
- MONGILLO, M., MCSORLEY, T., EVELLIN, S., SOOD, A., LISSANDRON, V., TERRIN, A., HUSTON, E., HANNAWACKER, A., LOHSE, M. J., POZZAN, T., HOUSLAY, M. D. & ZACCOLO, M. 2004. Fluorescence resonance energy transfer-based analysis of cAMP dynamics in live neonatal rat cardiac myocytes reveals distinct functions of compartmentalized phosphodiesterases. *Circ Res*, 95, 67-75.
- MONGILLO, M., TERRIN, A., EVELLIN, S., LISSANDRON, V. & ZACCOLO, M. 2005. Study of cyclic adenosine monophosphate microdomains in cells. *Methods Mol Biol*, 307, 1-13.
- MONGILLO, M., TOCCHETTI, C. G., TERRIN, A., LISSANDRON, V., CHEUNG, Y. F., DOSTMANN, W. R., POZZAN, T., KASS, D. A., PAOLOCCI, N., HOUSLAY, M. D. & ZACCOLO, M. 2006. Compartmentalized phosphodiesterase-2 activity blunts beta-adrenergic cardiac inotropy via an NO/cGMP-dependent pathway. *Circ Res*, 98, 226-34.
- MUKAI, H. 2003. The structure and function of PKN, a protein kinase having a catalytic domain homologous to that of PKC. *J Biochem*, 133, 17-27.
- MUKAI, H. & ONO, Y. 1998. [Structure and function of PKN]. *Tanpakushitsu Kakusan Koso*, 43, 1659-65.
- MULSANT, P., GATIGNOL, A., DALENS, M. & TIRABY, G. 1988. Phleomycin resistance as a dominant selectable marker in CHO cells. *Somat Cell Mol Genet*, 14, 243-52.
- NEWLON, M. G., ROY, M., MORIKIS, D., CARR, D. W., WESTPHAL, R., SCOTT, J. D. & JENNINGS, P. A. 2001. A novel mechanism of PKA anchoring revealed by solution structures of anchoring complexes. *Embo J*, 20, 1651-62.
- NEWLON, M. G., ROY, M., MORIKIS, D., HAUSKEN, Z. E., COGHLAN, V., SCOTT, J. D. & JENNINGS, P. A. 1999. The molecular basis for protein kinase A anchoring revealed by solution NMR. *Nat Struct Biol*, 6, 222-7.
- NGUEWA, P. A., CALVO, A., PULLAMSETTI, S. S., BANAT, G. A., GRIMMINGER, F. & SAVAI, R. 2011. Tyrosine kinase inhibitors with antiangiogenic properties for the treatment of non-small cell lung cancer. *Expert Opin Investig Drugs*, 20, 61-74.
- NIGG, E. A., SCHAFER, G., HILZ, H. & EPPENBERGER, H. M. 1985. Cyclic-AMP-dependent protein kinase type II is associated with the Golgi complex and with centrosomes. *Cell*, 41, 1039-51.
- NIKOLAEV, V. O., BUNEMANN, M., HEIN, L., HANNAWACKER, A. & LOHSE, M. J. 2004. Novel single chain cAMP sensors for receptor-induced signal propagation. *J Biol Chem*, 279, 37215-8.

- O'CONNELL, J. C., MCCALLUM, J. F., MCPHEE, I., WAKEFIELD, J., HOUSLAY, E. S., WISHART, W., BOLGER, G., FRAME, M. & HOUSLAY, M. D. 1996. The SH3 domain of Src tyrosyl protein kinase interacts with the N-terminal splice region of the PDE4A cAMP-specific phosphodiesterase RPDE-6 (RNPDE4A5). *Biochem J*, 318 ( Pt 1), 255-61.
- OLIVEIRA, R. F., TERRIN, A., DI BENEDETTO, G., CANNON, R. C., KOH, W., KIM, M., ZACCOLO, M. & BLACKWELL, K. T. 2010. The role of type 4 phosphodiesterases in generating microdomains of cAMP: large scale stochastic simulations. *PLoS One*, 5, e11725.
- PATTERSON, R. L., VAN ROSSUM, D. B. & GILL, D. L. 1999. Store-operated Ca<sup>2+</sup> entry: evidence for a secretion-like coupling model. *Cell*, 98, 487-99.
- PERRY, S. J., BAILLIE, G. S., KOHOUT, T. A., MCPHEE, I., MAGIERA, M. M., ANG, K. L., MILLER, W. E., MCLEAN, A. J., CONTI, M., HOUSLAY, M. D. & LEFKOWITZ, R. J. 2002. Targeting of cyclic AMP degradation to beta 2-adrenergic receptors by beta-arrestins. *Science*, 298, 834-6.
- PIDOUX, G. & TASKEN, K. Specificity and spatial dynamics of protein kinase A signaling organized by A-kinase-anchoring proteins. *J Mol Endocrinol*, 44, 271-84.
- PIEL, M., NORDBERG, J., EUTENEUER, U. & BORNENS, M. 2001. Centrosome-dependent exit of cytokinesis in animal cells. *Science*, 291, 1550-3.
- PONSIOEN, B., ZHAO, J., RIEDL, J., ZWARTKRUIS, F., VAN DER KROGT, G., ZACCOLO, M., MOOLENAAR, W. H., BOS, J. L. & JALINK, K. 2004. Detecting cAMP-induced Epac activation by fluorescence resonance energy transfer: Epac as a novel cAMP indicator. *EMBO Rep*, 5, 1176-80.
- PREMONT, R. T., CLAING, A., VITALE, N., FREEMAN, J. L., PITCHER, J. A., PATTON, W. A., MOSS, J., VAUGHAN, M. & LEFKOWITZ, R. J. 1998. beta2-Adrenergic receptor regulation by GIT1, a G protein-coupled receptor kinase-associated ADP ribosylation factor GTPase-activating protein. *Proc Natl Acad Sci U S A*, 95, 14082-7.
- PRYSTAY, L., GAGNE, A., KASILA, P., YEH, L. A. & BANKS, P. 2001. Homogeneous cell-based fluorescence polarization assay for the direct detection of cAMP. *J Biomol Screen*, 6, 75-82.
- PUCK, T. T., CIECIURA, S. J. & ROBINSON, A. 1958. Genetics of somatic mammalian cells. III. Long-term cultivation of euploid cells from human and animal subjects. *J Exp Med*, 108, 945-56.
- PUROHIT, A., TYNAN, S. H., VALLEE, R. & DOXSEY, S. J. 1999. Direct interaction of pericentrin with cytoplasmic dynein light intermediate chain contributes to mitotic spindle organization. *J Cell Biol*, 147, 481-92.
- QIAO, J., MEI, F. C., POPOV, V. L., VERGARA, L. A. & CHENG, X. 2002. Cell cycle-dependent subcellular localization of exchange factor directly activated by cAMP. *J Biol Chem*, 277, 26581-6.
- RALL, T. W. & SUTHERLAND, E. W. 1958. Formation of a cyclic adenine ribonucleotide by tissue particles. *J Biol Chem*, 232, 1065-76.
- RALL, T. W. & SUTHERLAND, E. W. 1962. Adenyl cyclase. II. The enzymatically catalyzed formation of adenosine 3',5'-phosphate and inorganic pyrophosphate from adenosine triphosphate. *J Biol Chem*, 237, 1228-32.
- RALL, T. W. & SUTHERLAND, E. W., JR. 1959. Action of epinephrine and norepinephrine in broken cell preparations. *Pharmacol Rev*, 11, 464-5.
- RANGEL-ALDAO, R. & ROSEN, O. M. 1976a. Dissociation and reassociation of the phosphorylated and nonphosphorylated forms of adenosine 3':5' - monophosphate-dependent protein kinase from bovine cardiac muscle. *J Biol Chem*, 251, 3375-80.

- RANGEL-ALDAO, R. & ROSEN, O. M. 1976b. Mechanism of self-phosphorylation of adenosine 3':5'-monophosphate-dependent protein kinase from bovine cardiac muscle. *J Biol Chem*, 251, 7526-9.
- RANGEL-ALDAO, R. & ROSEN, O. M. 1977. Effect of cAMP and ATP on the reassociation of phosphorylated and nonphosphorylated subunits of the cAMP-dependent protein kinase from bovine cardiac muscle. *J Biol Chem*, 252, 7140-5.
- REHMANN, H., ARIAS-PALOMO, E., HADDERS, M. A., SCHWEDE, F., LLORCA, O. & BOS, J. L. 2008. Structure of Epac2 in complex with a cyclic AMP analogue and RAP1B. *Nature*, 455, 124-7.
- REHMANN, H., DAS, J., KNIPSCHEER, P., WITTINGHOFER, A. & BOS, J. L. 2006. Structure of the cyclic-AMP-responsive exchange factor Epac2 in its auto-inhibited state. *Nature*, 439, 625-8.
- REINTON, N., COLLAS, P., HAUGEN, T. B., SKALHEGG, B. S., HANSSON, V., JAHNSEN, T. & TASKEN, K. 2000. Localization of a novel human A-kinase-anchoring protein, hAKAP220, during spermatogenesis. *Dev Biol*, 223, 194-204.
- RICH, T. C., FAGAN, K. A., NAKATA, H., SCHAACK, J., COOPER, D. M. & KARPEN, J. W. 2000. Cyclic nucleotide-gated channels colocalize with adenylyl cyclase in regions of restricted cAMP diffusion. *J Gen Physiol*, 116, 147-61.
- RICH, T. C., FAGAN, K. A., TSE, T. E., SCHAACK, J., COOPER, D. M. & KARPEN, J. W. 2001a. A uniform extracellular stimulus triggers distinct cAMP signals in different compartments of a simple cell. *Proc Natl Acad Sci U S A*, 98, 13049-54.
- RICH, T. C., TSE, T. E., ROHAN, J. G., SCHAACK, J. & KARPEN, J. W. 2001b. In vivo assessment of local phosphodiesterase activity using tailored cyclic nucleotide-gated channels as cAMP sensors. *J Gen Physiol*, 118, 63-78.
- RICH, T. C., XIN, W., MEHATS, C., HASSELL, K. A., PIGGOTT, L. A., LE, X., KARPEN, J. W. & CONTI, M. 2007. Cellular mechanisms underlying prostaglandin-induced transient cAMP signals near the plasma membrane of HEK-293 cells. *Am J Physiol Cell Physiol*, 292, C319-31.
- RICHTER, W. & CONTI, M. 2004. The oligomerization state determines regulatory properties and inhibitor sensitivity of type 4 cAMP-specific phosphodiesterases. *J Biol Chem*, 279, 30338-48.
- RIOS, R. M., CELATI, C., LOHMANN, S. M., BORNENS, M. & KERYER, G. 1992. Identification of a high affinity binding protein for the regulatory subunit RII beta of cAMP-dependent protein kinase in Golgi enriched membranes of human lymphoblasts. *EMBO J*, 11, 1723-31.
- ROBISON, G. A., BUTCHER, R. W. & SUTHERLAND, E. W. 1968. Cyclic AMP. *Annu Rev Biochem*, 37, 149-74.
- ROCHAIS, F., ABI-GERGES, A., HORNER, K., LEFEBVRE, F., COOPER, D. M., CONTI, M., FISCHMEISTER, R. & VANDECASTEELE, G. 2006. A specific pattern of phosphodiesterases controls the cAMP signals generated by different Gs-coupled receptors in adult rat ventricular myocytes. *Circ Res*, 98, 1081-8.
- RODRIGUEZ-COLLAZO, P., SNYDER, S. K., CHIFFER, R. C., BRESSLER, E. A., VOSS, T. C., ANDERSON, E. P., GENIESER, H. G. & SMITH, C. L. 2008a. cAMP signaling regulates histone H3 phosphorylation and mitotic entry through a disruption of G2 progression. *Exp Cell Res*, 314, 2855-69.
- RODRIGUEZ-COLLAZO, P., SNYDER, S. K., CHIFFER, R. C., ZLATANOVA, J., LEUBA, S. H. & SMITH, C. L. 2008b. cAMP signaling induces rapid loss of histone H3 phosphorylation in mammary adenocarcinoma-derived cell lines. *Exp Cell Res*, 314, 1-10.
- RODRIGUEZ-VILARRUPLA, A., JAUMOT, M., ABELLA, N., CANELA, N., BRUN, S., DIAZ, C., ESTANYOL, J. M., BACHS, O. & AGELL, N. 2005. Binding of calmodulin to the

- carboxy-terminal region of p21 induces nuclear accumulation via inhibition of protein kinase C-mediated phosphorylation of Ser153. *Mol Cell Biol*, 25, 7364-74.
- RONINSON, I. B., BROUDE, E. V. & CHANG, B. D. 2001. If not apoptosis, then what? Treatment-induced senescence and mitotic catastrophe in tumor cells. *Drug Resist Updat*, 4, 303-13.
- ROSS, E. M. & GILMAN, A. G. 1977a. Reconstitution of catecholamine-sensitive adenylate cyclase activity: interactions of solubilized components with receptor-replete membranes. *Proc Natl Acad Sci U S A*, 74, 3715-9.
- ROSS, E. M. & GILMAN, A. G. 1977b. Resolution of some components of adenylate cyclase necessary for catalytic activity. *J Biol Chem*, 252, 6966-9.
- RYAN, W. L. & HEIDRICK, M. L. 1968. Inhibition of cell growth in vitro by adenosine 3',5'-monophosphate. *Science*, 162, 1484-5.
- SARKAR, D., ERLICHMAN, J. & RUBIN, C. S. 1984. Identification of a calmodulin-binding protein that co-purifies with the regulatory subunit of brain protein kinase II. *J Biol Chem*, 259, 9840-6.
- SAURIN, A. T., DURGAN, J., CAMERON, A. J., FAISAL, A., MARBER, M. S. & PARKER, P. J. 2008. The regulated assembly of a PKCepsilon complex controls the completion of cytokinesis. *Nat Cell Biol*, 10, 891-901.
- SAVAI, R., PULLAMSETTI, S. S., BANAT, G. A., WEISSMANN, N., GHOFrani, H. A., GRIMMINGER, F. & SCHERMULY, R. T. 2010. Targeting cancer with phosphodiesterase inhibitors. *Expert Opin Investig Drugs*, 19, 117-31.
- SCAPIN, G., PATEL, S. B., CHUNG, C., VARNERIN, J. P., EDMONDSON, S. D., MASTRACCHIO, A., PARMEE, E. R., SINGH, S. B., BECKER, J. W., VAN DER PLOEG, L. H. & TOTA, M. R. 2004. Crystal structure of human phosphodiesterase 3B: atomic basis for substrate and inhibitor specificity. *Biochemistry*, 43, 6091-100.
- SCHALLMACH, E., STEINER, D. & VOGEL, Z. 2006. Adenylyl cyclase type II activity is regulated by two different mechanisms: implications for acute and chronic opioid exposure. *Neuropharmacology*, 50, 998-1005.
- SCHMIDT, P. H., DRANSFIELD, D. T., CLAUDIO, J. O., HAWLEY, R. G., TROTTER, K. W., MILGRAM, S. L. & GOLDENRING, J. R. 1999. AKAP350, a multiply spliced protein kinase A-anchoring protein associated with centrosomes. *J Biol Chem*, 274, 3055-66.
- SCHULTZ, R. 2009. PKA and CDC25B: at last connected. *Cell Cycle*, 8, 516-7.
- SEHRAWAT, S., CULLERE, X., PATEL, S., ITALIANO, J., JR. & MAYADAS, T. N. 2008. Role of Epac1, an exchange factor for Rap GTPases, in endothelial microtubule dynamics and barrier function. *Mol Biol Cell*, 19, 1261-70.
- SEREZANI, C. H., BALLINGER, M. N., ARONOFF, D. M. & PETERS-GOLDEN, M. 2008. Cyclic AMP: master regulator of innate immune cell function. *Am J Respir Cell Mol Biol*, 39, 127-32.
- SETTE, C. & CONTI, M. 1996. Phosphorylation and activation of a cAMP-specific phosphodiesterase by the cAMP-dependent protein kinase. Involvement of serine 54 in the enzyme activation. *J Biol Chem*, 271, 16526-34.
- SEYBOLD, J., NEWTON, R., WRIGHT, L., FINNEY, P. A., SUTTORP, N., BARNES, P. J., ADCOCK, I. M. & GIEMBYCZ, M. A. 1998. Induction of phosphodiesterases 3B, 4A4, 4D1, 4D2, and 4D3 in Jurkat T-cells and in human peripheral blood T-lymphocytes by 8-bromo-cAMP and Gs-coupled receptor agonists. Potential role in beta2-adrenoreceptor desensitization. *J Biol Chem*, 273, 20575-88.
- SHAKUR, Y., PRYDE, J. G. & HOUSLAY, M. D. 1993. Engineered deletion of the unique N-terminal domain of the cyclic AMP-specific phosphodiesterase RD1 prevents plasma membrane association and the attainment of enhanced thermostability

- without altering its sensitivity to inhibition by rolipram. *Biochem J*, 292 ( Pt 3), 677-86.
- SHANKS, R. A., LAROCCA, M. C., BERRYMAN, M., EDWARDS, J. C., URUSHIDANI, T., NAVARRE, J. & GOLDENRING, J. R. 2002a. AKAP350 at the Golgi apparatus. II. Association of AKAP350 with a novel chloride intracellular channel (CLIC) family member. *J Biol Chem*, 277, 40973-80.
- SHANKS, R. A., STEADMAN, B. T., SCHMIDT, P. H. & GOLDENRING, J. R. 2002b. AKAP350 at the Golgi apparatus. I. Identification of a distinct Golgi apparatus targeting motif in AKAP350. *J Biol Chem*, 277, 40967-72.
- SHARMA, R. K. & WANG, J. H. 1985. Differential regulation of bovine brain calmodulin-dependent cyclic nucleotide phosphodiesterase isoenzymes by cyclic AMP-dependent protein kinase and calmodulin-dependent phosphatase. *Proc Natl Acad Sci U S A*, 82, 2603-7.
- SHEPPARD, J. R. 1971. Restoration of contact-inhibited growth to transformed cells by dibutyryl adenosine 3':5'-cyclic monophosphate. *Proc Natl Acad Sci U S A*, 68, 1316-20.
- SHEPPARD, J. R. 1972. Difference in the cyclic adenosine 3',5'-monophosphate levels in normal and transformed cells. *Nat New Biol*, 236, 14-6.
- SHEPPARD, J. R. & PRESCOTT, D. M. 1972. Cyclic AMP levels in synchronized mammalian cells. *Exp Cell Res*, 75, 293-6.
- SHIMOMURA, O., JOHNSON, F. H. & SAIGA, Y. 1962. Extraction, purification and properties of aequorin, a bioluminescent protein from the luminous hydromedusan, *Aequorea*. *J Cell Comp Physiol*, 59, 223-39.
- SILLIBOURNE, J. E., MILNE, D. M., TAKAHASHI, M., ONO, Y. & MEEK, D. W. 2002. Centrosomal anchoring of the protein kinase CK1delta mediated by attachment to the large, coiled-coil scaffolding protein CG-NAP/AKAP450. *J Mol Biol*, 322, 785-97.
- SMITH, J. A. & MARTIN, L. 1973. Do cells cycle? *Proc Natl Acad Sci U S A*, 70, 1263-7.
- SONNENBURG, W. K., SEGER, D., KWAK, K. S., HUANG, J., CHARBONNEAU, H. & BEAVO, J. A. 1995. Identification of inhibitory and calmodulin-binding domains of the PDE1A1 and PDE1A2 calmodulin-stimulated cyclic nucleotide phosphodiesterases. *J Biol Chem*, 270, 30989-1000.
- STANGHERLIN, A., GESELLCHEN, F., ZOCCARATO, A., TERRIN, A., FIELDS, L. A., BERRERA, M., SURDO, N. C., CRAIG, M. A., SMITH, G., HAMILTON, G. & ZACCOLO, M. 2011. cGMP Signals Modulate cAMP Levels in a Compartment-Specific Manner to Regulate Catecholamine-Dependent Signaling in Cardiac Myocytes. *Circ Res*.
- STEFAN, E., WIESNER, B., BAILLIE, G. S., MOLLAJEW, R., HENN, V., LORENZ, D., FURKERT, J., SANTAMARIA, K., NEDVETSKY, P., HUNDSRUCKER, C., BEYERMANN, M., KRAUSE, E., POHL, P., GALL, I., MACINTYRE, A. N., BACHMANN, S., HOUSLAY, M. D., ROSENTHAL, W. & KLUSSMANN, E. 2006. Compartmentalization of cAMP-Dependent Signaling by Phosphodiesterase-4D Is Involved in the Regulation of Vasopressin-Mediated Water Reabsorption in Renal Principal Cells. *J Am Soc Nephrol*.
- STEINBERG, S. F. & BRUNTON, L. L. 2001. Compartmentation of G protein-coupled signaling pathways in cardiac myocytes. *Annu Rev Pharmacol Toxicol*, 41, 751-73.
- STEINER, A. L., KIPNIS, D. M., UTIGER, R. & PARKER, C. 1969. Radioimmunoassay for the measurement of adenosine 3',5'-cyclic phosphate. *Proc Natl Acad Sci U S A*, 64, 367-73.
- SUTHERLAND, E. W. 1972. Studies on the mechanism of hormone action. *Science*, 177, 401-8.

- SUTHERLAND, E. W. & ROBISON, G. A. 1966. The role of cyclic-3',5'-AMP in responses to catecholamines and other hormones. *Pharmacol Rev*, 18, 145-61.
- TABAKOFF, B., NELSON, E., YOSHIMURA, M., HELLEVUO, K. & HOFFMAN, P. L. 2001. Phosphorylation cascades control the actions of ethanol on cell cAMP signalling. *J Biomed Sci*, 8, 44-51.
- TAKAHASHI, M., MUKAI, H., OISHI, K., ISAGAWA, T. & ONO, Y. 2000. Association of immature hypophosphorylated protein kinase cepsilon with an anchoring protein CG-NAP. *J Biol Chem*, 275, 34592-6.
- TAKAHASHI, M., SHIBATA, H., SHIMAKAWA, M., MIYAMOTO, M., MUKAI, H. & ONO, Y. 1999. Characterization of a novel giant scaffolding protein, CG-NAP, that anchors multiple signaling enzymes to centrosome and the golgi apparatus. *J Biol Chem*, 274, 17267-74.
- TAKECHI, H., EILERS, J. & KONNERTH, A. 1998. A new class of synaptic response involving calcium release in dendritic spines. *Nature*, 396, 757-60.
- TAKIO, K., SMITH, S. B., KREBS, E. G., WALSH, K. A. & TITANI, K. 1984. Amino acid sequence of the regulatory subunit of bovine type II adenosine cyclic 3',5'-phosphate dependent protein kinase. *Biochemistry*, 23, 4200-6.
- TAN, C. M., KELVIN, D. J., LITCHFIELD, D. W., FERGUSON, S. S. & FELDMAN, R. D. 2001. Tyrosine kinase-mediated serine phosphorylation of adenylyl cyclase. *Biochemistry*, 40, 1702-9.
- TARASKA, J. W. & ZAGOTTA, W. N. 2007. Structural dynamics in the gating ring of cyclic nucleotide-gated ion channels. *Nat Struct Mol Biol*, 14, 854-60.
- TASKEN, K. & AANDAHL, E. M. 2004. Localized effects of cAMP mediated by distinct routes of protein kinase A. *Physiol Rev*, 84, 137-67.
- TASKEN, K. A., COLLAS, P., KEMMNER, W. A., WITCZAK, O., CONTI, M. & TASKEN, K. 2001. Phosphodiesterase 4D and protein kinase a type II constitute a signaling unit in the centrosomal area. *J Biol Chem*, 276, 21999-2002.
- TAVALIN, S. J., COLLEDGE, M., HELL, J. W., LANGEBERG, L. K., HUGANIR, R. L. & SCOTT, J. D. 2002. Regulation of GluR1 by the A-kinase anchoring protein 79 (AKAP79) signaling complex shares properties with long-term depression. *J Neurosci*, 22, 3044-51.
- TAYLOR, S. S. 1989. cAMP-dependent protein kinase. Model for an enzyme family. *J Biol Chem*, 264, 8443-6.
- TAYLOR, S. S., BUECHLER, J. A. & YONEMOTO, W. 1990. cAMP-dependent protein kinase: framework for a diverse family of regulatory enzymes. *Annu Rev Biochem*, 59, 971-1005.
- TAYLOR, S. S., KIM, C., CHENG, C. Y., BROWN, S. H., WU, J. & KANNAN, N. 2008. Signaling through cAMP and cAMP-dependent protein kinase: diverse strategies for drug design. *Biochim Biophys Acta*, 1784, 16-26.
- TAYLOR, S. S., KIM, C., VIGIL, D., HASTE, N. M., YANG, J., WU, J. & ANAND, G. S. 2005. Dynamics of signaling by PKA. *Biochim Biophys Acta*, 1754, 25-37.
- TERRENOIRE, C., HOUSLAY, M. D., BAILLIE, G. S. & KASS, R. S. 2009. The cardiac IKs potassium channel macromolecular complex includes the phosphodiesterase PDE4D3. *J Biol Chem*, 284, 9140-6.
- TERRIN, A., DI BENEDETTO, G., PERTEGATO, V., CHEUNG, Y. F., BAILLIE, G., LYNCH, M. J., ELVASSORE, N., PRINZ, A., HERBERG, F. W., HOUSLAY, M. D. & ZACCOLO, M. 2006. PGE(1) stimulation of HEK293 cells generates multiple contiguous domains with different [cAMP]: role of compartmentalized phosphodiesterases. *J Cell Biol*, 175, 441-51.
- TESMER, J. J., SUNAHARA, R. K., GILMAN, A. G. & SPRANG, S. R. 1997. Crystal structure of the catalytic domains of adenylyl cyclase in a complex with G $\alpha$ .GTP $\gamma$ S. *Science*, 278, 1907-16.

- THEURKAUF, W. E. & VALLEE, R. B. 1982. Molecular characterization of the cAMP-dependent protein kinase bound to microtubule-associated protein 2. *J Biol Chem*, 257, 3284-90.
- TROTTER, K. W., FRASER, I. D., SCOTT, G. K., STUTTS, M. J., SCOTT, J. D. & MILGRAM, S. L. 1999. Alternative splicing regulates the subcellular localization of A-kinase anchoring protein 18 isoforms. *J Cell Biol*, 147, 1481-92.
- TSIEN, R. Y. 1992. Intracellular signal transduction in four dimensions: from molecular design to physiology. *Am J Physiol*, 263, C723-8.
- VAASA, A., LUST, M., TERRIN, A., URI, A. & ZACCOLO, M. 2010. Small-molecule FRET probes for protein kinase activity monitoring in living cells. *Biochem Biophys Res Commun*, 397, 750-5.
- VERDE, I., PAHLKE, G., SALANOVA, M., ZHANG, G., WANG, S., COLETTI, D., ONUFFER, J., JIN, S. L. & CONTI, M. 2001. Myomegalin is a novel protein of the golgi/centrosome that interacts with a cyclic nucleotide phosphodiesterase. *J Biol Chem*, 276, 11189-98.
- VICINI, E. & CONTI, M. 1997. Characterization of an intronic promoter of a cyclic adenosine 3',5'-monophosphate (cAMP)-specific phosphodiesterase gene that confers hormone and cAMP inducibility. *Mol Endocrinol*, 11, 839-50.
- WALSH, D. A., PERKINS, J. P. & KREBS, E. G. 1968. An adenosine 3',5'-monophosphate-dependant protein kinase from rabbit skeletal muscle. *J Biol Chem*, 243, 3763-5.
- WANG, P., WU, P., EGAN, R. W. & BILLAH, M. M. 2003. Identification and characterization of a new human type 9 cGMP-specific phosphodiesterase splice variant (PDE9A5). Differential tissue distribution and subcellular localization of PDE9A variants. *Gene*, 314, 15-27.
- WANG, Z., DILLON, T. J., POKALA, V., MISHRA, S., LABUDDA, K., HUNTER, B. & STORK, P. J. 2006. Rap1-mediated activation of extracellular signal-regulated kinases by cyclic AMP is dependent on the mode of Rap1 activation. *Mol Cell Biol*, 26, 2130-45.
- WARRIER, S., BELEVYCH, A. E., RUSE, M., ECKERT, R. L., ZACCOLO, M., POZZAN, T. & HARVEY, R. D. 2005. Beta-adrenergic- and muscarinic receptor-induced changes in cAMP activity in adult cardiac myocytes detected with FRET-based biosensor. *Am J Physiol Cell Physiol*, 289, C455-61.
- WEHRENS, X. H., LEHNART, S. E., REIKEN, S., VEST, J. A., WRONSKA, A. & MARKS, A. R. 2006. Ryanodine receptor/calcium release channel PKA phosphorylation: a critical mediator of heart failure progression. *Proc Natl Acad Sci U S A*, 103, 511-8.
- WESTPHAL, R. S., SODERLING, S. H., ALTO, N. M., LANGE BERG, L. K. & SCOTT, J. D. 2000. Scar/WAVE-1, a Wiskott-Aldrich syndrome protein, assembles an actin-associated multi-kinase scaffold. *EMBO J*, 19, 4589-600.
- WESTPHAL, R. S., TAVALIN, S. J., LIN, J. W., ALTO, N. M., FRASER, I. D., LANGE BERG, L. K., SHENG, M. & SCOTT, J. D. 1999. Regulation of NMDA receptors by an associated phosphatase-kinase signaling complex. *Science*, 285, 93-6.
- WILLOUGHBY, D. & COOPER, D. M. 2006. Use of single-cell imaging techniques to assess the regulation of cAMP dynamics. *Biochem Soc Trans*, 34, 468-71.
- WILLOUGHBY, D. & COOPER, D. M. 2007. Organization and Ca<sup>2+</sup> regulation of adenylyl cyclases in cAMP microdomains. *Physiol Rev*, 87, 965-1010.
- WITCZAK, O., SKALHEGG, B. S., KERYER, G., BORNENS, M., TASKEN, K., JAHNSEN, T. & ORSTAVIK, S. 1999. Cloning and characterization of a cDNA encoding an A-kinase anchoring protein located in the centrosome, AKAP450. *Embo J*, 18, 1858-68.

- WONG, W. & SCOTT, J. D. 2004. AKAP signalling complexes: focal points in space and time. *Nat Rev Mol Cell Biol*, 5, 959-70.
- WU, R. S., PANUSZ, H. T., HATCH, C. L. & BONNER, W. M. 1986. Histones and their modifications. *CRC Crit Rev Biochem*, 20, 201-63.
- YARWOOD, S. J., STEELE, M. R., SCOTLAND, G., HOUSLAY, M. D. & BOLGER, G. B. 1999. The RACK1 signaling scaffold protein selectively interacts with the cAMP-specific phosphodiesterase PDE4D5 isoform. *J Biol Chem*, 274, 14909-17.
- YOUNG, A., DICTENBERG, J. B., PUROHIT, A., TUFT, R. & DOXSEY, S. J. 2000. Cytoplasmic dynein-mediated assembly of pericentrin and gamma tubulin onto centrosomes. *Mol Biol Cell*, 11, 2047-56.
- YU, F. H., YAROV-YAROVOY, V., GUTMAN, G. A. & CATTERALL, W. A. 2005. Overview of molecular relationships in the voltage-gated ion channel superfamily. *Pharmacol Rev*, 57, 387-95.
- ZACCOLO, M. 2002. Selection of functional antibodies on the basis of valency. *Methods Mol Biol*, 178, 255-8.
- ZACCOLO, M., DE GIORGI, F., CHO, C. Y., FENG, L., KNAPP, T., NEGULESCU, P. A., TAYLOR, S. S., TSIEN, R. Y. & POZZAN, T. 2000. A genetically encoded, fluorescent indicator for cyclic AMP in living cells. *Nat Cell Biol*, 2, 25-9.
- ZACCOLO, M. & POZZAN, T. 2000. Imaging signal transduction in living cells with GFP-based probes. *IUBMB Life*, 49, 375-9.
- ZACCOLO, M. & POZZAN, T. 2002. Discrete microdomains with high concentration of cAMP in stimulated rat neonatal cardiac myocytes. *Science*, 295, 1711-5.
- ZAKHARY, D. R., FINK, M. A., RUEHR, M. L. & BOND, M. 2000a. Selectivity and regulation of A-kinase anchoring proteins in the heart. The role of autophosphorylation of the type II regulatory subunit of cAMP-dependent protein kinase. *J Biol Chem*, 275, 41389-95.
- ZAKHARY, D. R., MORAVEC, C. S. & BOND, M. 2000b. Regulation of PKA binding to AKAPs in the heart: alterations in human heart failure. *Circulation*, 101, 1459-64.
- ZEILIG, C. E., JOHNSON, R. A., SUTHERLAND, E. W. & FRIEDMAN, D. L. 1976. Adenosine 3':5'-monophosphate content and actions in the division cycle of synchronized HeLa cells. *J Cell Biol*, 71, 515-34.
- ZHANG, G., LIU, Y., RUOHO, A. E. & HURLEY, J. H. 1997. Structure of the adenylyl cyclase catalytic core. *Nature*, 386, 247-53.
- ZHANG, J., HUPFELD, C. J., TAYLOR, S. S., OLEFSKY, J. M. & TSIEN, R. Y. 2005. Insulin disrupts beta-adrenergic signalling to protein kinase A in adipocytes. *Nature*, 437, 569-73.
- ZHANG, K. Y., CARD, G. L., SUZUKI, Y., ARTIS, D. R., FONG, D., GILLETTE, S., HSIEH, D., NEIMAN, J., WEST, B. L., ZHANG, C., MILBURN, M. V., KIM, S. H., SCHLESSINGER, J. & BOLLAG, G. 2004. A glutamine switch mechanism for nucleotide selectivity by phosphodiesterases. *Mol Cell*, 15, 279-86.
- ZHANG, L., MURRAY, F., ZAHNO, A., KANTER, J. R., CHOU, D., SUDA, R., FENLON, M., RASSENTI, L., COTTAM, H., KIPPS, T. J. & INSEL, P. A. 2008. Cyclic nucleotide phosphodiesterase profiling reveals increased expression of phosphodiesterase 7B in chronic lymphocytic leukemia. *Proc Natl Acad Sci U S A*, 105, 19532-7.
- ZHAO, Z. S., LIM, J. P., NG, Y. W., LIM, L. & MANSER, E. 2005. The GIT-associated kinase PAK targets to the centrosome and regulates Aurora-A. *Mol Cell*, 20, 237-49.
- ZHENG, J., TRUDEAU, M. C. & ZAGOTTA, W. N. 2002. Rod cyclic nucleotide-gated channels have a stoichiometry of three CNGA1 subunits and one CNGB1 subunit. *Neuron*, 36, 891-6.

- ZHENG, J. & ZAGOTTA, W. N. 2004. Stoichiometry and assembly of olfactory cyclic nucleotide-gated channels. *Neuron*, 42, 411-21.
- ZIMMERMAN, W. C., SILLIBOURNE, J., ROSA, J. & DOXSEY, S. J. 2004. Mitosis-specific anchoring of gamma tubulin complexes by pericentrin controls spindle organization and mitotic entry. *Mol Biol Cell*, 15, 3642-57.
- ZIPPIN, J. H., CHEN, Y., NAHIRNEY, P., KAMENETSKY, M., WUTTKE, M. S., FISCHMAN, D. A., LEVIN, L. R. & BUCK, J. 2003. Compartmentalization of bicarbonate-sensitive adenylyl cyclase in distinct signaling microdomains. *FASEB J*, 17, 82-4.
- ZMUDA-TRZEBIATOWSKA, E., OKNIANSKA, A., MANGANIELLO, V. & DEGERMAN, E. 2006. Role of PDE3B in insulin-induced glucose uptake, GLUT-4 translocation and lipogenesis in primary rat adipocytes. *Cell Signal*, 18, 382-90.